

CHARACTERIZATION OF THE SEISMIC RESPONSE OF RC FRAMES AT  
DIFFERENT PERFORMANCE LEVELS ESTABLISHED IN THE ASCE 41-06  
SEISMIC REHABILITATION CODE

by:

Merangelí Morales González

Project submitted as a partial requirement for the degree of:

MASTER OF ENGINEERING

in

Civil Engineering

UNIVERSITY OF PUERTO RICO

MAYAGÜEZ CAMPUS

MAYAGÜEZ, PUERTO RICO

2013

Approved by:

\_\_\_\_\_  
Luis E. Suárez Colche, Ph.D.  
Member, Graduate Committee

\_\_\_\_\_  
Date

\_\_\_\_\_  
José O. Guevara Guillén, Ph.D., P.E.  
Member, Graduate Committee

\_\_\_\_\_  
Date

\_\_\_\_\_  
Aidcer L. Vidot Vega, Ph.D., P.E.  
President, Graduate Committee

\_\_\_\_\_  
Date

\_\_\_\_\_  
Genock Portela, Ph.D., P.E.  
Representative of Graduate Studies

\_\_\_\_\_  
Date

\_\_\_\_\_  
Ismael Pagán Trinidad, MSCE  
Chairperson of the Department

\_\_\_\_\_  
Date

## ABSTRACT

Performance-based earthquake engineering is focused in the definition of limits states to represent different levels of damage, which can be described by material strains, drifts, displacements or even changes in dissipating properties and stiffness of the structure. This study presents a research plan to characterize the behavior of Reinforced Concrete (RC) moment resistant frames at different performance levels established by the ASCE 41-06 seismic rehabilitation code. A total of 16 RC special moment resisting frames (2D) with different aspect ratios (L/H) and one 3D RC frame were analyzed in order to evaluate the seismic behavior of the structure at different performance levels. The design guidelines used were taken from the ACI 318-08 and ASCE 7-05 building codes, which are the design guidelines used for United States constructions. For each aspect ratio, four longitudinal steel reinforcement ratios for the beams that varied from 0.85% to 2.5% were used. For columns the steel reinforcement ratio used was determined using the methodology presented in ACI 318-08. All 2D frames were subjected to seven compatible earthquakes and scaled to accelerations ranging from 0.1g to 1.5g (105 cases for each frame) obtained from the Pacific Earthquake Engineering Research (PEER) database. The 3D frame was subjected to four ground motion of increasing intensity levels. These ground motions were applied in sequence to the frame. The frames were analyzed using the program OpenSEES (Open System for Earthquake Engineering Simulation). As part of this research the impact of the aspect ratios and geometry at different performance levels and their contribution on the structural frames damage were evaluated. In addition, the relationship between material strains and energy dissipation changes for the different performance levels was studied. The goal is to characterize the seismic behavior of RC frames to improve the currently available design assessment techniques and damages limit states.

## RESUMEN

La Ingeniería Sísmica Basada en Desempeño está enfocada en definir varios límites para representar el nivel de daño en una estructura; éstos pueden estar definidos por los esfuerzos en los materiales, derivas de piso, desplazamientos e incluso por cambios en las propiedades de disipación de energía y rigidez de la estructura. Esta investigación presenta un estudio para identificar el comportamiento de pórticos de hormigón reforzado resistentes a momento a diferentes niveles de desempeño establecidos por el código de Rehabilitación Sísmica de Estructuras ASCE 41-06. Un total de 16 pórticos especiales resistentes a momentos (2D) con diferentes razones de largo entre altura de viga ( $L/H$ ) y un pórtico de hormigón reforzado en tres dimensiones fueron analizados para evaluar la respuesta sísmica de la estructura a diferentes niveles de desempeño. Las normas de diseño utilizadas fueron tomadas de los códigos ACI 318-08 y ASCE 7-05, los cuales son las guías utilizadas en las construcciones en Estados Unidos. Para cada razón de  $L/H$  se utilizaron 4 cuantías de acero longitudinal para las vigas, las cuales varían entre 0.85% a 2.5%. La cuantía de acero para las columnas fue determinada utilizando la metodología presentada en el ACI 318-08. Todos los pórticos en dos dimensiones fueron analizados con 7 sismos, obtenidos de la base de datos del Centro de Investigación de Ingeniería Sísmica del Pacífico (PEER), cuyas aceleraciones fueron escaladas entre 0.1g a 1.5 g (105 casos por pórticos). El pórtico en tres dimensiones fue sometido a 4 sismos de creciente y aplicados en secuencia. Los pórticos fueron analizados utilizando el programa OpenSEES (*Open System for Earthquake Engineering Simulation*). Como parte de esta investigación se evaluó el impacto de la razón entre el largo y altura de viga y la geometría de los elementos a diferentes niveles de desempeño y su contribución en los daños estructurales de los pórticos. Se estudió también la relación entre las deformaciones en los materiales y los cambios en disipación de energía para

los diferentes niveles de desempeño. El objetivo de esta investigación es caracterizar el comportamiento sísmico de los pórticos de hormigón reforzado para mejorar los métodos de rehabilitación y límites de daños existentes.

© Merangelí Morales-González 2013

To my lovely niece Ivanna Alejandra,

To my parents and sisters,

for being in every step of my life.

To my friends,

for the support provided during these years.

Thanks to all for being part of my life.

## **ACKNOWLEDGEMENTS**

I want to thank to the giver of life, God, for giving me the strength to complete this journey. I would like to give special thanks to my advisor, Dr. Aidcer L. Vidot Vega, for giving me the opportunity to work under her supervision, without her support and guidance would be impossible to finish this work. To my graduate committee, Dr. Luis E. Suárez and Dr. José O. Guevara, for his availability and knowledge transmitted for the completion of this work. To my family, for their unconditional support and patience on these years.

## TABLE OF CONTENTS

LIST OF TABLES .....	x
LIST OF FIGURES .....	xiii
CHAPTER 1: INTRODUCTION AND LITERATURE REVIEW .....	1
1.1 SCOPE .....	1
1.2 RESEARCH OBJECTIVES AND SIGNIFICANCE .....	1
1.3 BACKGROUND AND MOTIVATION .....	2
1.3.1 <i>Performance Based Design- Current and Past Efforts</i> .....	3
CHAPTER 2: METHODOLOGY AND MODELING CONSIDERATIONS .....	9
2.1. INTRODUCTION.....	9
2.2. MODELS GENERALITIES .....	9
2.3. MODEL GEOMETRY AND DIMENSIONS.....	10
2.3.1 <i>2D Frame</i> .....	10
2.3.2 <i>2D Frame Design</i> .....	14
2.3.3 <i>3D Frame</i> .....	14
2.4. MODELING APPROACHES AND MATERIALS .....	16
2.5. <i>BEAM AND COLUMNS CAPACITY- 2D FRAME</i> .....	21
CHAPTER 3: DYNAMIC ANALYSES .....	27
3.1. INTRODUCTION.....	27
3.2. GROUND MOTIONS AND DYNAMIC ANALYSIS FOR THE 2D FRAMES .....	27
3.2.1 <i>Imperial Valley</i> .....	27
3.2.2 <i>Northridge</i> .....	28
3.2.3 <i>Kobe</i> .....	28
3.2.4 <i>Loma Prieta</i> .....	29
3.2.5 <i>Tabas, Iran</i> .....	29
3.2.6 <i>Kocaeli</i> .....	29
3.2.7 <i>Chi-Chi</i> .....	29
3.3. GROUND MOTIONS AND DYNAMIC ANALYSIS FOR THE 3D FRAME .....	31
3.4. COMPATIBLE EARTHQUAKE ACCELERATIONS AND RESPONSE SPECTRUM ...	34
3.4.1 <i>2D Frame</i> .....	34
3.4.2 <i>3D Frame</i> .....	35
3.5. DYNAMIC ANALYSES CONSIDERATIONS .....	36
3.5.1 <i>2D Frames</i> .....	36
3.5.2 <i>3D Frame</i> .....	37
3.5.3 <i>3D Frame Model Validation</i> .....	38
3.6. ADDITIONAL PARAMETERS FOR THE GROUND MOTIONS.....	41
3.6.1 <i>Arias Intensity (AI)</i> .....	41

3.6.2 <i>Cumulative Absolute Velocity (CAV)</i> .....	43
3.6.3 <i>Specific Energy Density (SED)</i> .....	44
CHAPTER 4: DRIFT LIMIT RESULTS FROM THE DYNAMIC ANALYSIS .....	47
4.1 INTRODUCTION.....	47
4.2. DRIFT AS DAMAGE INDICATOR .....	47
4.3. DRIFT LIMIT STATES FROM ASCE 41-06.....	49
4.4. DRIFT RESULTS - 2D FRAMES .....	51
4.5. DRIFT RESULTS – 3D FRAME .....	57
CHAPTER 5: STRAIN LIMIT RESULTS FROM THE DYNAMIC ANALYSES .....	59
5.1. INTRODUCTION.....	59
5.2. STEEL AND CONCRETE STRAINS RESULTS-2D FRAME .....	59
5.2.1 <i>Strains as function of PGA values</i> .....	59
5.2.2 <i>Strains as function of drifts</i> .....	69
5.3. STEEL AND CONCRETE STRAINS RESULTS-3D FRAME.....	78
5.3.1 <i>Strain as function of PGA values</i> .....	78
5.3.2 <i>Strains as a function of drift</i> .....	80
CHAPTER 6: SEISMIC HYSTERETIC ENERGY LIMITS FOR 2D FRAMES.....	84
6.1. INTRODUCTION.....	84
6.2. SEISMIC HYSTERETIC ENERGY .....	84
6.3. SEISMIC HYSTERETIC ENERGY AT LIMIT STATES .....	97
CHAPTER 7: RESULTS SUMMARY, CONCLUSIONS AND RECOMMENDATIONS.....	100
7.1. INTRODUCTION.....	100
7.2. STRAIN RESULTS - SUMMARY.....	100
7.2.1 <i>2D Frames</i> .....	100
7.2.2 <i>3D Frame</i> .....	105
7.3. ADDITIONAL EVALUATION OF STRAINS VS. DRIFT – 2D FRAMES .....	106
7.4. DRIFT RESULTS SUMMARY .....	109
7.5. SEISMIC ENERGY RESULTS SUMMARY .....	109
7.6. CONCLUSIONS .....	110
7.7. RECOMMENDATIONS .....	113
REFERENCES .....	114
APPENDIX I: HYSTERETIC ENERGY PLOTS .....	120
APPENDIX II: STRAIN VALUES AT DIFFERENT LIMIT STATES .....	129

## LIST OF TABLES

Table 1 Beam Moment Capacities Obtained from Cumbia.....	22
Table 2 Column Moment Capacities Obtained from Cumbia .....	22
Table 3 Seismic Hysteretic Energy at Limit States- Frame 1-1.0% .....	98
Table 4 Seismic Hysteretic Energy at Limit States - Frame 2-1.0% .....	98
Table 5 Seismic Hysteretic Energy at Limit States - Frame 3-1.0% .....	99
Table 6 Seismic Hysteretic Energy at Limit States - Frame 4-1.0% .....	99
Table 7 Steel Strain at Asce 41-06 Limit States .....	107
Table 9 Concrete Strain at Limit States .....	112
Table 8 Steel Strain at Limit States.....	112
Table 10 Yield Beam and Yield Frame Strains - Frame 1 0.85% .....	130
Table 11 Steel Strain at Limit States - Frame 1 0.85%.....	130
Table 12 Concrete Strain at Limit States - Frame 1 0.85% .....	130
Table 13 Seismic Hysteretic Energy at Limit States (KJ) - Frame 1 0.85% .....	131
Table 14 Yield Beam and Yield Frame Strains - Frame 1 1.0% .....	131
Table 15 Steel Strain at Limit States - Frame 1 1.0%.....	131
Table 16 Concrete Strain at Limit States - Frame 1 1.0% .....	132
Table 17 Seismic Hysteretic Energy at Limit States (KJ) - Frame 1 1.0% .....	132
Table 18 Yield Beam and Yield Frame Strains - Frame 1 1.5% .....	132
Table 19 Steel Strain at Limit States - Frame 1 1.5%.....	133
Table 20 Concrete Strain at Limit States - Frame 1 1.5% .....	133
Table 21 Seismic Hysteretic Energy at Limit States (KJ) - Frame 1 1.5% .....	133
Table 22 Yield Beam and Yield Frame - Frame 1 2.0% .....	134
Table 23 Steel Strain at Limit States - Frame 1 2.0%.....	134
Table 24 Concrete Strain at Limit States - Frame 1 2.0% .....	134
Table 25 Seismic Hysteretic Energy at Limit States (KJ) - Frame 1 2.0% .....	135
Table 26 Yield Beam and Yield Frame - Frame 2 0.85% .....	135
Table 27 Steel Strain at Limit States - Frame 2 0.85%.....	135
Table 28 Concrete Strain at Limit States - Frame 2 0.85% .....	136
Table 29 Seismic Hysteretic Energy at Limit States (KJ) - Frame 2 0.85% .....	136
Table 30 Yield Beam and Yield Frame Strains - Frame 2 1.0% .....	136

Table 31 Steel Strain at Limit States - Frame 2 1.0%.....	137
Table 32 Concrete Strain at Limit States - Frame 2 1.0% .....	137
Table 33 Seismic Hysteretic Energy at Limit States (KJ) - Frame 2 1.0% .....	138
Table 34 Yield Beam and Yield Frame Strains - Frame 2 1.5% .....	138
Table 35 Steel Strain at Limit States - Frame 2 1.5%.....	138
Table 36 Concrete Strain at Limit States - Frame 2 1.5% .....	139
Table 37 Seismic Hysteretic Energy at Limit States (KJ) - Frame 2 1.5% .....	139
Table 38 Yield Beam and Yield Frame Strains - Frame 2 2.0% .....	139
Table 39 Steel Strain at Limit States - Frame 2 2.0%.....	140
Table 40 Concrete Strain at Limit States - Frame 2 2.0% .....	140
Table 41 Seismic Hysteretic Energy at Limit States (KJ) - Frame 2 2.0% .....	141
Table 42 Yield Beam and Yield Frame Strains - Frame 3 0.85% .....	141
Table 43 Steel Strain at Limit States - Frame 3 0.85%.....	141
Table 44 Concrete Strain at Limit States - Frame 3 0.85% .....	142
Table 45 Seismic Hysteretic Energy at Limit States (KJ) - Frame 3 0.85% .....	142
Table 46 Yield Beam and Yield Frame Strains - Frame 3 1.0% .....	142
Table 47 Steel Strain at Limit States- Frame 3 1.0%.....	143
Table 48 Concrete Strain at Limit States - Frame 3 1.0% .....	143
Table 49 Seismic Hysteretic Energy at Limit States (KJ) - Frame 3 1.0% .....	143
Table 50 Yield Beam and Yield Frame Strain - Frame 3 1.5% .....	144
Table 51 Steel Strain at Limit States - Frame 3 1.5%.....	144
Table 52 Concrete Strain at Limit States - Frame 3 1.5% .....	144
Table 53 Seismic Hysteretic Energy at Limit States (KJ) - Frame 3 1.5% .....	145
Table 54 Yield Beam and Yield Frame Strains - Frame 3 2.0% .....	145
Table 55 Steel Strain at Limit States - Frame 3 2.0%.....	145
Table 56 Concrete Strain at Limit States - Frame 3 2.0% .....	146
Table 57 Seismic Hysteretic Energy at Limit States (KJ) - Frame 3 2.0% .....	146
Table 58 Yield Beam and Yield Frame Strains - Frame 4 1.0% .....	146
Table 59 Steel Strain at Limit States - Frame 4 1.0%.....	147
Table 60 Concrete Strain at Limit States - Frame 4 1.0% .....	147
Table 61 Seismic Hysteretic Energy at Limit States (KJ) - Frame 4 1.0% .....	147

Table 62 Yield Beam and Yield Frame Strains - Frame 4 1.5% .....	148
Table 63 Steel Strain at Limit States - Frame 4 1.5% .....	148
Table 64 Concrete Strain at Limit States - Frame 4 1.5% .....	148
Table 65 Seismic Hysteretic Energy at Limit States (KJ) - Frame 4 1.5% .....	149
Table 66 Yield Beam and Yield Frame Strains - Frame 4 2.0% .....	149
Table 67 Steel Strain at Limit States - Frame 4 2.0% .....	149
Table 68 Concrete Strain at Limit States - Frame 4 2.0% .....	150
Table 69 Seismic Hysteretic Energy at Limit States (KJ) - Frame 4 2.0% .....	150
Table 70 Yield Beam and Yield Frame Strains - Frame 4 2.5% .....	150
Table 71 Steel Strain at Limit States - Frame 4 2.5% .....	151
Table 72 Concrete Strain at Limit States - Frame 4 2.5% .....	151
Table 73 Seismic Hysteretic Energy at Limit States (KJ) - Frame 4 2.5% .....	151

## LIST OF FIGURES

Figure 1 Performance Objectives for Buildings (SEAOC,1995).....	5
Figure 2 Geometry and Dimensions for Frames 1, 2 and 3 .....	11
Figure 3 Geometry and Dimensions for Frame 4 .....	12
Figure 4 Column Section for all Frames.....	12
Figure 5 Beam's Sections for all Frames .....	13
Figure 6 General Dimensions of 3D Model (15thWCEE Blind Test Challenge Report, 2012)...	15
Figure 7 Beam And Column Section for 3D Frame (15thWCEE Blind Test Challenge Report, 2012).....	15
Figure 8 Position of the Masses on the Slab (15thWCEE Blind Test Challenge Report, 2012)..	16
Figure 9 Fiber Element Modeling (Adapted From Opensees (Mc. Kenna Et Al., 2000)).....	17
Figure 10 Stress vs. Strain for Concrete01 Material (Kent And Park, 1971; Karsan-Jirsan 1969) .....	18
Figure 11 Stress vs. Strain for <i>Reinforcing Steel</i> Material (Mohle And Kunnath, 2006).....	19
Figure 12 Beam with Hinges Element (Scott And Fenves, 2006).....	20
Figure 13 Element Distribution For 2D RC Frames.....	20
Figure 14 Element Distribution For 3D RC Frame .....	21
Figure 15 Moment-Curvature Relation for Beams .....	23
Figure 16 Moment-Curvature Relation for Beam (Cont.) .....	24
Figure 17 Moment-Curvature Relation for Beams (Cont.).....	25
Figure 18 Moment-Curvature Relation for Columns.....	26
Figure 19 Acceleration Time History for the Seven Earthquakes .....	30
Figure 20 Ground Motion Accelerations (Longitudinal Direction).....	32
Figure 21 Ground Motion Acceleration for all Stages (Longitudinal Direction) .....	32
Figure 22 Ground Motion Acceleration (Transversal Direction) .....	33
Figure 23 Ground Motion Acceleration for all Stages (Transversal Direction) .....	33
Figure 24 Response Spectrum with Target Design Spectra for all Earthquakes .....	34
Figure 25 Design Spectra for 3D Frame Ground Motion .....	35
Figure 26 Mass Discretization for the 2D RC Frames.....	36
Figure 27 Mass Discretization for the 3D Frame.....	37

Figure 28 Position of Nodes A and B in 3D Frame (15th WCEE Blind Test Challenge Test Report, 2012).....	38
Figure 29 Displacement Time Histories for Node A in the 3D Frame.....	39
Figure 30 Displacement Time Histories for Node B in the 3D Frame.....	40
Figure 31 Arias Intensity (Ground Motions for the 2D Frames).....	42
Figure 32 Arias Intensity (Ground Motions for the 3D Frame).....	42
Figure 33 Cumulative Absolute Velocity (Ground Motions for the 2D Frames).....	43
Figure 34 Cumulative Absolute Velocity (Ground Motions for the 3D Frame).....	44
Figure 35 Specific Energy Density (Ground Motions for the 2D Frames).....	45
Figure 36 Specific Energy Density (Ground Motions for the 3D Frame).....	46
Figure 37 Drift in the 2D Frames.....	48
Figure 38 Drift in the 3D Frame.....	49
Figure 39 Drift vs. PGA - Frame 1.....	52
Figure 40 Drift vs. PGA - Frame 2.....	53
Figure 41 Drift vs. PGA - Frame 3.....	54
Figure 42 Drift vs. PGA - Frame 4.....	55
Figure 43 Drift vs. PGA.....	56
Figure 44 Drift vs. PGA.....	58
Figure 45 Positions of Steel and Concrete Strain Points.....	59
Figure 46 Steel Strain vs. PGA - Frame 1.....	60
Figure 47 Steel Strain vs. PGA - Frame 2.....	61
Figure 48 Steel Strain vs. PGA - Frame 3.....	62
Figure 49 Steel Strain vs. PGA - Frame 4.....	63
Figure 50 Concrete Strain vs. PGA - Frame 1.....	64
Figure 51 Concrete Strain vs. PGA - Frame 2.....	65
Figure 52 Concrete Strain vs. PGA - Frame 3.....	66
Figure 53 Concrete Strain vs. PGA - Frame 4.....	67
Figure 54 Steel Strain vs. Drift - Frame 1.....	70
Figure 55 Steel Strain vs. Drift - Frame 2.....	71
Figure 56 Steel Strain vs. Drift - Frame 3.....	72
Figure 57 Steel Strain vs. Drift - Frame 4.....	73

Figure 58 Concrete Strain vs. Drift - Frame 1 .....	74
Figure 59 Concrete Strain vs. Drift - Frame 2 .....	75
Figure 60 Concrete Strain vs. Drift - Frame 3 .....	76
Figure 61 Concrete Strain vs. Drift - Frame 4 .....	77
Figure 62 Strain vs. PGA (Beam And Girder).....	79
Figure 63 Strain vs. PGA (Columns).....	80
Figure 64 Strain vs. Drift .....	81
Figure 65 Steel Strain vs. Drift (Columns) .....	82
Figure 66 Concrete Strain vs. Drift (Columns).....	83
Figure 67 Seismic Hysteretic Energy vs. Drift - Frame 1.....	85
Figure 68 Seismic Hysteretic Energy vs. Drift - Frame 2.....	86
Figure 69 Seismic Hysteretic Energy vs. Drift - Frame 3.....	87
Figure 70 Seismic Hysteretic Energy vs. Drift - Frame 4.....	88
Figure 71 Seismic Hysteretic Energy vs. PGA - Frame 1 .....	89
Figure 72 Seismic Hysteretic Energy vs. PGA - Frame 2 .....	90
Figure 73 Seismic Hysteretic Energy vs. PGA - Frame 3 .....	91
Figure 74 Seismic Hysteretic Energy vs. PGA - Frame 4 .....	92
Figure 75 Seismic Hysteretic Energy vs. Ductility - Frame 1 .....	93
Figure 76 Seismic Hysteretic Energy vs. Ductility - Frame 2 .....	94
Figure 77 Seismic Hysteretic Energy vs. Ductility - Frame 3 .....	95
Figure 78 Seismic Hysteretic Energy vs. Ductility - Frame 4 .....	96
Figure 79 Concrete Strain vs. Aspect Ratio (0.85%).....	101
Figure 80 Concrete Strain vs. Aspect Ratio (1.0%).....	102
Figure 81 Concrete Strain vs. Aspect Ratio (1.5%).....	102
Figure 82 Concrete Strain vs. Aspect Ratio (2.0%).....	103
Figure 83 Steel Strain vs. Aspect Ratio (0.85%) .....	103
Figure 84 Steel Strain vs. Aspect Ratio (1.0%) .....	104
Figure 85 Steel Strain vs. Aspect Ratio (1.5%) .....	104
Figure 86 Steel Strain vs. Aspect Ratio (2.0%) .....	105
Figure 87 Steel Strain vs. Drift For 1.0% Of Steel Reinforcement Ratio.....	108
Figure 88 Hysteretic Energy Plots - Frame 1.....	121

Figure 89 Hysteretic Energy Plots - Frame 1 (Cont.) .....	122
Figure 90 Hysteretic Energy Plots - Frame 2.....	123
Figure 91 Hysteretic Energy Plots - Frame 2 (Cont.) .....	124
Figure 92 Hysteretic Energy Plots - Frame 3.....	125
Figure 93 Hysteretic Energy Plots - Frame 3 (Cont.) .....	126
Figure 94 Hysteretic Energy Plots - Frame 4.....	127
Figure 95 Hysteretic Energy Plots - Frame 4 (Cont.) .....	128

# **CHAPTER 1: Introduction and Literature Review**

## **1.1 SCOPE**

This study presents a research plan that will significantly advance our understanding about the seismic behavior of RC moment frame buildings under several damage or performance limit states. This will be accomplished by: (1) nonlinear time history analyses (NLTHA) of RC planar moment frames with different aspect ratios and longitudinal reinforcement ratios subjected to several scaled seismic ground motions; (2) nonlinear time history analyses of a 3D RC frame tested as part of the 15<sup>th</sup> WCEE (World Conference on Earthquake Engineering – 2012); and (3) detailed studies of the results obtained from the NLTHA focusing on the evaluation of material strains, drifts and energy dissipation changes at different performance limit states. The detailed objectives are described next.

## **1.2 RESEARCH OBJECTIVES AND SIGNIFICANCE**

In order to implement rapid assessment methods based on the concepts of performance-based seismic engineering for different damage limit states for structural systems like RC moment frames, it is crucial to have a clear understanding of how the energy dissipation is affected as different levels of inelastic demand are imposed to the structure during a seismic event. Also, it is necessary to study in detail how these parameters are linked to the material strains (concrete and steel reinforcement) to clearly identify the level of damage at both, member and system levels. The specific objectives of this research are the following: (1) to evaluate changes in energy dissipation capacity as function of ductility or different performance levels, material strains and geometric characteristics for RC moment frames, (2) to study in detail the

seismic response of RC moment frames at different damage limit states established in the ASCE 41-06 (2007) rehabilitation code, (3) to put forward recommendations about limits states that can be used to improve the seismic assessment of RC frames.

### **1.3 BACKGROUND AND MOTIVATION**

Buildings are subjected to gravity and lateral loads. The most critical lateral loads considered in the design are wind pressures and seismic ground motions. Among the structural systems, shear walls and bracings sometimes in combination with moment resisting frames (dual systems), are used to resist seismic forces or wind loads. This research was focused on the behavior of RC moment resistant frames subjected to several seismic ground motions. This type of system is composed of columns and beams, and the floor system is composed of RC slabs. Frames have the capacity to carry gravity loads and resist lateral forces on any direction. The use of frames maximizes the space distribution on buildings and makes it more efficient (Paulay and Priestley, 1992).

Moment resisting frames are often used in seismic zones due to its capacity for energy dissipation and deformation. There are three types of moment resisting frames: ordinary moment resisting concrete frames (OMRCF), intermediate moment resisting concrete frames (IMRCF) and special moment resisting concrete frames (SMRCF). The selection of the type of moment frame depends on the classification of the seismic zones. For seismic zones with low and moderate classification, the OMRCF and IMRCF are the most commonly used. For high seismic zones the SMRCF provides superior ductility and energy dissipation capacity (Wan Han and Jee, 2005).

Recent earthquakes damages (e.g., 2010 Mw 8.8 Chile, 2009 Mw 6.3 Italy, and 2011 Mw 9.0 Japan) and life losses make us to continue improving and searching for new and better ways to design or rehabilitate structures. The USGS Earthquake Hazard program indicated that 374,092 structures were destroyed by the 2010 Chile earthquake and tsunami, and 10,000 buildings were destroyed by the 2009 Italy earthquake in the L'Aquila area. For the 2011 Japan earthquake and tsunami more than 1 million buildings were damaged (Tanaka and Shigekawa, 2012). These events showed the vulnerability of existing RC buildings and the need to change or improve the existing seismic design guidelines. Design and rehabilitation codes are constantly changing due to earthquake events which helps to better understand the seismic performance of buildings and to produce better designs methods to reduce earthquake losses. Several of these documents were developed based on concepts of performance based seismic engineering (PBSE). The earlier documents (ATC-40, 1996; FEMA 273/274, 1997 and FEMA 356, 2000) focused on the retrofitting of existing buildings, but more recent documents (ATC 58-2, 2004; FEMA 445, 2006) are focused on expanding the efforts to new construction. PBSE concepts have been the subject of discussion since the early 1970's and have evolved as an option for better designs.

### ***1.3.1 Performance Based Design- Current and Past Efforts***

On February, 1971 the San Fernando Valley experienced a very damaging earthquake, 6.6 magnitude ground motion with approximately 60 seconds of duration. This earthquake took away 65 lives, more than 2,000 persons were injured and left property damages of about \$505 million dollars. Two hospitals and other emergency facilities exhibited structural damages causing that injured people were unable to have access to medical services. As a consequence of the infrastructure damage, the reconstruction and recovery process of the city was more

complicated (Hamburger, 2003). Due to this event, US engineers began to collect information about the seismic performance of the structures and started conceptualizing the performance based seismic design (PBSD) in the United States (Hamburger, 2004).

The damage observed during the Northridge earthquake of 1994 again opened questions about the seismic performance of structures. The PBSD resurged and captured again the attention of the government agencies as an answer to better designs (Hamburger, 2004). The Federal Emergency Management Agency (FEMA) created an association with the Applied Technology Council (ATC), the Building Seismic Safety Council and the American Society of Civil Engineers (ASCE), to develop seismic rehabilitation guidelines for existing buildings and other performance-based related guidelines. Their efforts initially produced the FEMA 273 report, which later became the Seismic Evaluation report (ASCE 31, 2003) and Seismic Rehabilitation report (ASCE 41, 2007). Both reports use the PBSD concepts for the design and evaluation of existing structures.

The Structural Engineering Association of California (SEAOC), ATC and FEMA were responsible for proposing methods for the implementation of the PBSD. On 1995, the SEAOC defined the goal of the PBSD as to “develop design methodologies that produce structures of predictable and intended seismic performance under stated levels of seismic hazards” (ATC 40, 1996). This is accomplished by the definition of performance objectives that are selected by the owner and engineer prior to the design. SEAOC (1995) defined three main objectives which depend on the importance of the structure such as: Basic Safety Objective (BSO), Enhanced Objective 1 (EO1), and Enhanced Objective 2 (EO2). The document Vision 2000 (SEAOC, 1995) introduced some engineering response parameters to consider during the assessment (drift,

stress, plastic hinge rotation angle, acceleration, and others) and limits for a particular performance objective.

These criteria were for the most part based on consensus, rather than on test data or quantitative field observation (Whitaker et al., 2007). Figure 1 shows the performance objectives described in SEAOC (1995). They divided the performance levels into structural (SP) and non-structural (NP) levels. These definitions can vary according to the different PBSD guidelines available in the literature.

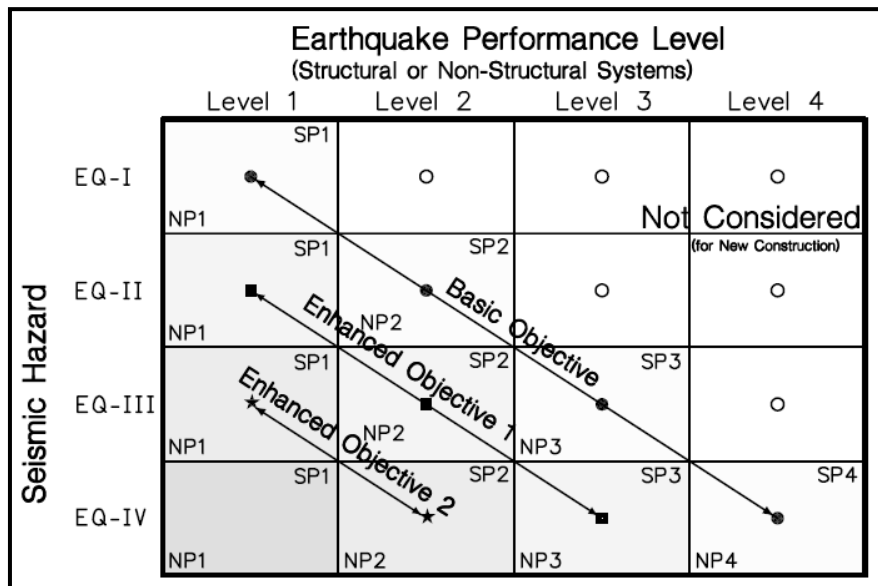


**Figure 1** Performance objectives for buildings (SEAOC,1995)

Furthermore, ASCE 41-06 defines the four performance categories as Operational (OP), Immediate Occupancy (IO), Life Safety (LS) and Collapse Prevention (CP). Depending on the use of the structure, the owner can choose the performance level they want for the structure. The Operational level maintains the structure capable to function during and after the event with some minor cracks on non-structural elements. Non-structural components remain operational. In the Immediate Occupancy level, the structure has minor cracks on non-structural elements but

the service systems can be affected. At these levels, the structure does not present permanent drifts and remains with the original strength and stiffness (ASCE 41-06).

In the life safety (LS) occupancy level, the structure has a residual stiffness and strength in all stories, with permanent drift and no out-of-plane failure of walls. Also, non-structural component and partitions could exhibit some damages. Finally, in the collapse prevention (CP) level, the structures have a minimal stiffness and strength in all stories, but columns and walls remain working. At this stage, non-structural components are damaged and the building is near to collapse (ASCE 41-06).

Moreover, the report ATC 40 (1996) specified that PBSB is “the methodology in which structural criteria are expressed in terms of achieving a performance objective” (ATC 40, 1996). Also they stated that the main difference between the PBSB and the Force Based Design (FBD) is that on the FBD the structural criterion is limited on member forces by a prescribed level of applied shear force (ATC 40, 1996). FEMA 273 (1997) established that PBSB is composed “of methods and design criteria to achieve several different levels and ranges of seismic performance”.

Ghobarah (2001) defined the PBSB as a “general design philosophy in which the design criteria are expressed in terms of achieving stated performance objectives when the structure is subjected to stated levels of seismic hazard”. Ghobarah also stated that the performance targets may be a level of stress, load, displacement, limit state or a damage state that cannot be exceeded.

Hamburger (2003) identified various shortcomings with the first PBSB methodologies. The first deficiency was a lack between the calculated demands and component performance. This was caused by the use of static and linear methods to calculate the engineering demands.

The second deficiency was the definition of the relation between the engineering demands and the calculated performance. It was based on the engineering judgment or calculated using analytical models. Hamburger (2003) stated that this relationship needs to be established by approaches based on relevant data in order to produce reliable information (ATC-58, 2004). The third point was based on the performance of the structure; he said that on the PBSB the structural performance was obtained by the component performance. It was taken as the worst performance of any component of the structure, and not as an entire behavior of the structure (ATC-58, 2004).

Based on these deficiencies the FEMA and ATC organizations began in 2001 to work on the ATC-58 project. This project developed guidelines for design and upgrade of new and existing buildings. This new concept is called the Next Generation Performance Based Design (NGPBD). Hamburger (2004) established that these guidelines allow the design to have a more reliable performance than those produced by other codes. With this method, the performance of the structure would be shown in terms of the risk of earthquake induced losses. These categories are financial losses, earthquake-induced life losses and lost use of facilities. Financial losses include the cost of the repair and replacement of the damages structures; earthquake-induced life losses consist of the dead and seriously injured people; and the lost use of facilities include the downtime associated with the repair, replacement or restoration to service (Hamburger, 2004).

One of the disadvantages of the current PBSB is that it does not provide guidelines to determine how to select the desired performance level for the structure. Using the NGPBD, the designer has all the necessary tools to make a better decision selecting the appropriate performance level (Hamburger, 2004). But unfortunately, as stated by Hamburger (2007), the

inexperience and lack of knowledge on how to use the NGPBD causes a lack of confidence in users and still needs improvement.

**In summary, there are several shortcomings to existing performance based or displacement based assessment procedures:** (1) the drifts levels suggested in several codes or documents (e.g., FEMA 356, 2000; ASCE 41-06, 2007; Vision 2000,1995) are stipulated for a type of system and ductile detailing, (2) drifts relationships should be based on geometric characteristics (e.g., length aspect ratios) and other parameters (e.g., stiffness degradation) and not only on system type, (3) the effects of energy dissipation have not been clearly evaluated in the development of damage levels used in performance-based assessment procedures. These limitations motivated this research. The methodology is described in detail next.

## **CHAPTER 2: Methodology and Modeling Considerations**

### **2.1. INTRODUCTION**

This chapter describes the models of the 2D frames and the 3D frame, from the dimensions to the materials used. The geometry and reinforcement characteristics of the beams and columns sections are presented. The modeling of these frames is described in detail as well all the materials used in the analyses. The program OpenSees (McKenna et al., 2000) was used to perform all the analysis. In addition, the program CUMBIA (Montejo and Kowalsky, 2007) was used to perform a moment-curvature analyses to check the beam and column capacities of the frames.

### **2.2. MODELS GENERALITIES**

A total of 16 RC plane frames and one 3D RC frame were designed and analyzed using the Open System for Earthquake Engineering Simulation (OpenSees). OpenSees (McKenna et al., 2000) is a DOS system developed by the University of California, Berkeley with the support of the National Science Foundation (NSF) and the Pacific Earthquake Engineering Research (PEER). It is an open platform software that allows earthquake engineering researchers and engineers to improve existing models or create new ones. The frames were designed using the ASCE 7-05 and ACI 318-05 design codes. For the design, it was assumed that the structure is located in a place with a soil classification type D.

In this research, sixteen different designs of RC frames were used, with two bays and four stories. Four beam aspect ratios are used and for each one four different longitudinal reinforcement ratios were specified. The values of aspect ratio (L/H) vary from 7.5 to 12. For the first three aspect ratios (7.5, 9 and 10), the percentage of reinforcement steel ratios are

0.85%, 1%, 1.5% and 2%, and for  $L/H=12$  the reinforcement ratios were 1%, 1.5%, 2% and 2.5%. The aspect ratios varied for the frames since they can have a significant effect on the frame drifts and performance limit states. There is no rule or guide that specifies what values can be used. Sener et al. (2002) used a value for  $L/H$  of 5 to verify and calibrate the size effect on concrete beams with and without steel fibers. Wang and Shi (2012) used values of 2.5, 10 and 20 for cantilevered beams with uniform load and 5, 10 and 20 for clamped-clamped beam with concentrated force at the midspan. Wang and Shi (2012) used these values to study the effects of the boundary layer solutions on the deflections, shear forces and stresses using analytical methods (sixth order differential equilibrium equations) on clamped end beams.

With this information, values of aspect ratios ( $L/H$ ) in the range of 6 to 16 are used in this study. In order to obtain more practical beam height values, the beam length was fixed for the first three  $L/H$  values. For the last value of  $L/H$ , another beam length was used to obtain a more common beam height size. The variation in aspect ratio permits to study their impact in the damage levels for frames with varied geometrical characteristics.

## **2.3. MODEL GEOMETRY AND DIMENSIONS**

### ***2.3.1 2D Frame***

The models were composed of columns with height of 3.05 m (10'), for a total structural height of 12.2 m (40'). Figure 2 shows the frame configuration and dimensions for frames with  $L/H$  of 7.5, 9 and 10. The value of beam length for these frames was fixed to 4.57 m (15'). For  $L/H=12$  the beam's length was 6.1 m (20'). Figure 3 shows the frame model for the frame with  $L/H=12$ . The height of the beam was changed maintaining the beam length fixed for each aspect ratio. The beam section heights for frame 1 ( $L/H=7.5$ ) was 609.6 mm (24"). For frame 2

(L/H=9) and frame 4 (L/H=12) was 508 mm (20”) and for frame 3 (L/H=10) was 457.2 mm (18”). All beams have a width of 304.88 mm (12”) and slab thickness of 152.44 mm (6”). The slab was used only for the mass distribution; one half of the mass slab in each side of the frame was assigned to the beams. All columns sections have dimensions of 609.76 mm (24”) x 609.76 mm (24”), but the size of the steel reinforcement varies for certain frames. Frame 1 with  $\rho=2\%$  has column section 3. Meanwhile, frames 1 with  $\rho=1.5\%$ , frame 2  $\rho=2\%$  and frame 4 with  $\rho=2\%$  and 2.5% have column section 2 and all other frame cases have column section 1. This modification in steel reinforcement was performed to achieve the weak beam strong column behavior. Figures 4 and 5 illustrate the column design and beam sections for all frames, respectively.

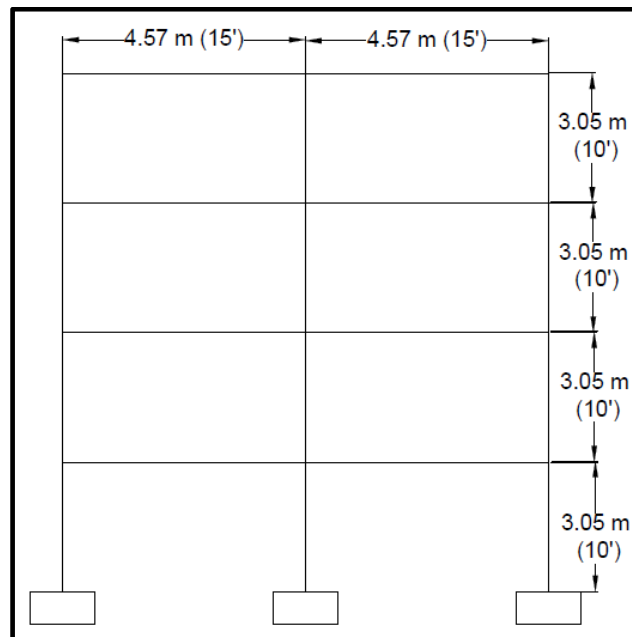


**Figure 2** Geometry and Dimensions for frames 1, 2 and 3

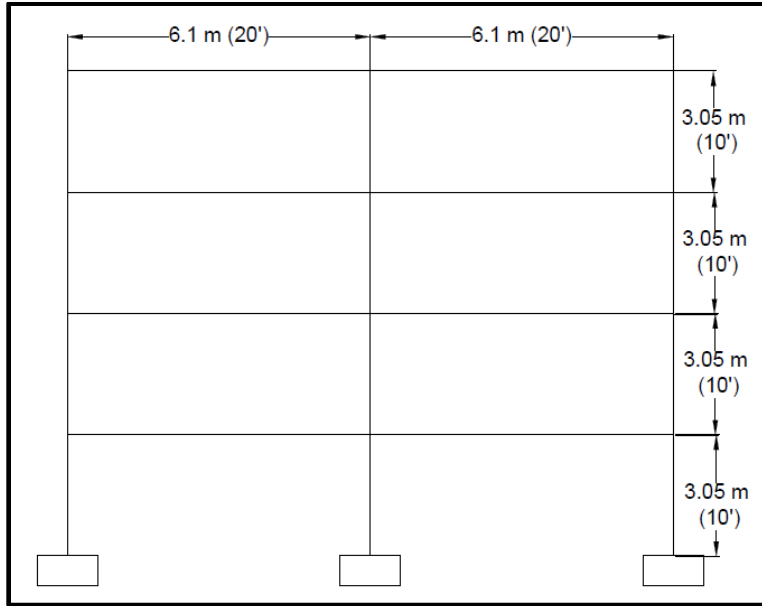


**Figure 3** Geometry and Dimensions for frame 4

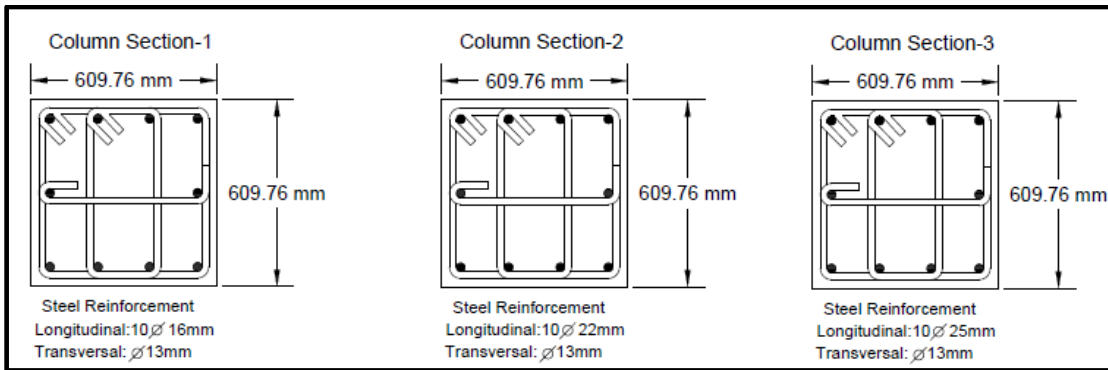


**Figure 4** Column section for all frames

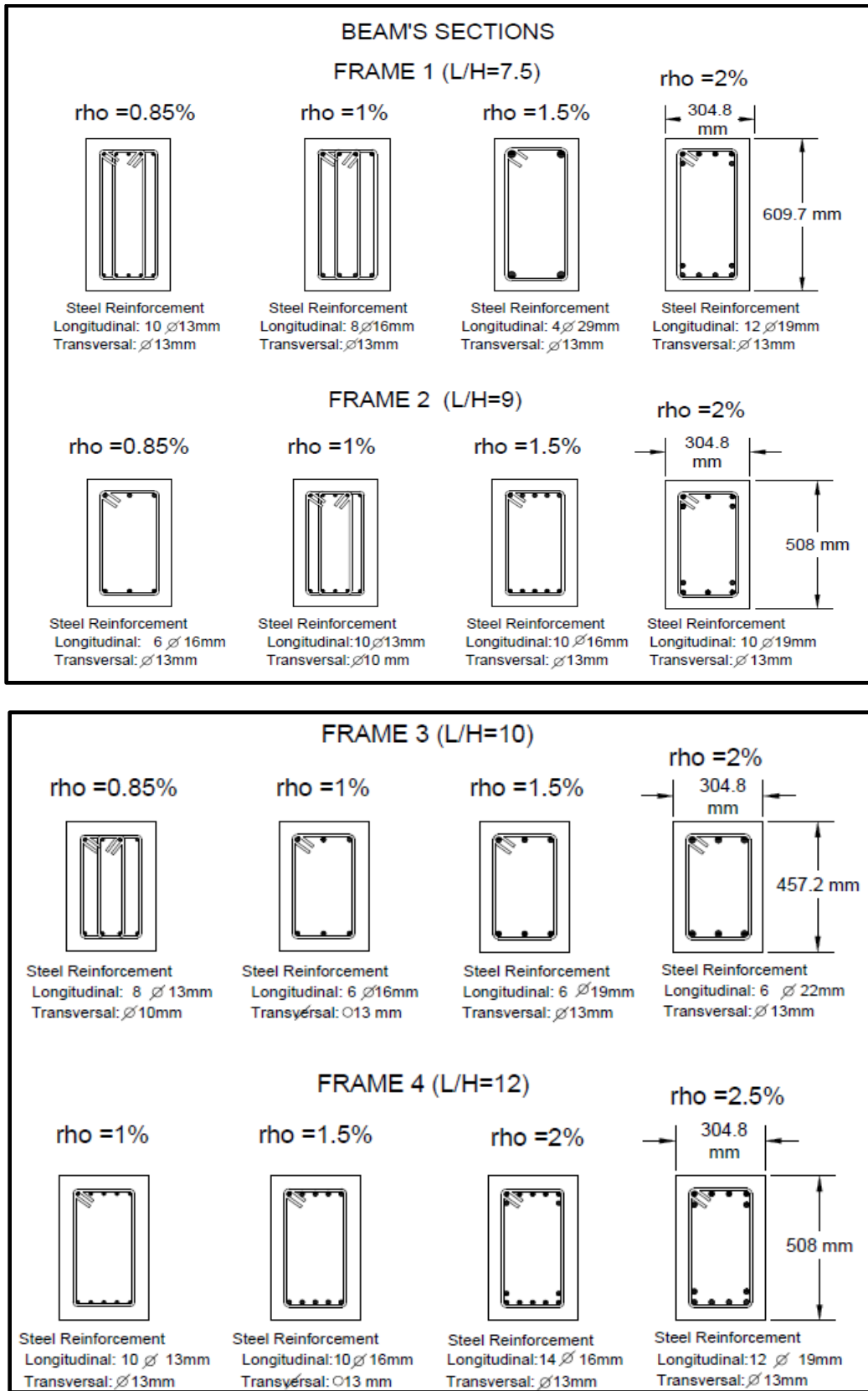


**Figure 5** Beam's sections for all frames

### ***2.3.2 2D Frame Design***

During the design stage of the 2D frame models, the program ETABS was used to obtain the design moment and shears diagrams. For this purpose, the live load was taken from the ASCE 7-05 using the residential building classification. The value used was  $1.92 \text{ KN/m}^2$  ( $40 \text{ lb/ft}^2$ ), and the dead load was obtained from the weight of the frame. For the superimposed dead load (partitions) a value of  $0.708 \text{ KN/m}^2$  ( $15 \text{ psf}$ ) was used. The seismic lateral force was determined using the equivalent lateral force procedure described in the ASCE 7-05 code. In this method, the effective seismic weight of the structure and the seismic response coefficient was used to determine the seismic base shear. The lateral force was distributed vertically using the formulas described in ASCE 7-05, which use the base shear and a vertical distribution coefficient. The lateral force distribution is proportional to the displacements during a ground motion event, and to the floor masses and heights of the structure. For structures with periods less than 0.5 sec., assuming that the floor mass distribution is uniform and floors with equal height, the force distribution has a triangular shape varying from zero at the base to the maximum force at the top (ASCE 7-05). To obtain a better behavior of the structure, the seismic force per floor was equally distributed to each node in the same story.

### ***2.3.3 3D Frame***

A 3D frame was included in this research. The frame was composed of one story, one bay in each direction and slab until half the girder length, shown in Figure 6. The frame dimensions were: beam's length of 3.5m (11.48'), girder's length of 4 m (13.12') and columns of 3m (9.84') height. The beam's depth and width was 40 cm (15.75") and 20 cm (7.87"), respectively. The column dimensions were 20 cm (7.87") x 20 cm (7.87"). Figure 7 shows the beam and column sections for this model. The slab is extended 2 m (6.6') from one edge to the

girder's length. Nine additional masses of 1200 kg (2645.6 lb) each one was placed on this slab. Each mass was fixed to the slab using 4 bolts, 8 steel plates, 8 washers and 8 nuts which represents an additional mass of 36 kg (79.4 lb). The location of the masses is shown in Figure 8. This frame was tested as part of the activities of the 15<sup>th</sup> World Conference on Earthquake Engineering (Lisbon, 2012).

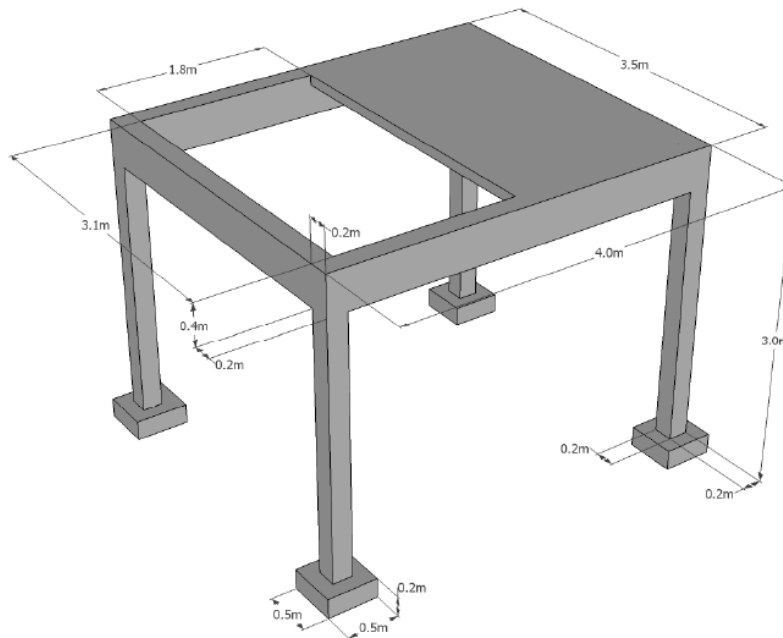


**Figure 6** General Dimensions of 3D model (15thWCEE Blind Test Challenge Report, 2012)

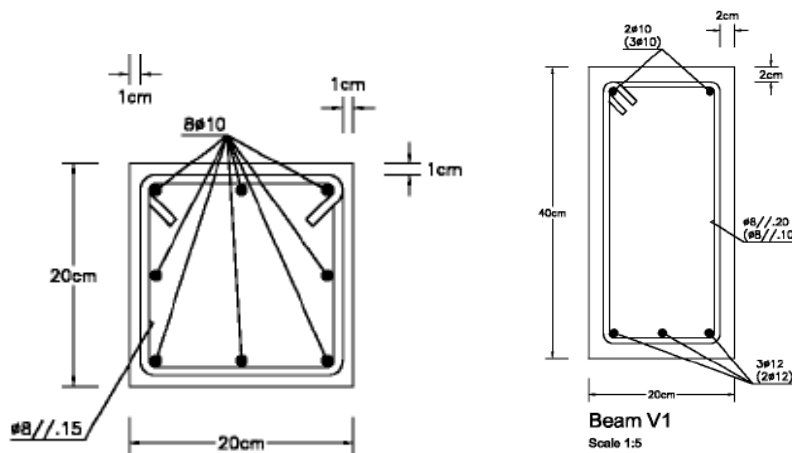


**Figure 7** Beam and Column section for 3D frame (15thWCEE Blind Test Challenge Report, 2012)

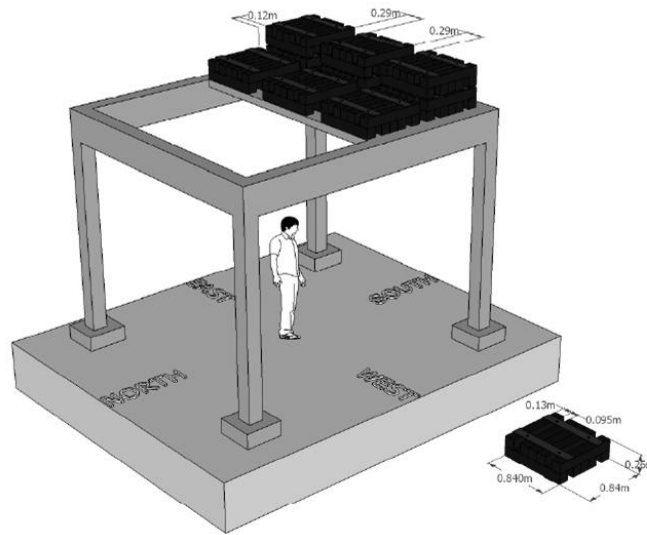


**Figure 8** Position of the masses on the slab (15thWCEE Blind Test Challenge Report, 2012)

For this model, the design and seismic data was provided by the 15<sup>th</sup> World Conference on Earthquake Engineering Blind Test Committee (2012). There were 4 seismic intensity levels, namely low, moderate, reference and high. The mass distribution was performed using the principle of the tributary masses, similar as for the 2D frames.

## 2.4. MODELING APPROACHES AND MATERIALS

The beams and columns sections were modeled using the fiber element approach. This approach consists of the division of each material that comprises the section into several fibers. In the case of a reinforced concrete section it is divided in unconfined, confined and steel fibers as shown in Figure 9. Adequate transversal steel reinforcement provides higher ductility levels and prevents buckling of the longitudinal steel reinforcement, restraining in combination with longitudinal steel reinforcement the lateral expansion of the concrete (Paulay and Priestley, 1992). Each fiber is assigned to a material which is represented by a stress-strain relationship.

The OpenSEES (McKenna et al., 2000) database has different types of concrete and steel materials. For this research the *Concrete01* material based on the concrete constitutive model of Kent and Park (1971) with modifications performed by Karsan and Jirsa (1969) was used. It is a uniaxial material with degraded linear unloading/reloading and no tensile strength. For the 2D frames the concrete compressive strength for all elements was 32 MPa (4.64 ksi) and for the 3D model the  $f'_c$  was 30.03 MPa (4.36 ksi) for the beams and 35.63 MPa (5.17 ksi) for the columns. Figure 10 shows an example of the Stress vs. Strain variation obtained using the Concrete01 material (Kent and Park, 1971; Kirsan and Jirsan, 1969).

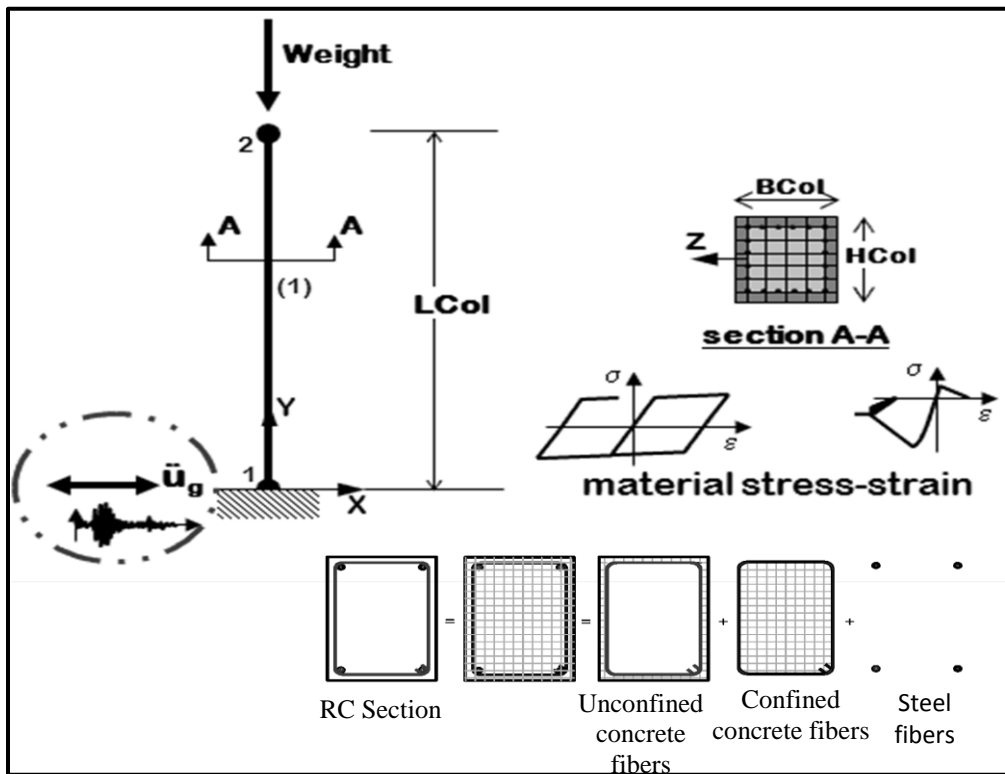


**Figure 9** Fiber Element Modeling (adapted from OpenSEES (Mc. Kenna et al., 2000))

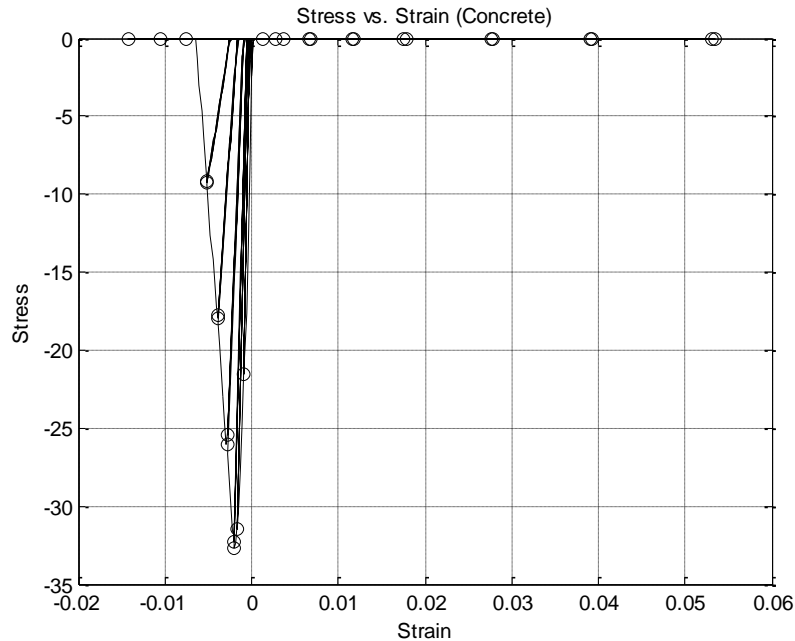


**Figure 10** Stress vs. Strain for Concrete01 material (Kent and Park, 1971; Karsan-Jirsan 1969)

The steel material used was the uniaxial *ReinforcingSteel* which is based on the work performed by Moehle and Kunnath (2006). The Moehle and Kunnath (2006) steel constitutive model is based on the steel model proposed by Chang and Mander (1994). For this material, Moehle and Kunnath (2006) used the Coffin-Manson equations for plastic strain amplitude to determine the fatigue parameters. Also they used a variation from the Gomes and Appleton (1997) and Dhakal and Maekawa (2002) research to incorporate buckling simulations. The steel yield stress used was 450 MPa (65.3 ksi) for all elements of the 2D frames and for 3D frame was 561.67 MPa (81.46 ksi), it was assumed that on 3D frame were used a conventional steel reinforcement. Figure 11 shows an example of the Stress and Strain relationship obtained with the *ReinforcingSteel* material from Moehle and Kunnath (2006). In order to obtain the concrete and steel data the frames were modeled using the OpenSEES program.

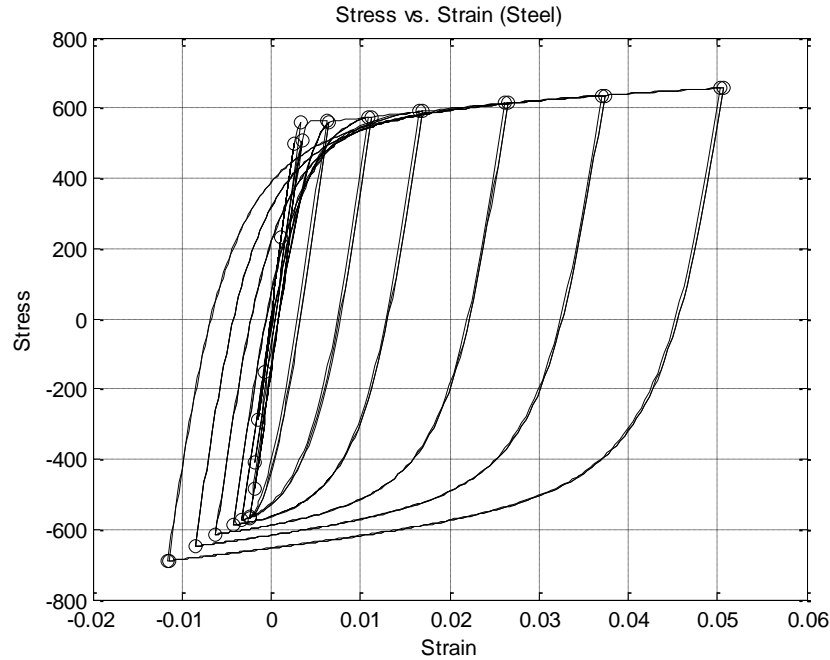


**Figure 11** Stress vs. Strain for *Reinforcing Steel* material (Moehle and Kunnath, 2006)

All 2D frames are divided in 57 elements, 20 of them were modeled using the beam with hinges (BWH) element (Scott and Fenves, 2006) of the OpenSEES program and the other 37 elements were modeled as elastic elements. The effect of the slab on the 2D frames was added as an additional mass to the frame. The 3D frame is divided into 32 elements, 12 of them were modeled using elastic elements and 20 using beam with hinges elements. On this frame the slab was modeled as a rigid diaphragm and his mass was also added to the frame. Figure 12 shows a model of a beam with hinges element. Figures 13 and 14 show the elements distribution for the 2D and 3D frame, respectively. These elastic elements were extended from each joint half of the beam or column height. This was done to obtain a better behavior of the beam-column joint by having a linear elastic section with the beam or column elastic stiffness (Priestley et al., 2007). By using beam with hinges, it was considered that the plasticity of the element is concentrated at a specified hinge length at the element ends. The plastic hinge length for each element was

calculated using equations 1.1-1.2, from the methodology presented by Priestley et al. (1996) as follows:

$$L_p = kL_c + L_{SP} \leq 2L_{SP} \quad (1.1)$$

$$L_{SP} = 0.022f_s d_{bl} ; f_s \leq f_y \quad (1.2)$$

$$k = 0.2 \frac{f_{su}}{f_y} - 1 \leq 0.08$$

where:

$L_p$  = equivalent plastic hinge length,

$L_{sp}$  = strain penetration length,

$L_c$  = length from the critical section to the point of contraflexure,

$f_s$  = tension stress in the longitudinal bars,

$f_y$  = longitudinal bars yielding stress, and

$d_{bl}$  = longitudinal bar diameter.

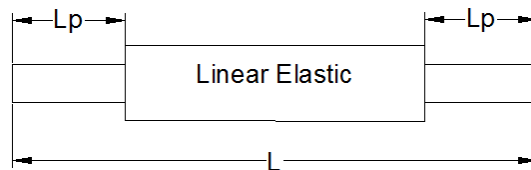


**Figure 12** Beam with Hinges element (Scott and Fenves, 2006)

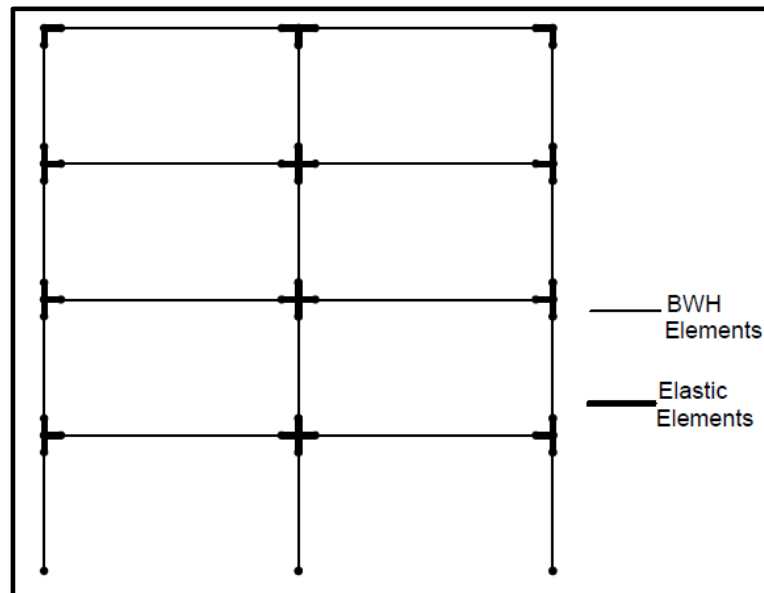


**Figure 13** Element distribution for 2D RC frames

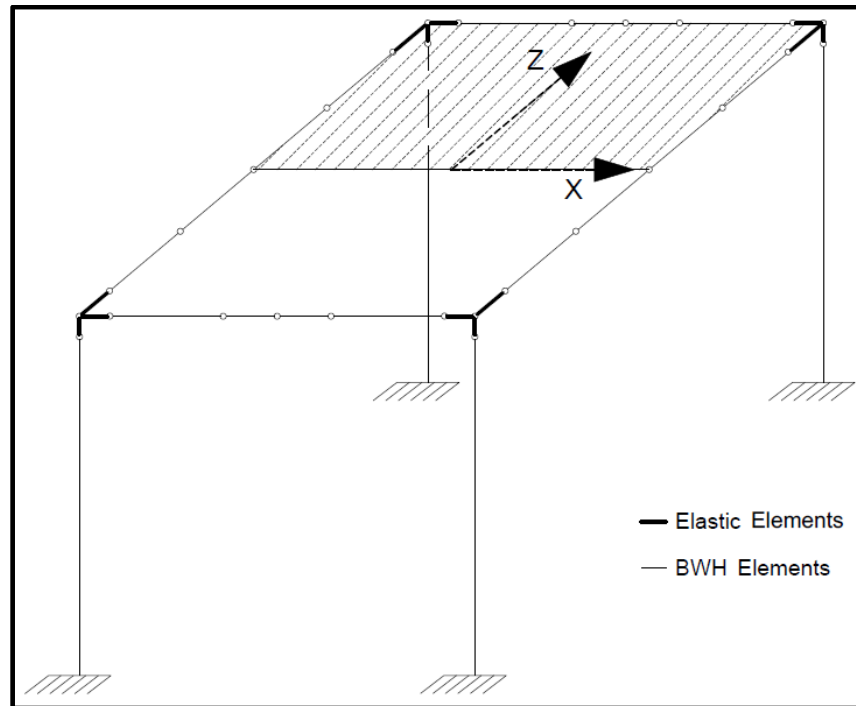


**Figure 14** Element distribution for 3D RC frame

## **2.5. BEAM AND COLUMNS CAPACITY- 2D FRAME**

The frame design was performed to satisfy the weak beam strong column mechanism. To ensure this mechanism, the summation of the beam flexural moment capacities in a frame joint have to be smaller than the summation of the nominal flexural moment capacities of the column framing in that joint. A factor of 6/5 has to be also applied to the summation of beam flexural capacities in the joint (ACI 318-05). The CUMBIA program (Montejo and Kowalsky, 2007) was used to obtain the flexural nominal capacity values. This program calculates the nominal moments from a moment-curvature analysis. From the analyses were obtained that more than one section for columns were needed. The results obtained are presented in Tables 1

and 2. Also the moment-curvature curves for each beam and columns are presented in Figures 15 to 18. The frame analyses performed are discussed in the next chapter.

**Table 1** Beam moment capacities obtained from CUMBIA

	CUMBIA			
FRAME 1	2*Mn (KN-m)	(6/5)*Mnb (KN-m)	2*Mn (Kip-ft)	(6/5)*Mnb (Kip-ft)
0.85	337.22	404.66	248.72	298.46
1	397.48	476.98	293.17	351.80
1.5	630.46	756.55	465.00	558.00
2	792.08	950.50	584.21	701.05
FRAME 2				
0.85	247.82	297.38	182.78	219.34
1	272.14	326.57	200.72	240.86
1.5	397.00	476.40	292.81	351.37
2	531.10	637.32	391.72	470.06
FRAME 3				
0.85	196.14	235.37	144.67	173.60
1	218.98	262.78	161.51	193.81
1.5	297.70	357.24	219.57	263.49
2	388.08	465.70	286.23	343.48
FRAME 4				
1	270.98	325.18	199.86	239.84
1.5	397.00	476.40	292.81	351.37
2	535.16	642.19	394.71	473.66
2.5	631.98	758.38	466.12	559.35

**Table 2** Column moment capacities obtained from CUMBIA

	CUMBIA			
	dbl (m)	2*Mn (KN-m)	dbl (ft)	2*Mn (Kip-ft)
COL 1	0.016	505.29	0.052	372.68
COL 2	0.022	944.2	0.072	696.41
COL 3	0.025	1209.06	0.082	891.76

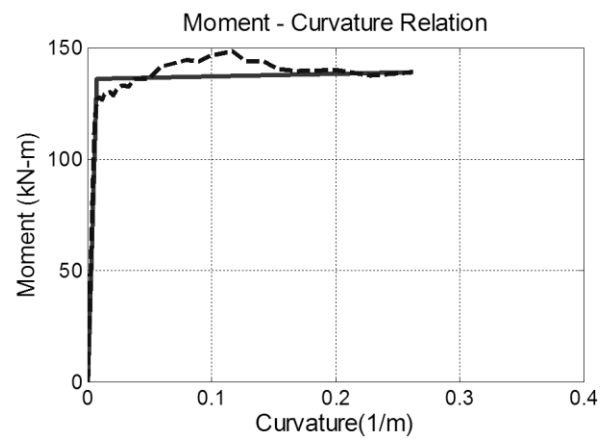
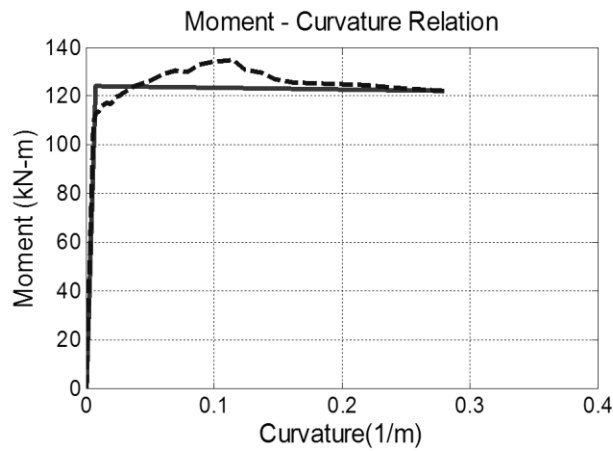
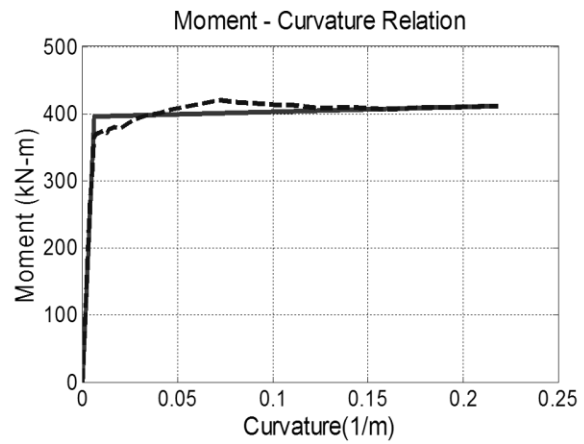
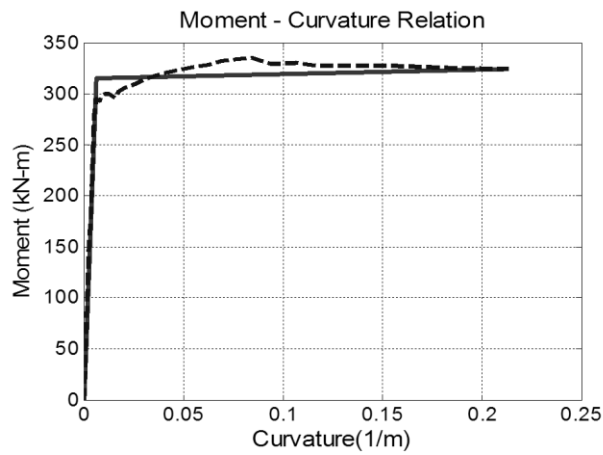
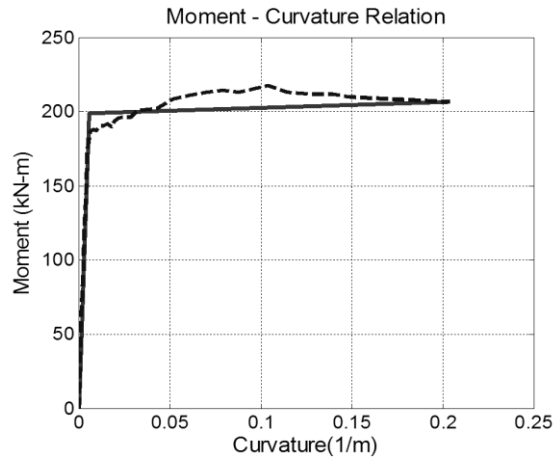
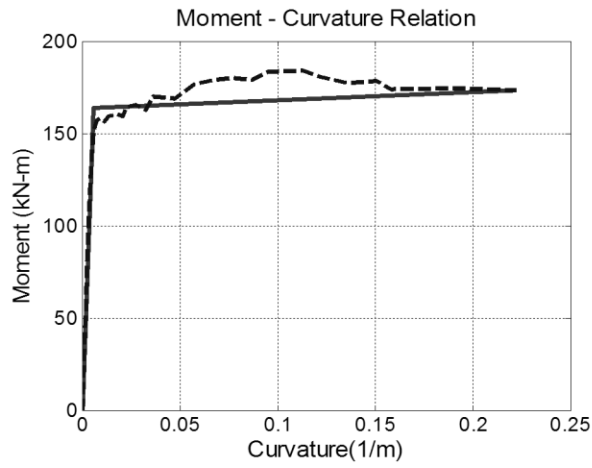


Figure 15 Moment-Curvature relation for beams

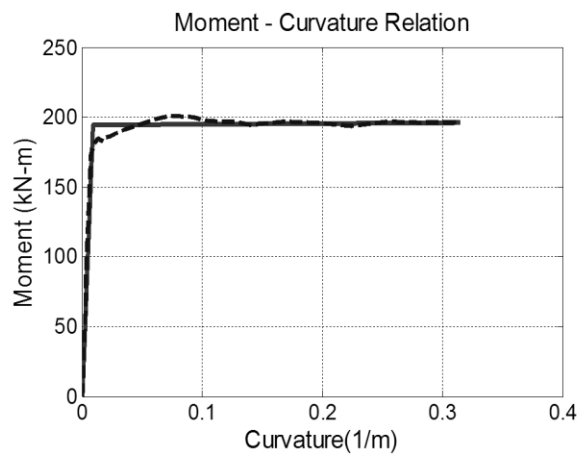
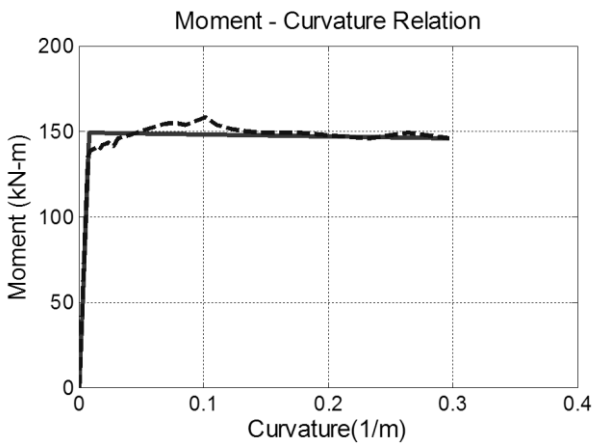
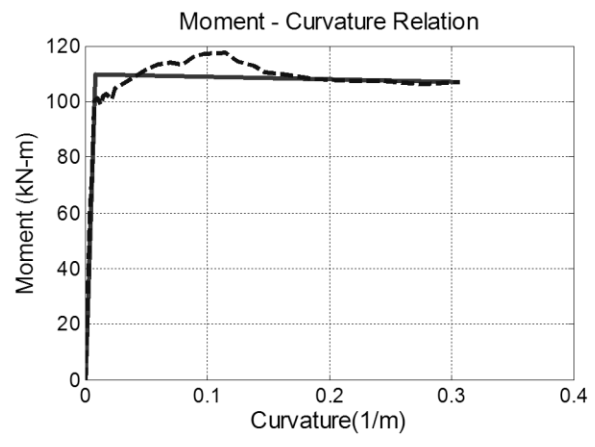
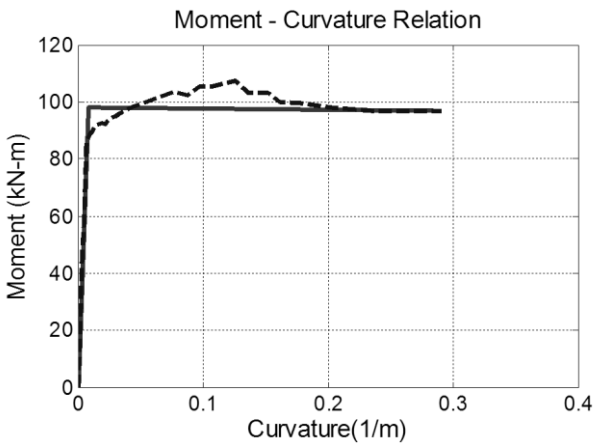
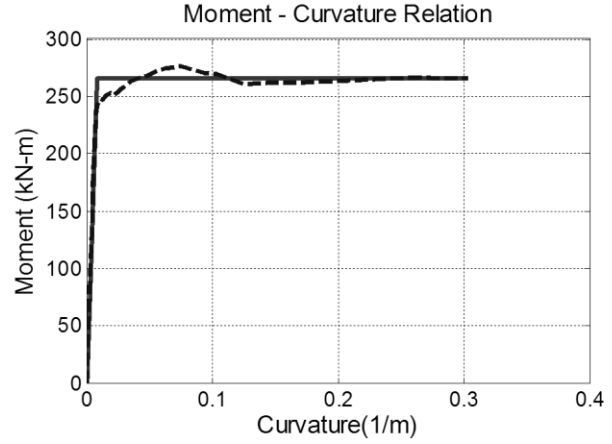
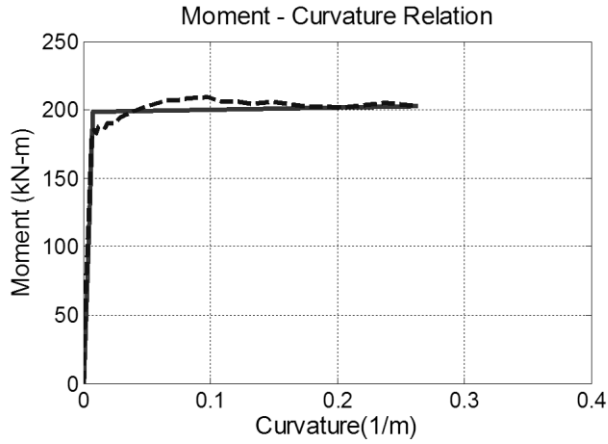
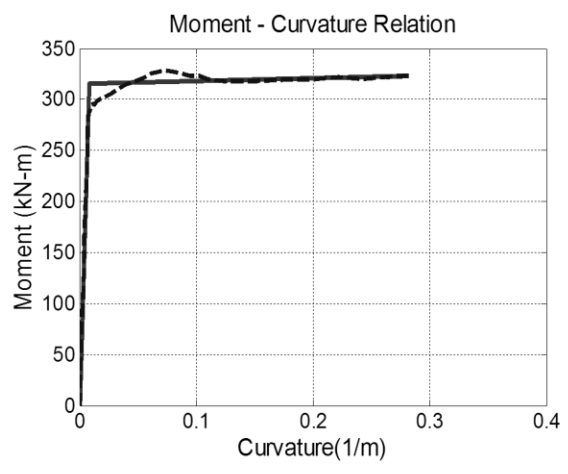
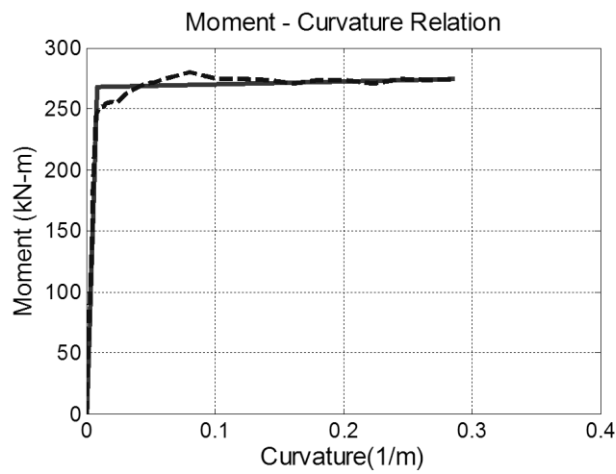
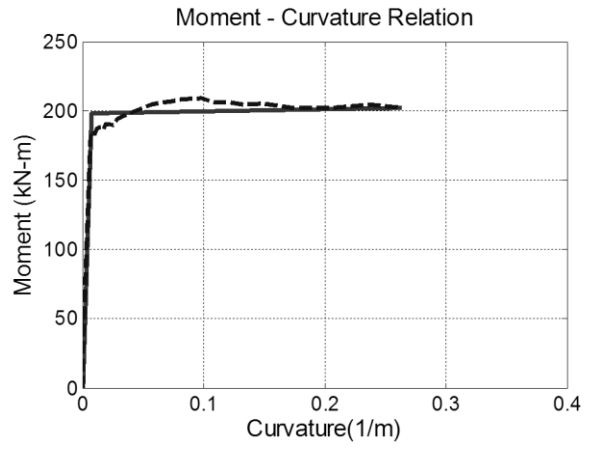
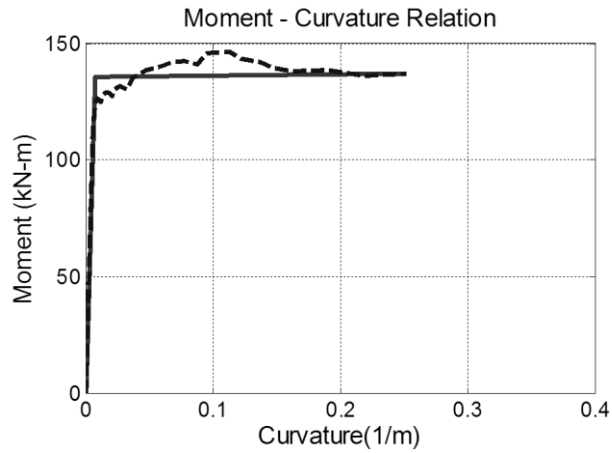
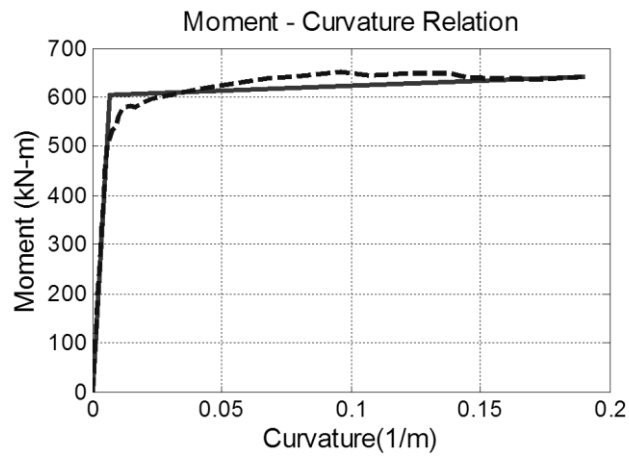
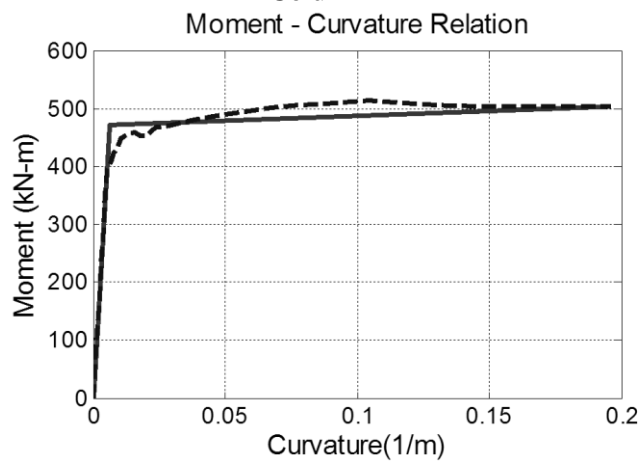
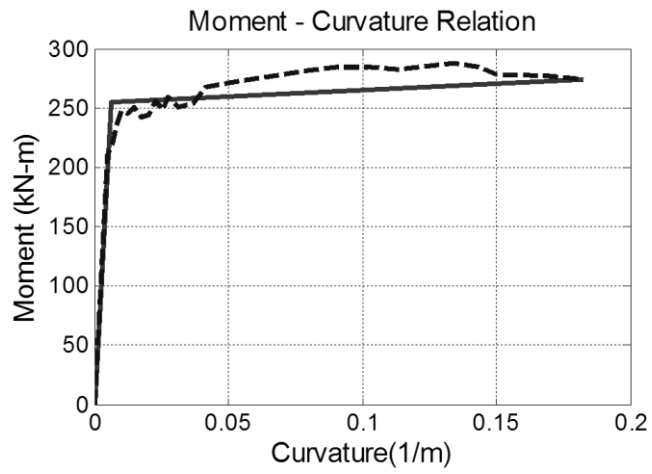


Figure 16 Moment-Curvature relation for beam (cont.)



**Figure 17** Moment-Curvature relation for beams (cont.)



**Figure 18** Moment-Curvature relation for columns

## **CHAPTER 3: Dynamic Analyses**

### **3.1. INTRODUCTION**

Dynamic analyses were performed for all the frames using OpenSEES. For the 2D frames seven earthquakes were chosen from the PEER database. For the 3D frame, a seismic ground motion scaled to four intensity levels was used, and was provided by the 15<sup>th</sup> WCEE blind test committee. The ground motions and generalities of the dynamic analyses are described next.

### **3.2. GROUND MOTIONS AND DYNAMIC ANALYSIS FOR THE 2D FRAMES**

From the PEER database seven earthquakes with magnitudes that varied from 6 to 8.5 were chosen. The earthquakes that were selected included the Imperial Valley (1979), Northridge (1994), Kobe (1995), Loma Prieta (1989), Tabas (1978), Kocaeli (1999) and the Chi-Chi (1999) earthquake. All earthquakes were scaled from 0.1g to 1.5g with increments of 0.1. The original seismic ground motions are shown in Figure 19. The criteria for the selection of these earthquakes were based on their impact to the society (economic and social) and structural damages within the specified magnitude range. The different earthquakes are described next.

#### ***3.2.1 Imperial Valley***

The Imperial Valley Earthquake with a 6.5 magnitude occurred in October 15, 1979 within the Mexico-California border. The USGS reported approximately 90 injured people and property damage estimated on around \$30 million. There were 1,565 houses and 440 commercial buildings with major structural damages. There were two houses and 11 commercial buildings destroyed. The most severe damage occurred on the Imperial County Services building

in “El Centro”. The structural system of this structure was composed of a six story reinforced concrete frame designed under the 1967 provisions of the California Uniform Building Code (USGS, 2013). During this event, the irrigation system of the Imperial Valley and the water system from the Colorado River to the Imperial Valley were damaged. This ground motion followed the same characteristics of the well known May 18, 1940 earthquake. USGS estimates the maximum lateral and vertical displacements as 55 cm and 19 cm respectively.

### ***3.2.2 Northridge***

The Northridge earthquake occurred in January 17, 1994 with a magnitude of 6.69 in California, USA. The Earthquake Hazard program of the USGS (2013) reports that approximately 57 people were dead; more than 7,000 were injured and 20,000 people were left homeless. They found more than 40,000 buildings with structural damages (at a \$20 billion cost). The most severe structural damages were observed on the Santa Monica, Antelope Valley, Simi Valley and Golden State freeway systems. The maximum soil uplift recorded by USGS was about 15 cm and caused liquefaction in some areas. As mentioned before, this earthquake encouraged scientists and engineers to continue improving seismic design.

### ***3.2.3 Kobe***

On January 16, 1995 occurred the Kobe earthquake in Japan with a magnitude of 6.9. This event caused 5,502 people killed and 36,896 people injured. Around 200,000 buildings had some structural damages or were destroyed. In the epicenter area occurred liquefaction and the service lines (gas) exploded causing some fires. The USGS estimates damages in \$100 billion dollars (USGS, 2013).

### ***3.2.4 Loma Prieta***

The Loma Prieta earthquake occurred in the Santa Cruz Mountains in California on October 18, 1989. It had a magnitude of 6.9, causing 63 people dead and 3,757 injured. The Earthquake Hazard program of the USGS (2013) reports that property damage was estimated on \$6 billion. The most severely affected area was on the San Francisco Marina District, Oakland and San Francisco in which houses and a reinforced concrete viaduct collapsed. Structural damages on bridges were observed; 10 presented severe structural damages, another 10 required temporary support and 80 displayed minor damages. Liquefaction was present and caused more damages to structures (USGS, 2013).

### ***3.2.5 Tabas, Iran***

The Tabas 7.35 magnitude earthquake occurred on September 16, 1978 in Iran. There were approximately 20,000 people dead. It was a three minutes event that caused damages on 40 villages. Approximately 15,000 houses and 30 underground water canals were destroyed (Berberian, 1979).

### ***3.2.6 Kocaeli***

On August 17,1999, the Kocaeli earthquake struck the western zone of Turkey, with a magnitude of 7.51 (USGS, 2013). The life losses were estimated on 13,479 and 27,164 people were injured. The buildings with structural damages were estimated on 54,295; from this number a total of 27,000 buildings collapsed or were demolished for their severe damage (Ansal et al., 1999).

### ***3.2.7 Chi-Chi***

The Chi-Chi earthquake with a magnitude of 7.62 occurred on September 21, 1999 in Taiwan, China. According to the *Event Report of Chi-Chi, Taiwan Earthquake Risk*

*Management Solutions* document (2000), approximately 2,400 persons died and more than 10,700 were injured. Over 14,700 buildings showed some structural damages, from this 8,500 were destroyed and 6,200 have severe damages. More than 100,000 people were left homeless, and economical losses were estimated in \$12 billion (USGS, 2013).

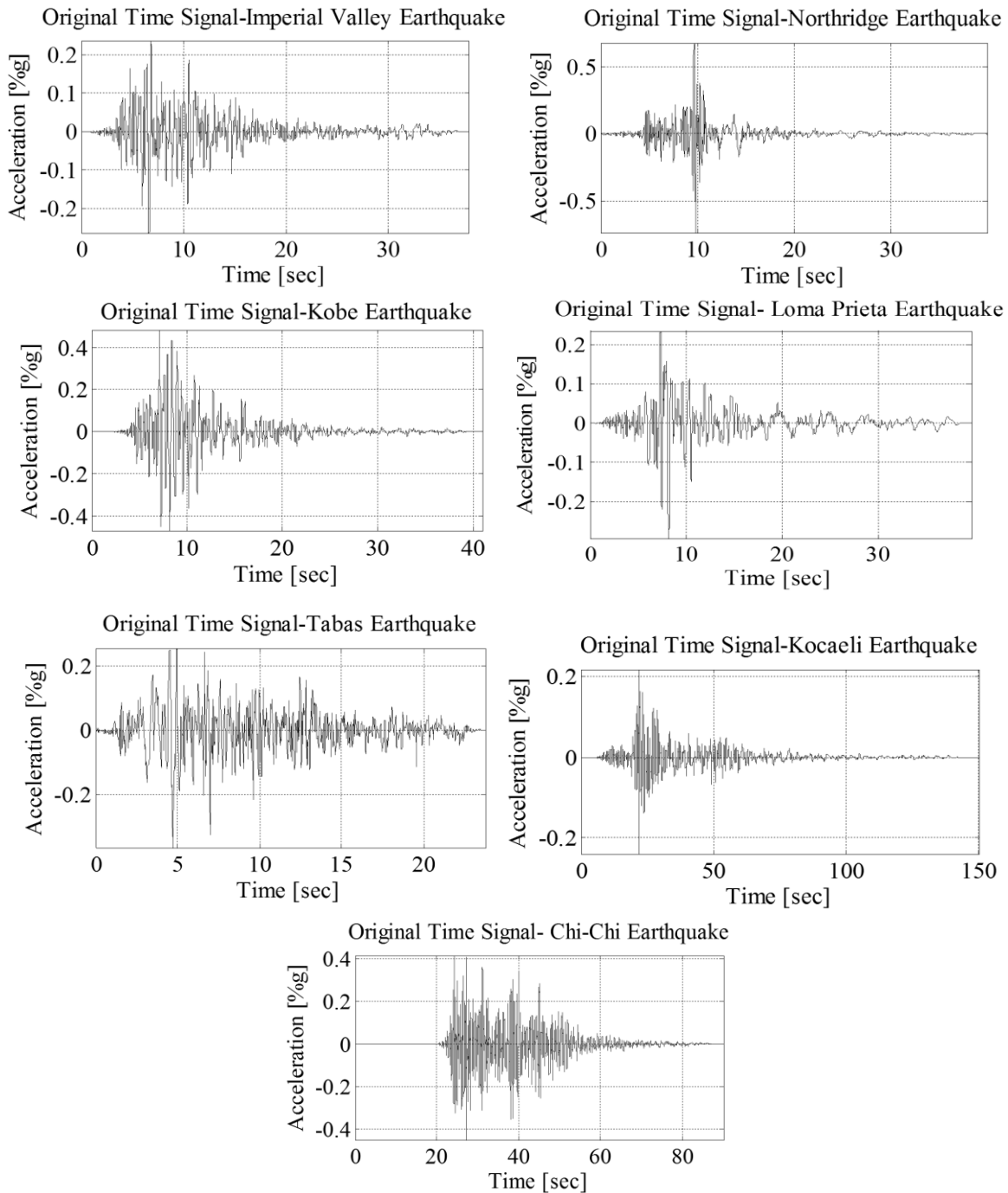


**Figure 19** Acceleration Time History for the seven earthquakes

### **3.3. GROUND MOTIONS AND DYNAMIC ANALYSIS FOR THE 3D FRAME**

Similar to the 2D frame, the dynamic analysis was performed using OpenSEES. The ground motion data was provided by the 15<sup>th</sup> World Conference of Earthquake Engineering (WCEE) Blind Test Committee. The frame was tested as part of a Blind Prediction Challenge Competition. They chose two horizontal orthogonal components of a strong motion signal registered during the Great East Japan earthquake and tsunami (15WCEE Blind Test Challenge Preliminary Test Report, 2012). The ground motions were applied into two components along the longitudinal and transversal direction (bidirectional analysis). The transversal direction is parallel to the beams (x axis in Fig. 14) and the longitudinal direction parallel to the girders (z axis). Figures 20 and 22 show the ground motions time histories in the longitudinal and transversal direction for each stage. The duration of the time signal selected is of 40.96 seconds with a Peak Ground Acceleration (PGA) of 0.265g and 0.254g in the transversal and longitudinal direction, respectively. This ground motion was scaled to four stages: low, medium, reference and high. The low and medium intensity levels correspond to a 20% and 70% of the original ground motion, respectively. The reference level is 100% of the original ground motion. The high intensity level corresponds to a 200% of the original ground motion (15WCEE Blind Test Challenge Preliminary Test Report, 2012).

The ground motions with the four intensity levels were applied simultaneously to simulate test conditions. During the test experiment, each ground motion was applied after the frame suffered damage from previous test. Around 15 seconds of zero ground motion were included between each intensity levels in order to assure that the structure comes to rest before the next ground motion was applied. Figures 21 and 23 shows the ground motions time histories with the zeros for the longitudinal and transversal direction, respectively.

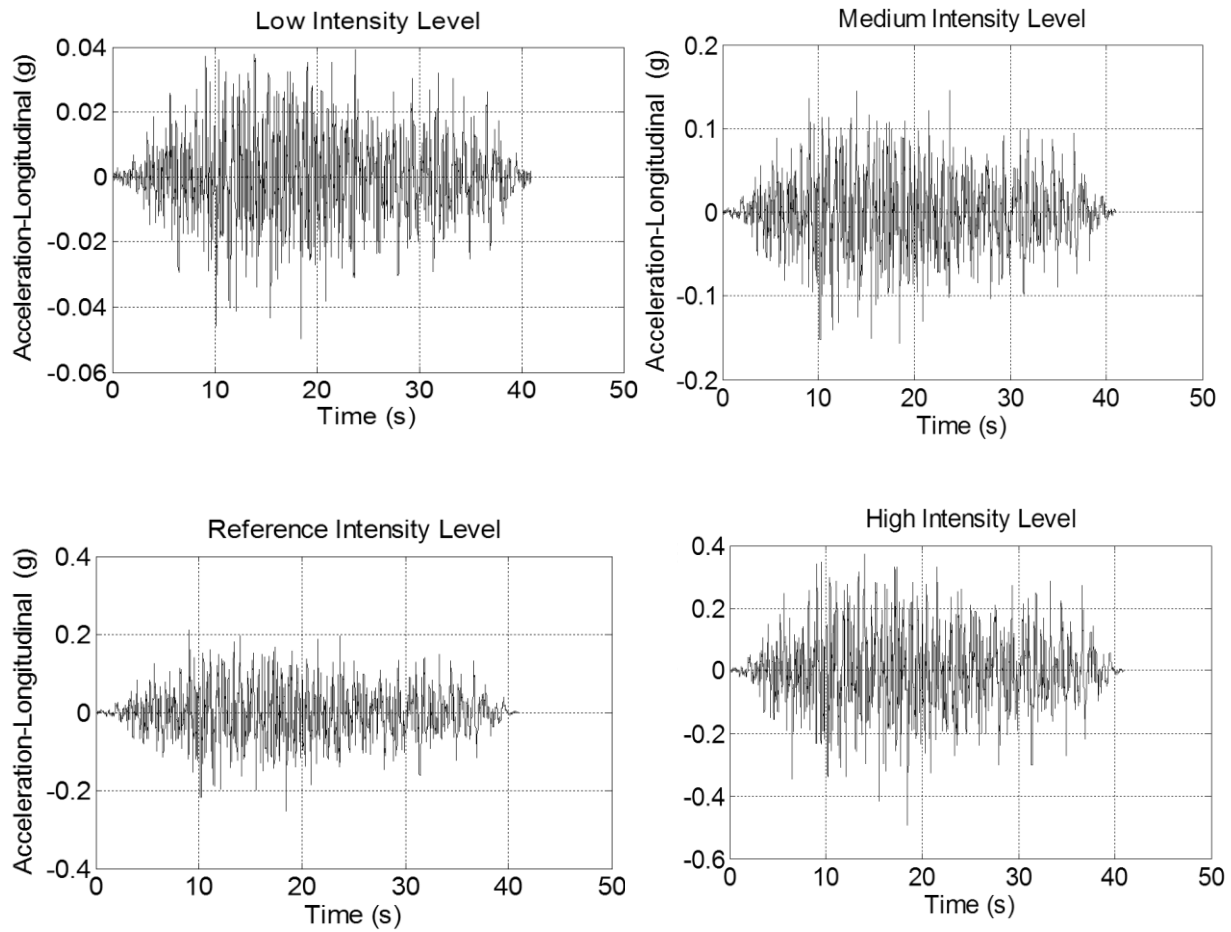


**Figure 20** Ground Motion Accelerations (Longitudinal direction)

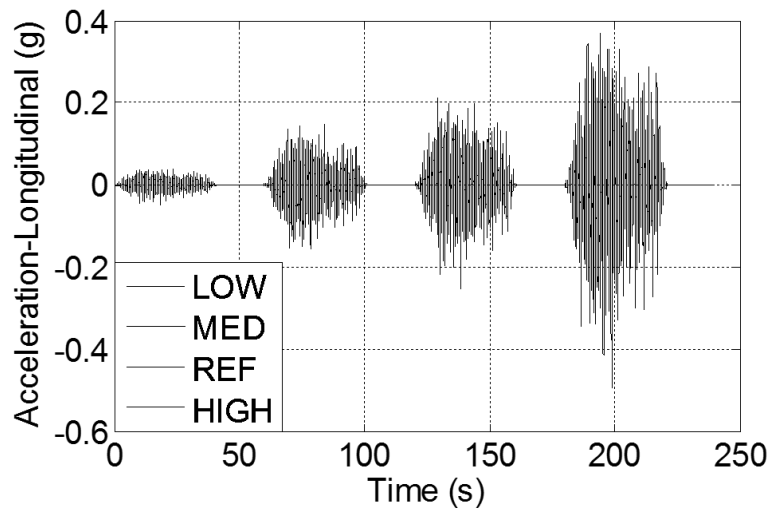


**Figure 21** Ground Motion Acceleration for all stages (Longitudinal direction)

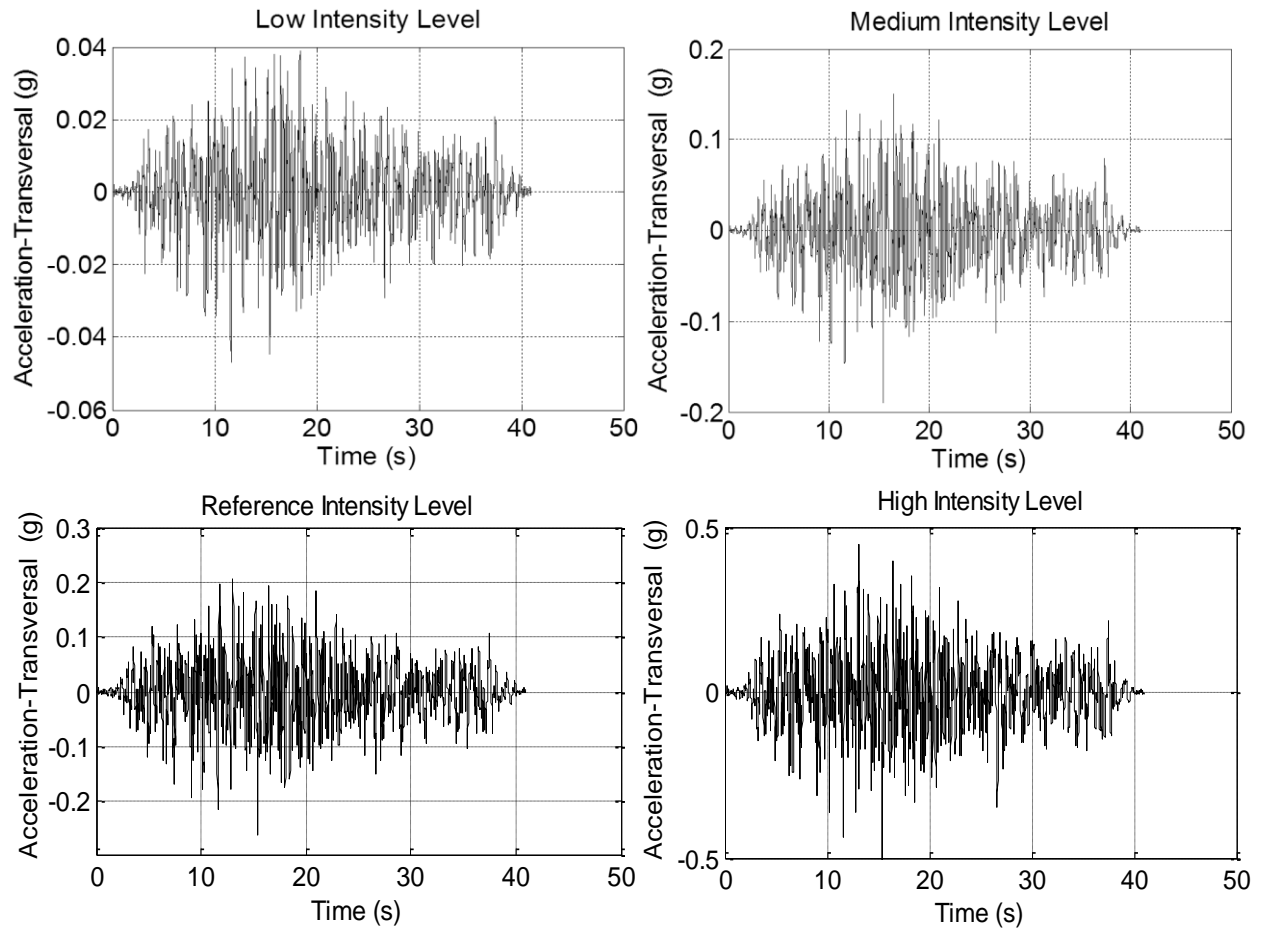


**Figure 22** Ground Motion Acceleration (Transversal direction)

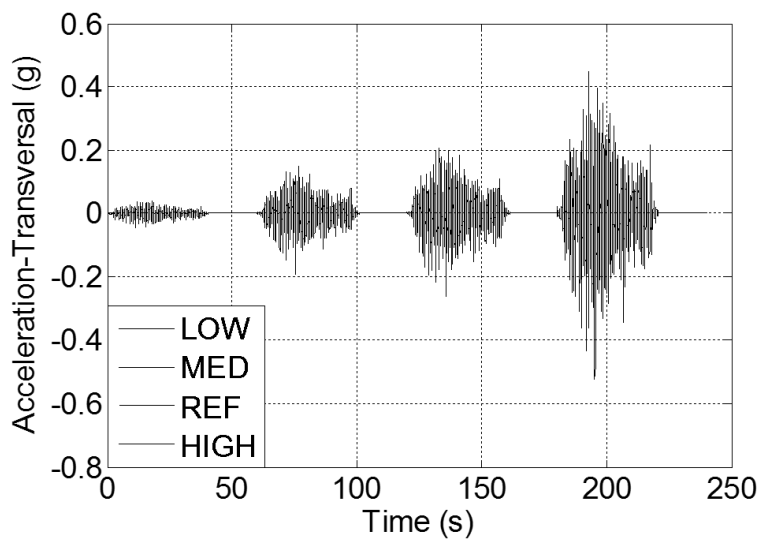


**Figure 23** Ground Motion Acceleration for all stages (Transversal direction)

### 3.4. COMPATIBLE EARTHQUAKE ACCELERATIONS AND RESPONSE SPECTRUM

#### 3.4.1 2D Frame

The original ground motion accelerations shown in Figure 19 were made it compatible with a design spectrum. Figure 24 shows the response spectra with the target design spectrum for all earthquakes. The values of the design spectral response acceleration parameter at short period ( $S_{DS}$ ), design spectral response acceleration parameter at 1 second ( $S_{D1}$ ) and the long period transition period ( $T_L$ ) for Mayagüez, Puerto Rico were obtained using the ASCE 7-05. The MATLAB<sup>®</sup> programs ArtifQuakeLet and AccelCorrect (Montejo-Valencia, 2004) were used to make the records compatible with the design spectrum as shown in Figure 24. The program ArtifQuakeLet uses wavelet theory to match the response spectrum of each earthquake to the design or target spectrum.

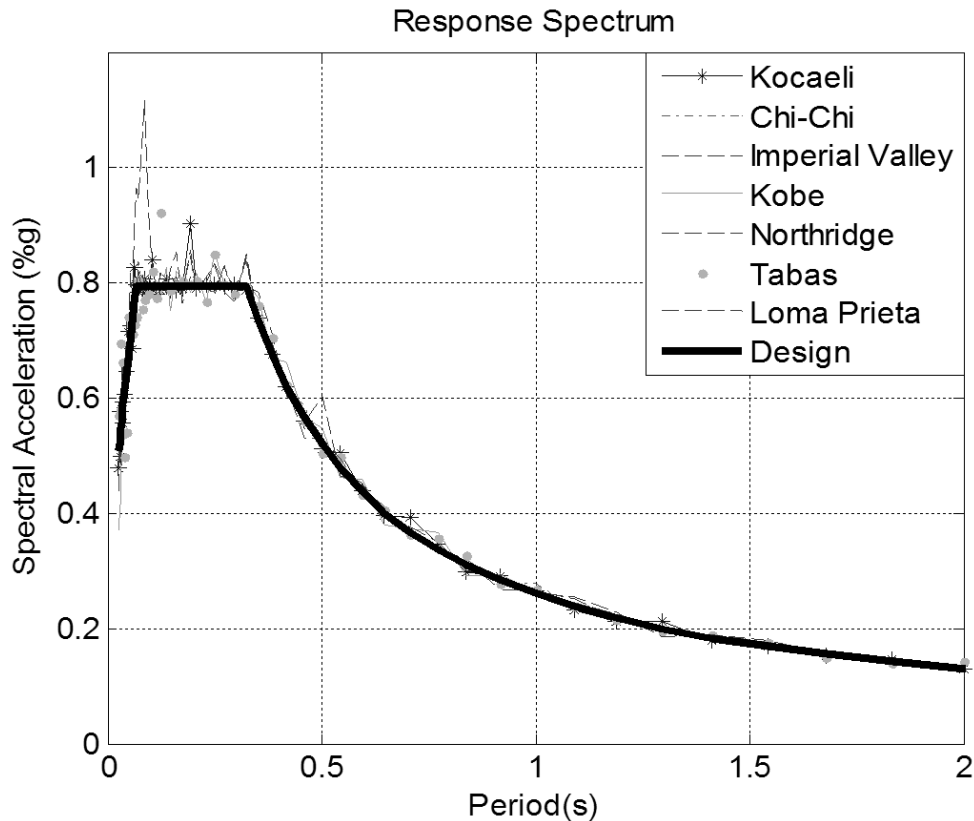


**Figure 24** Response Spectrum with Target Design Spectra for all earthquakes

### 3.4.2 3D Frame

As mentioned before the 3D frame was part of a blind prediction competition during the 15<sup>th</sup> WCEE, celebrated in Lisbon, Portugal (2012). The blind test challenge committee used the Eurocode (EC8) equations, that uses the reference peak ground acceleration ( $A_{GR}$ ), the lower ( $T_B$ ) and upper ( $T_C$ ) limit of the period of the constant spectral acceleration branch (Eurocode, 1998) and the beginning of the constant displacement response range of the spectrum ( $T_D$ ) to determine the elastic response spectrum to which the selected ground motion was made compatible. This spectrum is also dependent of the soil factor  $S$ , which describes the shape of the elastic response (Bisch et al., 2011). The  $T_B$ ,  $T_C$ ,  $T_D$ , and  $S$  values depend on the soil type. These parameters were provided by the 15<sup>th</sup> WCEE Blind Test Committee, and there are:  $A_{GR} = 1.5 \text{ m/s}^2$ ,  $S=1.3$ ,  $T_B=0.1\text{s}$ ,  $T_C=0.6\text{s}$  and  $T_D=2 \text{ s}$ . Using these values and the equations from the EC8 the design spectrum shown in Figure 25 was obtained.

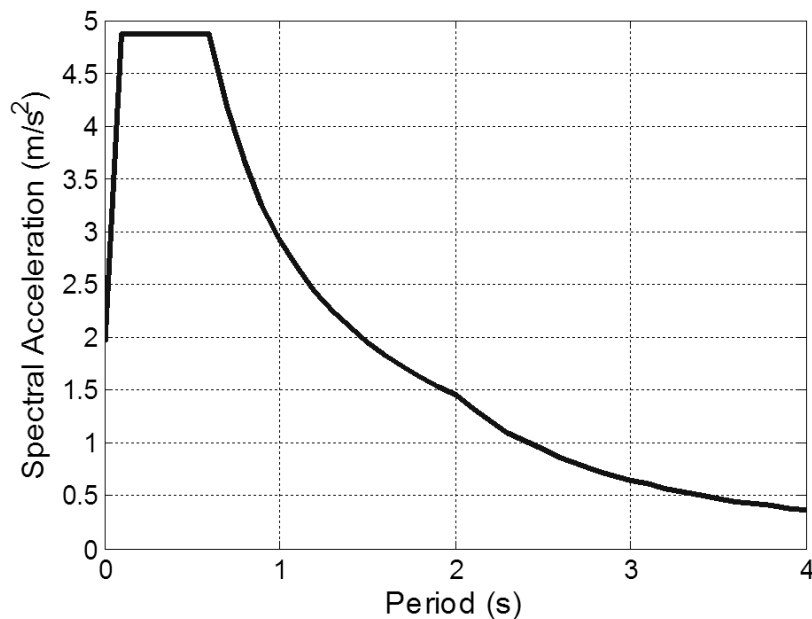


**Figure 25** Design Spectra for 3D frame ground motion

### 3.5. DYNAMIC ANALYSES CONSIDERATIONS

#### 3.5.1 2D Frames

For the dynamic analyses the masses were concentrated at the nodes connecting the columns and beams. Half of the masses of each element that is connected at the same joint were assigned to each node as shown in Figure 26 (principle of tributary masses). As stated by Priestley et al. (2007), this type of discretization provides realistic values for seismic axial forces. The effect of damping was also considered in the dynamic analysis. The damping is responsible for the reduction in dynamic building response due to energy dissipation of structural and nonstructural components of the building, its foundation, and the underlying soil/rock materials. In general, is composed of an elastic and hysteretic part (due to energy absorbed during the inelastic response). The damping ratio ( $\xi$ ) typically used in analyses of structures without artificial dampers can varied from 0.02 to 0.10 (Chopra, 1995). A value of damping ratio of 2% was used in this research since in fiber-element modeling the hysteretic rules used for the materials model the nonlinearity in the elastic range. Therefore, lower values of damping ratios are needed in the nonlinear time history analyses (Priestley et al., 2007).

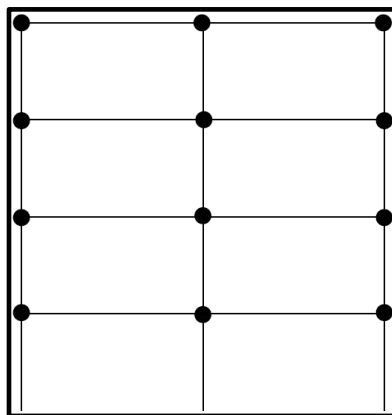


**Figure 26** Mass discretization for the 2D RC frames

### 3.5.2 3D Frame

For the 3D frame the beams and girders were divided several times in order to obtain a better behavior of the structure and to accommodate changes in reinforcing steel along the beams and girders (the reinforcement content was shown in Chapter 2). As shown in Figure 27, the mass discretization was performed using the same principle of the 2D frames (tributary masses). The beams were divided into three equal lengths, and then additional mass nodes were located at the sides of the elastic elements, concentrating the masses into 6 nodes for each beam. In the girders, a similar procedure was performed, now with an additional node located at the middle of the girders. As mentioned before (Chapter 2), additional masses were placed above the slab of the Lab model; therefore 67% of these masses were distributed in the nodes located at the beam connected with the slab. The remaining 33% of the masses were equally distributed into the nodes located at the half of the girders, which connects the slab with the girders.

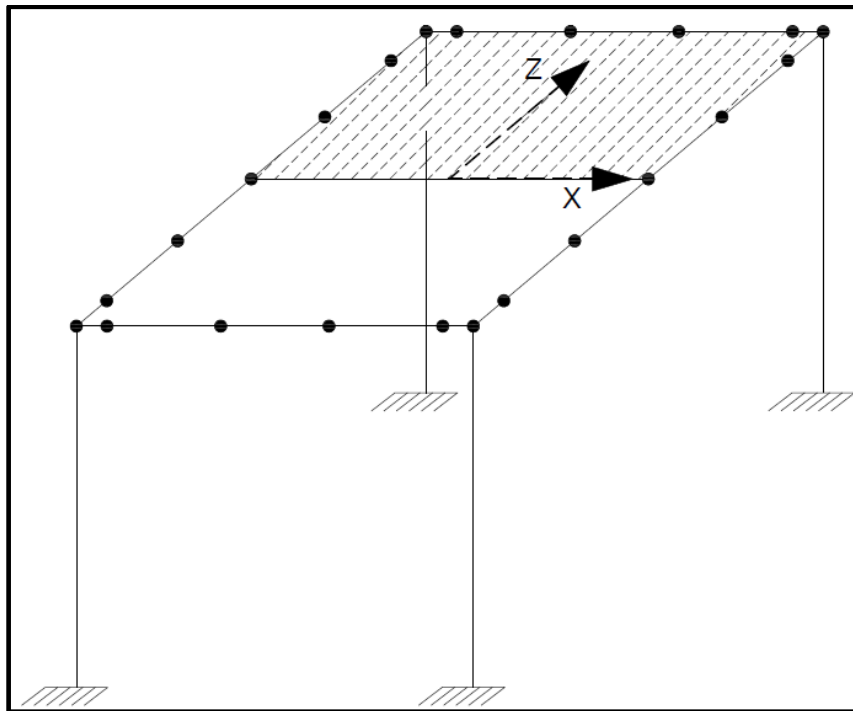


**Figure 27** Mass discretization for the 3D frame

### 3.5.3. 3D Frame Model Validation

The displacement results for nodes A and B, illustrated in Figure 28, obtained from the shaking table were provided by the test committee. This information was used to compare with the results obtained from the OpenSEES model. Figures 29 and 30 illustrate the displacement time histories for each node in x and y direction, predicted by OpenSEES and the experimental values.

Both nodes in the two directions have almost the same behavior for all earthquake intensities. For the medium and reference ground motions the values obtained from the OpenSEES model are compatible with the results obtained from the challenge. In the high intensity level the difference between each case are more visible. The low intensity level is the one with the greater differences between the OpenSEES and challenge results. In general, the results obtained from the OpenSEES model are a good representation of the real behavior of a structure. Further calibration of the model is recommended to improve the results for low and high intensity ground motions; however this was out of the scope of this project.

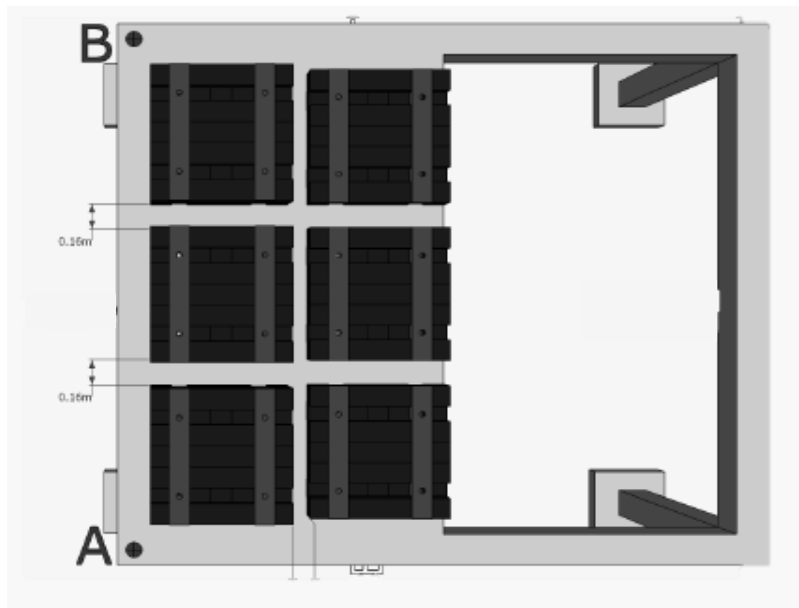


**Figure 28** Position of Nodes A and B in 3D Frame (15th WCEE Blind Test Challenge Test Report, 2012)

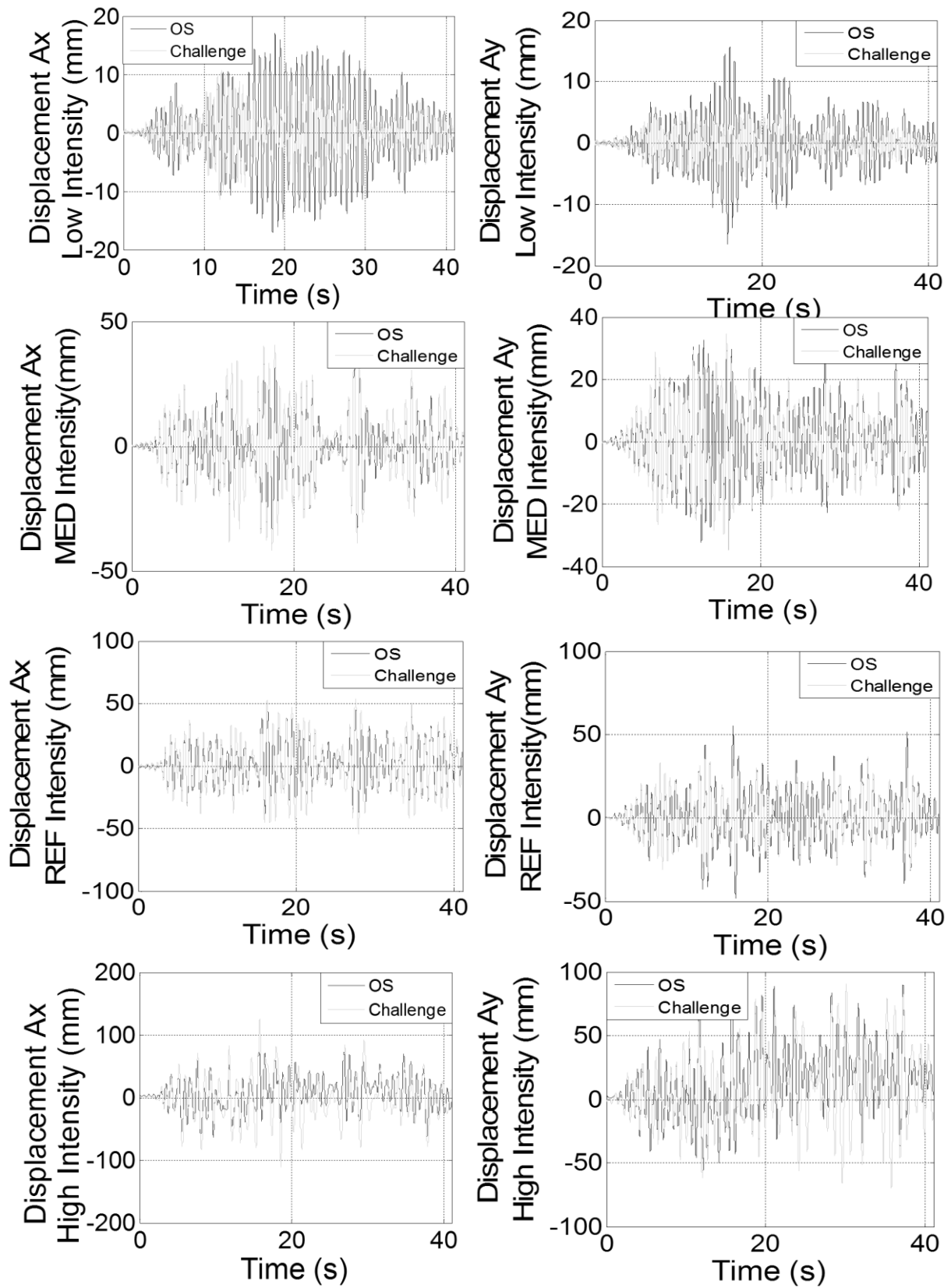


**Figure 29** Displacement Time Histories for node A in the 3D frame

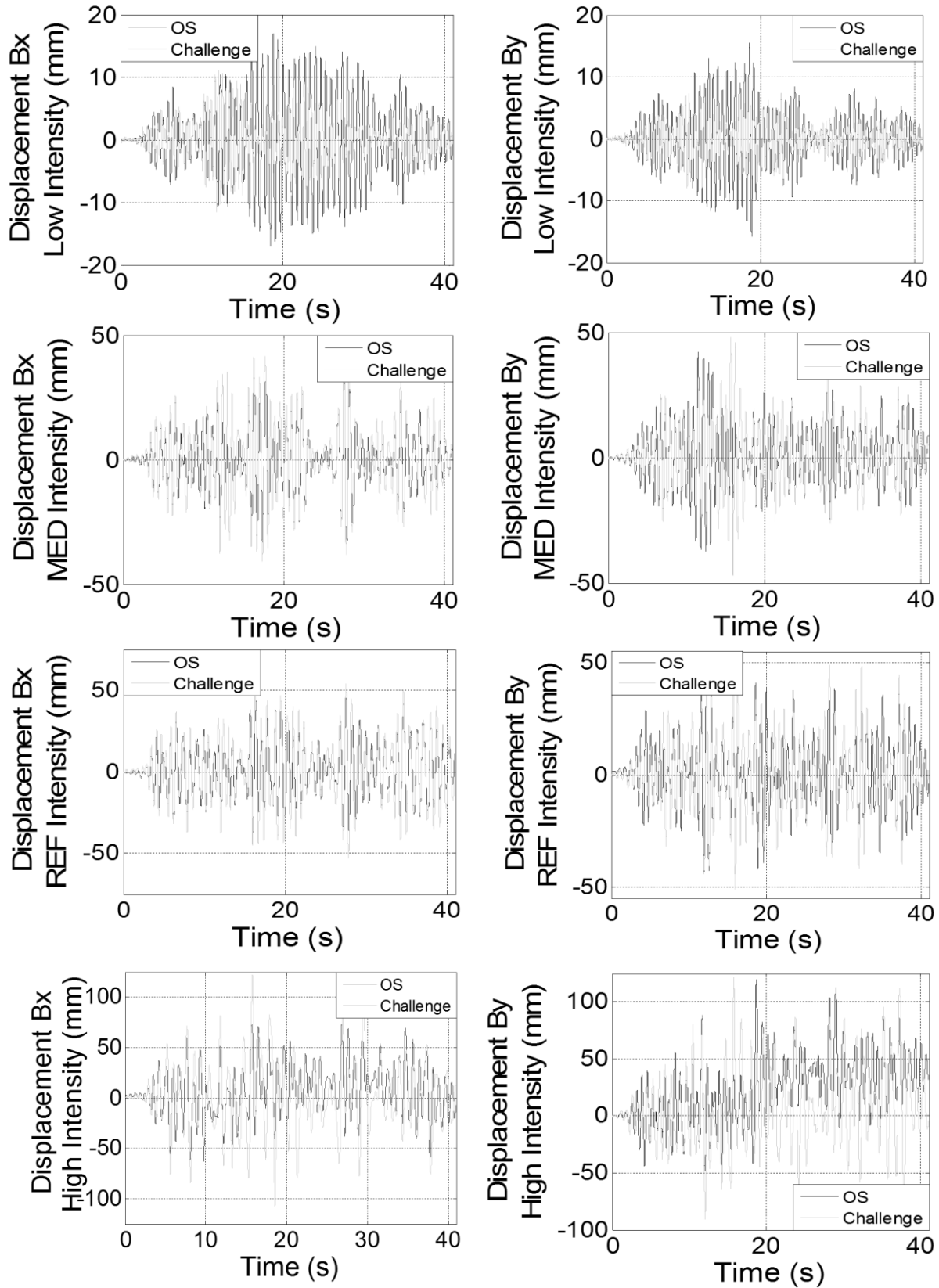


**Figure 30** Displacement Time Histories for Node B in the 3D Frame

### 3.6. ADDITIONAL PARAMETERS FOR THE GROUND MOTIONS

In order to understand the behavior of the structure under seismic motions and dynamic analyses, it is important to obtain certain ground motions parameters that represent the characteristics of the earthquake. Using the SeismoSignal<sup>®</sup> program (Seismosoft Ltd., 2013) and the acceleration time histories of each earthquake the Arias Intensity (AI), Cumulative Absolute Velocity (CAV), and Specific Energy Density (SED) were obtained.

#### *3.6.1. Arias Intensity (AI)*

The AI is a measure of the strength of a ground motion (EPRI, 1988). This parameter quantifies the potential destructiveness of an earthquake (Travasarou et al., 2002). It is calculated as the integral of the square of the acceleration time histories (Arias, 1970), which is the same formulation used in the SeismoSignal<sup>®</sup> program.

For the ground motion used in the 2D frames, the earthquake with the largest AI was the Chi-Chi earthquake, which has a value of 0.33 m/s, followed by the Kocaeli earthquake with a value of 0.24 m/s. On the other hand, the earthquakes with the lowest AIs were Tabas, with a value of 0.10 m/s, and Northridge earthquake with 0.12 m/s. The values of Kobe, Imperial Valley and Loma Prieta earthquakes were 0.19 m/s, 0.137 m/s and 0.134 m/s, respectively. These values are shown in Figure 31.

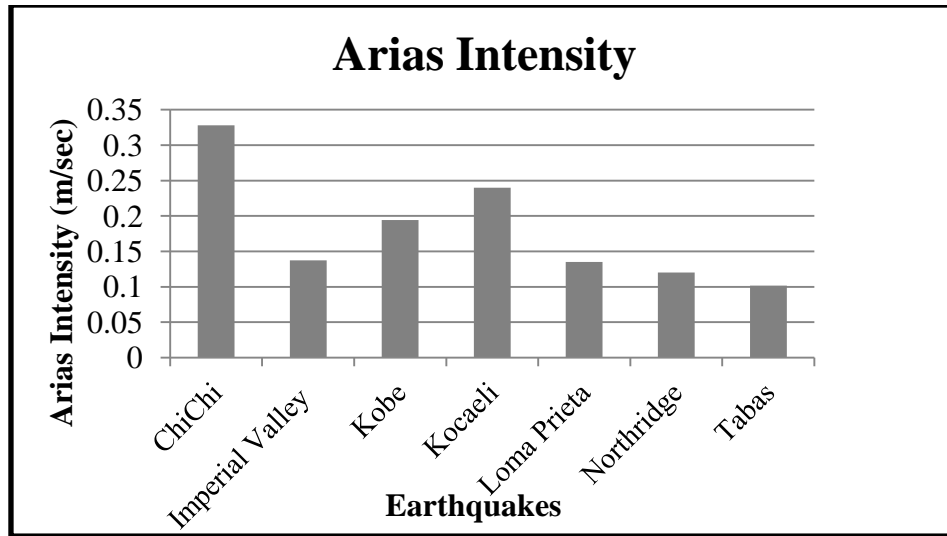


**Figure 31** Arias Intensity (ground motions for the 2D frames)

For the 3D model, the AI for both directions of the ground motions are shown in Figure 32, which shows as expected that the greater AI was obtained for the high intensity ground motion. Also, for all intensity stages the AI in the longitudinal direction is greater than the values in the transversal direction. The greatest values in the longitudinal and transversal direction are 6.83 m/s and 6.05 m/s, respectively. For the low intensity level, the AI values were 0.084m/s in the longitudinal direction and 0.069 m/s in the transversal direction.

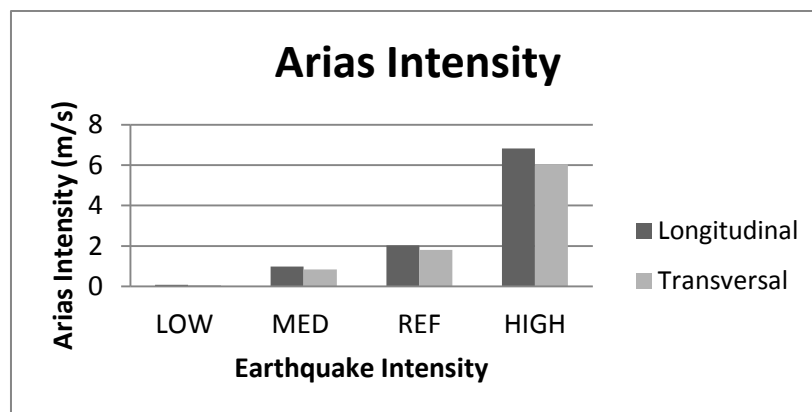


**Figure 32** Arias Intensity (ground motions for the 3D frame)

### 3.6.2. Cumulative Absolute Velocity (CAV)

Another parameter obtained is the CAV, which represents the possible onset of structural damage. It is calculated as the area under the absolute acceleration time histories (EPRI,1988). For the earthquakes used in the 2D frames, those with the greater CAV values were Kocaeli, with a value of 722.8 cm/s, and Chi-Chi with 690.5 cm/s. The lowest values of CAV were obtained for the Tabas and Northridge earthquakes, with values of 275 cm/s and 318.5 cm/s, respectively. The values obtained for the Kobe, Loma Prieta and Imperial Valley earthquakes were 440.76 cm/s, 374.18 cm/s and 367.54 cm/s respectively. Figure 33 illustrates the values of CAV for these earthquakes.

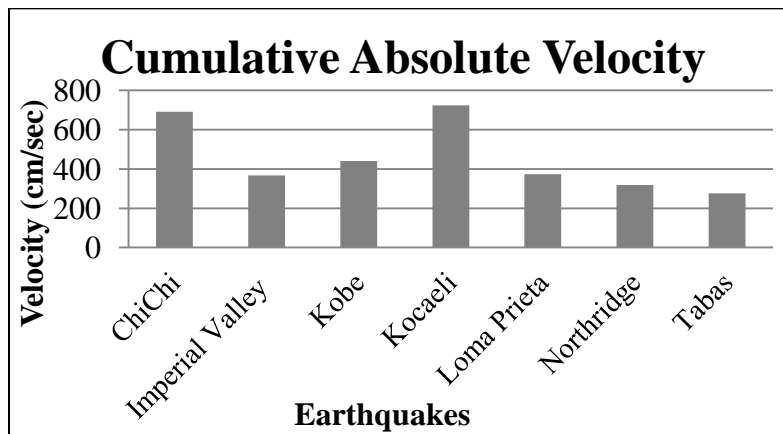


**Figure 33** Cumulative Absolute Velocity (ground motions for the 2D frames)

The CAV values for the longitudinal and transversal direction of the earthquakes used for the 3D frame are shown in Figure 34. The minimum values were obtained in the low intensity level, 345.70 cm/s in the longitudinal direction and 312.98 cm/s in the transversal direction. The maximum values were obtained in the high intensity level, which are 3072.24 cm/s in the longitudinal direction and 2867.59 cm/s in the transversal direction. For all earthquake intensities the values obtained from the longitudinal direction are greater than the values in the transversal direction.

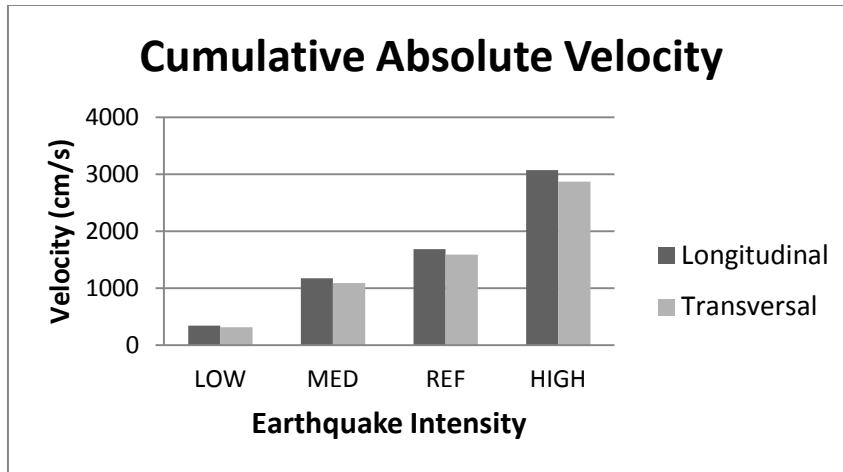


**Figure 34** Cumulative Absolute Velocity (ground motions for the 3D frame)

### 3.6.3. Specific Energy Density (SED)

The Specific Energy Density (SED) is defined as the sum of the square of the velocity time histories. Using the same program, the SED values were obtained for the ground motions used in the 2D frames and are shown in Figure 35. The earthquakes with the largest SED values are the Chi-Chi, with  $390.43 \text{ cm}^2/\text{s}$ , followed by the Kocaeli earthquake with a value of  $388.77 \text{ cm}^2/\text{s}$ . Meanwhile, the lowest values of SED occur for the Tabas and Northridge earthquakes. They have values of  $147.98 \text{ cm}^2/\text{s}$  and  $165 \text{ cm}^2/\text{s}$ , respectively. The values for the Kobe, Loma Prieta and Imperial Valley earthquakes are  $289.9 \text{ cm}^2/\text{s}$ ,  $275.6 \text{ cm}^2/\text{s}$  and  $247.9 \text{ cm}^2/\text{s}$ , respectively.

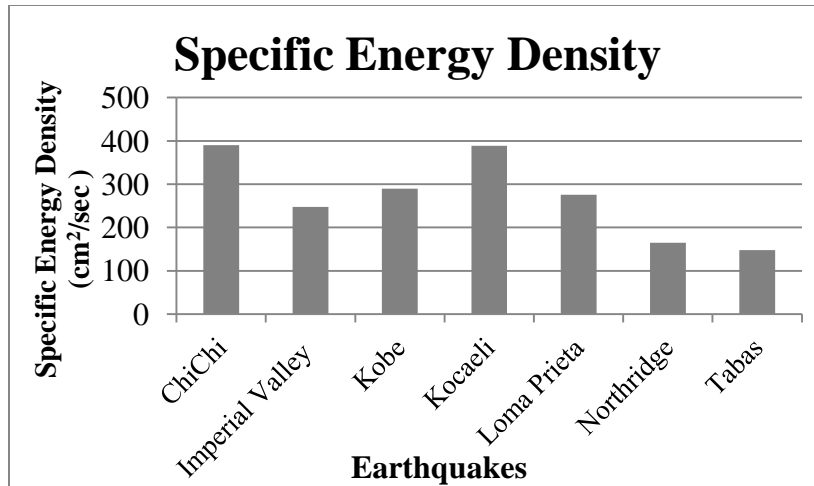


**Figure 35** Specific Energy Density (ground motions for the 2D frames)

For the motions used for the 3D frame the SED for the four earthquake intensities is illustrated in Figure 36. The values obtained for the longitudinal and transversal direction has a minimal difference between them. As expected, the maximum value of SED obtained occurs in the high intensity level, with values of 4859.21 cm<sup>2</sup>/s in the longitudinal direction and 4787.23 cm<sup>2</sup>/s in the transversal direction. The minimum values were obtained in the low intensity level, which are 56.45 cm<sup>2</sup>/s in the longitudinal direction and 56.88 cm<sup>2</sup>/s in the transversal direction.

All the parameters described before (AI, CAV and SED) will help to understand some of the results obtained from the dynamic analyses, in special the energy dissipation values. A discussion is included in the next chapters.

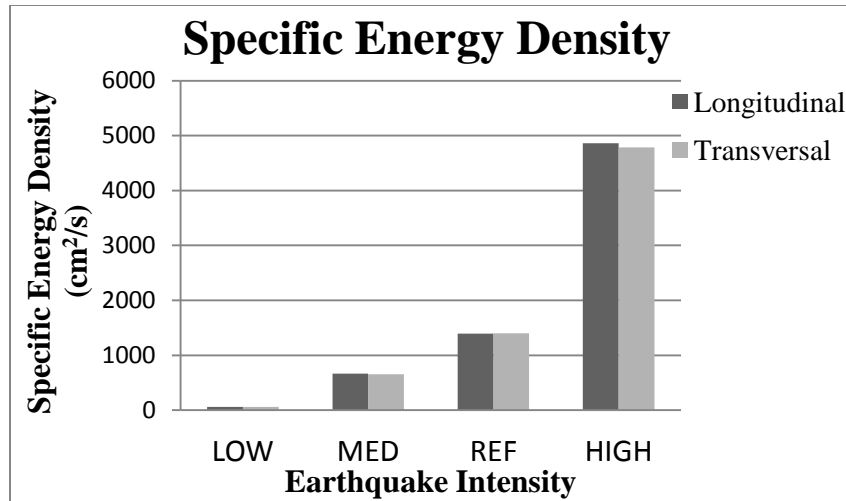


**Figure 36** Specific Energy Density (ground motions for the 3D frame)

## **CHAPTER 4: Drift Limit Results from the Dynamic Analysis**

### **4.1 INTRODUCTION**

An Incremental Dynamic Analyses was performed to analyze the behavior of the frames described previously. The IDA was defined by Vamvatsikos and Cornell (2002<sup>a</sup>) as an analysis method “*which involves performing nonlinear dynamic analyses of the structural model under a suite of ground motion records, each scaled to several intensity levels designed to force the structure all the way from elasticity to final global dynamic instability*”. This analysis provides a connection between the response of the structure under a Static Pushover analysis (SPO) and Dynamic analysis (Vamvatsikos and Cornell, 2002<sup>b</sup>). As stated before, in this research all frames were subjected to seven earthquakes and each earthquake was scaled from 0.1g to 1.5g. The maximum values of drifts and material strains (steel and concrete) were obtained for each intensity and earthquake. Also, energy dissipation values were obtained. The values obtained for each IDA analyses, including drift, steel strain, concrete strain and seismic hysteretic energy are shown in Appendix II. This chapter presents the drift results that were obtained from the IDA for all the frames. The following chapter presents the results obtained for the material strain limits.

### **4.2. DRIFT AS DAMAGE INDICATOR**

The inter-story drift is defined as the ratio of the relative displacement between each story over the height of the story. This parameter is used as an indicator of the damage presented in a structure. For the 2D frame, the drift values were obtained for each node in all stories, as illustrated in Figure 37. An average value for each story was calculated and the maximum values for each earthquake and intensity were obtained. The position of the maximum drift was

used to obtain the values of steel strain, concrete strain, moment and rotations. For the 3D model the drift values were obtained for the longitudinal (Z axis) and transversal (X axis) direction, as illustrated in Figure 38. The position of the maximum drift in the X direction was used to found the maximum strains in the beams, and the maximum drift in the Z direction was used to found the maximum strain at the girders. For this frame the resultant drift values were calculated as the square root of the sum of the squares of the drift in X and Z direction. For the columns the same procedure was used with the corresponding resultant drift values.

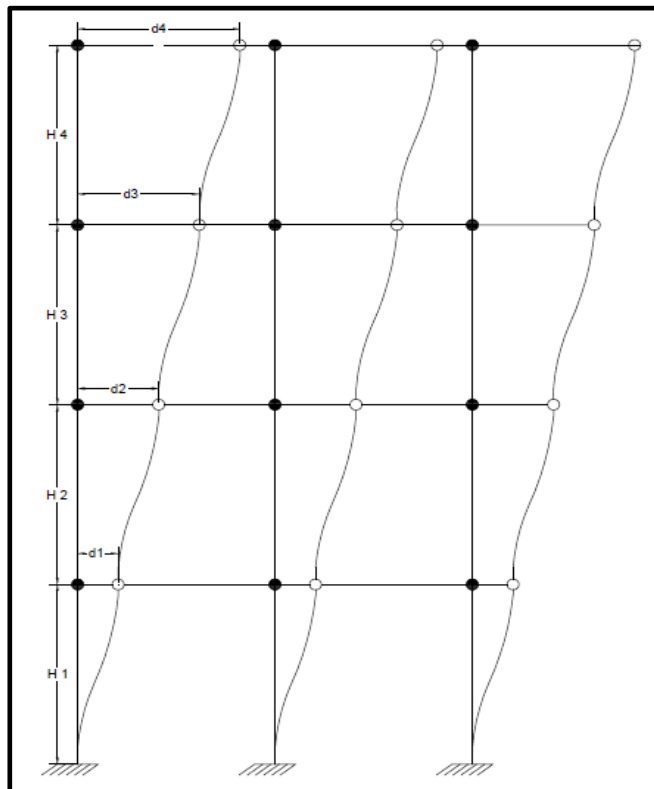


**Figure 37** Drift in the 2D frames

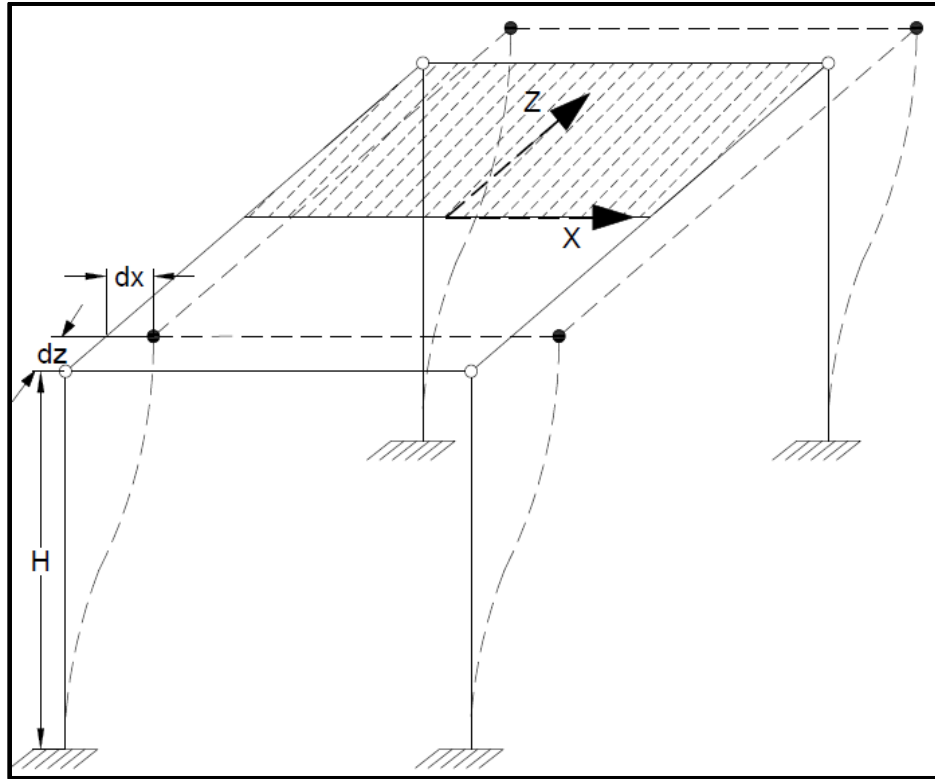


**Figure 38** Drift in the 3D frame

### 4.3. DRIFT LIMIT STATES FROM ASCE 41-06

The ASCE 41-06 code was used to obtain values of drift limit states which provide a measurement of the performance of the structure. These values will be used to compare them with the drift results from the IDA. Drift limits at several occupancy levels were obtained and are defined as Immediate Occupancy (IO), Life Safety (LS) and Collapse Prevention (CP) limit states. They were taken from Table 6-7, “Modeling Parameters and Numerical Acceptance Criteria for Nonlinear Procedures-Reinforced Concrete Beams”, of the ASCE/SEI 41-06 code. In order to find these values it is required to calculate the ratio between the difference of the steel reinforcement ratio ( $\rho$ ) in compression and in tension over the balanced steel reinforcement ratio. For all beam sections the quantity of steel reinforcement in compression and in tension is equal, therefore this ratio is zero. Other parameters needed to obtain the drift limit values is the ratio

between the shear force over the width, depth to the tension fiber (d) and the concrete nominal compressive strength ( $f'_c$ ). These parameters are shown in Equations 4.1 and 4.2. They are used with U.S. customary units.

$$(\rho - \rho') / \rho_{bal} \quad (4.1)$$

$$V / (bd\sqrt{f'_c}) \quad (4.2)$$

The shear force was obtained using the formulas of the ACI 318-08 code (Eq. 4.3 to 4.5), which is composed of the contribution of the concrete and steel reinforcement to the shear force capacity of the section.

$$V = V_c + V_s \quad (4.3)$$

$$V_c = 2 * b * d * \sqrt{f'_c} \quad (4.4)$$

$$V_s = \frac{A_v * f_y * d}{s} \quad (4.5)$$

The transverse reinforcement was classified as conforming (“C”) and as primary component type. Since all the values of the ratio  $V / (bd\sqrt{f'_c})$  for the 2D frames are greater than 6, the drift values for the IO, LS and CP limits are 0.005, 0.01 and 0.02, respectively. For the 3D frame, the values of drift limits from ASCE 41-06 for the beam and girders are the same as for the 2D frame. However, for this frame the final drift limits were found at the columns since it follows a weak column-strong beam mechanism. The drift limits for the columns were determined using Table 6-8 of the ASCE 41-06. This table has the same parameters as the beam table, except for the steel reinforcement ratio. This was replaced by the ratio between the axial force over the product of the gross area and the concrete compressive strength ( $f'_c$ ). The axial force was determined with the dead load, using the mass discretization principle. With these

values the drift limits for the columns were the following: IO = 0.005, LS = 0.01365 and CP = 0.01820.

#### 4.4. DRIFT RESULTS - 2D FRAMES

As mentioned before, for all frames the maximum drift was obtained for each earthquake and intensity. For all frames a linear behavior was obtained from the drift vs. PGA curves, which confirms the directly proportional relation between drift and the peak ground acceleration. Figures 39 through 42 show the drift vs. PGA curves with the drift limit-states, yield beam drift and yield frame drift and average drift. The yield beam and yield frame drifts were calculated using Equations 4.6 through 4.8, and the drift limit states were obtained as indicated in the previous section.

$$\varphi_Y = \frac{2.1 * ey}{h_b} \quad (4.6)$$

$$\theta_b = \frac{\varphi_Y * L_b}{6} \quad (4.7)$$

$$\theta_F = \frac{0.5 * ey * L_b}{h_b} \quad (4.8)$$

where:

$\varphi_Y$ = yield curvature,

$ey$ = $F_y/E_s$ , yield steel strain,

$h_b$ = beam height,

$\theta_b$ = Yield beam drift,

$L_b$ = beam length and,

$\theta_F$ = Yield frame drift.

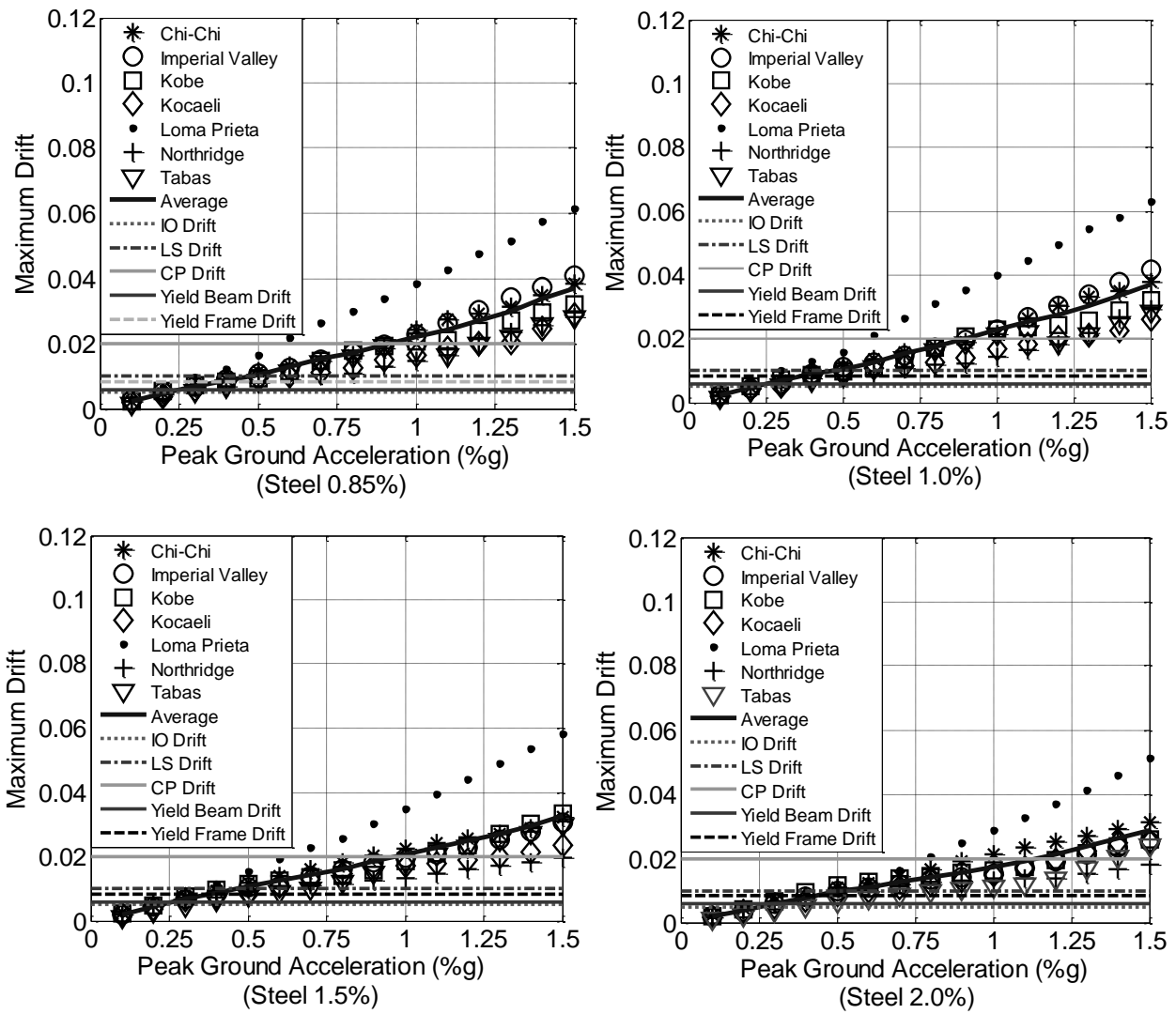
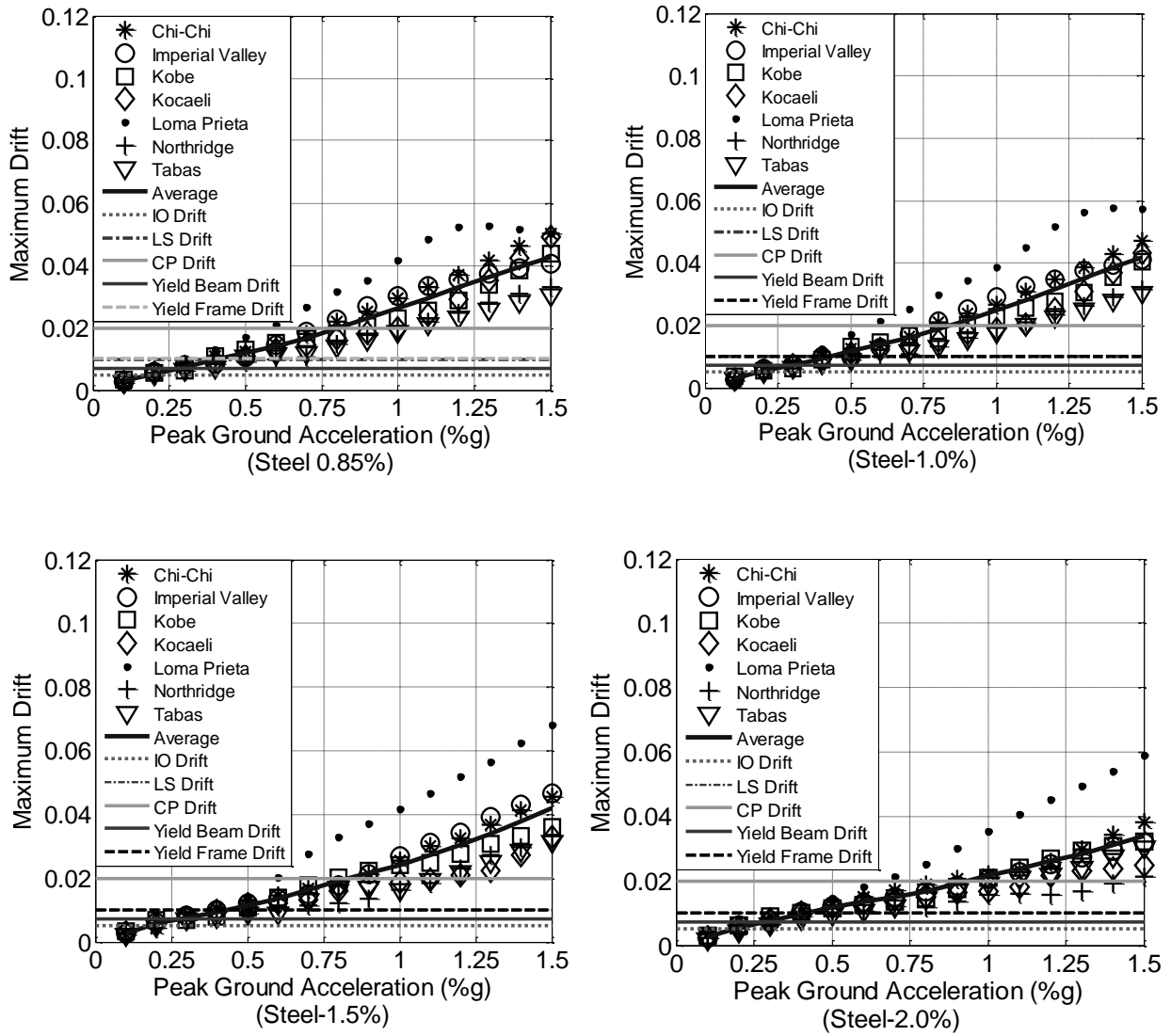


Figure 39 Drift vs. PGA - Frame 1



**Figure 40** Drift vs. PGA - Frame 2

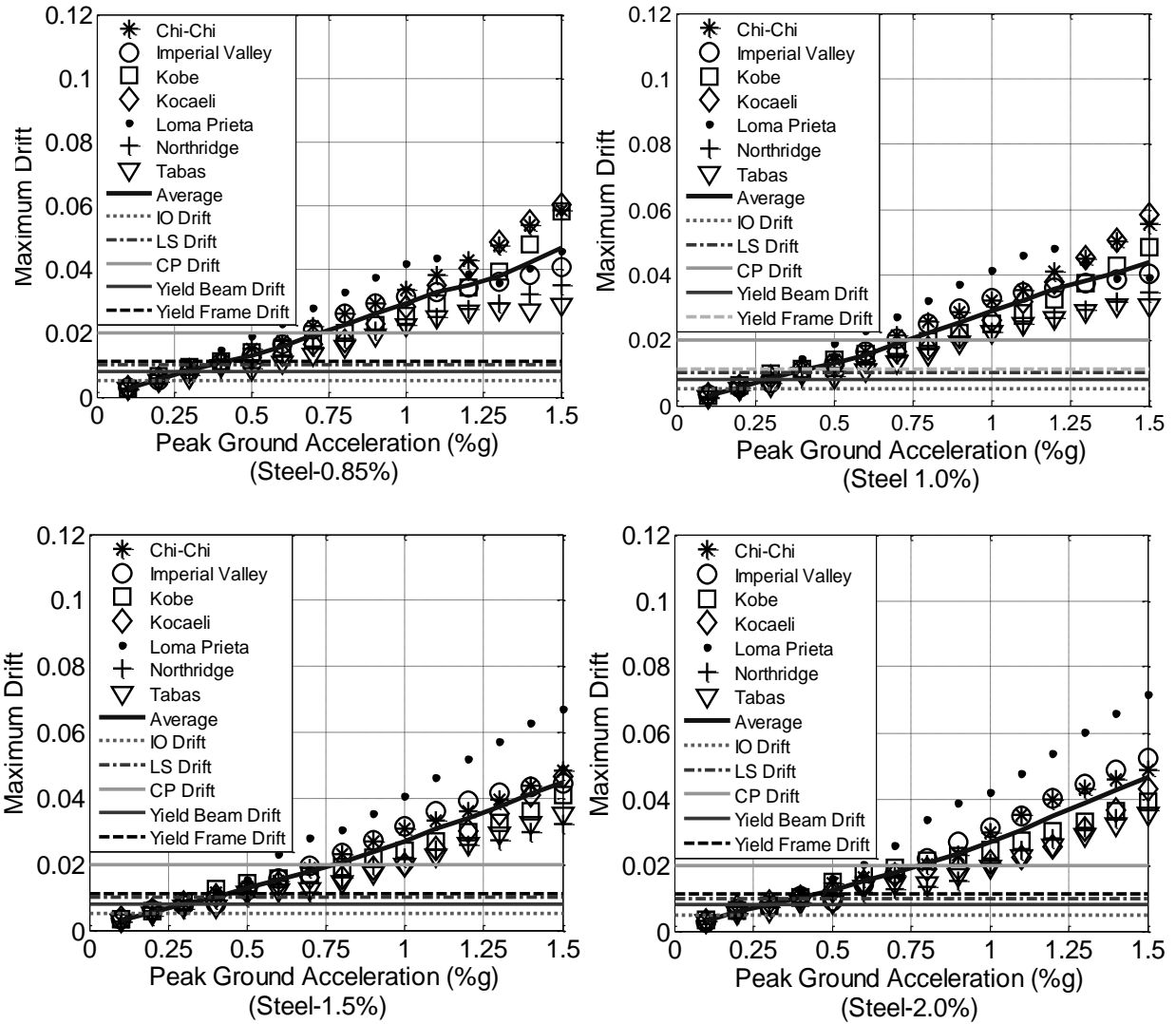


Figure 41 Drift vs. PGA - Frame 3

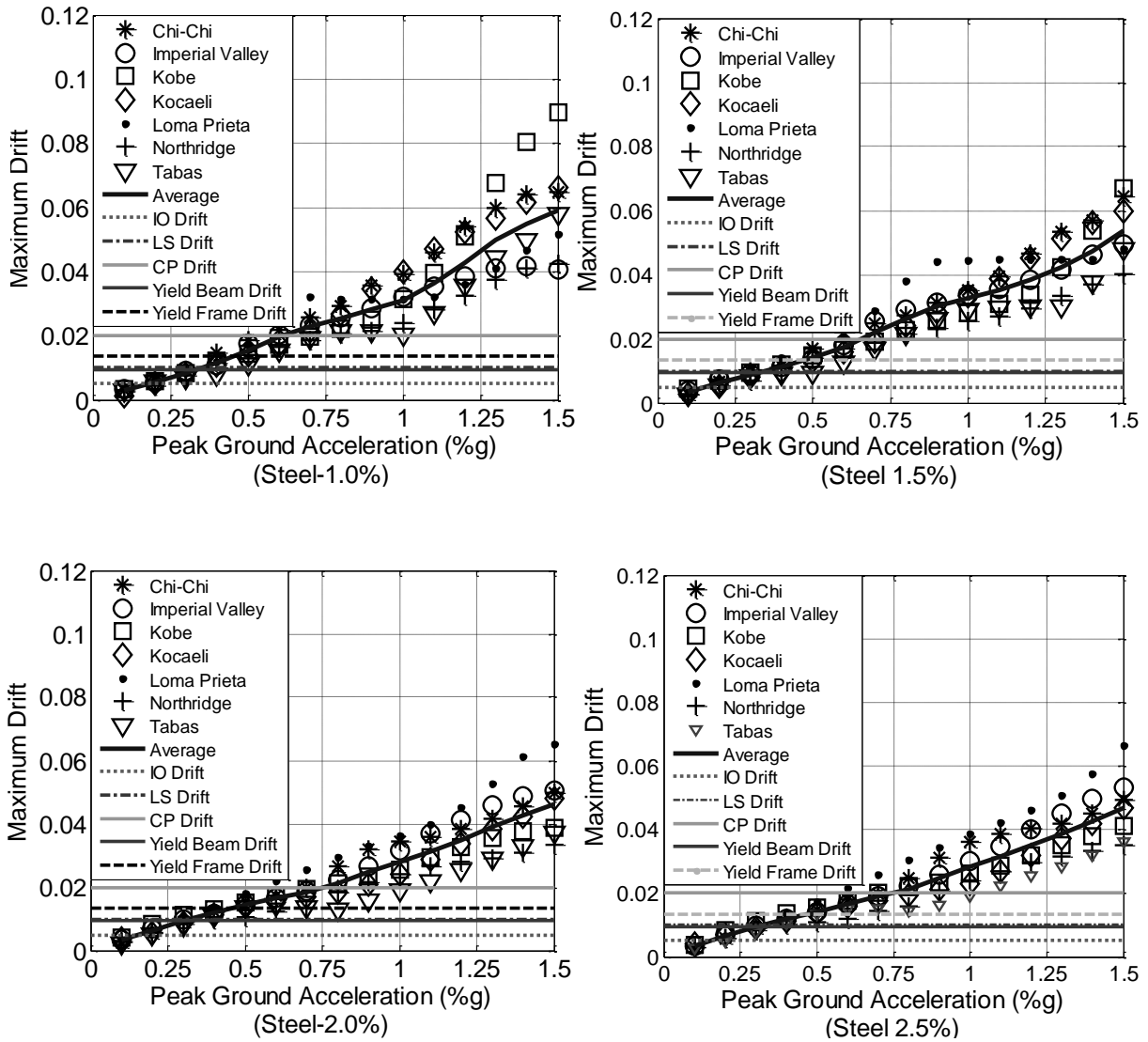
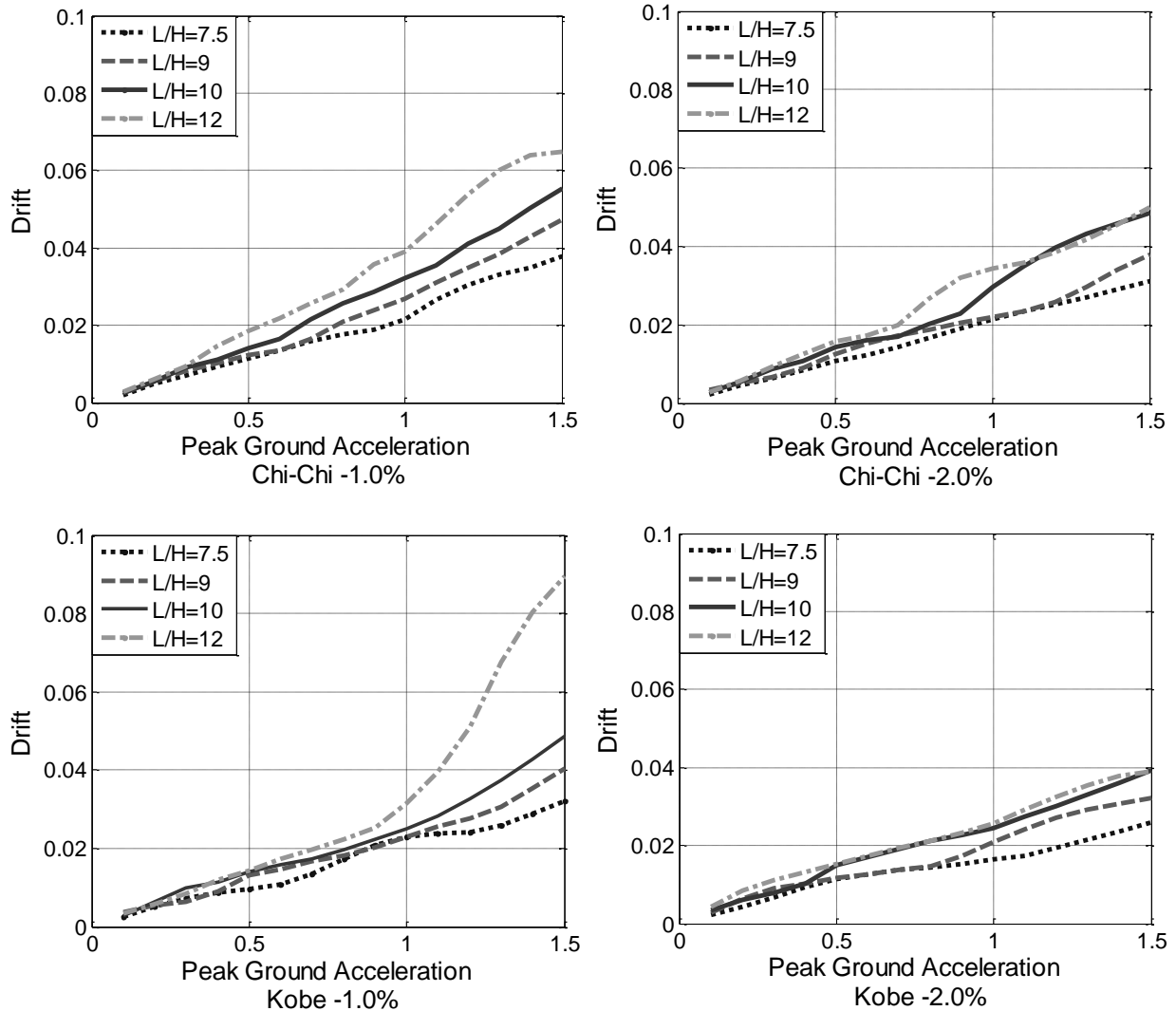


Figure 42 Drift vs. PGA - Frame 4



**Figure 43** Drift vs. PGA

From these curves it is observed that for each frame the drift values decrease as the steel reinforcement ratio increases. Figure 43 shows the variability of the drift between aspect ratios for the Chi-Chi and Kocaeli ground motions for 1.0% and 2.0% of steel reinforcement. It is confirmed in this Figure that the drift values increase as the aspect ratio increases. The highest values of drift were obtained for the frame 4, with an aspect ratio of 12, followed by the frame 3, with an aspect ratio of 10. In third place is the frame 2 with  $L/H = 9$ , and the lowest values of drift were obtained from the frame 1 with an aspect ratio of 7.5. This behavior demonstrates the

importance of the effect of the aspect ratio and reinforcing steel content on the frame drift limits. Also, it can be seen that the slope of the drift curves increases when the aspect ratio increase. Collapse prevention (CP) limit states (Figs. 39-42) are exceeded for frame 1 for PGA values higher than 0.6g to 1.4 g depending on the reinforcing steel ratio. For frame 2, 3, and 4 the CP limit is exceeded for PGA values higher than 0.6g, higher than 0.6g, and from 0.6-1.1g respectively. The life safety (LS) limits are reached at average PGA values of 0.6g, 0.5g, 0.5g, 0.4g for frames 1, 2, 3, 4, respectively. The IO is exceeded at 0.3g for frame 1 and 0.2g for frames 2, 3 and 4. From these plots, it can be deducted that code limits (IO, LS, CP) based on constant drifts ratios are not necessarily appropriate if the goal is to ensure constant damage for the same type of frame structure since the drift ratios are dependent of the aspect ratios and seismic level demands. It will be more appropriate to include in the definition of drift limits for rehabilitation codes parameters like aspect ratio and reinforcing steel in a more detailed fashion in order to predict much better the level of seismic performance desired for the structure.

#### **4.5. DRIFT RESULTS – 3D FRAME**

The results from the IDA are shown in Figure 44 together with the drift limit states from ASCE 41-06 and lines for the yield drift values obtained using the same equations of the 2D frames (Eq. 4.6 to 4.8). The behavior obtained was the same as the 2D frames, the drift and PGA show a directly proportional relationship. In both directions, the drift value for the low intensity level is under the IO, LS and Yield beam or girder drift limits. The drifts of the medium intensity level in both directions are equal to or lower than the yield frame drift value. Also, the drift value for the reference intensity, in both directions, is under the CP limit state. Finally, the drift for the high intensity level motion are beyond the CP limit state.

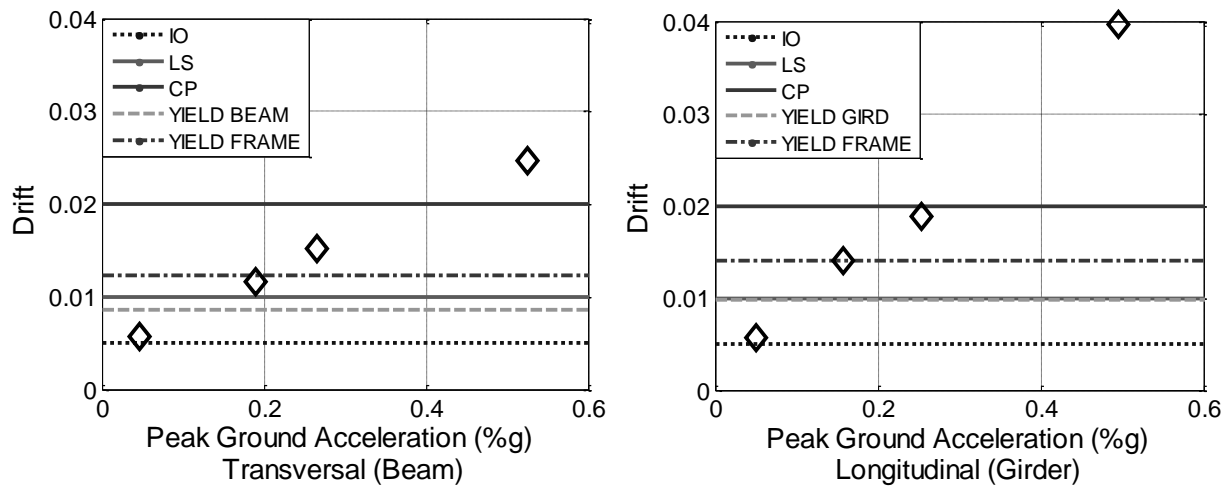


**Figure 44** Drift vs. PGA

# CHAPTER 5: Strain Limit Results from the Dynamic Analyses

## 5.1. INTRODUCTION

For both types of frames (2D and 3D) the concrete and steel reinforcing strains were measured at four points along the beam sections after the IDA was performed. The steel strain was obtained in tension and the concrete strain in compression. The values of the steel strain were obtained at the center of the steel reinforcement as shown in Figure 45 with points labeled as A, B, C, and D. The concrete strain values were found at the edges of the beam's section (points E-H in Figure 45). These strains were obtained at each end of the beam with hinges elements, taking a total of eight strain values per element and per material.

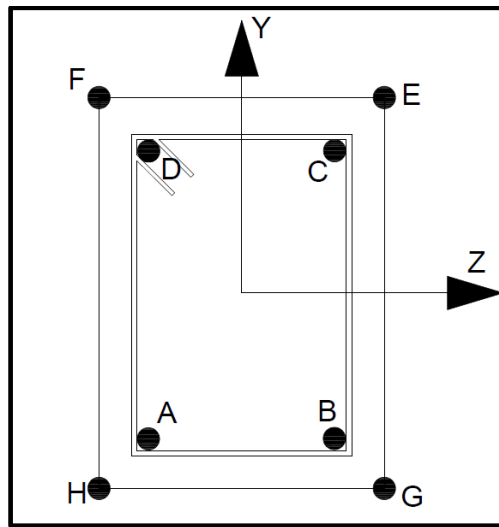


Figure 45 Positions of steel and concrete strain points

## 5.2. STEEL AND CONCRETE STRAINS RESULTS-2D FRAME

### 5.2.1. Strains as function of PGA values

The position in the time history where the maximum drift value occurred was obtained during the dynamic analysis for all ground motions and peak ground accelerations (PGA). At this time, the material (concrete and steel) strain values in the beam were retrieved to develop the

strains vs. PGA plots shown in Figures 46 through 53. Gaps between strain values on the same earthquakes may be presented in any case; this occurs when there is a change in the story in which the maximum drift occurs.

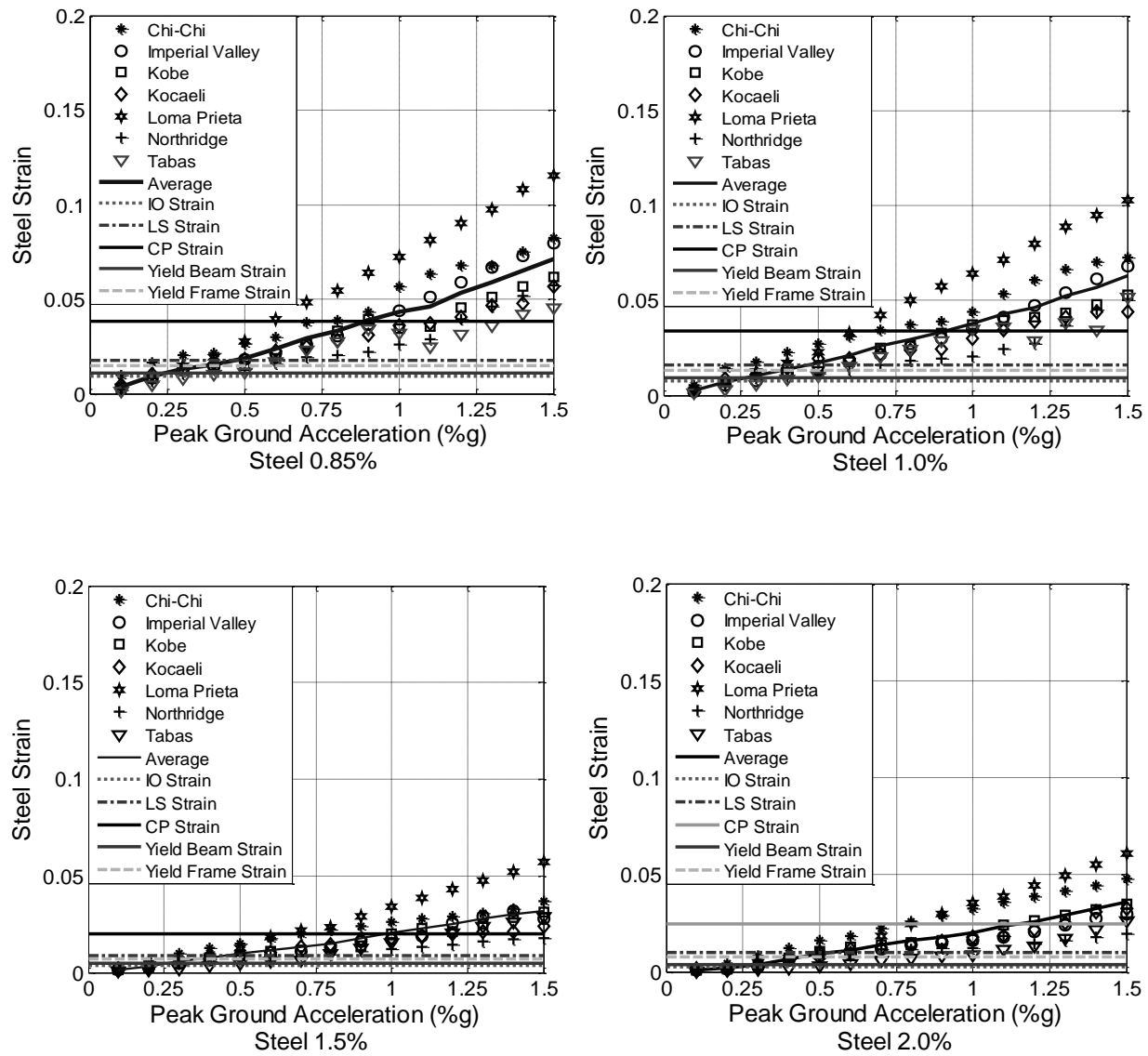


Figure 46 Steel Strain vs. PGA - Frame 1

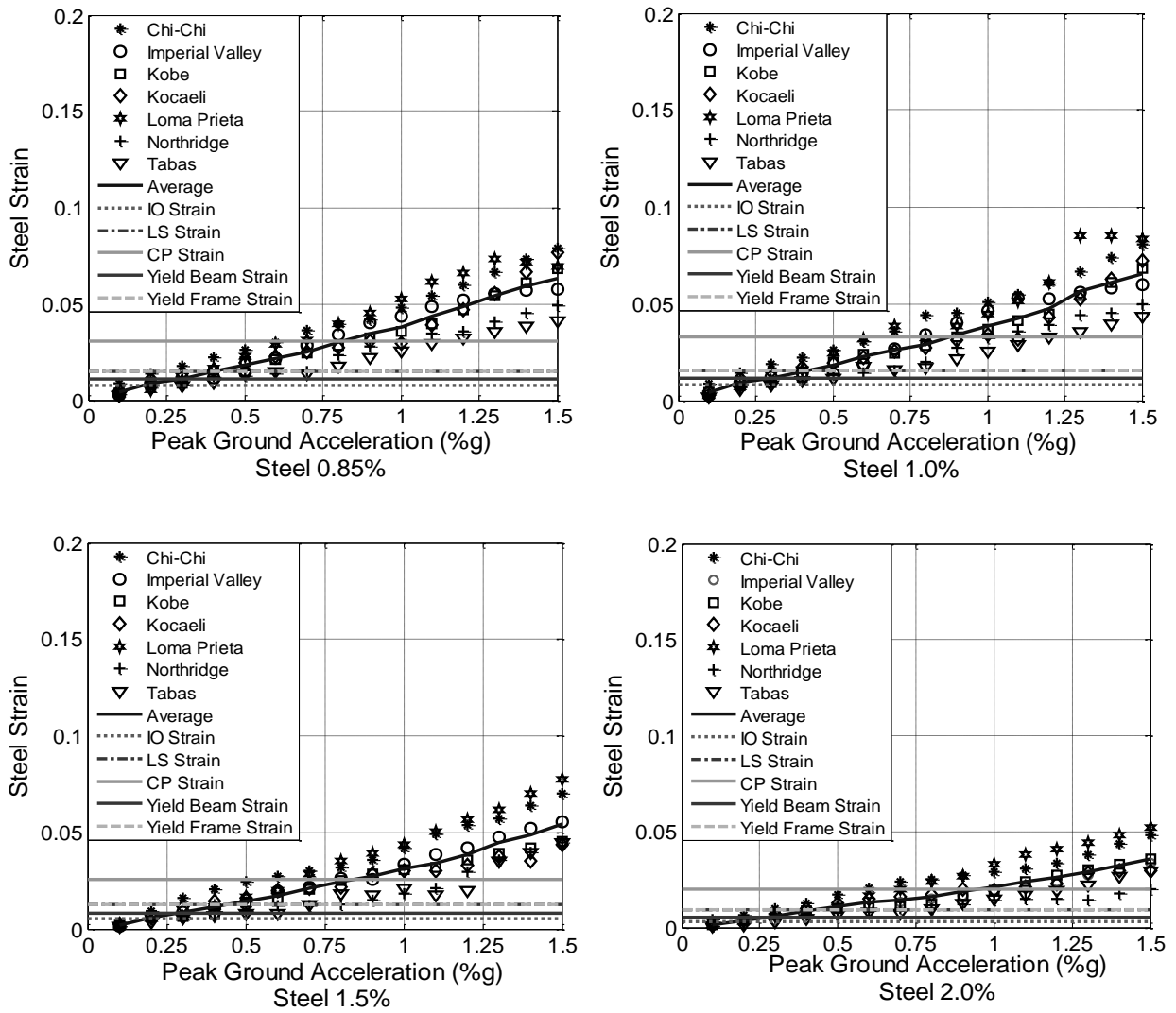


Figure 47 Steel Strain vs. PGA - Frame 2

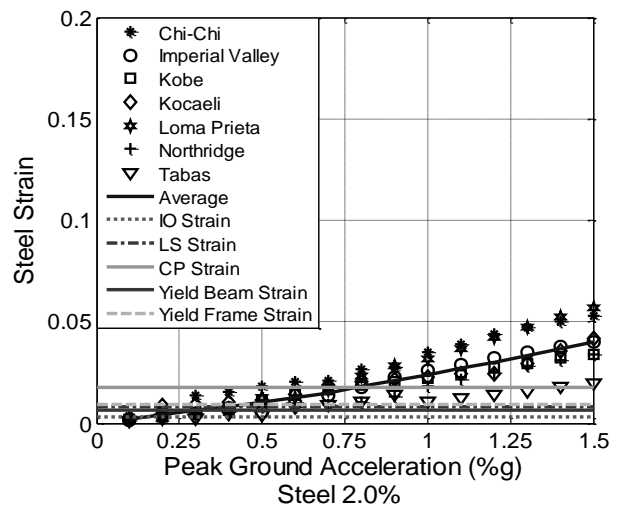
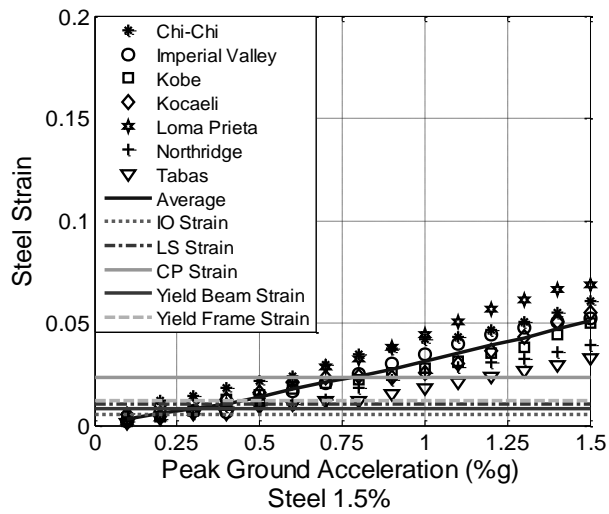
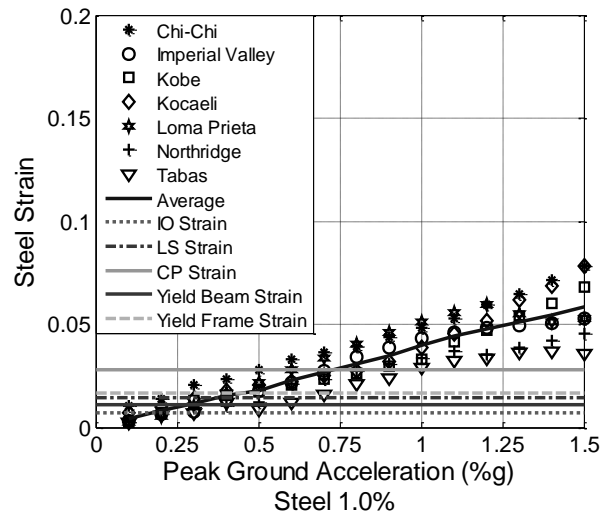
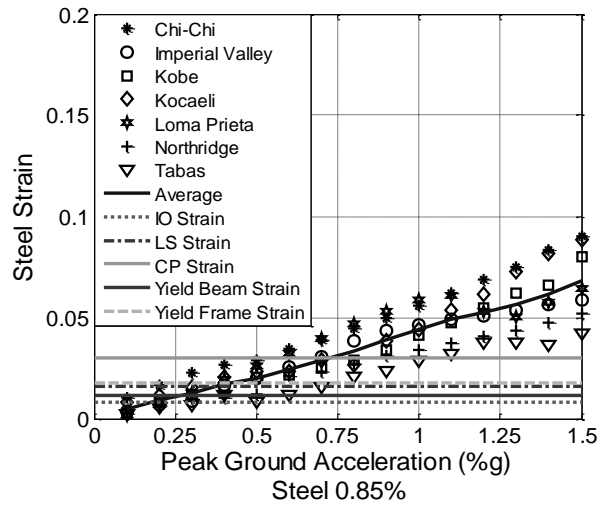


Figure 48 Steel Strain vs. PGA - Frame 3

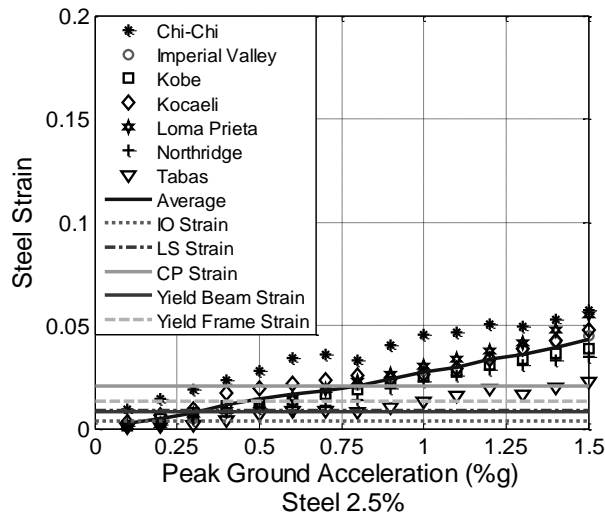
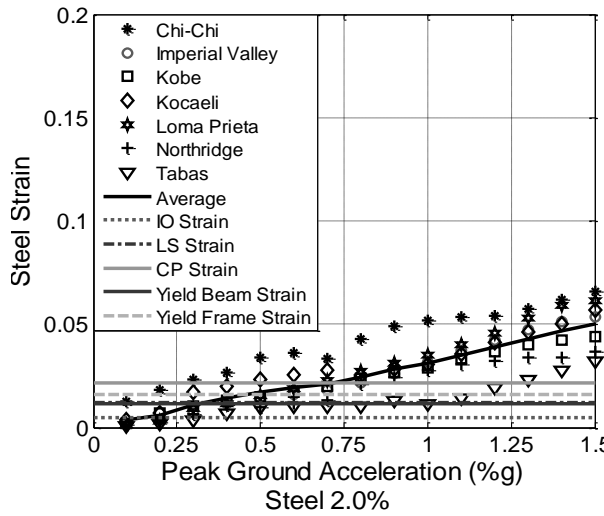
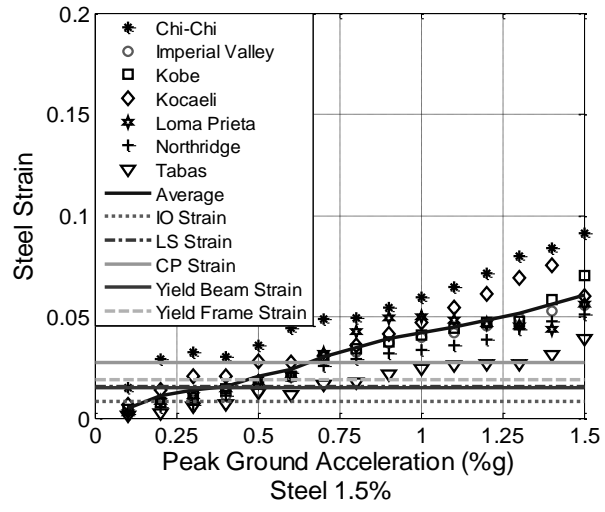
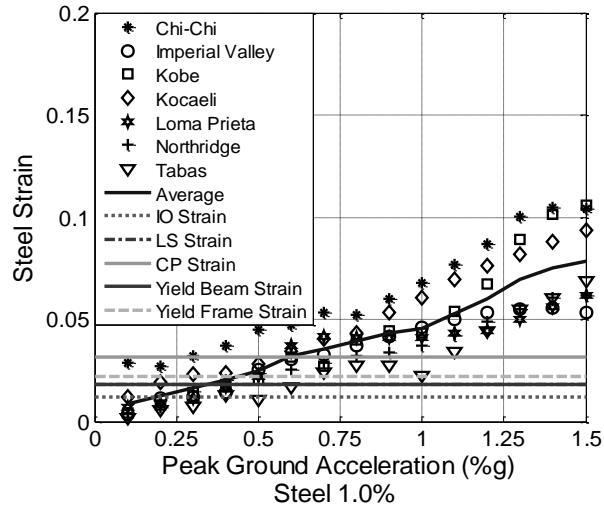


Figure 49 Steel Strain vs. PGA - Frame 4

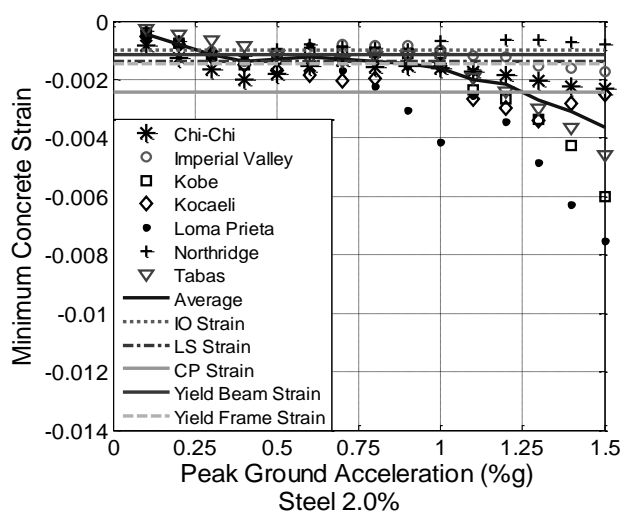
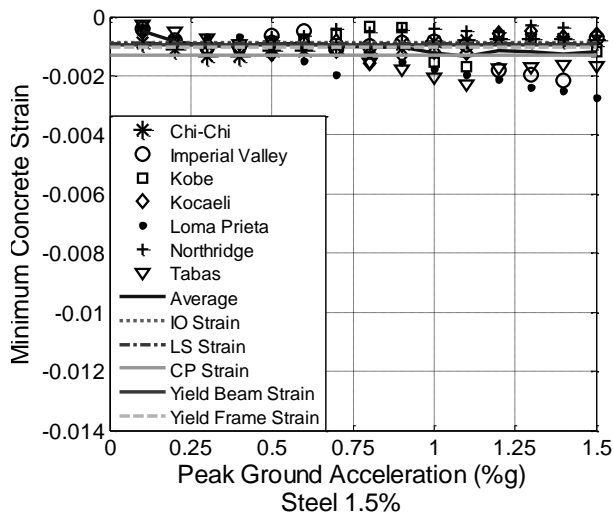
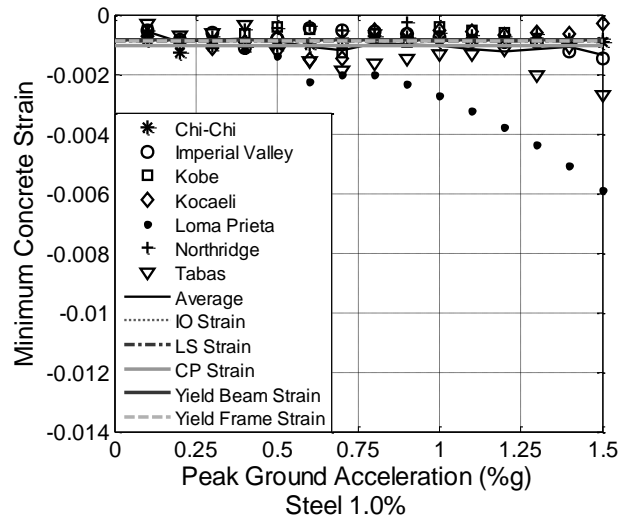
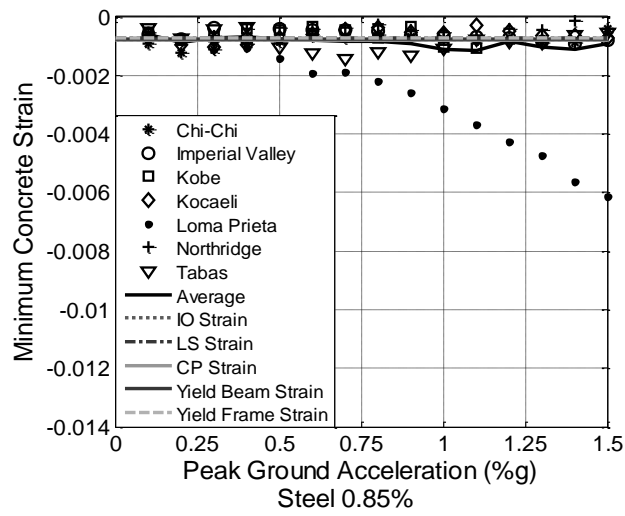


Figure 50 Concrete Strain vs. PGA - Frame 1

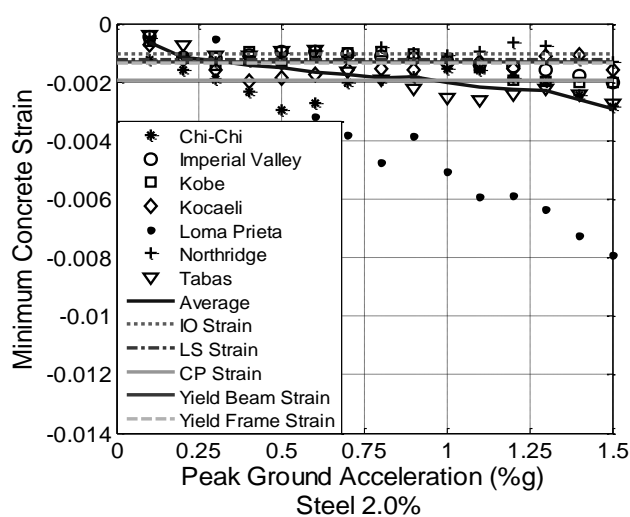
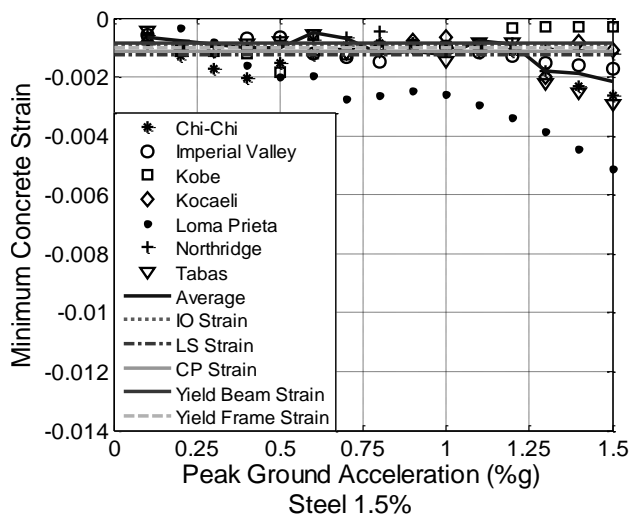
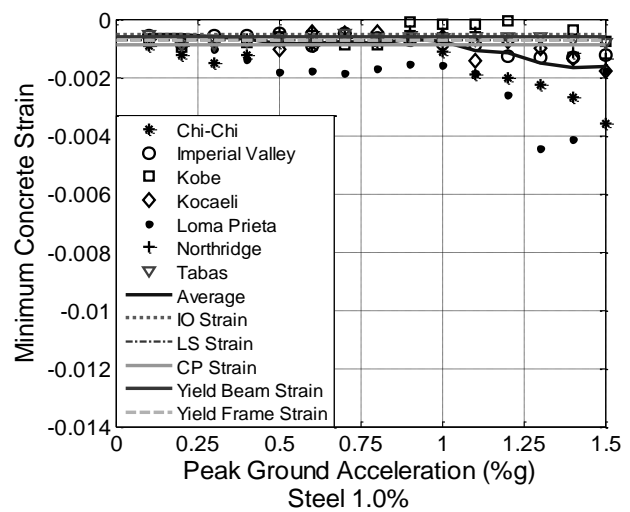
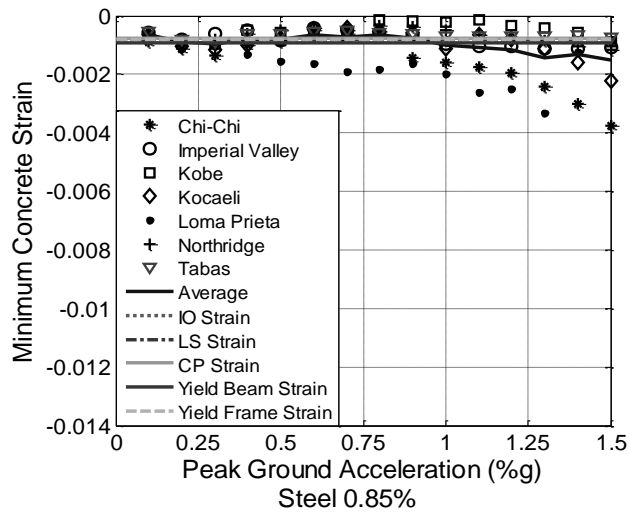
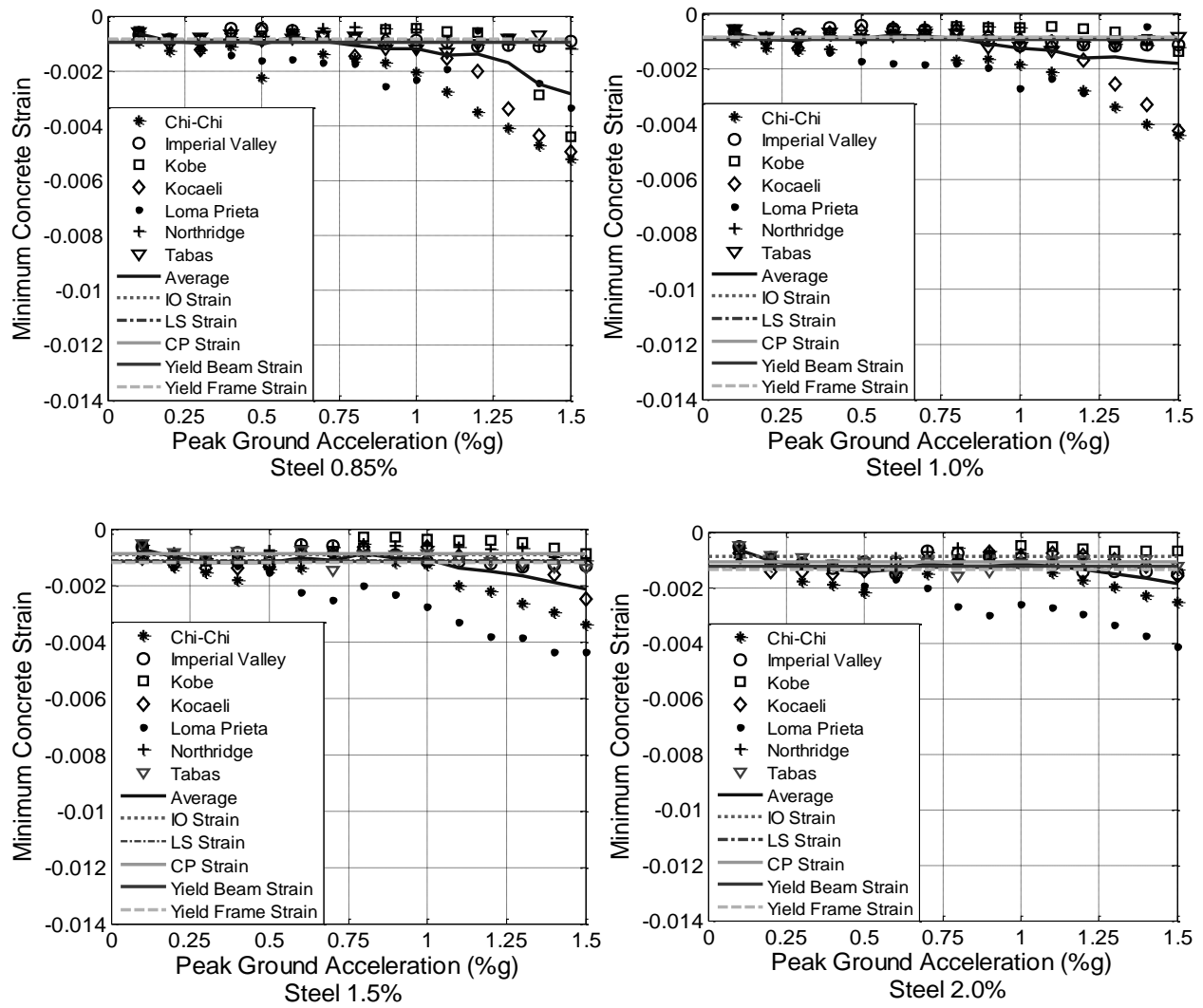
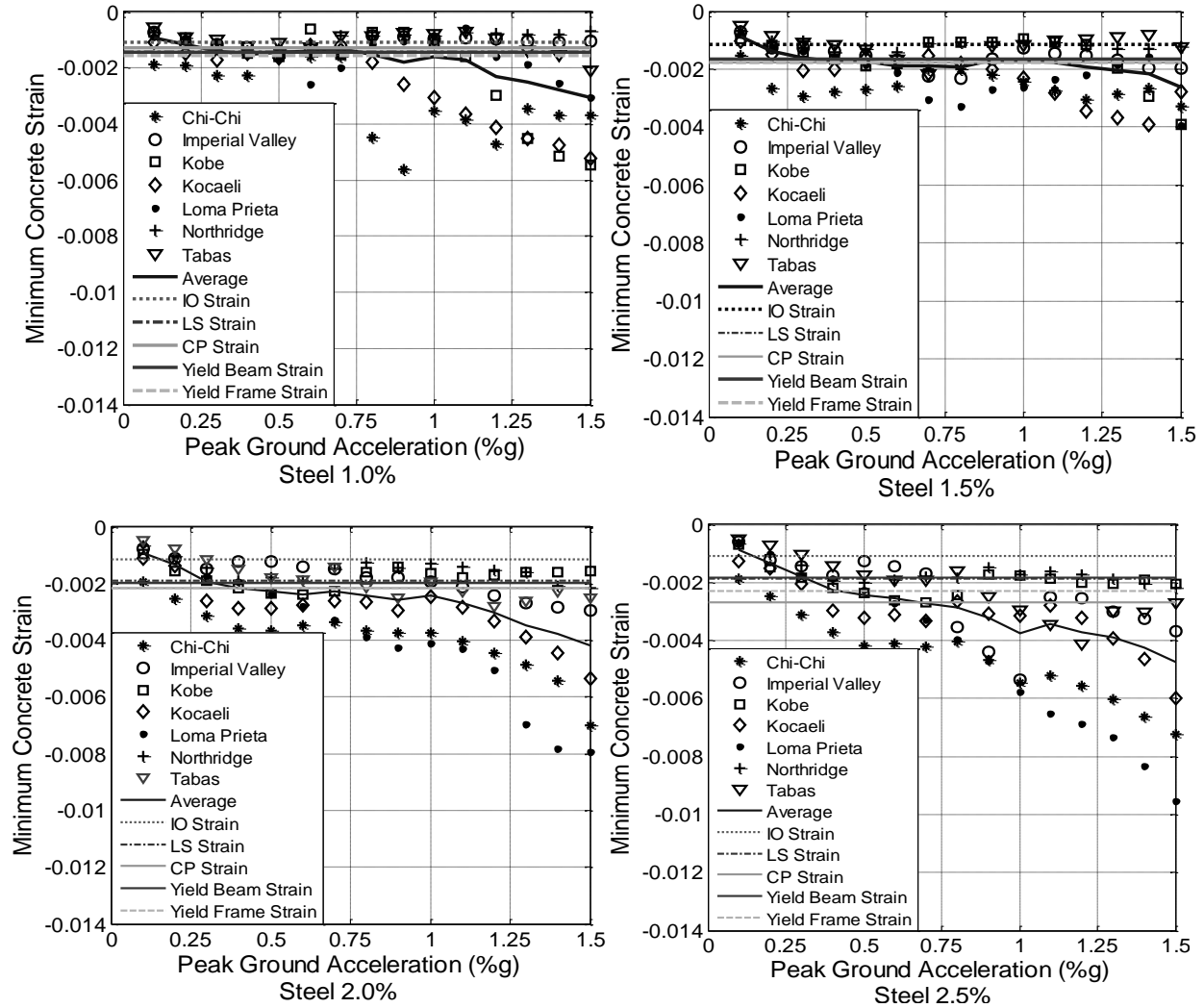


Figure 51 Concrete Strain vs. PGA - Frame 2



**Figure 52** Concrete Strain vs. PGA - Frame 3



**Figure 53** Concrete Strain vs. PGA - Frame 4

In these Figures 46-53, it can be seen that the steel strain limits present an almost linear relationship with the PGA values. The behavior of compression concrete strain limits is more erratic and in some cases does not present a linear relationship. The values of the compression concrete strain are very small for some of the earthquakes and those levels can be a challenge for the program to capture them with enough precision. Included in the Figure are the lines for the average steel or concrete strains obtained for the ASCE 41-06 limit states (IO, LS, CP) and for the strains corresponding to the yield beam drift and yield frame drift calculated with Equations

4.6 through 4.8. From the IDA, the strains (steel and concrete) were interpolated for the corresponding drift limits of the code and an average was performed among earthquake results. The strain values for each earthquake and limit state are included in Appendix II. It can be noted that the strains for the CP limit state are exceeded for all frames (1, 2, 3 and 4) at 0.6g. The life safety (LS) limits are reached at average PGA values of 0.6g, 0.5g, 0.5g, 0.4g for frames 1, 2, 3, 4, respectively. The IO is exceeded at 0.3g for frame 1 and 0.2g for frames 2, 3 and 4.

The IO limit state average steel tension strain value for frames 1, 2, 3, 4 were 0.0059, 0.0060, 0.0061 and 0.0072, respectively. For the LS limit states the average values were found as 0.013 for frames 1 and 2, and 0.0122, 0.0138 for frames 3 and 4, respectively. In the CP limit state the steel strain average values were found as 0.029, 0.0272, 0.0248 and 0.0253 for frames 1, 2, 3 and 4, respectively. From these values can be noted that the average value of steel tension strain for all frames at IO, LS, CP limit states were 0.0063, 0.013 and 0.0265, respectively. For the concrete compression strain the average values at IO limit for frames 1, 2, 3 was 0.0009 and for frame 4 was 0.0012. The LS limit average concrete strain values were 0.00097 and 0.0018 for frames 1 and 4, and 0.001 for frames 2 and 3. For the CP limit state the concrete strain values were 0.0013, 0.0011, 0.00093 and 0.002 for frames 1, 2, 3, 4, respectively. The average value of concrete compression strain at IO, LS, and CP limits for all frames were 0.00097, 0.0012 and 0.0013, respectively. From these results (specially for the steel strain limits) it can be noted that the strain vs. drift relationship is unique and independent of the load history. This has been proven by some researchers (Vidot and Kowalsky 2011, Goodnight et. al 2013).

The serviceability limit state is defined at a concrete compression strain of 0.004 or steel tension strain of 0.015 as suggested by Priestley et al. (2007). The damage control limit state is defined as a concrete compression strain of 0.018 or steel tension strain of 0.060, whichever

occurs first in the section. The LS and CP limit states are equivalent to the serviceability and damage control presented by Priestley et al. (2007). As mentioned before, the average value for all frames of steel tension strains were 0.013 and 0.026 for the LS and CP limits, respectively. For the concrete compression strains the values obtained were 0.0012 and 0.0013 for LS and CP limit states. These values are smaller than the serviceability and damage control limit state values presented before. This represents that the ASCE 41-06 limits are more conservative based on the strains than the presented by Priestley et al. (2007).

### ***5.2.2. Strains as function of drifts***

Using IDA results, the compression concrete and tension steel strains as function of the drifts were obtained, which are shown in Figures 54 through 61. From these graphs is confirmed that a directly proportional behavior occurs between these parameters in the case of steel strain limits. As presented before, concrete strain limits show more variability in the results. A static pushover analysis was performed in which the maximum drift and strain were also obtained (line marked as PO in the Figure 54 to 61). Vertical lines that represent the IO, LS and CP drift limits are also included in these Figures. It can be observed that the peak strains (concrete and steel) obtained for a given peak drift are very similar among all earthquakes and for the PO analysis for the steel strain limits. The difference between the PO and dynamic analysis is more noticeable as the aspect ratio of the frame increases. For concrete compression strains limits the PO results have more variability that for the steel strain limits. In general, it can be concluded that the monotonic envelope can be used to describe the envelope of the response from the dynamic analysis with sufficient accuracy for frames with aspect ratios lower than 10 based on the results obtained in this study. This of course has to be verified with a major number of analyses.

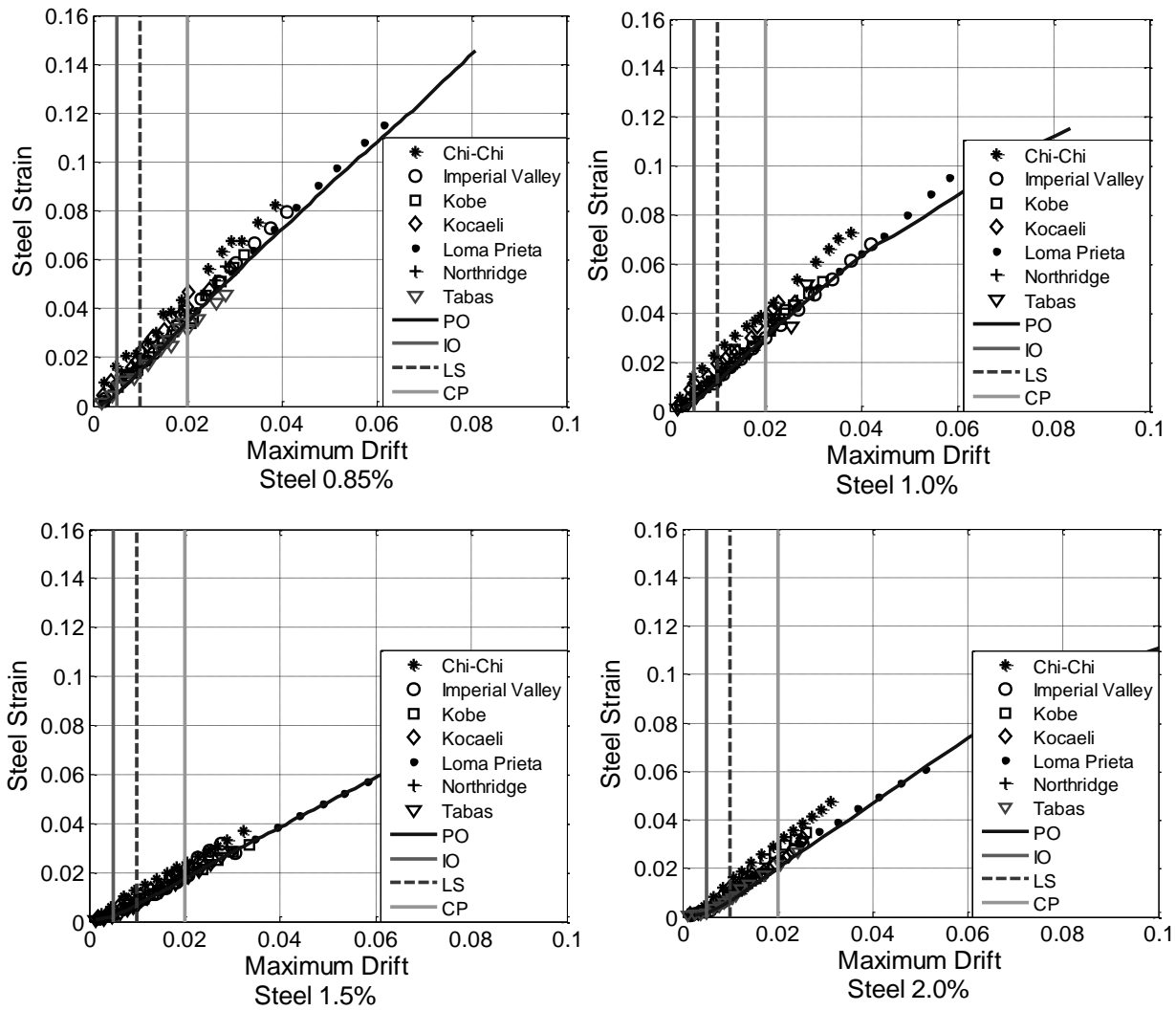


**Figure 54** Steel Strain vs. Drift - Frame 1

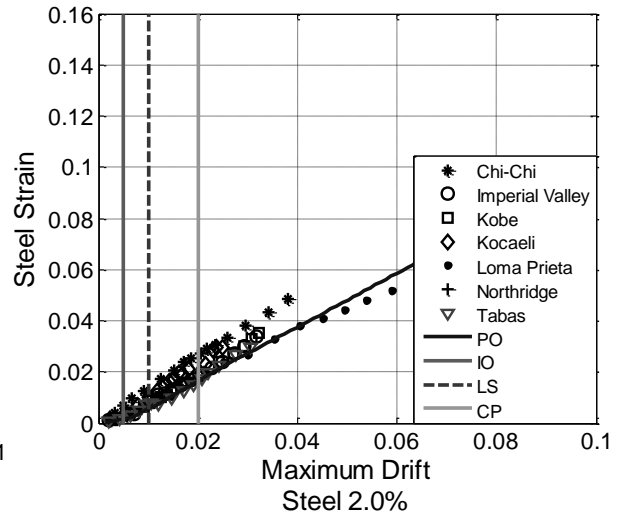
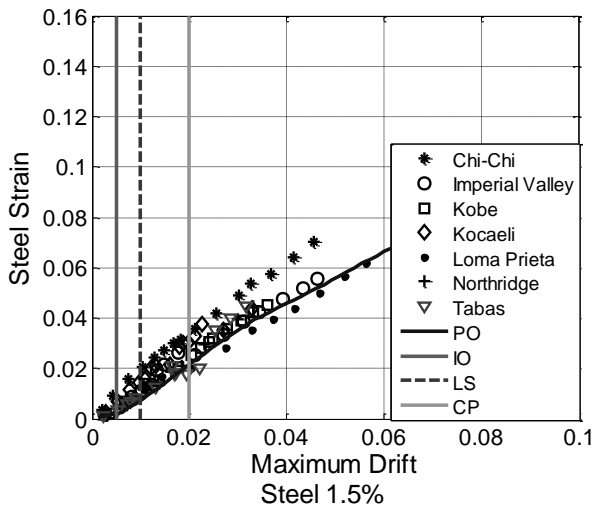
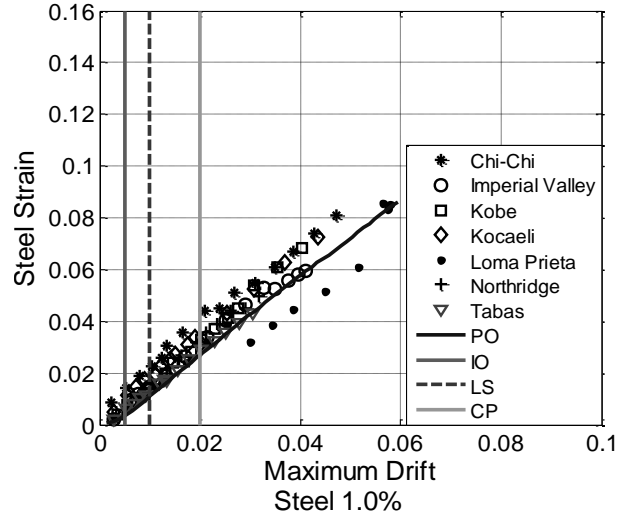
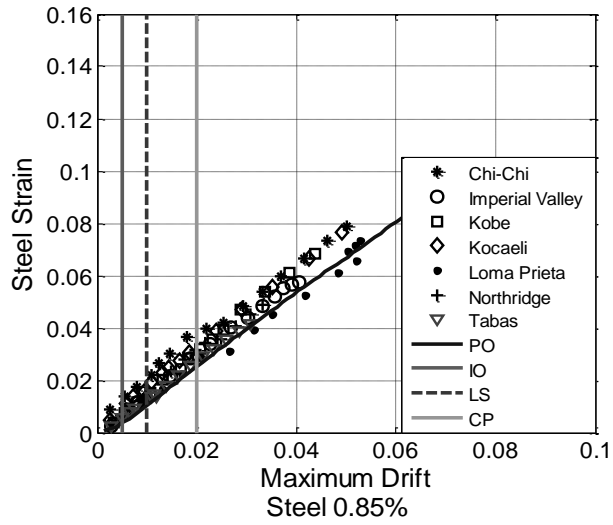
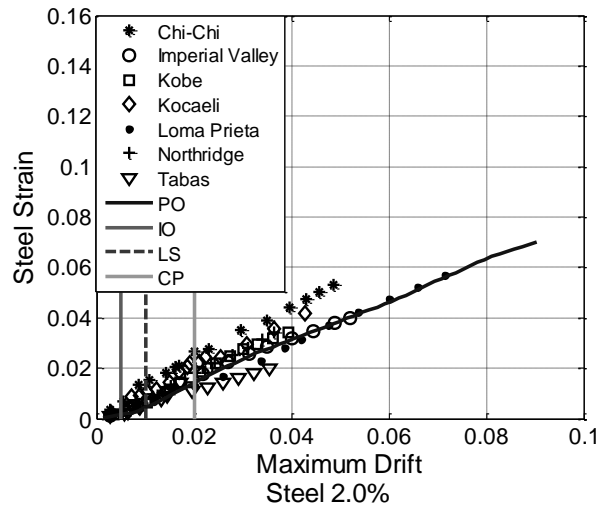
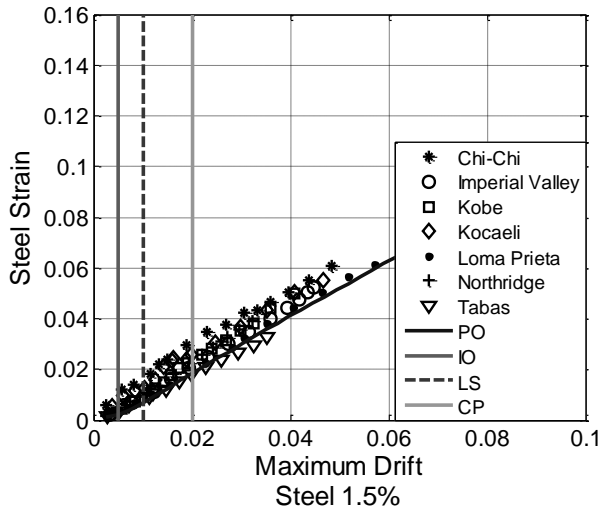
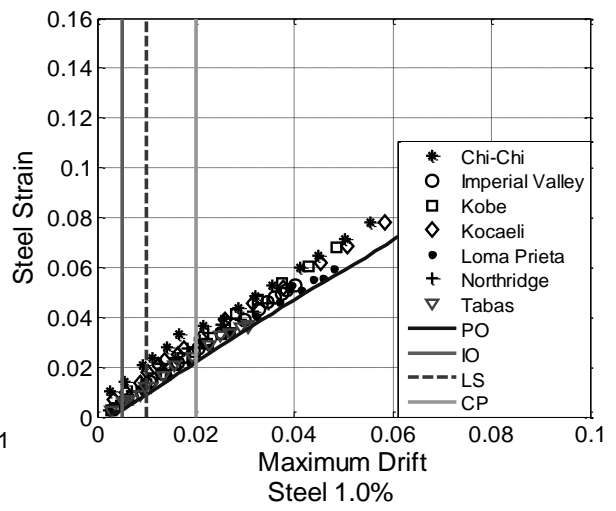
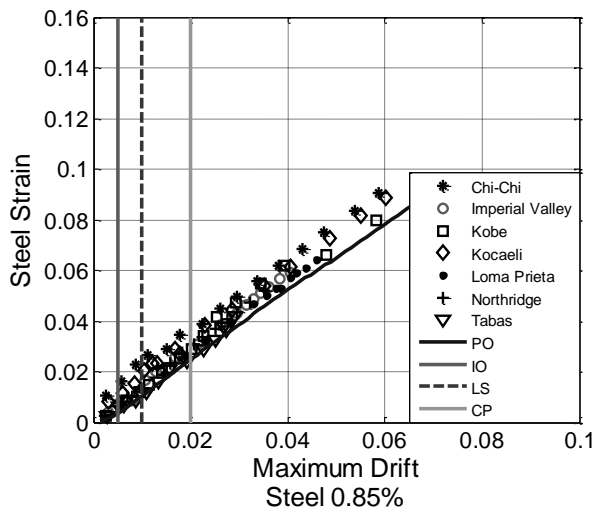


Figure 55 Steel Strain vs. Drift - Frame 2



**Figure 56** Steel Strain vs. Drift - Frame 3

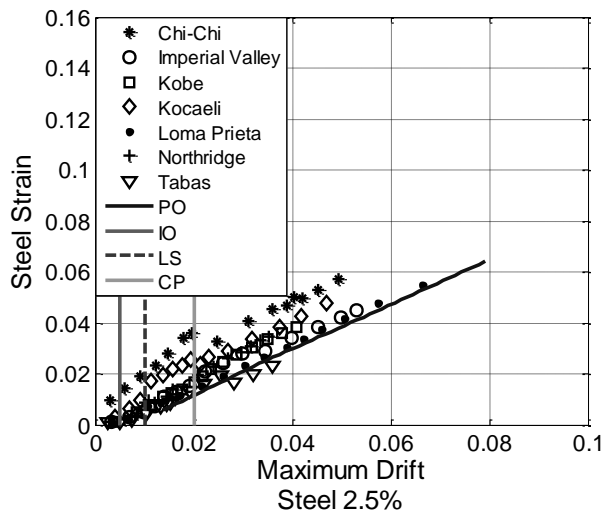
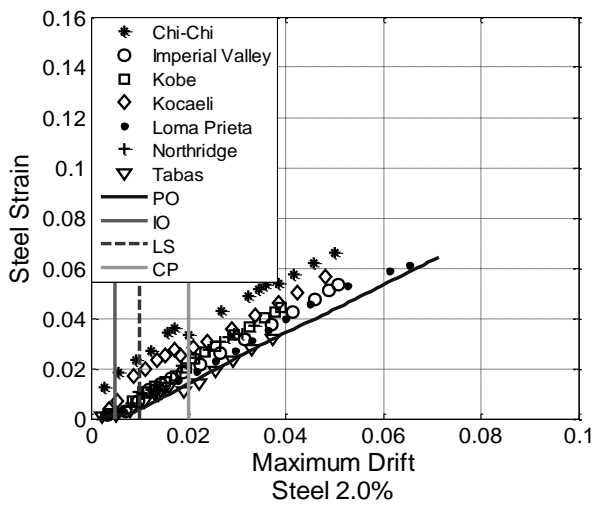
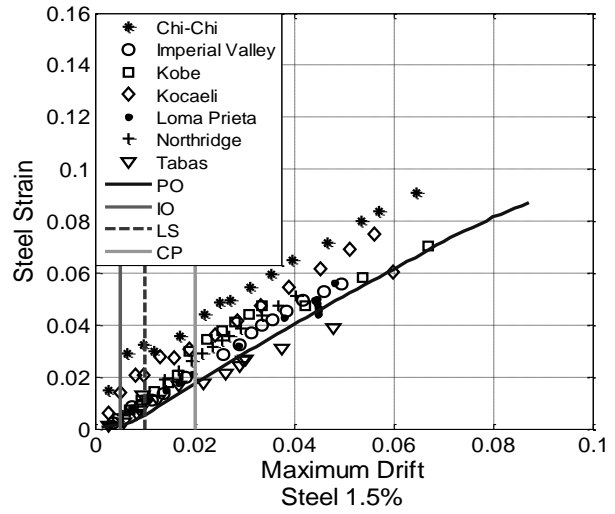
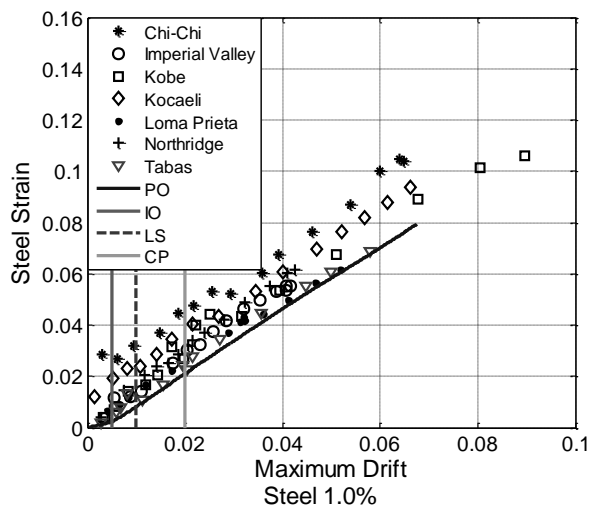
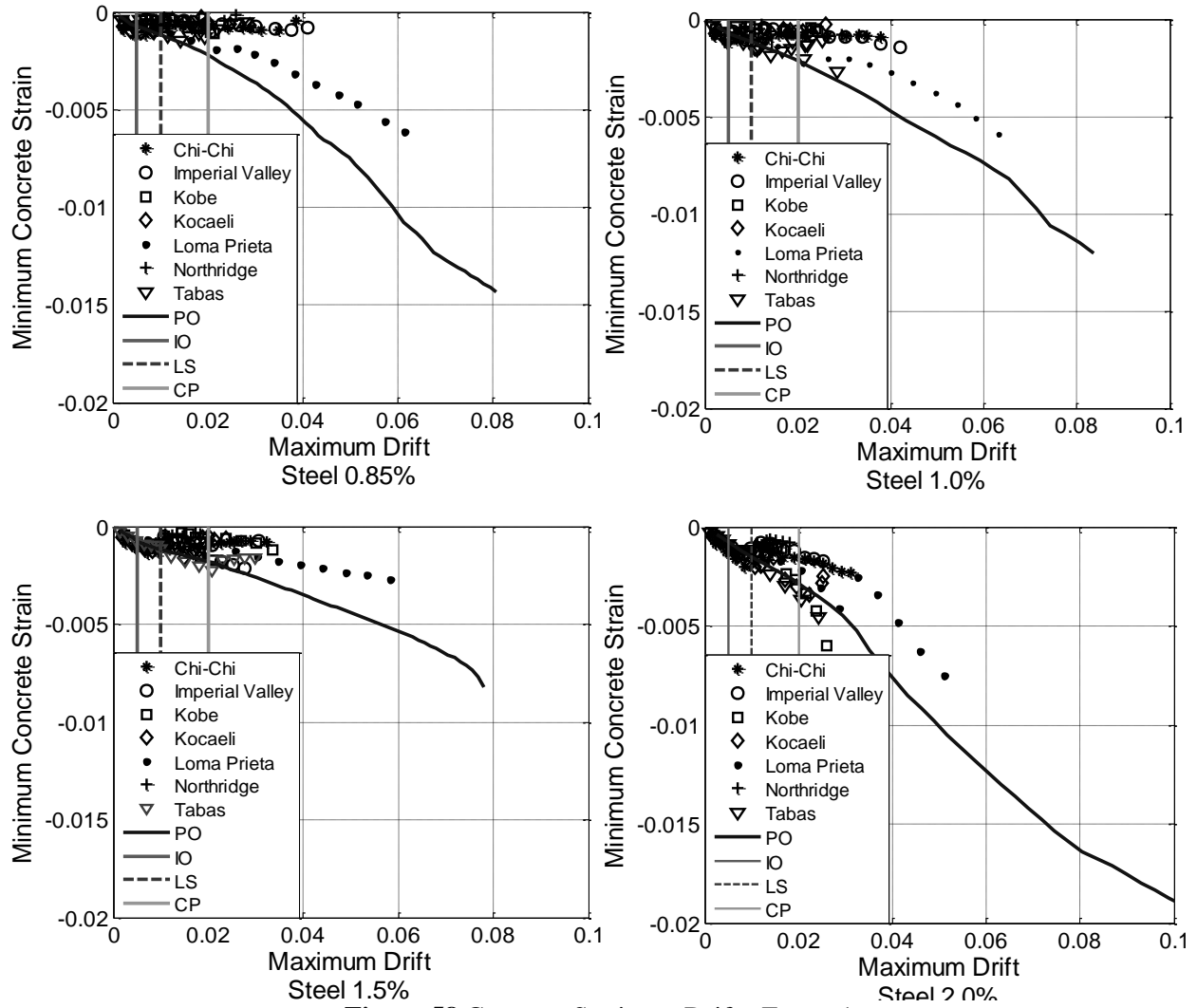
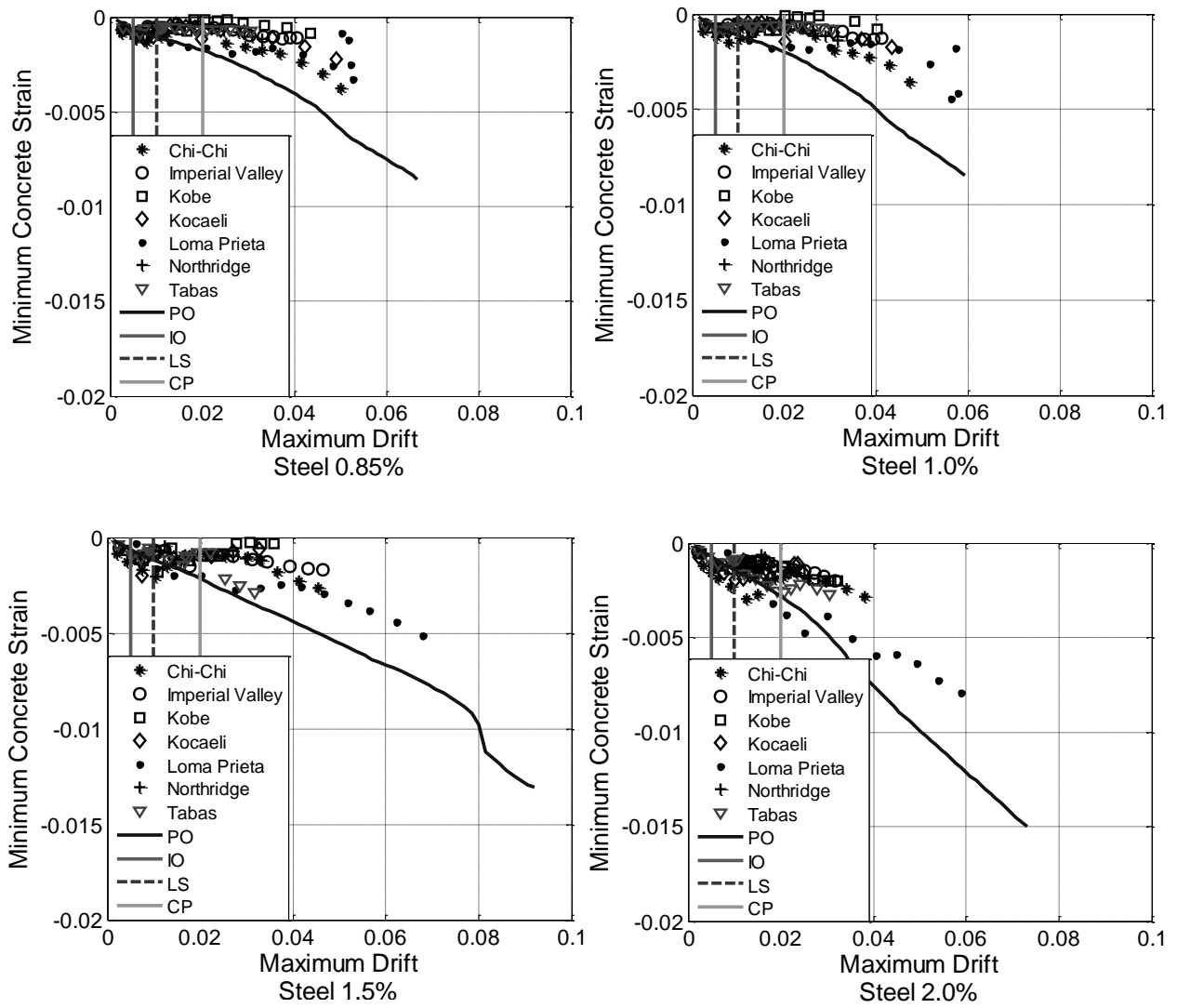


Figure 57 Steel Strain vs. Drift - Frame 4



**Figure 58** Concrete Strain vs. Drift - Frame 1



**Figure 59** Concrete Strain vs. Drift - Frame 2

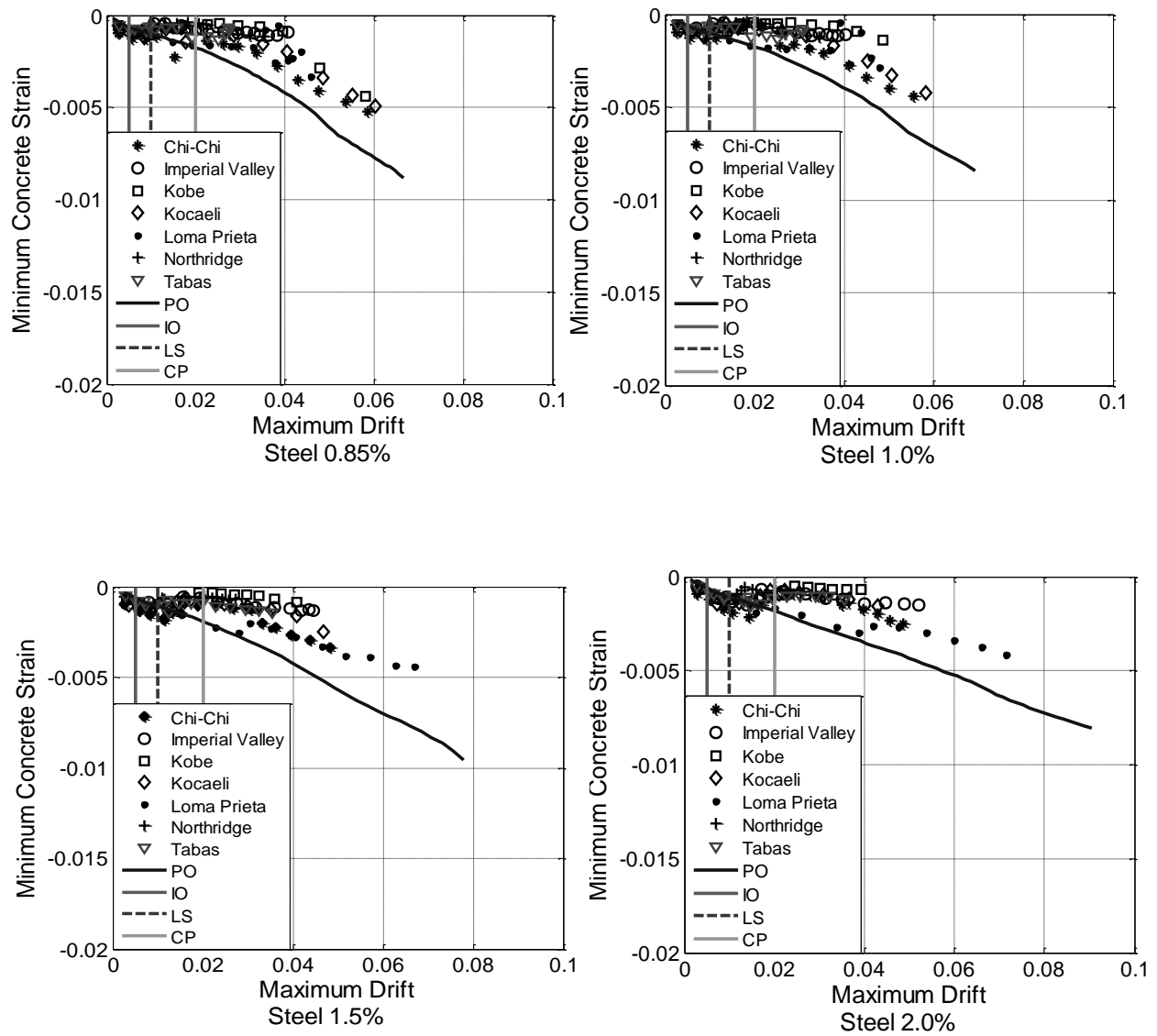


**Figure 60** Concrete Strain vs. Drift - Frame 3

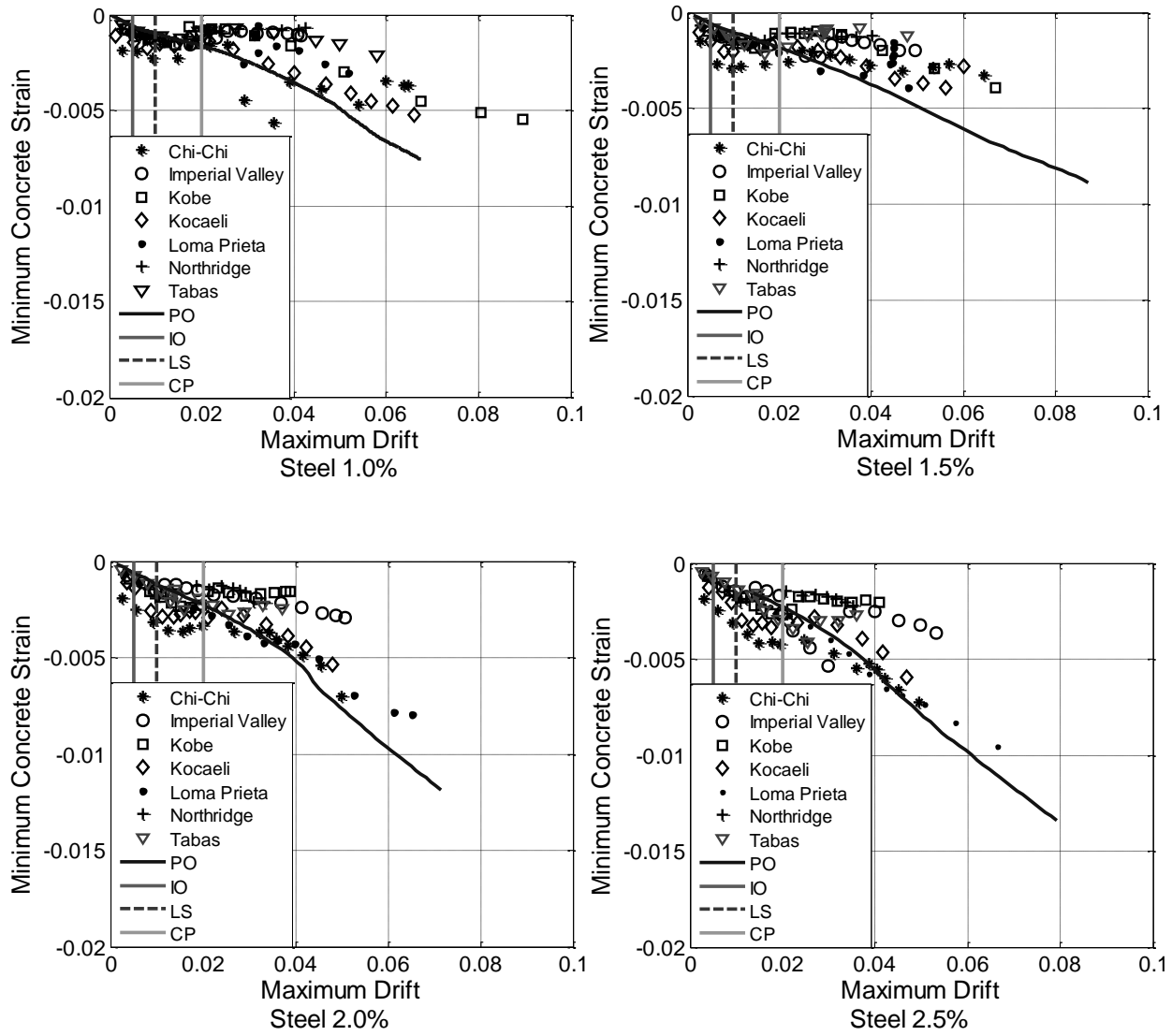


**Figure 61** Concrete Strain vs. Drift - Frame 4

### 5.3. STEEL AND CONCRETE STRAINS RESULTS-3D FRAME

#### 5.3.1. Strain as function of PGA values

For the 3D frame the maximum drift value was determined in the X direction and Z for the beams and girders. Also, in this model the strains and other parameters were obtained in the columns. Maximum values of drifts and strains were found for each intensity level of the earthquakes (Low, Medium, Reference and High). Similar to the 2D frames, with the values of drift limit states (IO, LS, CP), from ASCE 41-06, an interpolation was performed to find the values of tension steel and concrete compression strains at these limits. The yield beam and yield frame drifts were also used to obtain the strains at these limits. The strain (steel and concrete) results are shown in Figures 62 as function of PGA including the values of strains at ASCE 41-06 limit-states. Figure 63 displays the results obtained for the columns. The strains for the columns are the average values obtained from the four columns of the 3D frame.

In the beams (transversal direction) and girders (longitudinal direction), the steel strain has a linear relation with the PGA. However, for the compression concrete strains in the beams and girders the behavior displays a higher variability. For the columns, the behavior shown in the plots (Figure 63) suggests a directly proportional relationship of the strain and the PGA. It can also be observed that the steel and concrete strains obtained at the columns are higher than the strains in the beams, due to the weak columns-strong beam mechanism. This 3D frame, tested at the 15<sup>th</sup> WCEE, simulated conditions of frames with insufficient seismic detailing. All cases exceed the IO limits in the four intensity levels for the beams and girders. In addition, the medium and reference intensity level also exceeded the LS limits, and the high intensity level is the only that exceeded the CP limits for beam and girders. Also, for the columns, all cases exceed the IO limit, the medium intensity level also exceeded the LS limit. The CP limit state was exceeded for the reference and high ground motion intensity.

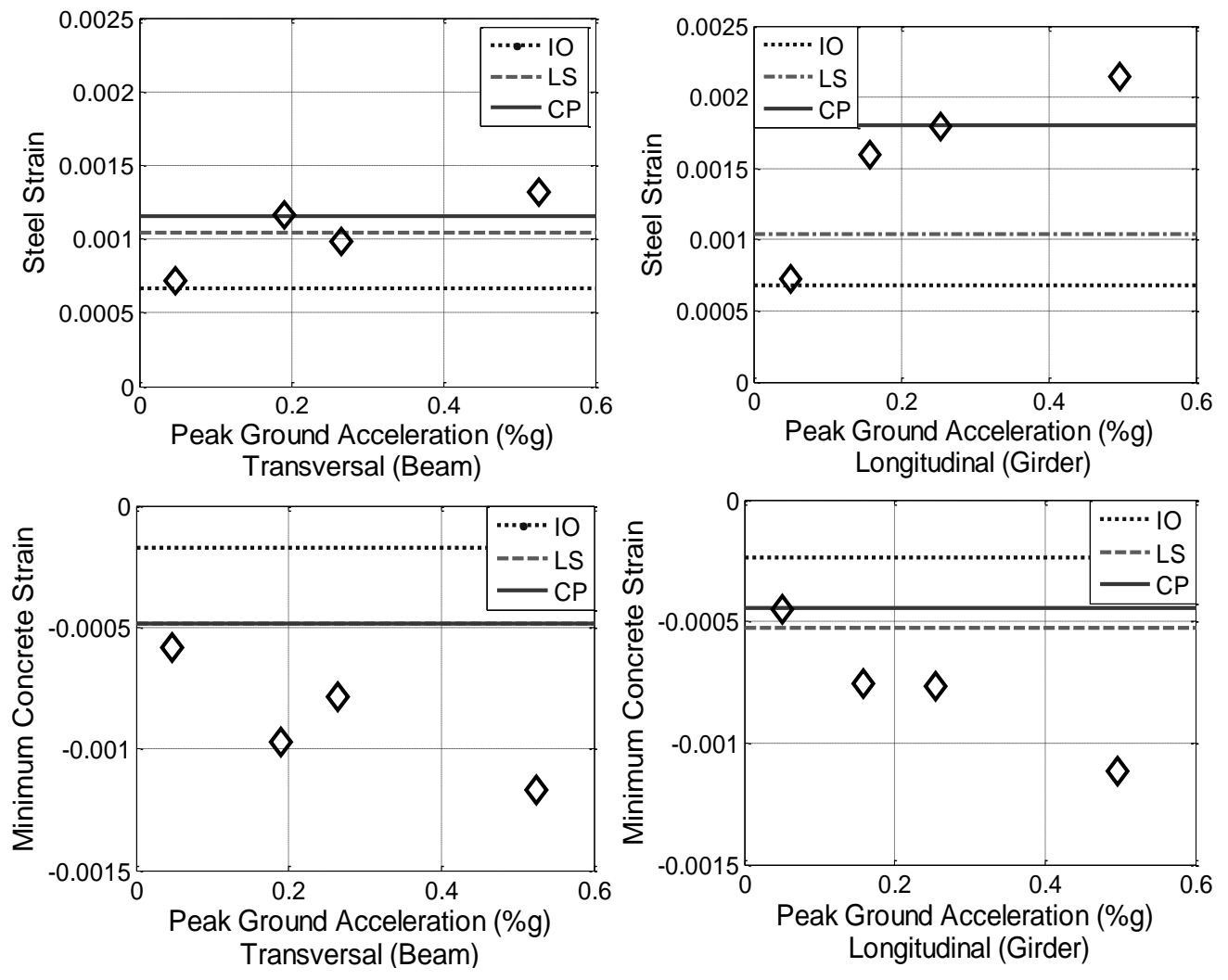


**Figure 62** Strain vs. PGA (Beam and Girder)

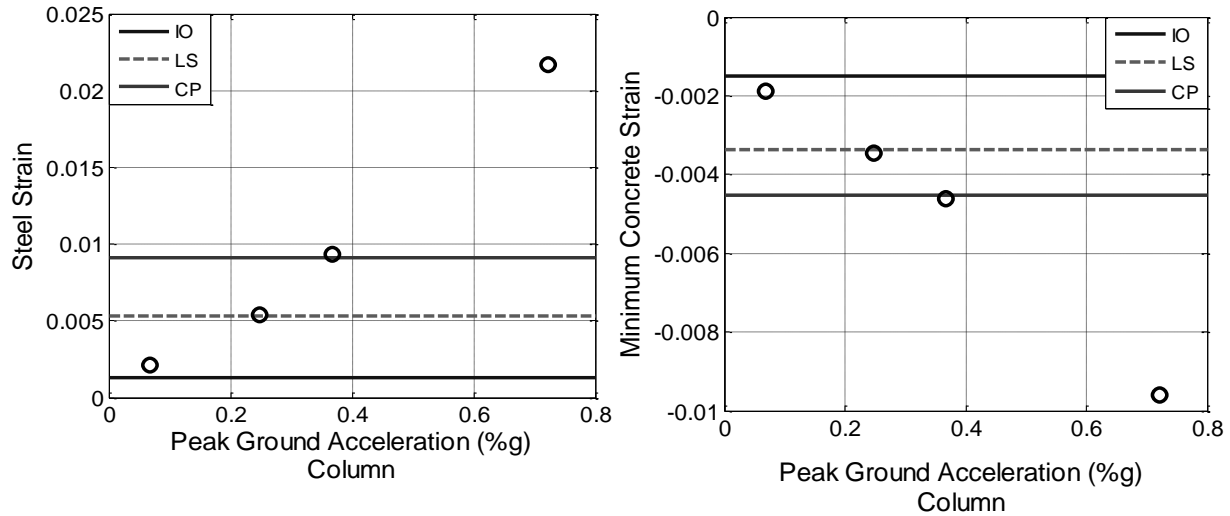


**Figure 63** Strain vs. PGA (Columns)

### 5.3.2. Strains as a function of drift

For the beams, girders, and columns the steel and concrete strains as function of maximum drift values are shown in Figure 64 through 66. On these plots are also shown the values of ASCE 41-06 drift limit states and the pushover analysis (PO) response. Figure 64 shows that for both directions and materials, the results from the pushover analyses have a good correlation with the results obtained from the dynamic analyses. This helps to gain confidence in the definition of limit states for rehabilitation codes based on monotonic analyses.

For the 3D frame the strain and drift at the columns were analyzed and are shown in Figure 65-66. These figures present the maximum values of strains and drifts for the four columns of the frame. Columns 1 and 2 are the ones connected with the slab and columns 3 and 4 are in the opposite side. The drift values shown for the columns were calculated as the square root of the sum of the squares of the drift in X and Z directions. In Figures 65 and 66 are presented the strain and drift values for each column and in the fifth plot in each figure the average values of all columns are shown. From the average results (fifth graph) of both figures

(65 and 66), it can be seen that the pushover analysis results have an excellent correlation with the values obtained from the dynamic analysis. For the pushover analysis the total dead load was located at the master node, which was at the center of the slab. The discussion of the implications of these limits on the results was included in the previous section.

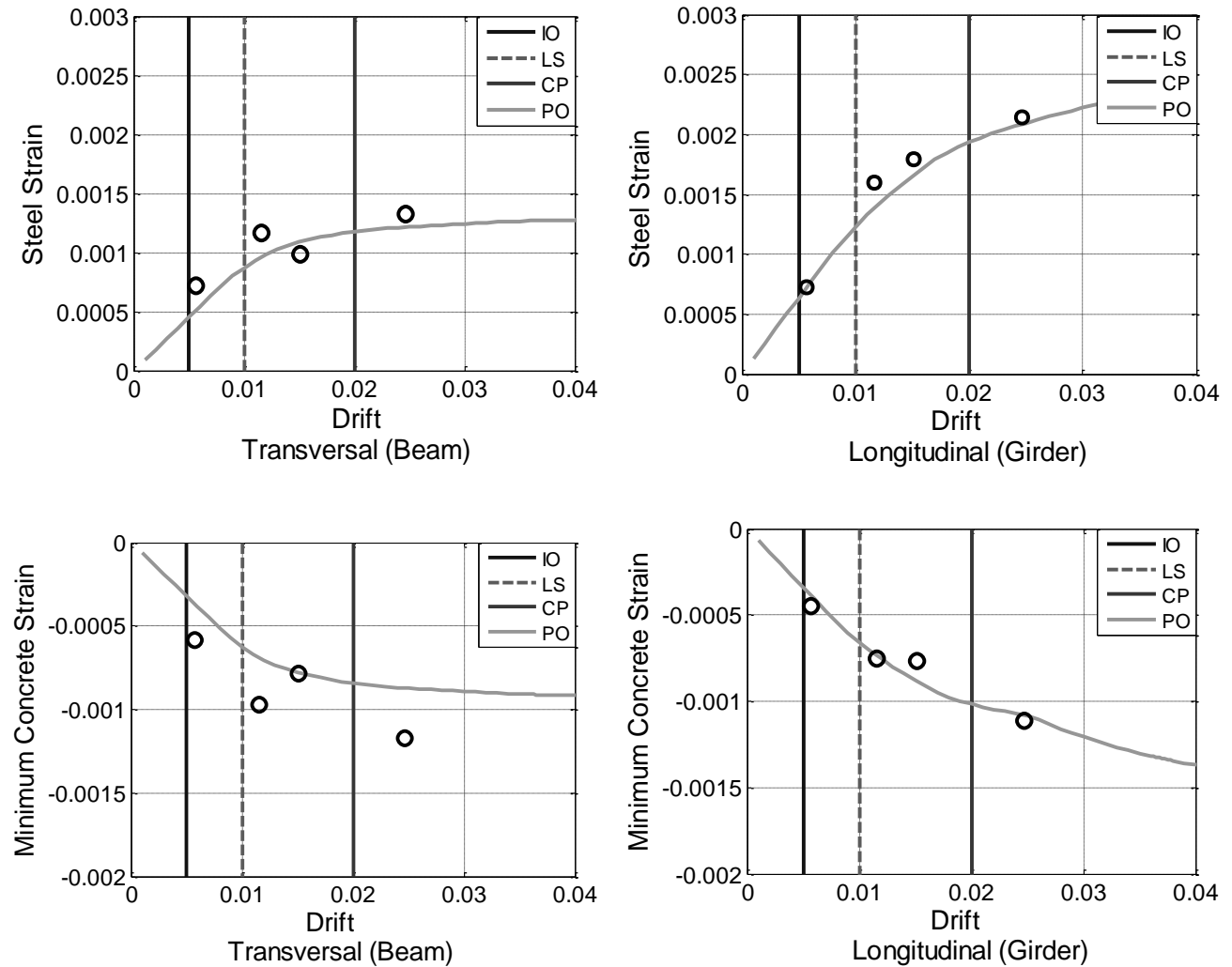


**Figure 64** Strain vs. Drift

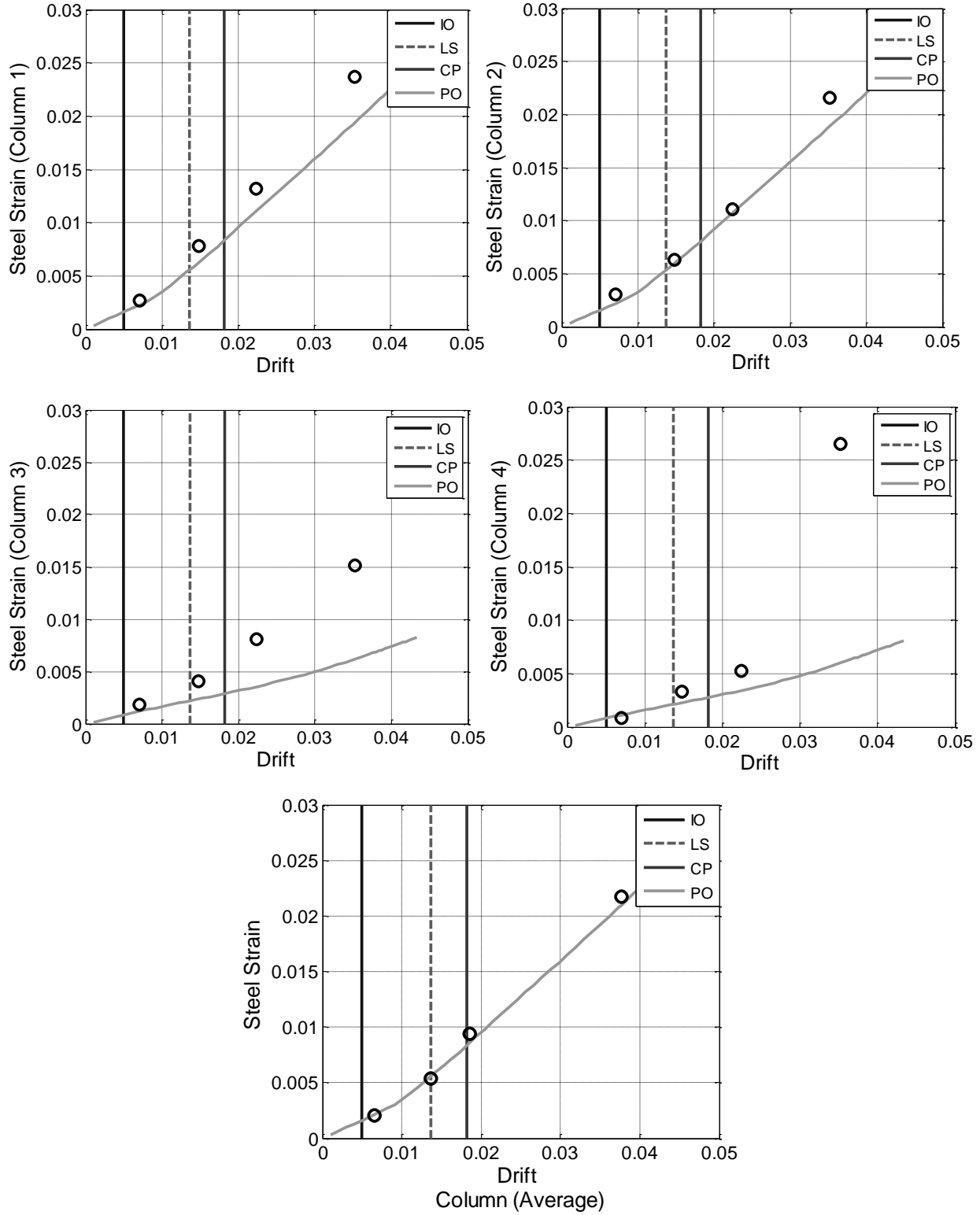


**Figure 65 Steel Strain vs. Drift (Columns)**

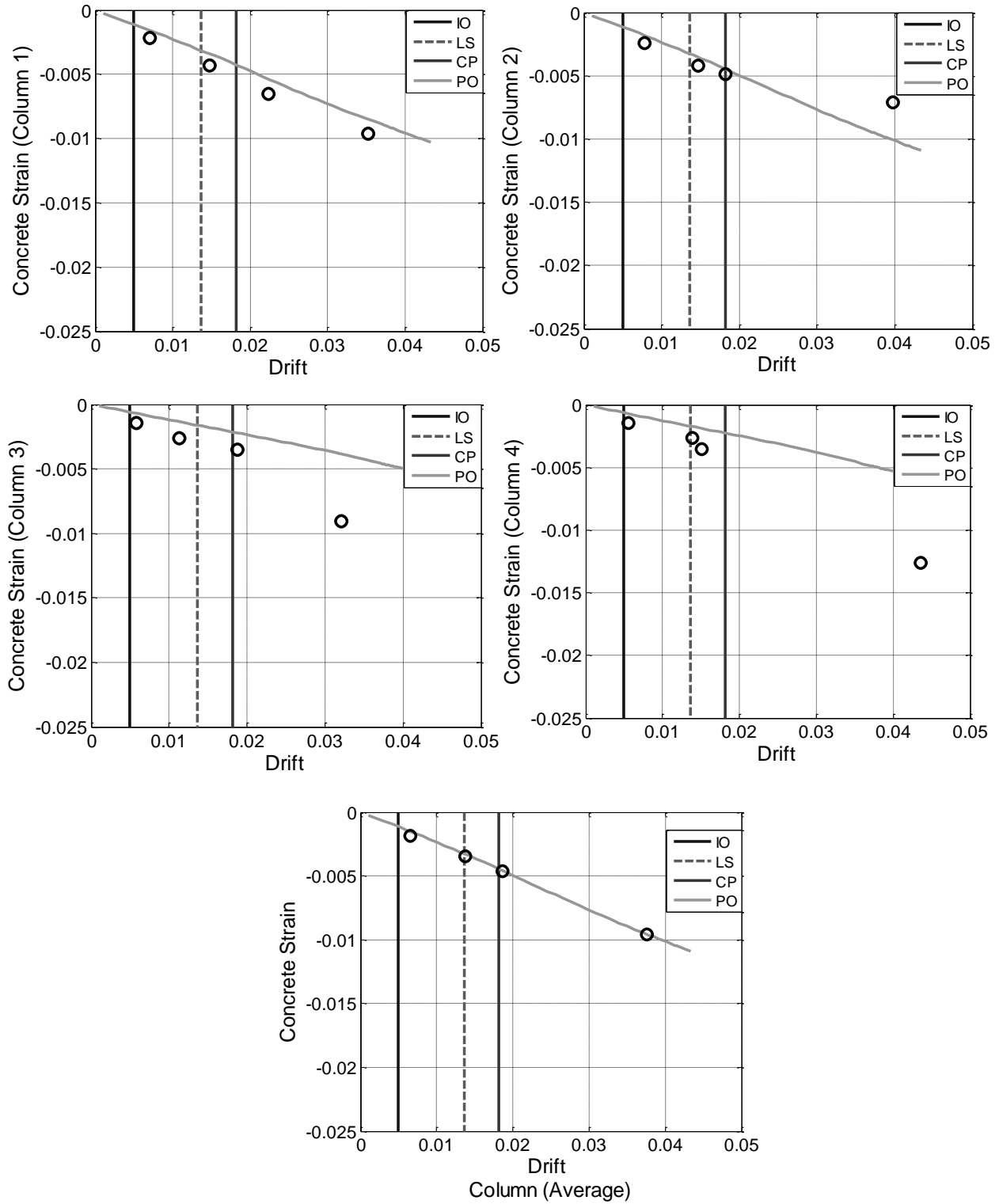


**Figure 66** Concrete Strain vs. Drift (Columns)

## CHAPTER 6: Seismic Hysteretic Energy Limits for 2D frames

### 6.1. INTRODUCTION

As stated by Estes and Anderson (2002) in his study “*Hysteretic Energy Demands in Multistory Buildings*”, the hysteretic energy dissipation needs to be used in the analysis and design process for frames because it represents a measure of the amount of damage that structure can withstand. Also, from the direct relation of the hysteretic energy and cumulative ductility the inelastic deformations in structural members can be obtained (Estes and Anderson, 2004). In this chapter, the methodology used to calculate the seismic hysteretic energy in the 2D frames is described.

### 6.2. SEISMIC HYSTERETIC ENERGY

The seismic hysteretic energy was calculated using the area under the moment vs rotation curve obtained during the analyses of the 2D frames. The moment and rotation at the beams on the story with the maximum drift were obtained from the OpenSEES runs. The hysteretic energy was calculated at each hinge and added to each one to obtain the total hysteretic energy dissipated in the story. This was performed using the *polyarea* function of the Matlab<sup>®</sup> computer program. For each frame and four earthquakes (only at 1.5 g) a curve of the displacement and seismic hysteretic energy vs time is presented in Appendix I. For these curves the earthquakes shown are the Chi-Chi (EQ 1) , Kocaeli (EQ 4), Northridge (EQ 6) and Tabas (EQ 7), which are the two with the highest (EQ 1 and 2) and lowest (EQ 6 and 7) Mw intensity.

In Figures 67 through 78 are illustrated the Seismic Hysteretic Energy vs. Drift, PGA and Ductility curves obtained from the analyses and calculations for the 2D frames (aspect ratios varied from 7.5 to 12 and with different reinforcing steel ratios). The energies are shown as

function of these three parameters for comparison purposes. The ductility can give a better sense of the displacement capacity of the frame. For all 2D frames the seismic hysteretic energy dissipated by the Chi-Chi and Kocaeli earthquake were greater than for the rest of the earthquakes. As shown in Chapter 3, these earthquakes are the ones with the largest Arias Intensity, Cummulative Absolute Velocity and Specific Energy Density. Maximum drifts that varied from 3% to almost 7% were found depending on the earthquake, which are translated into ductility values ranging from 3 to almost 10.

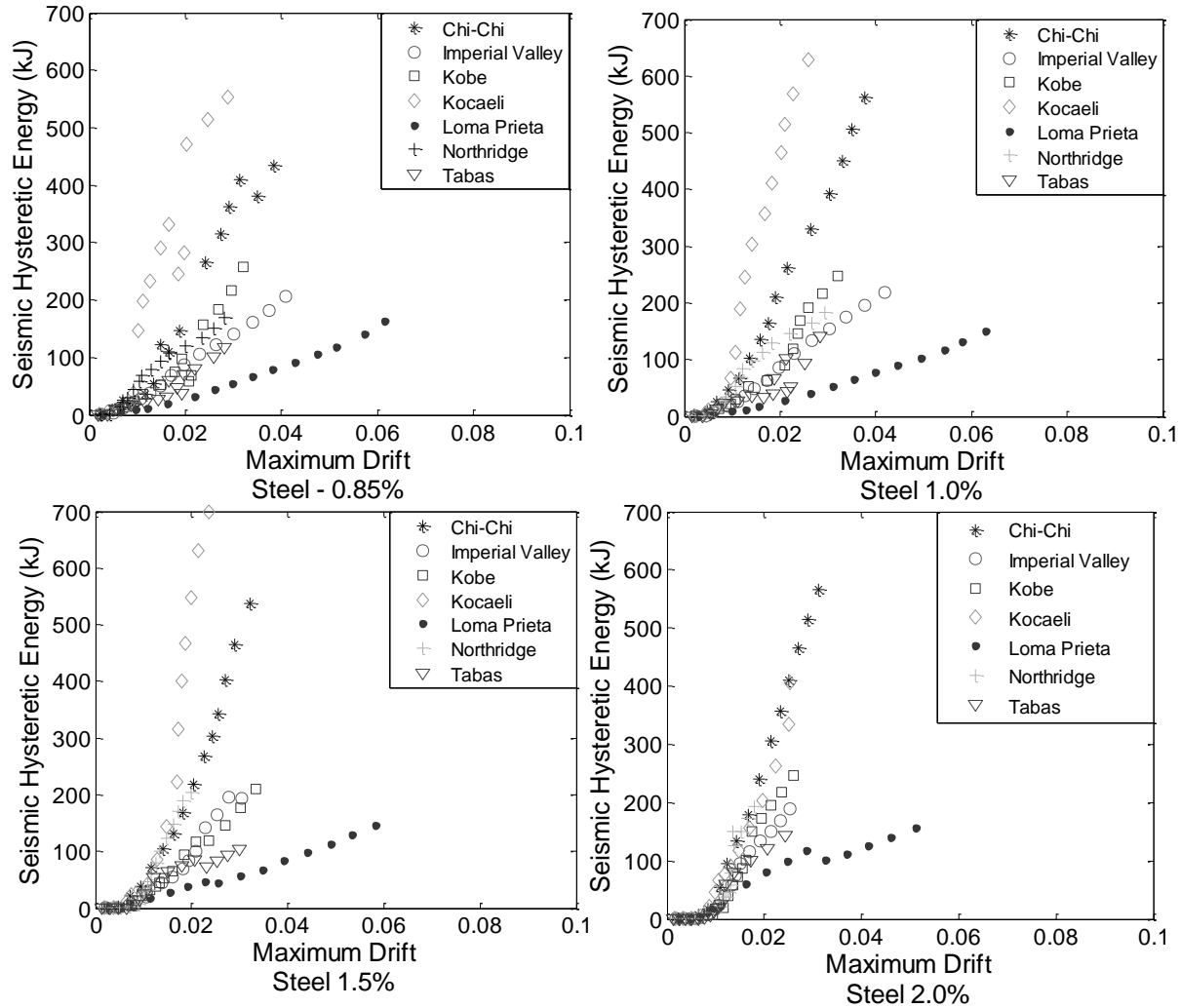


**Figure 67** Seismic Hysteretic Energy vs. Drift - Frame 1

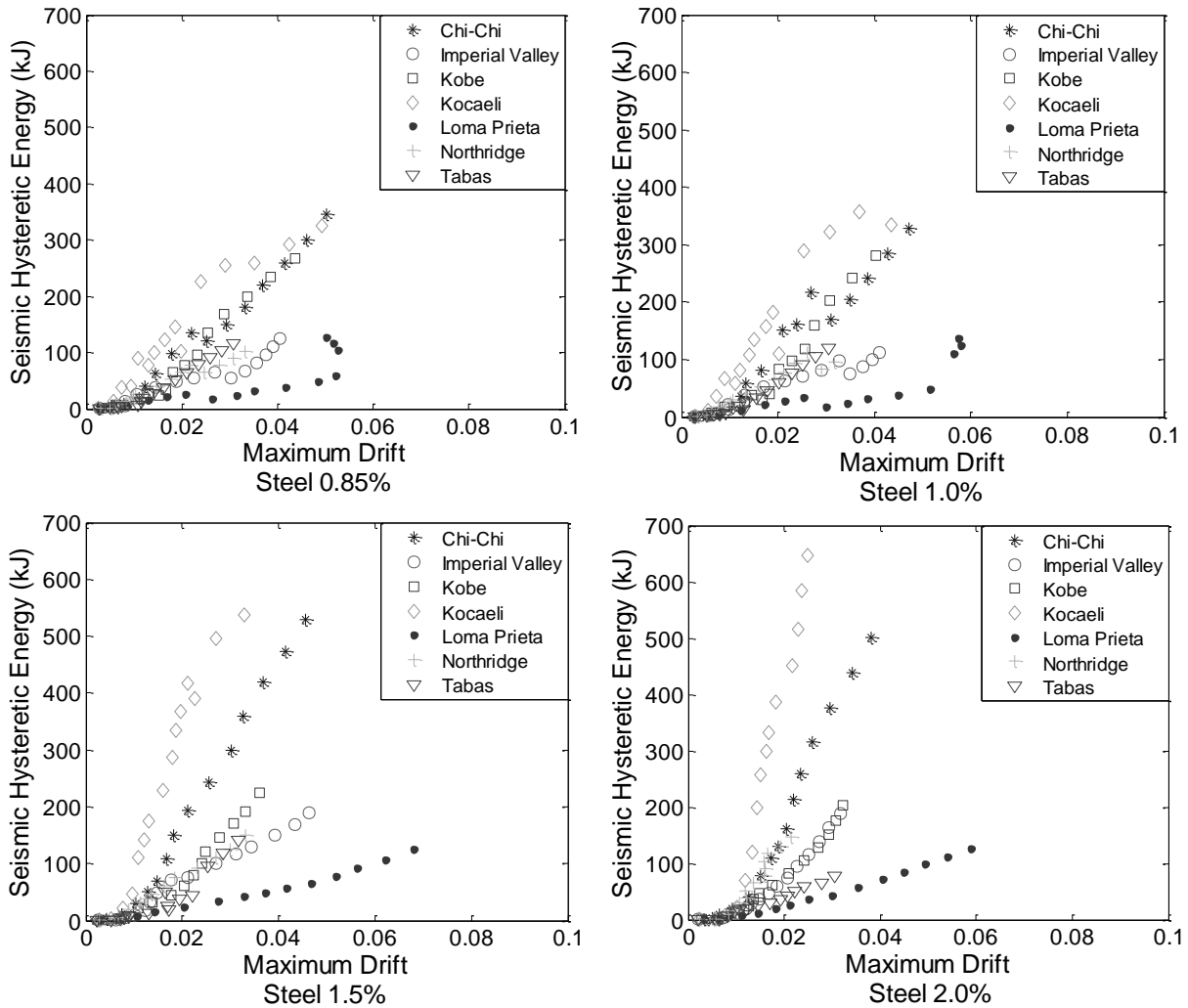


**Figure 68** Seismic Hysteretic Energy vs. Drift - Frame 2

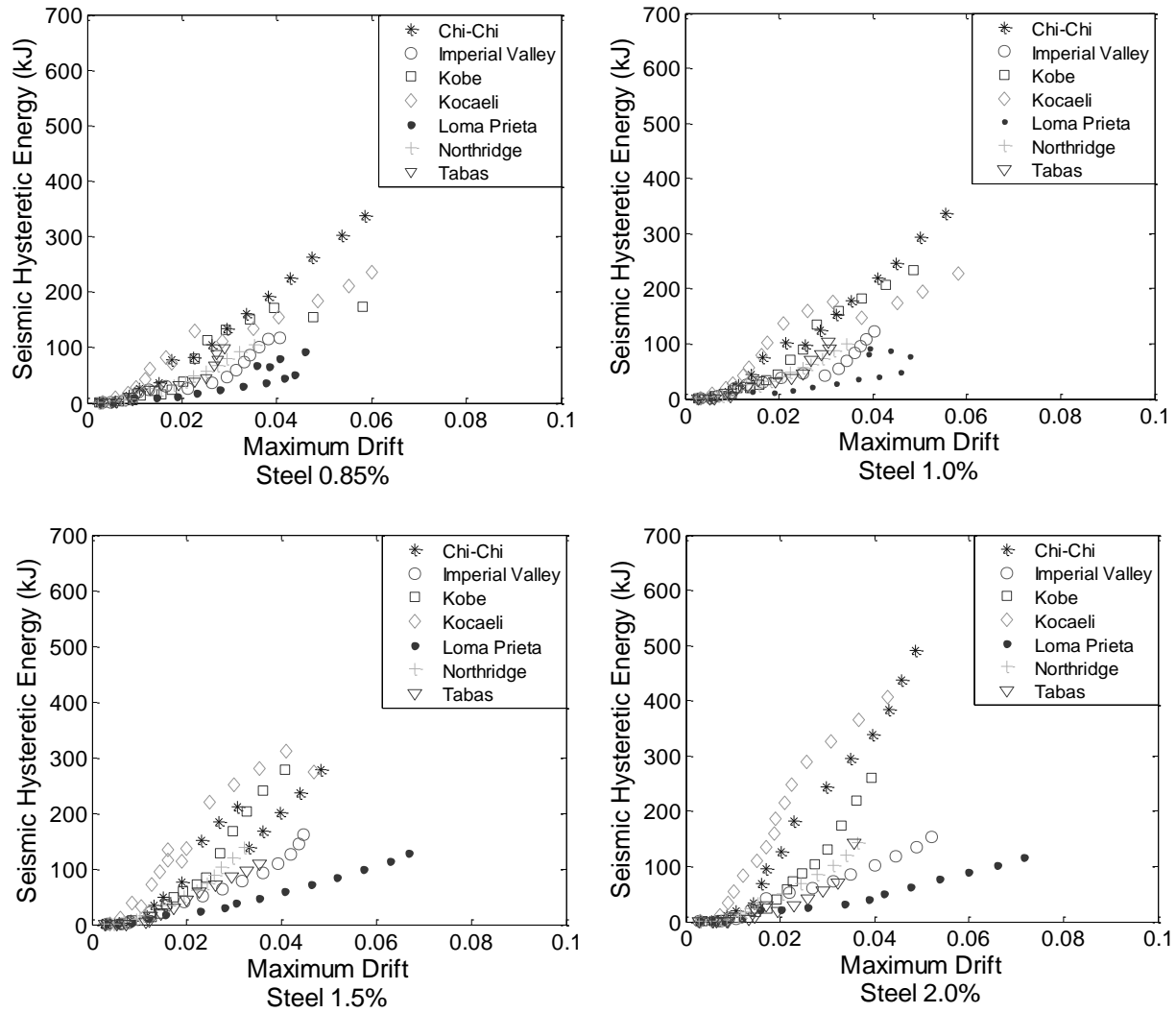


**Figure 69** Seismic Hysteretic Energy vs. Drift - Frame 3

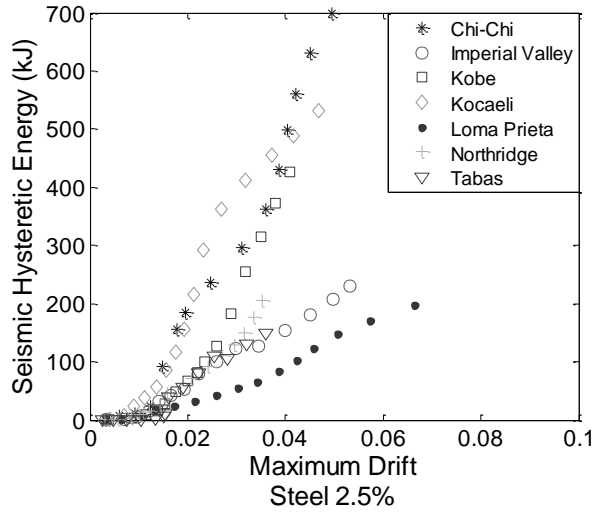
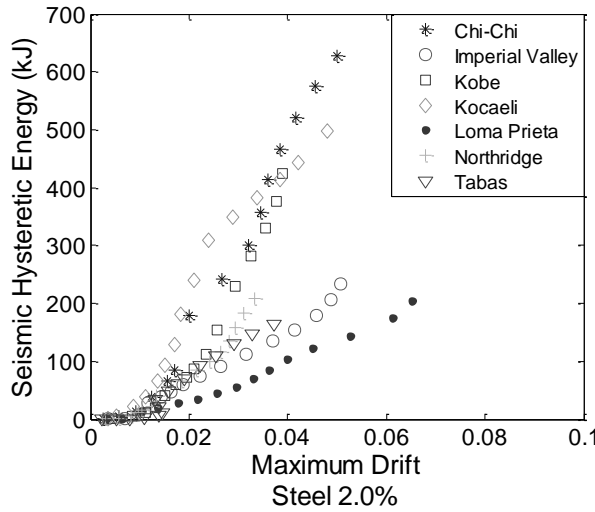
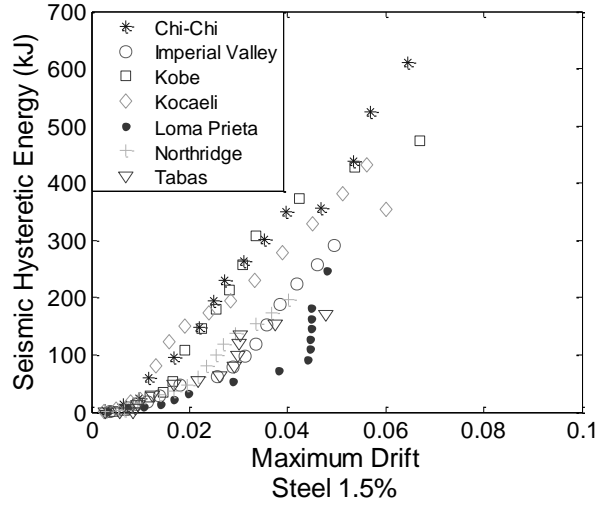
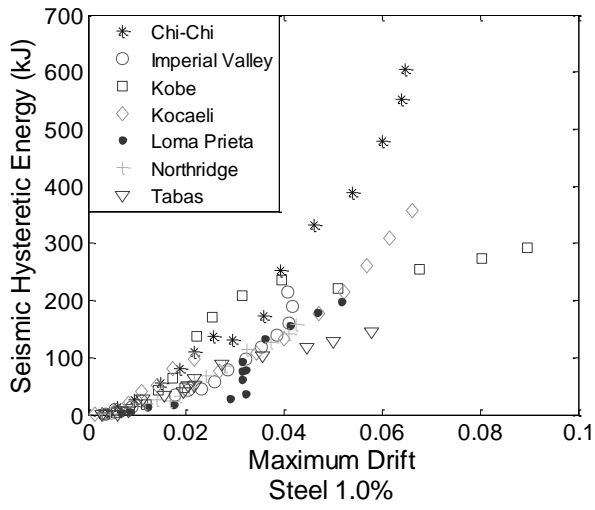


**Figure 70** Seismic Hysteretic Energy vs. Drift - Frame 4

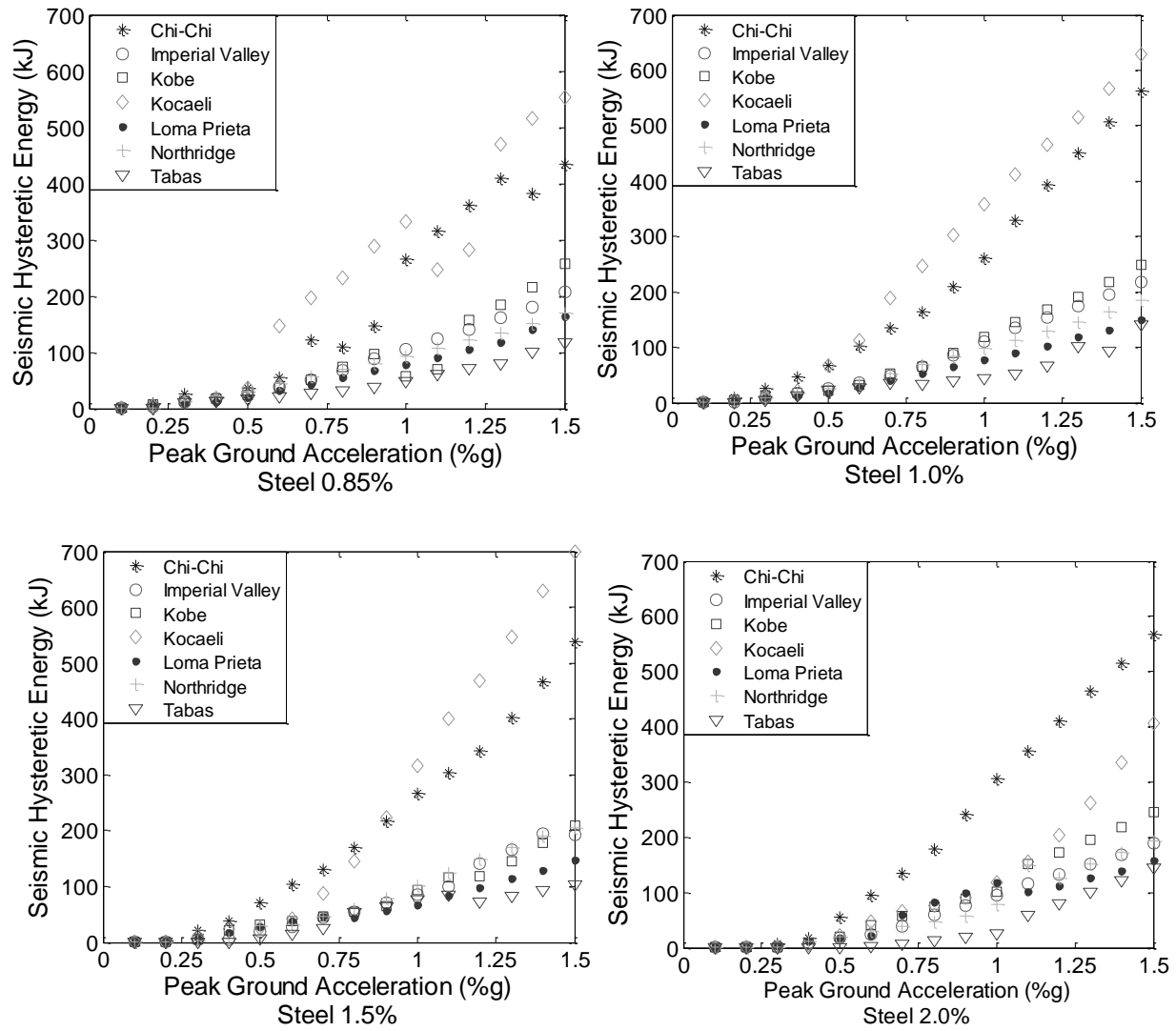


**Figure 71** Seismic Hysteretic Energy vs. PGA - Frame 1

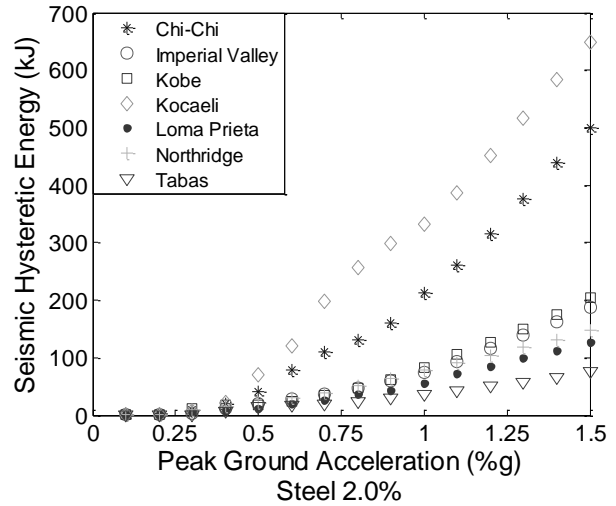
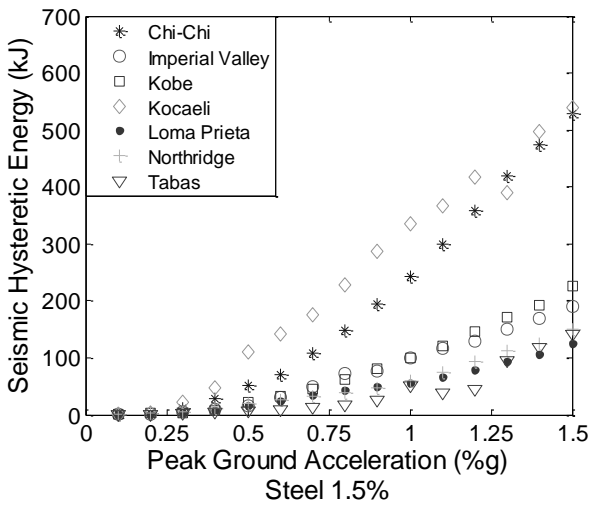
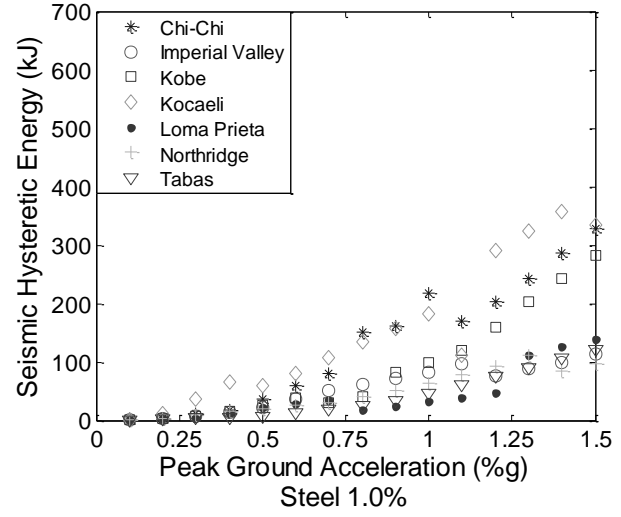
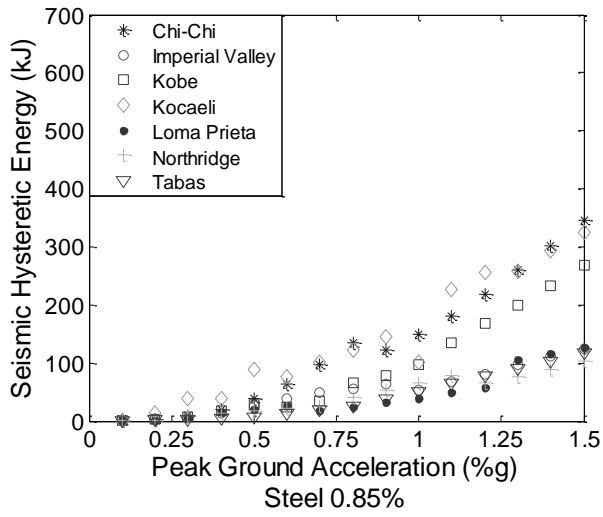


**Figure 72** Seismic Hysteretic Energy vs. PGA - Frame 2

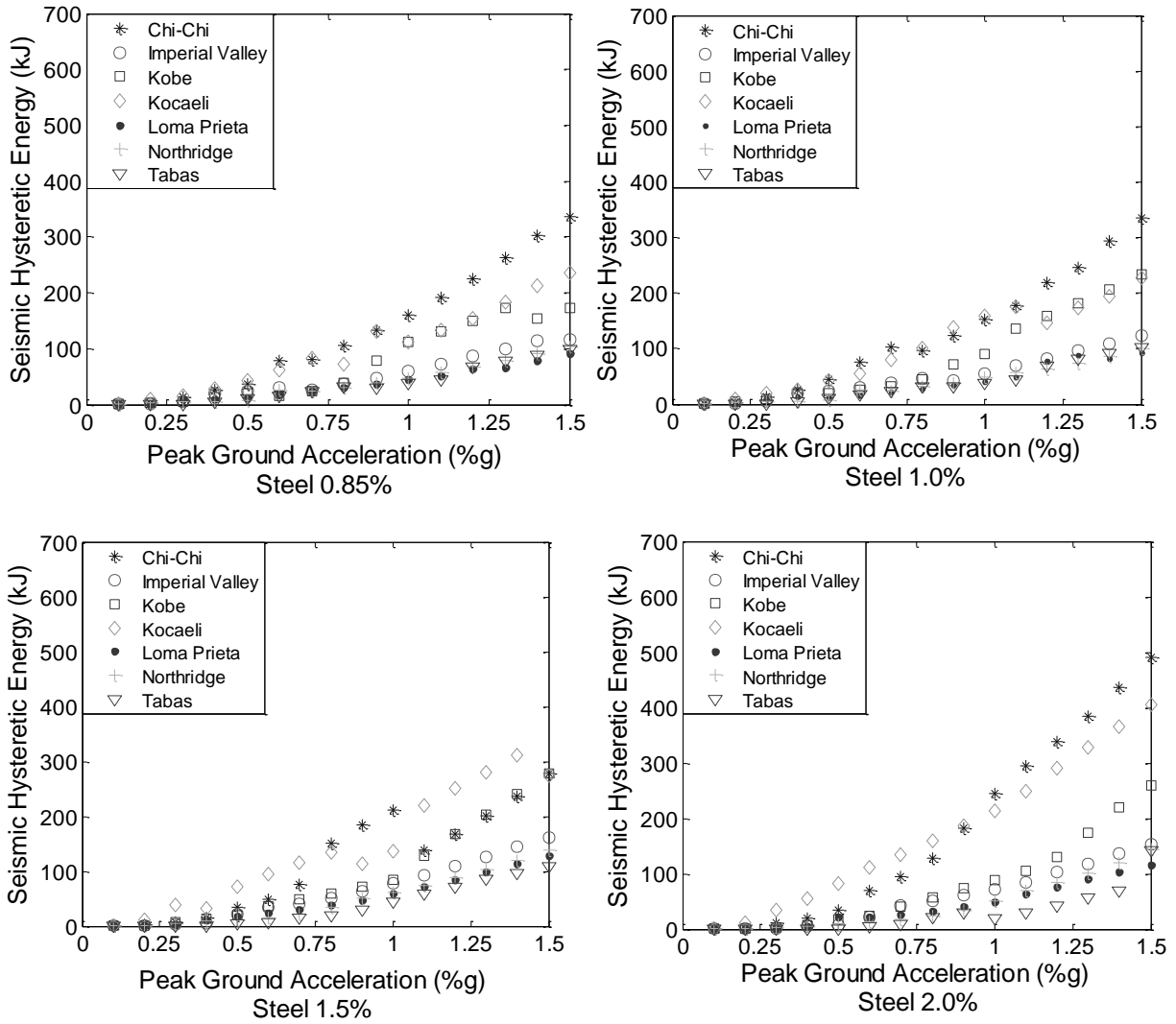


**Figure 73** Seismic Hysteretic Energy vs. PGA - Frame 3

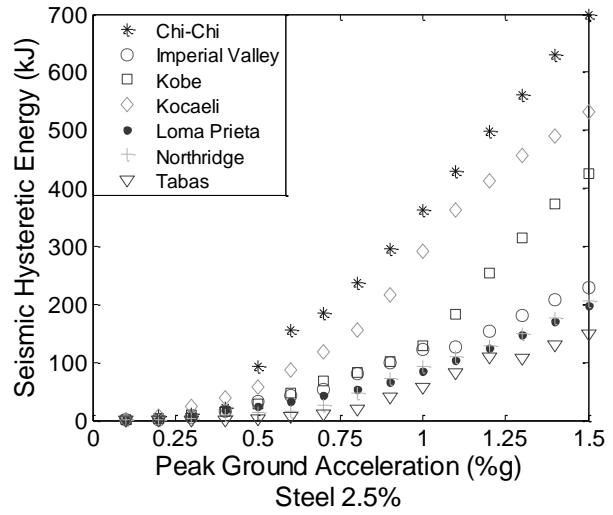
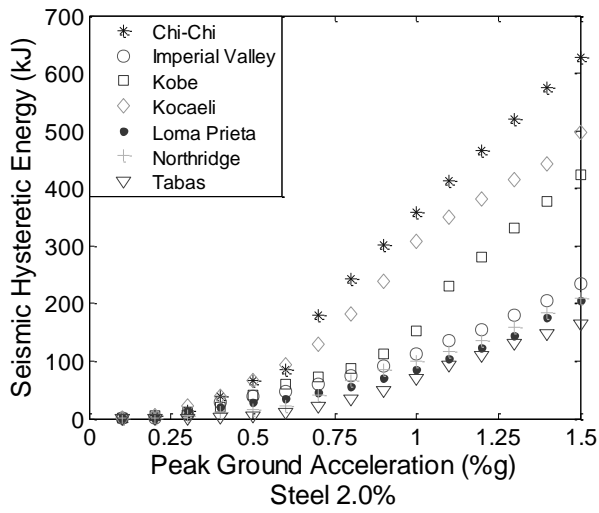
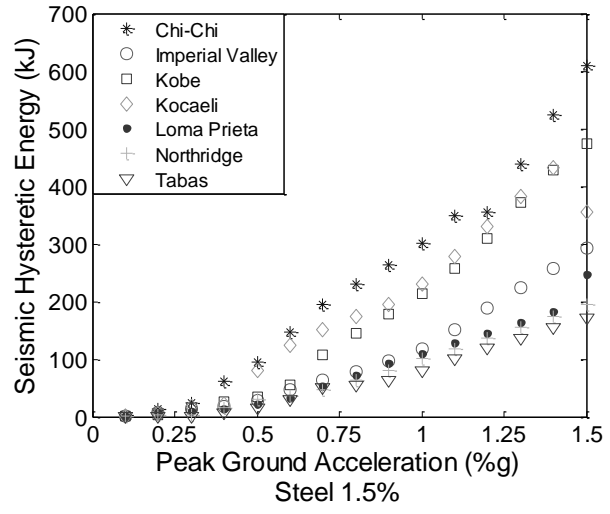
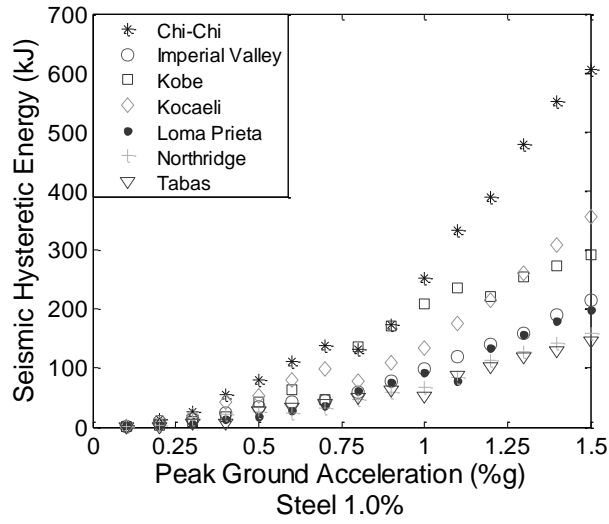


**Figure 74** Seismic Hysteretic Energy vs. PGA - Frame 4

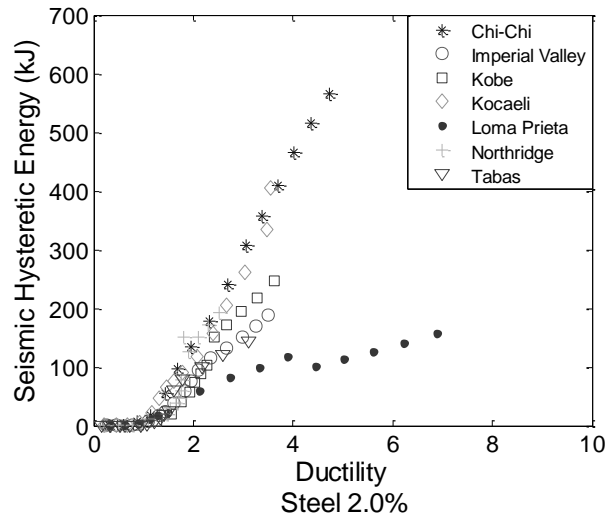
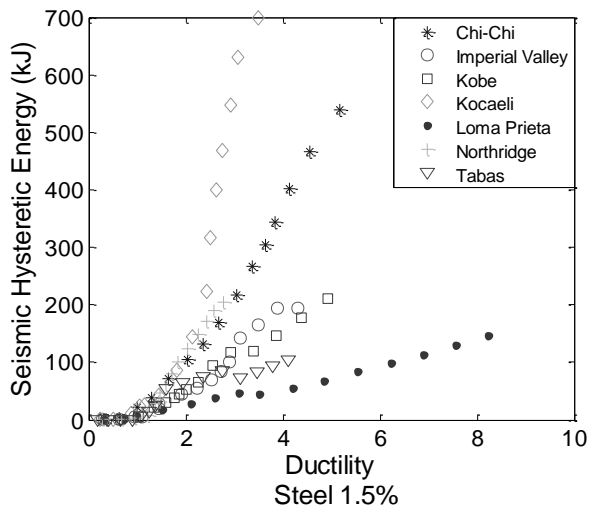
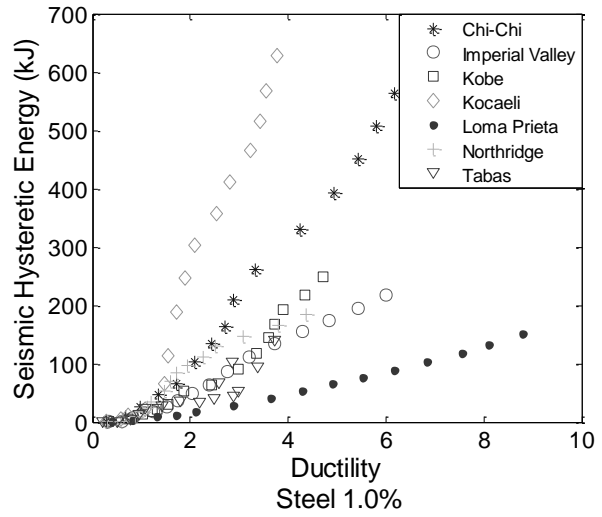
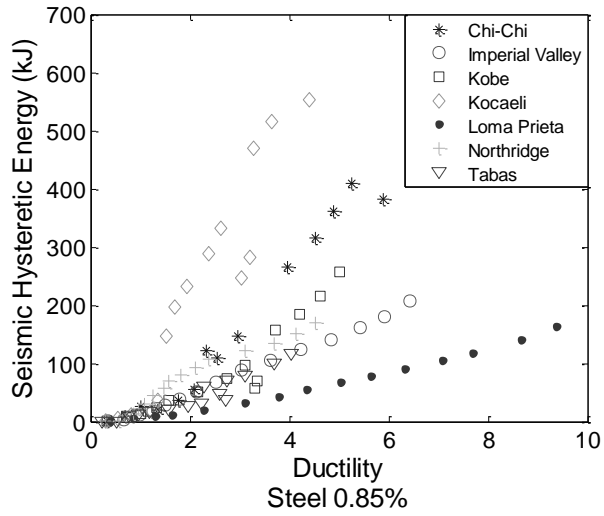


**Figure 75** Seismic Hysteretic Energy vs. Ductility - Frame 1

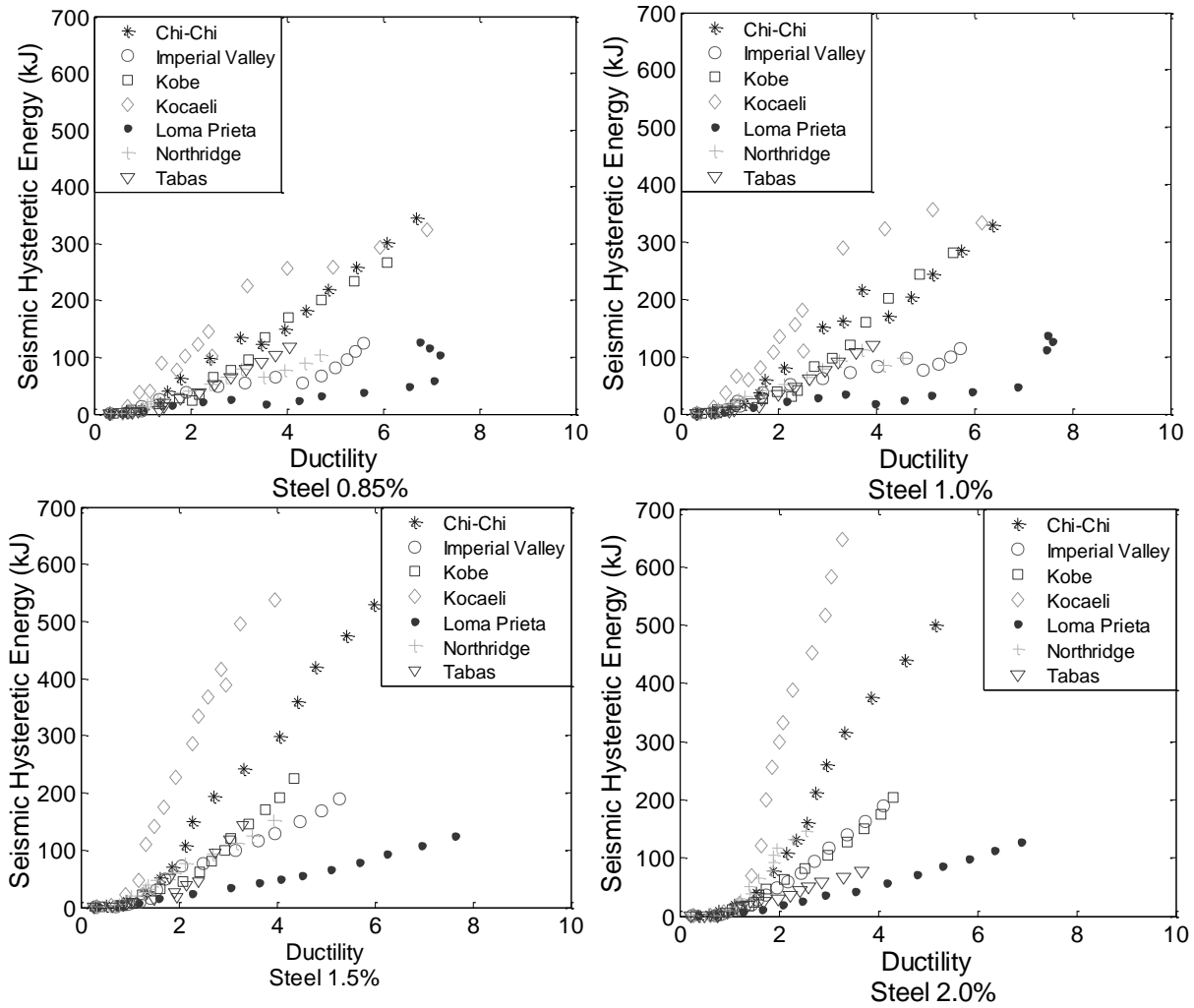


**Figure 76** Seismic Hysteretic Energy vs. Ductility - Frame 2

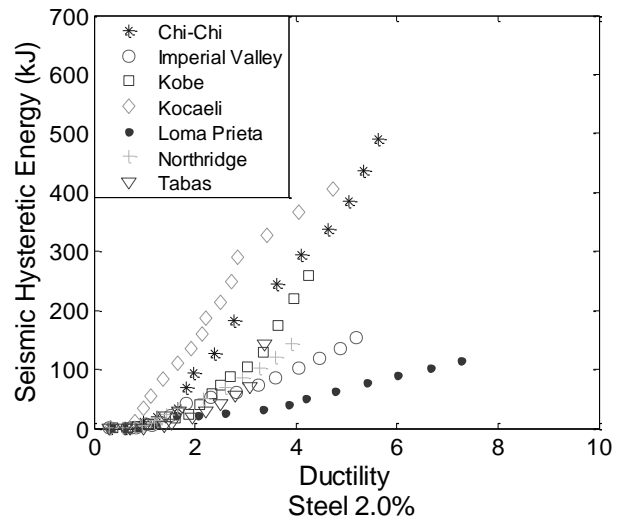
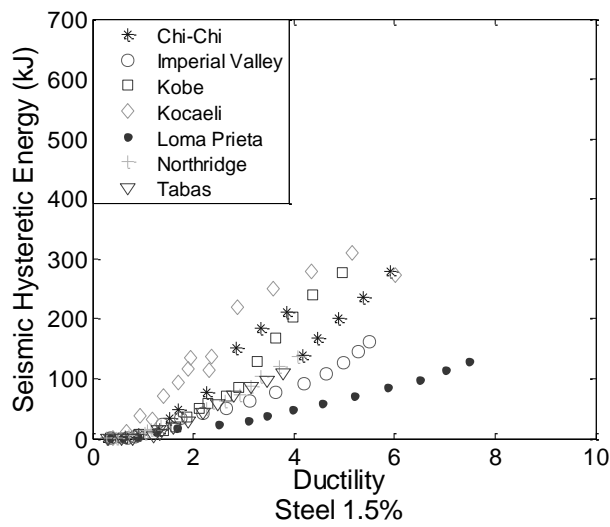
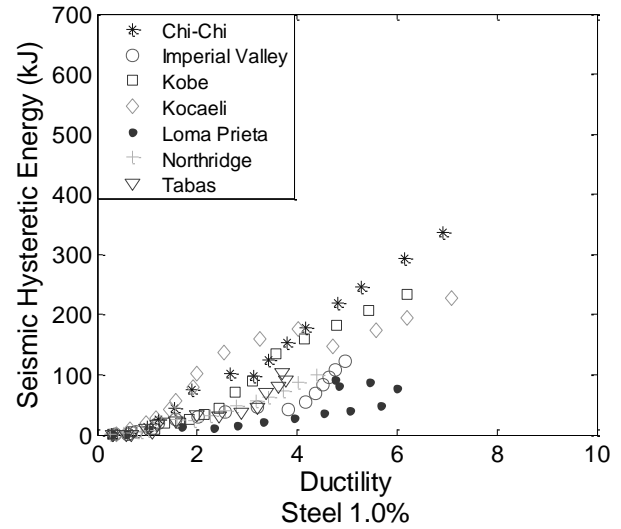
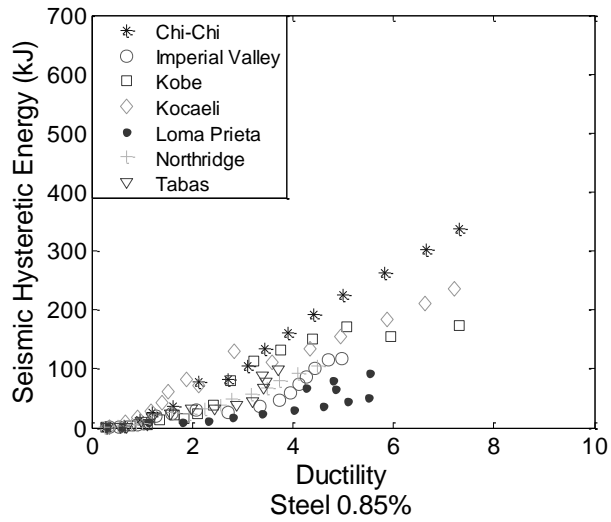


**Figure 77** Seismic Hysteretic Energy vs. Ductility - Frame 3

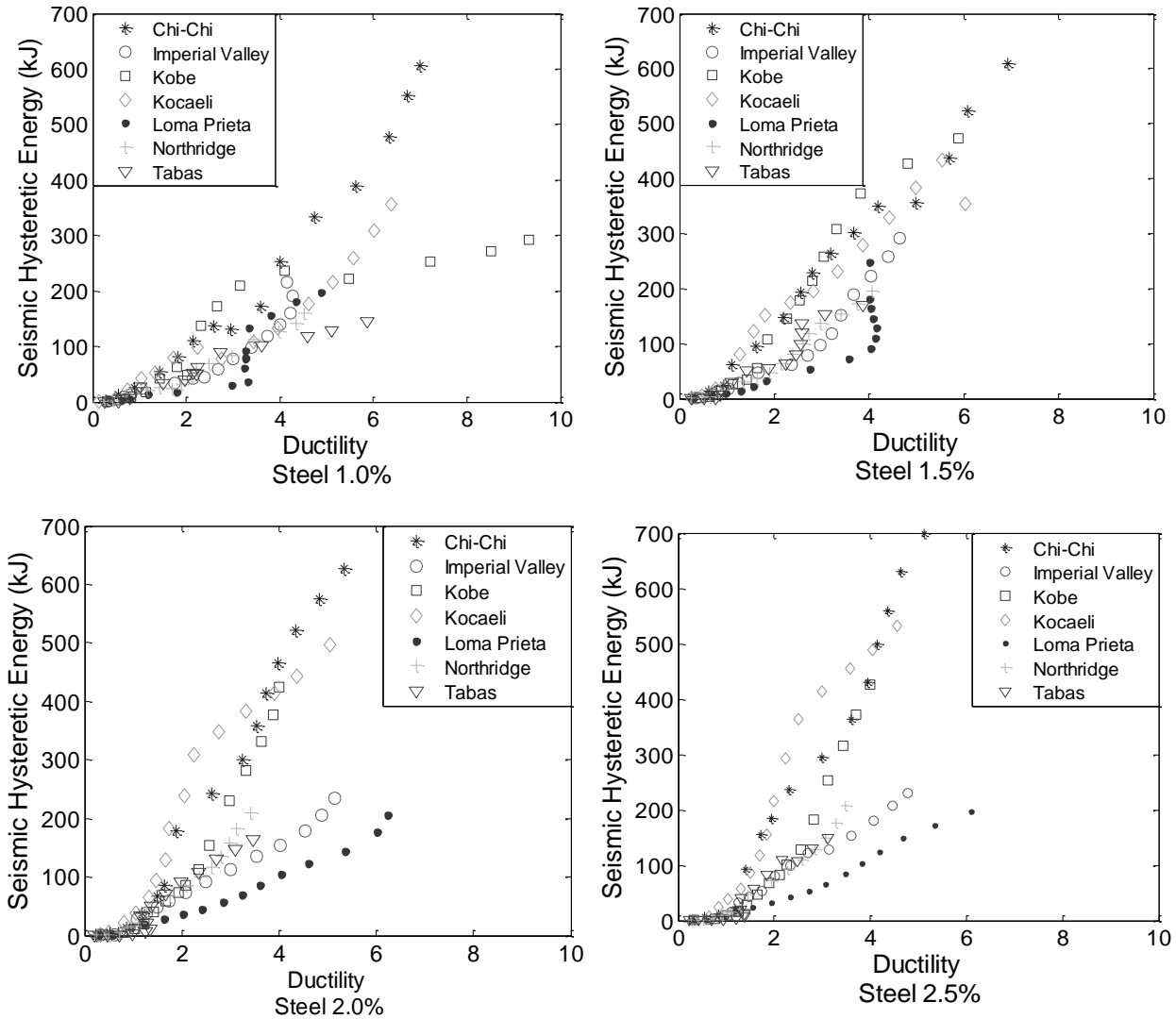


**Figure 78** Seismic Hysteretic Energy vs. Ductility - Frame 4

In the majority of the cases a proportional relationship between the seismic hysteretic energy and the drift, PGA and ductility can be perceived. As mentioned before, some gaps are observed on these curves, when there is a change in the story where the maximum drift occurs. In general, it is shown from the seismic hysteretic energy that for the first 3 frames (1, 2 and 3) the energy decreases as the aspect ratio increases. However, an increase in the energy can be seen in frame 4, this frame has a greater beam's length than the others. It can also be noted that there is strong variability of the results among the seven earthquakes considered in this study.

As discussed in Chapter 3, they have different characteristics which have a strong influence in the seismic hysteretic energy. These results have been confirmed by many researchers (Park et al. 1987, Bommer and Martinez-Pereira 2000, Wong 2002, Kazantzi and Vamvatsikos 2012 and others). The hysteretic energy has also been recognized by several researchers as a potentially useful seismic performance indicator (e.g., Park et al., 1987; Bojorquez et al., 2011). However, the strong dependence with the seismic input presents a drawback if it is to be used as a parameter for definition of code limit states.

### **6.3. SEISMIC HYSTERETIC ENERGY AT LIMIT STATES**

From the IDA, the seismic hysteretic energy was interpolated for the corresponding ASCE 41-06 drift limit states. Tables 3 through 6 present the energy at each limit states for all earthquakes with 1.0% of steel reinforcement ratio. These values are presented in Appendix II for all frame cases. The CP limit state is exceeded for all frames (1, 2, 3 and 4) at 0.6g to 1.3g. The life safety (LS) limits are reached at an average PGA value of 0.6g and 0.4g for frames 1 and 4, and 0.5g, for frames 2 and 3. The IO is exceeded at an average value of 0.3g for frame 1 and 0.2g for frames 2, 3 and 4. From these tables, it can be noted the variability of the energy values between each limit states and earthquakes.

**Table 3** Seismic Hysteretic Energy at Limit States- Frame 1-1.0%

<b>Seismic Hysteretic Energy (kJ)</b>						
<b>Earthquake</b>	<b>PGA<sub>IO</sub></b>	<b>IO</b>	<b>PGA<sub>LS</sub></b>	<b>LS</b>	<b>PGA<sub>CP</sub></b>	<b>CP</b>
Chi-Chi	0.3	9.635293	0.5	53.14558	1	230.7358
Imperial Valley	0.3	2.834515	0.5	21.2011	1	87.04341
Kobe	0.2	3.882614	0.6	24.90995	0.9	83.91635
Kocaeli	0.3	10.72546	0.6	76.65787	1.2	456.162
Loma Prieta	0.2	2.637609	0.4	9.753388	0.6	26.03795
Northridge	0.3	3.710111	0.7	45.75272	1.3	137.2385
Tabas	0.3	3.261295	0.6	26.67779	1	84.16224
<b>Average</b>		5.2410		36.8712		157.8995
<b>Max</b>		10.7255		76.6579		456.1620
<b>Min</b>		2.6376		9.7534		26.0379
<b>standard deviation</b>		3.4173		22.9297		146.0658

**Table 4** Seismic Hysteretic Energy at Limit States - Frame 2-1.0%

<b>Seismic Hysteretic Energy (kJ)</b>						
<b>Earthquake</b>	<b>PGA<sub>IO</sub></b>	<b>IO</b>	<b>PGA<sub>LS</sub></b>	<b>LS</b>	<b>PGA<sub>CP</sub></b>	<b>CP</b>
Chi-Chi	0.2	2.53863	0.4	17.149907	0.8	135.039049
Imperial Valley	0.2	2.586197	0.4	15.249404	0.8	58.863029
Kobe	0.2	2.336921	0.5	18.963949	0.9	77.687209
Kocaeli	0.2	9.942591	0.5	62.611604	1.1	125.757339
Loma Prieta	0.2	2.092575	0.4	7.38602	0.6	26.365045
Northridge	0.2	2.58646	0.6	25.097644	1.1	69.750915
Tabas	0.2	2.792545	0.6	10.84272	1.1	59.917299
<b>Average</b>		3.5537		22.4716		79.0543
<b>Max</b>		9.9426		62.6116		135.0390
<b>Min</b>		2.0926		7.3860		26.3650
<b>standard deviation</b>		2.8259		18.5908		38.6306

**Table 5** Seismic Hysteretic Energy at Limit States - Frame 3-1.0%

Seismic Hysteretic Energy (kJ)						
Earthquake	PGA <sub>IO</sub>	IO	PGA <sub>LS</sub>	LS	PGA <sub>CP</sub>	CP
Chi-Chi	0.2	2.347806	0.4	17.904137	0.7	94.549863
Imperial Valley	0.2	1.239073	0.4	17.38619	0.7	36.352281
Kobe	0.2	2.867228	0.4	10.940913	0.9	48.169927
Kocaeli	0.2	6.979053	0.4	25.447562	0.9	126.775653
Loma Prieta	0.2	0.921529	0.4	9.626477	0.6	12.239561
Northridge	0.3	2.966103	0.6	12.462804	0.9	37.141672
Tabas	0.2	0.927138	0.6	8.209369	1	32.814155
<b>Average</b>		2.6068		14.5682		55.4347
<b>Max</b>		6.9791		25.4476		126.7757
<b>Min</b>		0.9215		8.2094		12.2396
<b>standard deviation</b>		2.1179		6.0536		40.3084

**Table 6** Seismic Hysteretic Energy at Limit States - Frame 4-1.0%

Seismic Hysteretic Energy (kJ)						
Earthquake	PGA <sub>IO</sub>	IO	PGA <sub>LS</sub>	LS	PGA <sub>CP</sub>	CP
Chi-Chi	0.2	9.455912	0.4	29.00956	0.6	93.67952
Imperial Valley	0.2	7.082956	0.4	18.99733	0.6	41.26598
Kobe	0.2	1.842077	0.4	13.33501	0.8	56.5631
Kocaeli	0.2	5.71639	0.4	35.0726	0.7	91.35505
Loma Prieta	0.2	2.438046	0.4	8.8906	0.6	20.40644
Northridge	0.3	3.897393	0.4	18.20968	0.8	42.73277
Tabas	0.2	0.716518	0.5	19.93892	0.8	46.62486
<b>Average</b>		4.4499		20.4934		56.0897
<b>Max</b>		9.4559		35.0726		93.6795
<b>Min</b>		0.7165		8.8906		20.4064
<b>standard deviation</b>		3.1275		8.9322		27.1351

# **CHAPTER 7: Results Summary, Conclusions and Recommendations**

## **7.1. INTRODUCTION**

In this chapter a summary of the results is presented. All frames were analyzed using the OpenSEES program by performing incremental dynamic analyses. 2D frames and one 3D frame were considered. The 2D frames were analyzed with varying aspect ratios and reinforcement steel contents. For the dynamic analyses of the 2D frames, a total of 7 compatible earthquakes with PGA increasing from 0.1 to 1.5g were used. The analysis of the 3D frame was performed with one ground motion scaled to four different intensities which were applied simultaneously. From these analyses, the values of drifts, steel and concrete strains, moments and rotations, were obtained. Seismic hysteretic energies were calculated for the 2D frames. A program in MATLAB® was developed to process the data and obtain the desired results. The ASCE 41-06 rehabilitation limit states were included as part of the study. The implications of these limits in the results were discussed and will be summarized next.

## **7.2. STRAIN RESULTS - SUMMARY**

### ***7.2.1. 2D Frames***

As mentioned before, the data obtained from the OpenSEES analyses were organized, evaluated and managed with a program developed in MATLAB®. Using this program the steel and concrete strains at each limit-state were obtained with the methodology described in Chapter 5. The strains for the IO, LS and CP were obtained from interpolation of the IDA results (Chapter 5). The values obtained for the different frames are shown in the tables of Appendix II.

For the 2D frames, the average value of the strains at each limit state (IO, LS, CP) obtained for each earthquake in the same frame case were calculated. These results are presented in Figures 79 through 86 for the steel and concrete strains as function of the frame aspect ratio for different beam reinforcing steel ratios (from 0.85% to 2.0%). As shown in Chapter 5, steel strain limits shows a linear tendency, whereas concrete strain limits show a less linear tendency in function of aspect ratios. These plots demonstrated that for a single limit-state value the strain varies for each aspect ratio. This could imply that the damage level represented by the code limits does not necessary represents the same level of damage for different frame types.

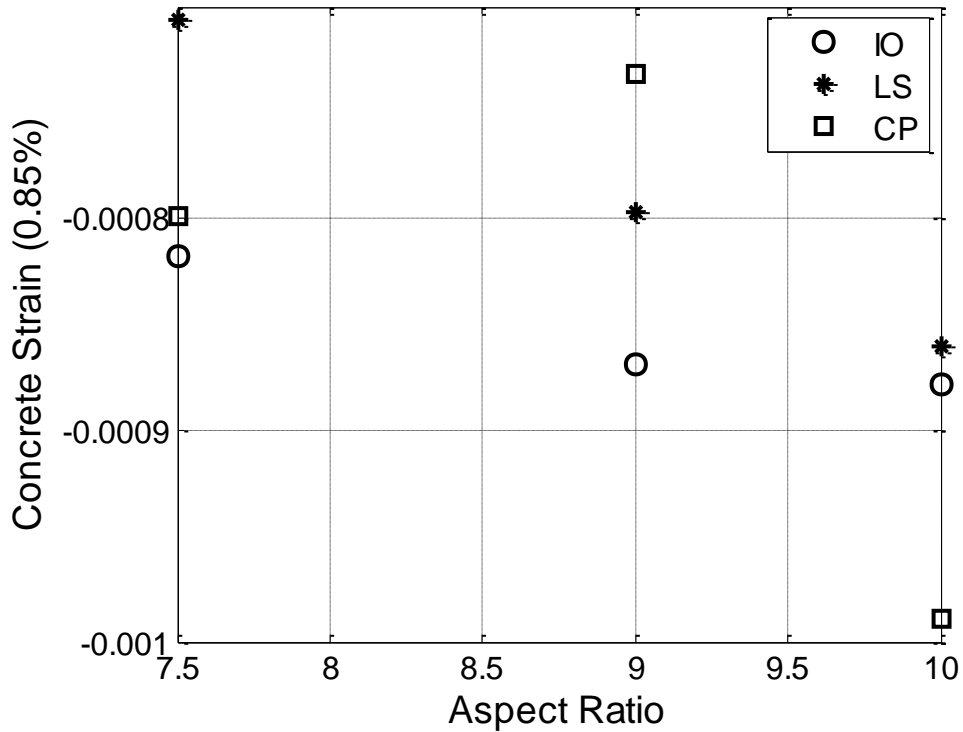


**Figure 79** Concrete Strain vs. Aspect Ratio (0.85%)

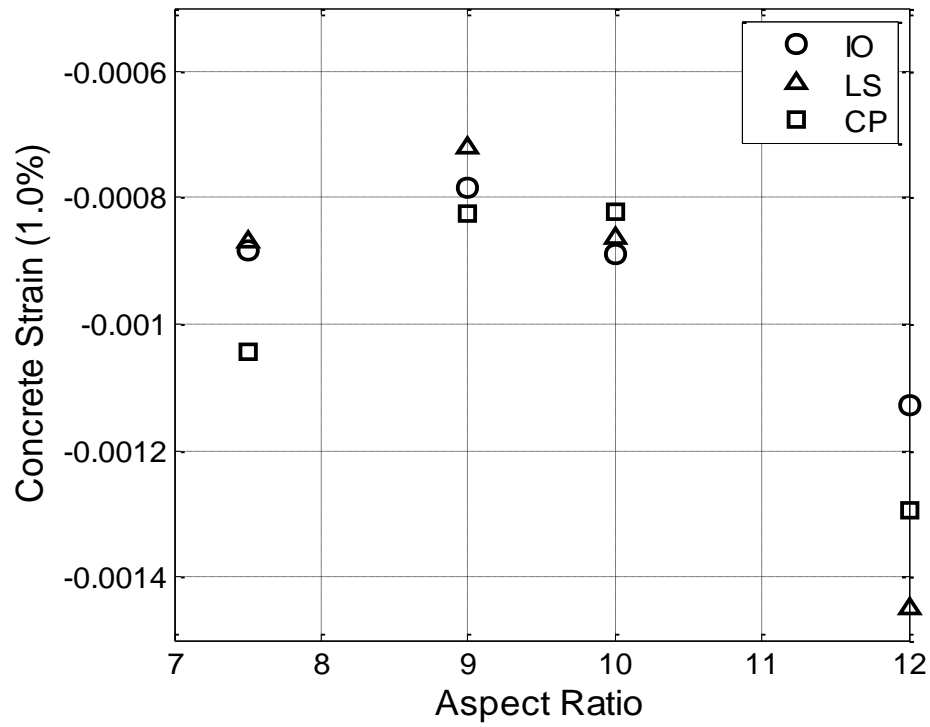


**Figure 80** Concrete Strain vs. Aspect Ratio (1.0%)

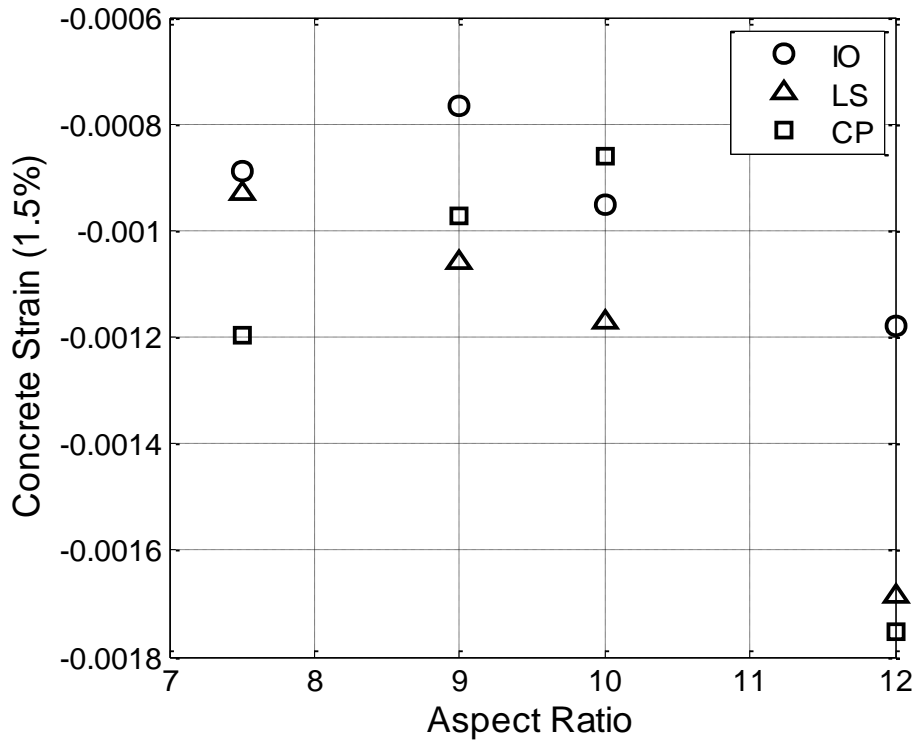


**Figure 81** Concrete Strain vs. Aspect Ratio (1.5%)

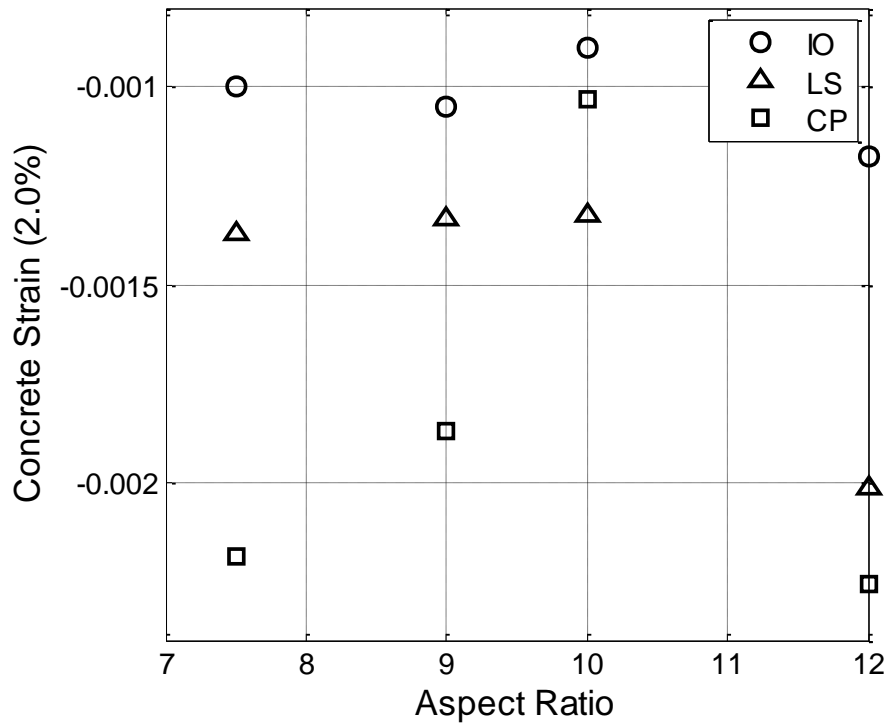


**Figure 82** Concrete Strain vs. Aspect Ratio (2.0%)

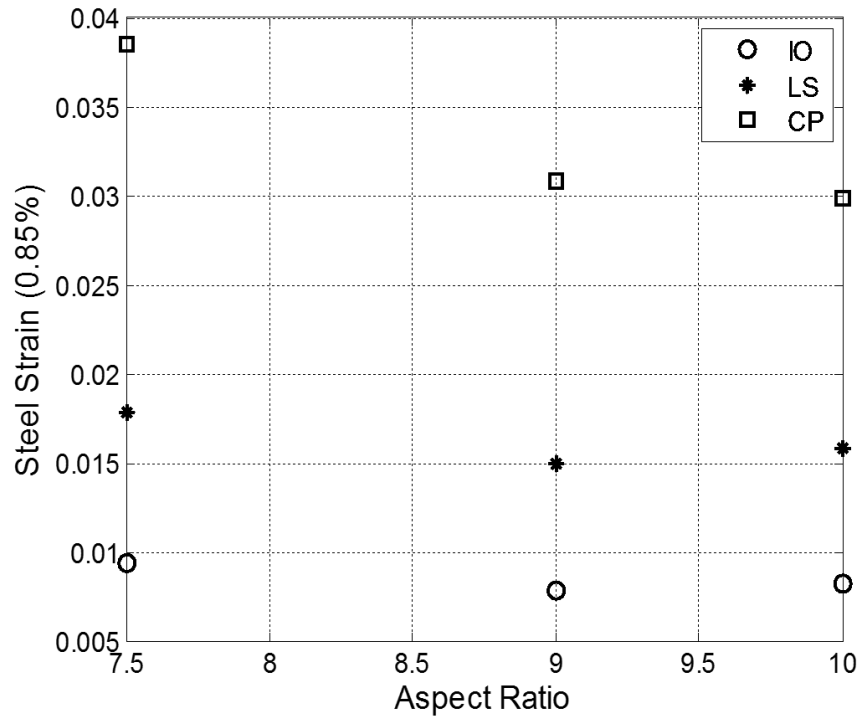


**Figure 83** Steel Strain vs. Aspect Ratio (0.85%)

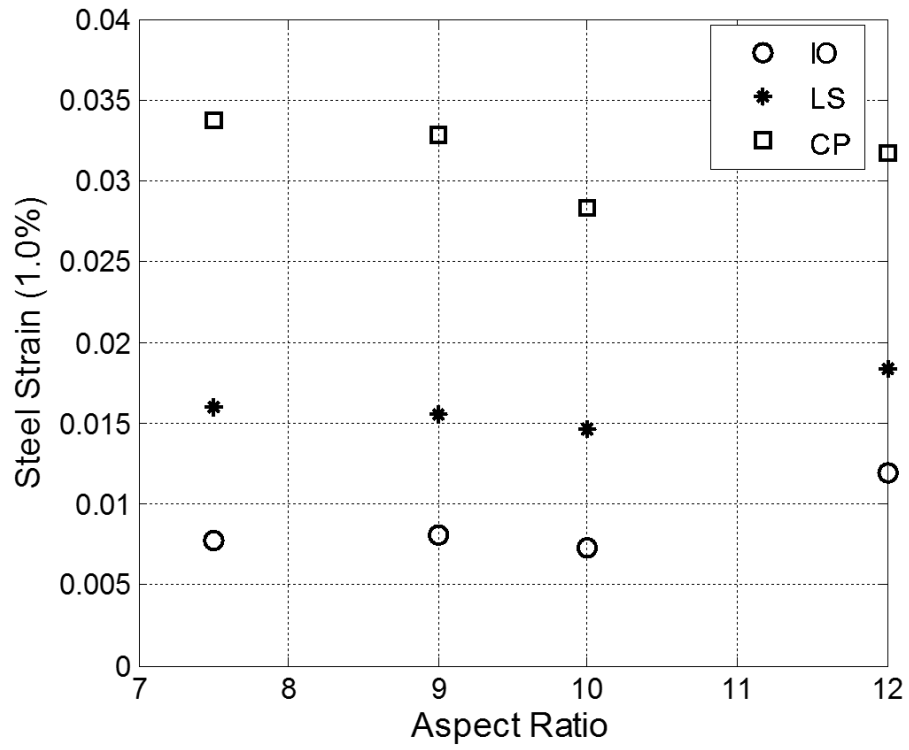


**Figure 84** Steel Strain vs. Aspect Ratio (1.0%)

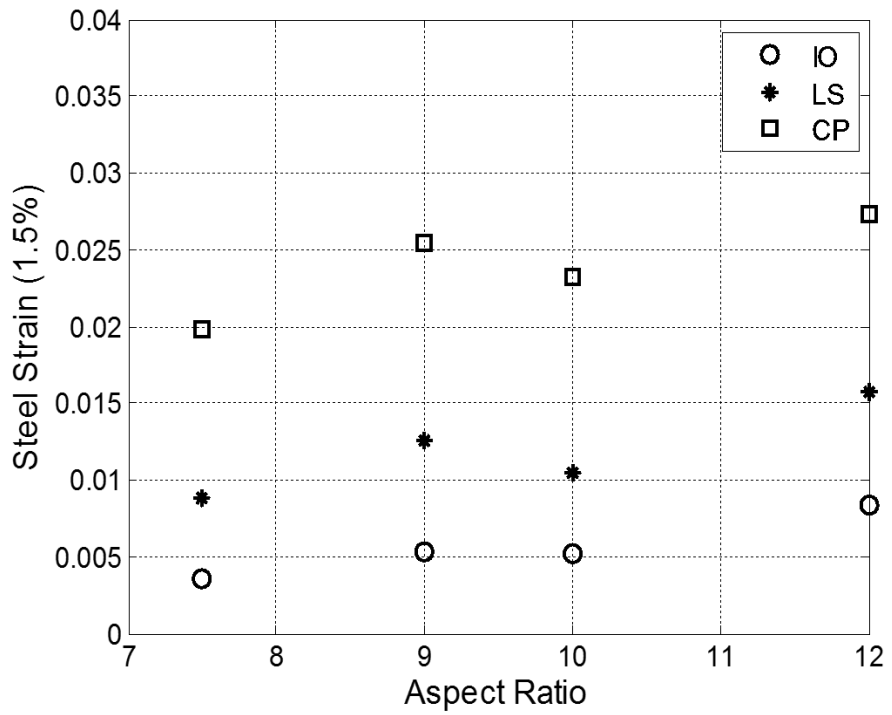


**Figure 85** Steel Strain vs. Aspect Ratio (1.5%)

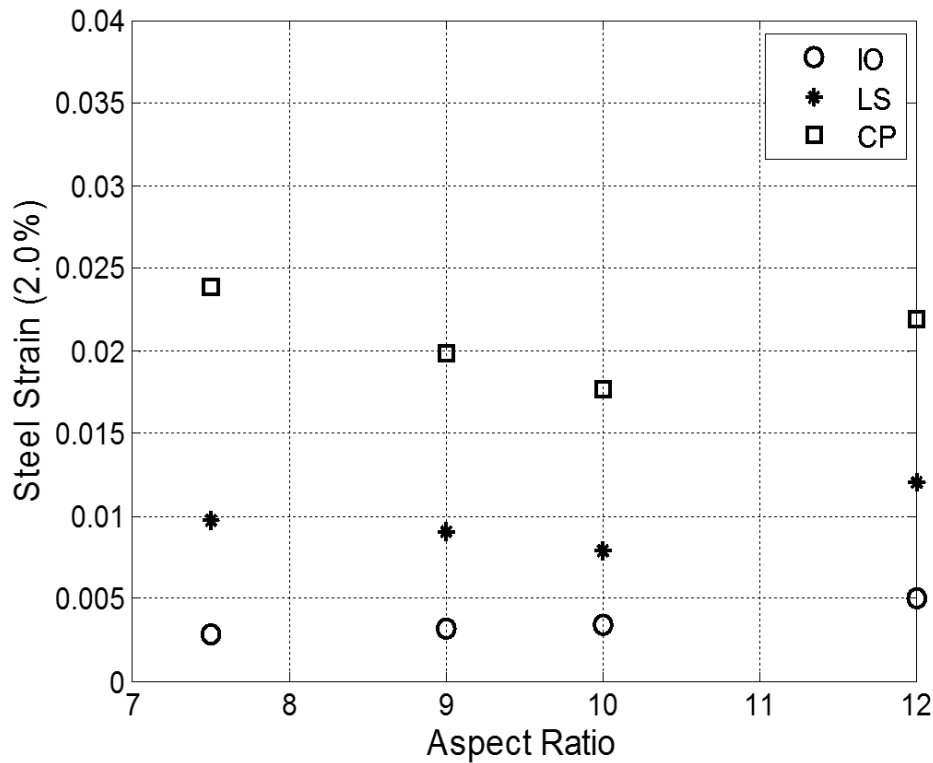


**Figure 86** Steel Strain vs. Aspect Ratio (2.0%)

### 7.2.2. 3D Frame

For the 3D frame, the same methodology from the 2D frames to obtain the strains at each limit state was used. As mentioned before, this frame has a weak column-strong beam mechanism. For this reason, the drift and strains at columns were analyzed in addition to the beams and girders. From the strain analyses on the beams and girders, a linear relationship between the steel strain and the PGA was observed and for the concrete strain and PGA, there was a greater variability among the results. For both materials, steel and concrete, a linear behavior was obtained between the strains and the PGA in the columns. The strains values were greater at the columns than in the beams and girders, due to the weak column-strong beam mechanism. As described in Chapter 5, a pushover (PO) analysis was performed and compared with the strain and drift results obtained from the dynamic analysis. These analyses revealed

obtained a linear behavior between the strains and drifts. For the beams and girders, the results obtained from the PO analyses have a good correlation with those from the dynamic analyses. Similarly, at the columns the PO analyses showed an excellent correlation with the results obtained from the dynamic analyses.

### 7.3. ADDITIONAL EVALUATION OF STRAINS VS. DRIFT – 2D FRAMES

Using the steel strain values obtained from the pushover analysis and Equation 9.1, the drift at different limit states were calculated. This equation depends on the mechanical reinforcing ratio, the materials strains, the beam aspect ratio, the concrete cover ratio and yield curvature (Vidot and Kowalsky, 2010). The mechanical reinforcing ratio was obtained using Equation 9.2 and the yield dimensionless curvature from Equation 9.3. Using the values of ASCE 41-06 drift limit-states and interpolating between them, the values of strain at each limit state per steel reinforcement and aspect ratio were obtained; they are shown in Table 7. These values have a minor discrepancy with the original steel strain values as shown in Figure 87. This figure shows the steel strain as function of drift obtained from the dynamic analysis, pushover (PO) and using the Equation. 9.1, for 1.0% of steel reinforcement ratio. From this figure it can be concluded that both results, pushover and Equation 9.1, are consistent with the dynamic analyses results. Similar results were obtained for the other frame cases. This equation (9.1) could be used to calculate drift limits as a function of strain values.

$$\theta_j = \left[ 0.5 * \varepsilon_y * \left( \frac{L_b}{H_B} \right) + (1.75 * \varepsilon_s * \omega_s^{0.15} - K_y) \left( \frac{L_p}{H_B} \right) \right] * 0.70 * \varepsilon_s^{-0.08} \quad (9.1)$$

$$\omega_s = \rho_{long} * \left( \frac{f_y}{f'_c} \right) \quad (9.2)$$

$$K_y = 2.1 * \epsilon_y \quad (9.3)$$

$\theta_j$ =drift,

$\epsilon_y$ = steel yield strain,

$L_b$ = length of beam,

$H_b$ =depth of beam,

$\epsilon_s$ =steel strain,

$\rho_{long}$ = longitudinal steel ratio,

$\omega_s$ = mechanical steel ratio and,

$K_y$ =yield dimensionless curvature.

$L_p$ = plastic hinge length (Equation 1.1);

**Table 7** Steel Strain at ASCE 41-06 limit states

% Steel	FRAME 1			FRAME 2		
	IO	LS	CP	IO	LS	CP
0.85	0.00057	0.00658	0.02534	0.00042	0.00341	0.01756
1	0.00096	0.00610	0.02267	0.00039	0.00327	0.01852
1.5	0.00052	0.00467	0.01350	0.00030	0.00306	0.01599
2	0.00061	0.00517	0.01851	0.00025	0.00294	0.01402

% Steel	FRAME 3			FRAME 4		
	IO	LS	CP	IO	LS	CP
0.85	0.00036	0.00154	0.01591			
1	0.00065	0.00174	0.01434	0.00004	0.00009	0.01190
1.5	0.00053	0.00186	0.01238	0.00053	0.00106	0.01046
2	0.00024	0.00203	0.01052	0.00014	0.00028	0.00996
2.5				0.00012	0.00025	0.00909

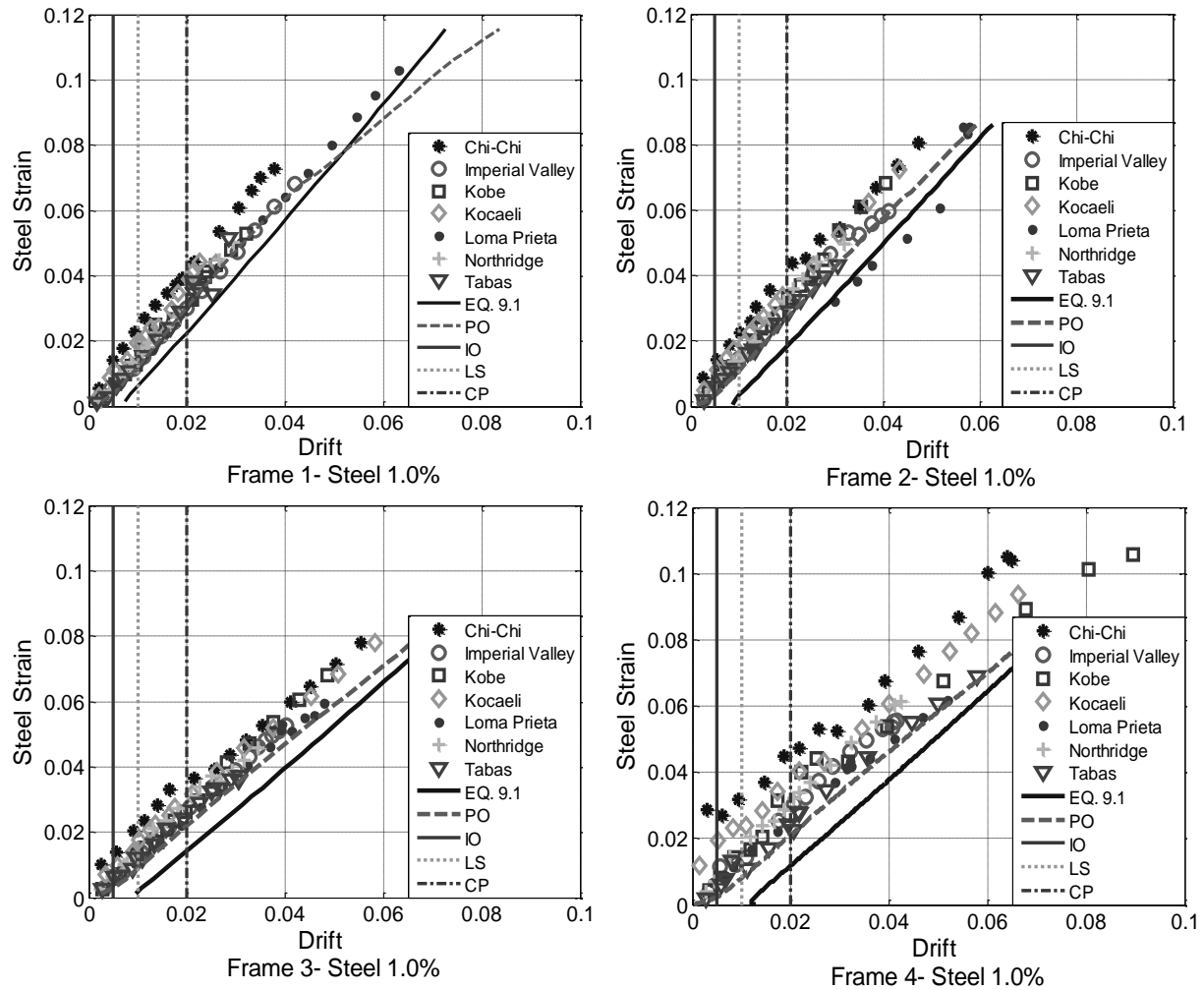


**Figure 87** Steel Strain vs. Drift for 1.0% of Steel Reinforcement Ratio

The concrete strains were not evaluated using the equation developed by Vidot and Kowalsky 2010, as it was done for the steel strain values, because the concrete strain values obtained from the analysis were smaller and beyond the scope of the equation. It is recommended to develop an equation, or to improve the existing ones, to calculate drift limits based on concrete strain levels covering a major range of values.

#### **7.4. DRIFT RESULTS SUMMARY**

The inter-story drift is an indicator of the damage presented in a structure during a ground motion event. Using the ASCE 41-06 document, the drift limits (IO, LS, CP) for the beams at the 2D and 3D frame were obtained. For the 3D frame the drift obtained was that in the columns, because this model presents a weak column-strong beam mechanism. From the drift analyses it was observed that there is a proportional behavior with the PGA. Also, because the PGA is greater in the transversal direction for the 3D frame, the drift obtained in this direction was greater than the values in the longitudinal direction. For all beams (2D and 3D) the values of ASCE 41-06 drift limits obtained were 0.005, 0.01 and 0.02 for IO, LS and CP, respectively. For the columns on the 3D frame the code values observed were 0.005, 0.01365 and 0.0182 for IO, LS and CP, respectively. These values were compared with the results obtained from the dynamic analyses. As mentioned in Chapter 4, the drift decreases as the steel reinforcement ratio increases. The principal conclusion obtained from these analyses was that the code limits (IO, LS, CP) based on constant drift ratios are not necessarily appropriate if the goal is to ensure constant damage for the same type of frame structure. This is so because the drift ratios are dependent of the aspect ratios and seismic level demands.

#### **7.5. SEISMIC ENERGY RESULTS SUMMARY**

For all 2D frames the seismic hysteretic energy was obtained using the area under the moment vs. rotation curves. This energy measures the amount of damage that a structure can withstand. From the results presented on Chapter 6, it was concluded that for the majority of the cases a proportional relationship exists between the seismic hysteretic energy and the drifts, PGA and ductility. Also it was seen that for the first 3 frames (1, 2 and 3) the energy decreases as the

aspect ratio increases, but for frame 4 an increase in the energy was observed. The results obtained for each earthquake indicates that there was a strong variability within the seven ground motions. The values of energy at each limit states were obtained using the drift limits of the ASCE 41-06 and presented in Appendix II. The seismic hysteretic energy displays a strong dependence on the ground motion, and due to this situation it cannot be used alone to develop performance limit states.

## **7.6. CONCLUSIONS**

1. From the seismic hysteretic energy results, it was found that the earthquakes with the highest Arias Intensity, Cumulative Absolute Velocity and Specific Energy Density dissipate more energy than the others. This confirms a proportional relationship between these parameters and the hysteretic energy dissipated.
2. The dependence of the seismic hysteretic energy with the characteristics of the ground motion was confirmed. Although this energy is a useful parameter to describe in some sense the seismic performance of a structure at different seismic demands, the use of this parameter to define damage limits states for seismic rehabilitation codes can be challenging.
3. Limit-state strains (steel and concrete) vary for each frame aspect ratio and longitudinal steel reinforcement ratio. This behavior implies that limit-states should be based on aspect ratio and longitudinal steel reinforcement ratio instead of using a constant value.
4. From the strain vs. drift curves, it was demonstrated that the results from the pushover analyses are consistent with those obtained from the dynamic analyses. It is confirmed that the IDA and pushover analysis have a connection, as stated by Vamvatsikos and Cornell

(2002<sup>b</sup>). This situation adds confidence to the use of monotonic analyses to define damages limit states.

5. From the strain and drift vs. PGA curves presented on Chapter 4-5, it was demonstrated that a directly proportional behavior occurs between these parameters (strain and drift) and the aspect ratio. As the aspect ratio increases, the drift and strain values of the frames increase, with the greatest drift value the frame 4 with  $L/H=12$  and the lowest values the frame 1 with  $L/H=7.5$ .
6. The inclusion of strains in the definition of limits states to be used in rehabilitation codes is recommended since they allow for a better indication of the damage across the structure than the drift alone.
7. Better equations to obtained limit states based on concrete strains are needed, specially when low values of concrete strain are expected. The equations described in section 7.3 for the calculation of the steel strains limits proved to be effective.
8. From the analysis performed were obtained the average value of steel and concrete strain at each limit states, which are presented below.

**Table 8 Steel Strain at Limit States**

% Steel Reinforcement	Steel Strain					
	Frame 1			Frame 2		
	IO	LS	CP	IO	LS	CP
0.85	0.0093	0.0179	0.0385	0.0078	0.0149	0.0308
1	0.0077	0.0160	0.0338	0.0081	0.0155	0.0328
1.5	0.0036	0.0088	0.0198	0.0053	0.0126	0.0254
2	0.0028	0.0097	0.0238	0.0032	0.0090	0.0199

% Steel Reinforcement	Steel Strain					
	Frame 3			Frame 4		
	IO	LS	CP	IO	LS	CP
0.85	0.0082	0.0158	0.0298			
1	0.0073	0.0147	0.0283	0.0119	0.0183	0.0317
1.5	0.0053	0.0104	0.0232	0.0083	0.0157	0.0273
2	0.0033	0.0079	0.0177	0.005	0.0121	0.0219
2.5				0.0037	0.0090	0.0201

**Table 9 Concrete Strain at Limit States**

% Steel Reinforcement	Concrete Strain					
	Frame 1			Frame 2		
	IO	LS	CP	IO	LS	CP
0.85	-0.0008	-0.0007	-0.0008	-0.0009	-0.0008	-0.0007
1	-0.0009	-0.0009	-0.001	-0.0005	-0.0007	-0.0008
1.5	-0.0009	-0.0009	-0.0012	-0.0007	-0.001	-0.0006
2	-0.001	-0.0014	-0.0022	-0.001	-0.0013	-0.0019

% Steel Reinforcement	Concrete Strain					
	Frame 3			Frame 4		
	IO	LS	CP	IO	LS	CP
0.85	-0.0009	-0.0009	-0.001			
1	-0.0009	-0.0009	-0.0008	-0.0011	-0.0014	-0.0013
1.5	-0.001	-0.0012	-0.0009	-0.0012	-0.0017	-0.0018
2	-0.0009	-0.0013	-0.001	-0.0012	-0.0020	-0.0023
2.5				-0.0011	-0.0020	-0.0027

## **7.7. RECOMMENDATIONS**

For future works it is recommended to study the stiffness changes among different displacement or performance levels. The stiffness can be obtained during the analyses, calculating the ratio between the shear and displacement at different limit states. This parameter, as well as the energy dissipated, has an important role in the ductility of a system and its capacity to resist different cycles of inelastic action. It also provides a measure of the performance level of the structure (Paulay and Priestley, 1992). It is also recommended to include frames with different number of stories in the analyses and to revise new experimental data as it become available to improve existing limit states and equations.

## REFERENCES

- 15WCEE Blind Test Challenge Design Report, (2012), 15<sup>th</sup> World Conference on Earthquake Engineering, Lisbon, Portugal.
- 15WCEE Blind Test Challenge Test Report, (2012), 15<sup>th</sup> World Conference on Earthquake Engineering, Lisbon, Portugal.
- 15WCEE Blind Test Challenge Preliminary Test Report, (2012), 15<sup>th</sup> World Conference on Earthquake Engineering, Lisbon, Portugal.
- ACI 318-08. (2008). *Building Code Requirements for Structural Concrete and Commentary*, American Concrete Institute, Farmington Hills, Michigan, USA.
- Ansar, A., Bardet, J.P., Bray, J., Cetin, O., Durgunoglu, T., Erdik, M., Kaya, A., Ural, D., Yilmaz, T. and Youd, L., (1999). *Initial Geotechnical Observations of the August 17, 1999, Izmit Earthquake, A Report of the Turkey-US Geotechnical Reconnaissance Team*, National Information Service for Earthquake Engineering, University of California, Berkeley.
- ASCE 7-05 (2006). *Minimum Design Loads for Buildings and Other Structures*, American Society of Civil Engineers, ASCE, Reston, VA, pp.12, 115-116, 121, 129-132.
- ASCE 41-06 (2007). *Seismic Rehabilitation of Existing Building*, American Society of Civil Engineers, ASCE, Reston, VA, pp. 7-21.
- ATC 40 (1996). *Seismic Evaluation and Retrofit of Concrete Buildings, Volume 1*. Report No. SSC 96-01, Seismic Safety Commission, Redwood City, CA, pp. 3.1-3.13.
- ATC 58. (2004). *Engineering Demand Parameters for Structural Framing Systems*. Project Task Report, Phase 2, Task 2.2, Redwood City, CA.
- Bechtoula, H., Sakashita, M, Kono, S., Watanabe, F. and Eberhard, M. O., (2006). *Cyclic Performance of Lower Stories of a Mid-Rise Reinforced Concrete Frame Building*, ACI Structural Journal, Vol. 103, pp. 513-521.
- Berberian, M. (1979), *Tabas-E-Golshan (Iran) Catastrophic Earthquake of 16 September 1978: A Preliminary Field Report*, Disasters, Vol. 4, pp. 207-219.
- Bisch, P., Carvalho, E., Degee, H., Fajfar, P., Fardis, M., Franchin, P., Kreslin, M., Pecker, A., Pinto, P., Plumier, A., Somja, H. and Tsionis, G., (2011). *Eurocode 8: Seismic Design of Buildings Worked Examples*. Proceedings of the Workshop “EC 8: Seismic Design of Buildings”, Lisbon, Portugal.

Bojorquez, E., Teran-Gilmore, A., Ruiz, S.E. and Reyes-Salazar, A. (2011). *Evaluation of structural reliability of steel frames: Interstory drift versus plastic hysteretic energy*. Earthquake Spectra. Vol. 27, No. 3, pp.661–682.

Bommer, J.J. and Martinez-Pereira, A. (2000). *Strong Motion Parameters: Definition, Usefulness and Predictability*. Proceedings of the 12th World Conference on Earthquake Engineering, Auckland, New Zealand; Paper No. 206.

Chang, G. and Mander, J. (1994). *Seismic Energy Based Fatigue Damage Analysis of Bridge Columns: Part I – Evaluation of Seismic Capacity*. NCEER Technical Report 94-0006.

Chopra, A.K. (1995). *Dynamics of Structures: Theory and Applications to Earthquake Engineering*, 1<sup>st</sup> edition, Prentice Hall, Englewood Cliff, New Jersey, pp. 414-416.

Dhakal, R. and Maekawa, K. , (2002). *Reinforcement stability and fracture of cover concrete in reinforced concrete members*, ASCE Journal of Structural Engineering, Vol. 128, No. 10, pp. 1253–1262.

EPRI NP-5930, (1988). *A Criterion for Determining Exceedance of the Operating Basis Earthquake*, Electric Power Research Institute, Research Project 2848-16, Jack R. Benjamin and Associates, Inc. Mountain View, California.

Estes, K.R. and Anderson, J.C., (2002). *Hysteretic Energy Demands in Multistory Buildings*, Proceedings of the Seventh U.S. National Conference on Earthquake Engineering, Earthquake Engineering Research Institute, Oakland, CA.

Estes, K.R. and Anderson, J.C., (2004). *Earthquake Resistant Design using Hysteretic Energy Demands for Low Rise buildings*, Proceedings of the 13<sup>th</sup> World Conference on Earthquake Engineering, Paper No.3276, Vancouver, B.C., Canada.

Eurocode 8, EN 1998-1:2003, (2003). *Design of Structures for Earthquake Resistance*, European Committee for Standardization, Brussels, Belgium, pp. 23-26.

FEMA 273, (1997). *NEHRP Guidelines for the Seismic Rehabilitation of Buildings*, Federal Emergency Management Agency, Washington, DC, pp. 2.4 -2.19.

FEMA 274 (1997). *Commentary on the Guidelines for the Seismic Rehabilitation of Buildings: FEMA 274*, Federal Emergency Management Agency, Washington, DC, pp. 442.

FEMA 356 (2000). *Prestandard and Commentary for the Seismic Rehabilitation of Buildings (FEMA 356)*, Federal Emergency Management Agency, Washington, DC, pp. 1.9-1.17.

FEMA 450 (2003). *The 2003 NEHRP Recommended Provisions for New Buildings and Other Structures Part 1: Provisions (FEMA 450)*, Federal Emergency Management Agency, Washington, DC, pp. 452.

FEMA 445 (2006). *Next-Generation Performance-Based Seismic Design Guidelines (FEMA 445)*, Federal Emergency Management Agency, Washington, DC, pp.1-9

Ghobarah, A. (2001). *Performance-Based Design in earthquake engineering: state of development*, Engineering Structures, Vol. 23, pp. 878-884

Goodnight, J., Kowalsky, M., and Nau, J. (2013). *The Effect of Load History on Performance Limit States of Circular Bridge Columns*. Accepted Manuscript of ASCE Journal of Bridge Engineering.

Gomes, A. and Appleton, J. (1997). *Nonlinear Cyclic Stress-Strain Relationship of Reinforcing Bars Including Buckling*. Engineering Structures, Vol. 19, No.10, pp. 822–826.

Hamburger, R.O. (2003). *A Vision for Performance Based Earthquake Engineering*, Unpublished White Paper for the ATC- 58 Project, Applied Technology Council, Redwood City, CA, 2003.

Hamburger, R. O. (2004). *Development of Next Generation Performance-Based Seismic Design Guidelines*, Performance-Based Seismic Design Concepts and Implementation, Proceedings of The International Workshop, Bled, Slovenia, and PEER Report 2004/05, pp. 89-100.

Hamburger, R. and Hooper, J. (2011). *Performance Based Seismic Design*, Modern Steel Construction, April, 2011, Proceedings of the NASCC: The Steel Conference, Pittsburgh, Pennsylvania.

Hill, H.J., (1998). *Proportioning: Missing Step in Model Building Code Seismic Design* Practice Periodical on Structural Design and Construction, Vol. 3, No. 1, pp. 25-33.

Karsan, I. and Jirsa, J. (1969). *Behavior of Concrete Under Compressive Loadings*, ASCE Journal of Structural Division, Vol. 95, No. 12, pp. 2543–2563.

Kazantzi, A.K. and Vamvatsikos D. (2012). *A study on the Correlation Between Dissipated Hysteretic Energy and Seismic Performance*. Proceedings of the 15th World Conference on Earthquake Engineering, Lisbon, Portugal.

Kent, D. C. and Park, R. (1971). *Flexural Members with Confined Concrete*, ASCE Journal of Structural Engineering, Vol. 97, No. 7, pp.1969–1990.

- Leelataviwat, S., Goel, S. and Stojadinovic, B. (1999). *Toward Performance-Based Seismic Design of Structures*, Earthquake Spectra, Vol. 15, No. 3, pp. 435-461.
- Liao, W., Goel, S. and Chao, S. (2010). *Performance Based Plastic Design of RC Special Moment Frame Structures*, Proceedings of the 6<sup>th</sup> International Conference on Concrete under Severe Conditions (CONSEC'10), Mérida, Yucatán, México, pp. 1631-1638.
- McKenna, F., Fenves, G., Filippou, F., Mazzoni, S., Scott, M., Jeremic, B., Elgamal, A., Yang, Z., Lu, J., Arduino, P., McKenzie, P., Deierlein, G. and Law, K., (2000). *Open System for Earthquake Engineering Simulation (OpenSEES)*, <http://opensees.berkeley.edu/>
- Miyamoto, H.K., Gilani, A.S.J., Wada, A., (2012). *The 2011 Eastern Japan Earthquake: Facts and Reconstruction Recommendations*. Proceedings of the 15<sup>th</sup> World Conference on Earthquake Engineering, Lisbon, Portugal.
- Moehle, J. and Kunnath, S. (2006). *Reinforcing Steel: OpenSees User's Manual*, pp. 112-114 <http://opensees.berkeley.edu/>
- Montejo-Valencia, L.A. (2004). *Generation and Analysis of Spectrum-Compatible Earthquake Time-Histories Using Wavelets*, University of Puerto Rico-Mayaguez, MS Thesis.
- Montejo, L.A., and Kowalsky, M.J., (2007). *CUMBIA-Set of codes for the Analysis of Reinforced Concrete Members*, CFL Technical Report No. IS-07-01, Dept. of Civil, Construction and Environmental Engineering, North Carolina State University, Raleigh, NC.
- Moyer, M. and Kowalsky, M. (2003). *Influence of Tension Strain on Buckling of Reinforcement in Concrete Columns*, ACI Structural Journal, Vol. 100, pp. 75-85.
- Park, Y.J., Ang, A.H. and Wen, Y.K. (1987). *Damage-Limiting a Seismic Design of Buildings*. Earthquake Spectra, Vol. 3, No. 1, pp. 1-26.
- Pauley, T. and Priestley, M.J.N., (1992). *Seismic Design of Reinforced Concrete and Masonry Buildings*, 1<sup>st</sup> edition, John Wiley and Sons, Inc., pp. 11-15, 99, 158-186.
- Priestley, M.J.N., Calvi, G.M. and Kowalsky, M. (2007). *Displacement-Based Seismic Design of Structures*, 1<sup>st</sup> edition, IUSS Press, Pavia, Italy, 2007, pp. 193-194.
- Priestley, M.J.N., Seible, F. and Calvi G.M., (1996), *Seismic Design and Retrofit of Bridge Structures*, John Wiley and Sons, New York, NY.

Rathje, E. M., Abrahamson, N. A., Bray, J. D., (1998). *Simplified Frequency Content Estimates of Earthquake Ground Motions*, Journal of Geotechnical and Geoenvironmental Engineering, Vol. 124, No. 2, pp. 150-159.

Risk Management Solutions, Inc., Event Report Chi-Chi Taiwan Earthquake (2000), [https://www.rms.com/Publications/Taiwan\\_Event.pdf](https://www.rms.com/Publications/Taiwan_Event.pdf)

Seismosoft Ltd., Earthquake Engineering Software Solutions, Pavia, Italy, Accessed on March, 2013, <http://www.seismosoft.com/en/HomePage.aspx>.

Scott, M.H. and Fenves, G.L. (2006). *Plastic Hinge Integration Methods for Force-Based Beam-Column Elements*, Journal of Structural Engineering, Vol. 132, No. 2, pp. 244-252.

Searer, G., Parret, T. and Freeman, S., (2008). *ASCE-31 and ASCE-41: What Good Are They?* ASCE Structures Congress 2008: Crossing Borders, Vancouver, Canada, pp. 1-8.

SEAOC, (1995), *Recommended Lateral Force Requirements and Commentary, 7th Ed* , Seismology Committee, Structural Engineering Association of California, Sacramento, California.

Sener,S., Begimgil,M. and Belgin,C. (2002). *Size effect on Failure of Concrete Beams With and Without Steel Fiber*, Journal of Materials in Civil Engineering, Vol. 14, No. 5, pp. 436-440.

Tanaka, S., and Shigekawa, K., (2012). *Analysis of the Building Damage Evaluation for the 2011 Great East Japan Earthquake*, Proceedings of the 15<sup>th</sup> World Conference on Earthquake Engineering, Lisbon, Portugal.

Travasarou, T., Bray, J.D., and Abrahamson, N.A. (2002). *Empirical Attenuation Relationship for Arias Intensity*, submitted to *Earthquake Engineering and Structural Dynamics*, April, 2002.

USGS *Earthquake Hazard Program, Historic Earthquakes*  
<http://earthquake.usgs.gov/earthquakes>, Accessed on March, 2013

Vamvatsikos, D. and Cornell, CA., (2002<sup>a</sup>) *Incremental dynamic analysis*. Earthquake Engineering and Structural Dynamics, Vol. 31, No.3, pp. 491–514.

Vamvatsikos, D. and Cornell, CA. (2002<sup>b</sup>). *The Incremental Dynamic Analysis and its Application to Performance-Based Earthquake Engineering*, Proceedings of the 12<sup>th</sup> European Conference on Earthquake Engineering, London, U.K.

Vidot-Vega, A.L. and Kowalsky, M.J. (2010). *Relationship between Strain, Curvature, and Drift in Reinforced Concrete Moment Frames in Support of Performance-Based Seismic Design*, ACI Structural Journal, Vol. 107, No. 3, pp. 291-299.

Vidot-Vega, A.L. and Kowalsky, M.J., (2011). *Impact of Seismic Input on Strain/Displacement Response of RC Members and Frames*, ACI Structural Journal, Vol. 108, No. 2, pp. 178-187.

Wang, X. and Shi, G. (2012). *The boundary layer solutions induced by displacement boundary conditions of shear deformable beams and accuracy study of several higher order beam theories*, Accepted Manuscript of ASCE Journal of Engineering Mechanics.

Wan Han, S. and Jee, N. (2005). *Seismic behaviors of columns in ordinary and intermediate moment resisting concrete frames*, Engineering Structures, Vol. 27, pp.951–962

Whittaker, A., Hamburger, R. O. and Huang, Y.N. (2007). *Next-Generation Performance Based Earthquake Engineering*, EJSE Special Issue: MDCMS 11<sup>st</sup> International Conference on Modern Design, Construction and Maintenance of Structures - Hanoi, Vietnam, December 2007.

Wong, K. (2002). *Inelastic Seismic Response Analysis based on Energy Density Spectra*, Journal of Earthquake Engineering. Vol. 8, No.2, pp. 315-334.

Zhang, Z. and Cho, C., (2009), *Experimental Study on Damping Ratios of in-situ Buildings*, International Journal of Engineering and Applied Sciences, Vol. 5, No. 4, pp. 264-268.

## Appendix I: Hysteretic Energy Plots

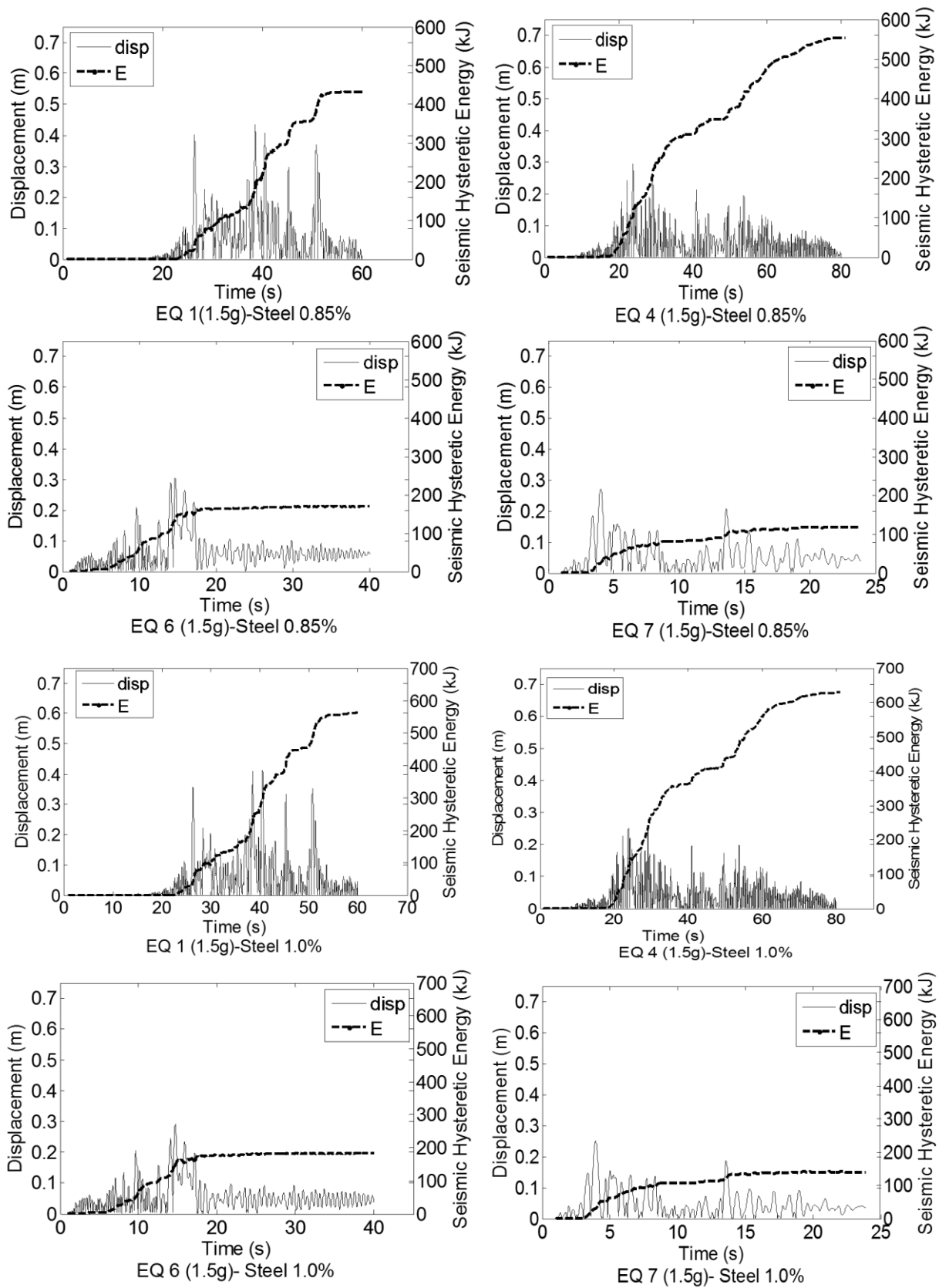


**Figure 88** Hysteretic Energy Plots - Frame 1

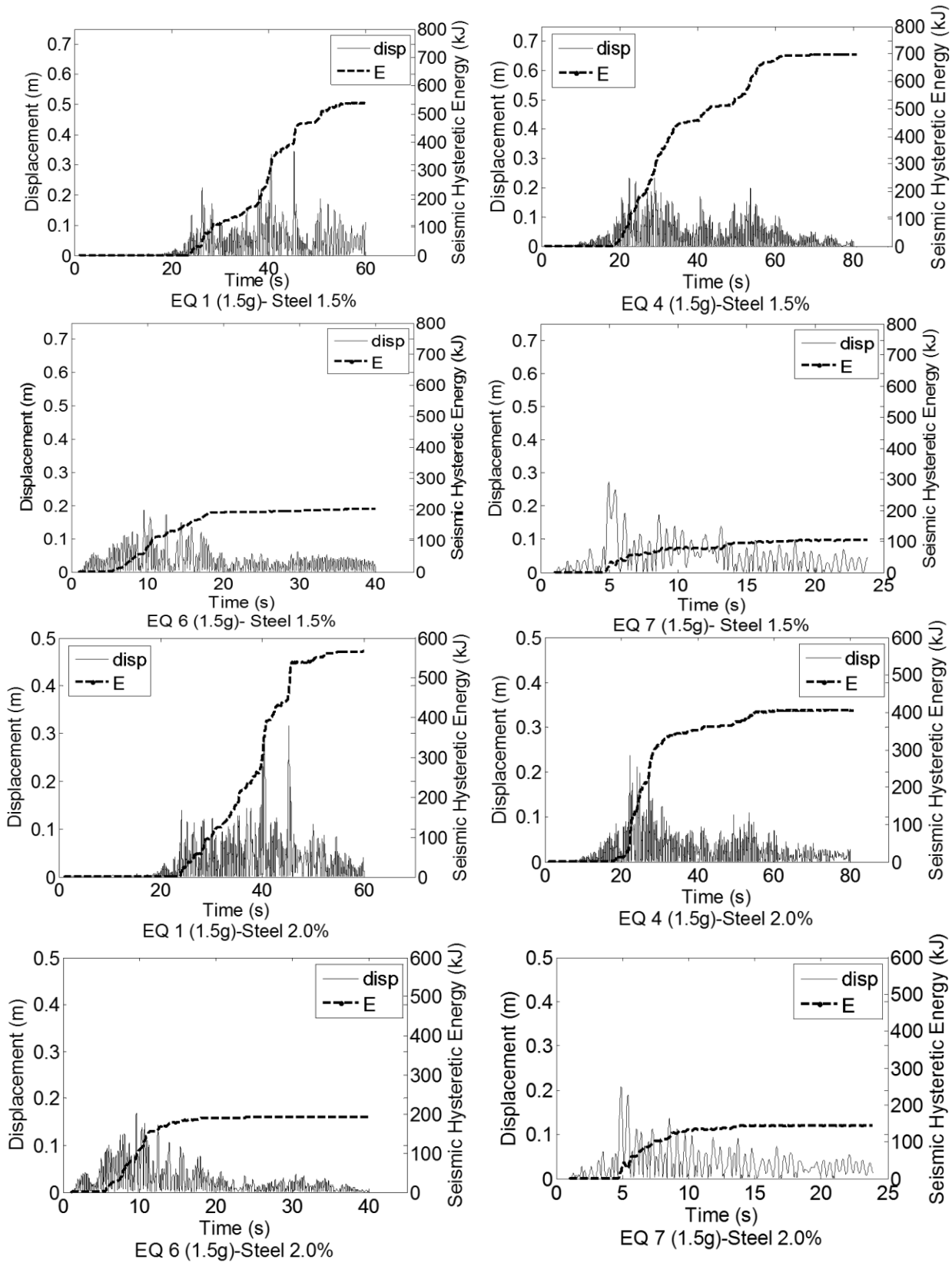


**Figure 89** Hysteretic Energy Plots - Frame 1 (cont.)

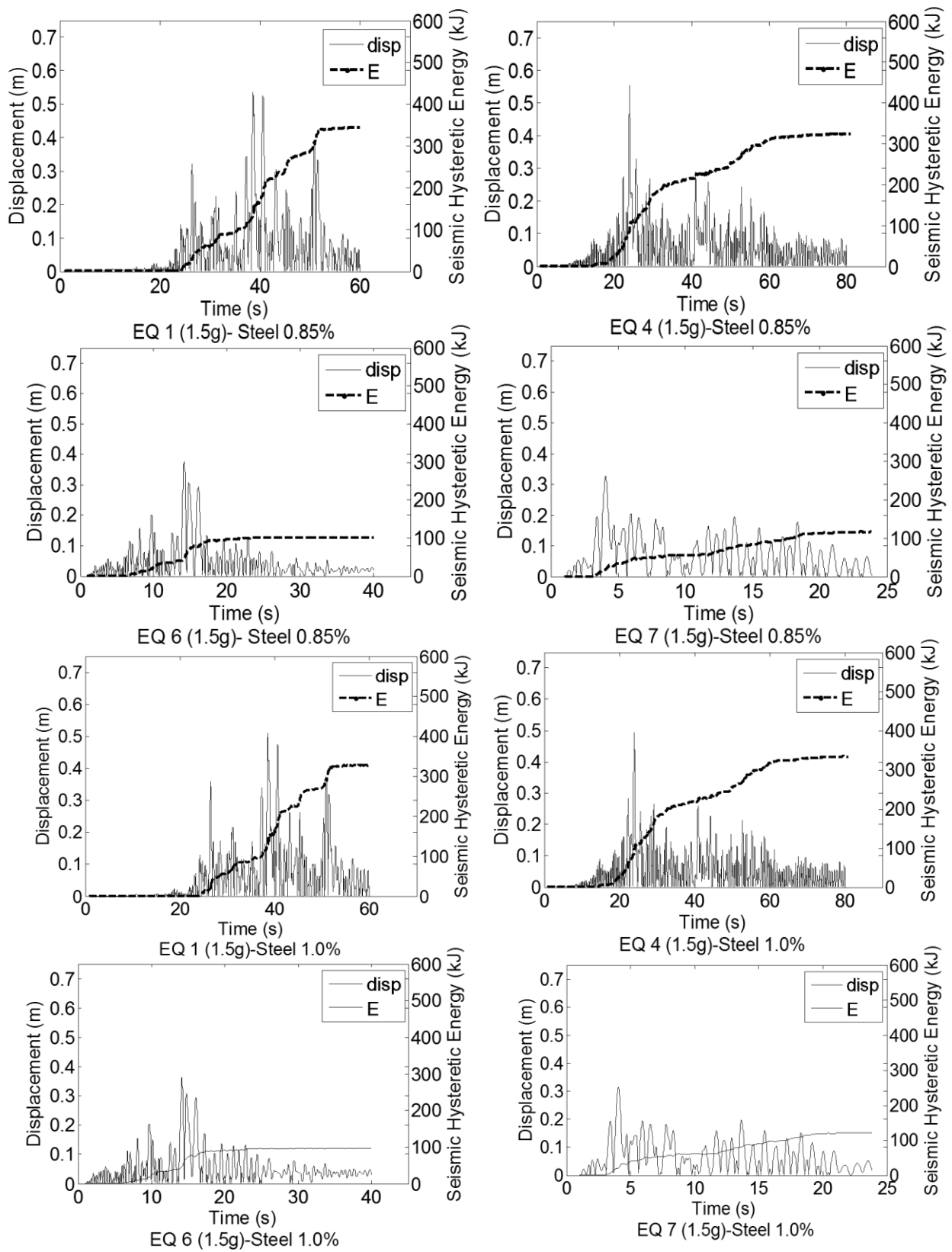


**Figure 90** Hysteretic Energy Plots - Frame 2

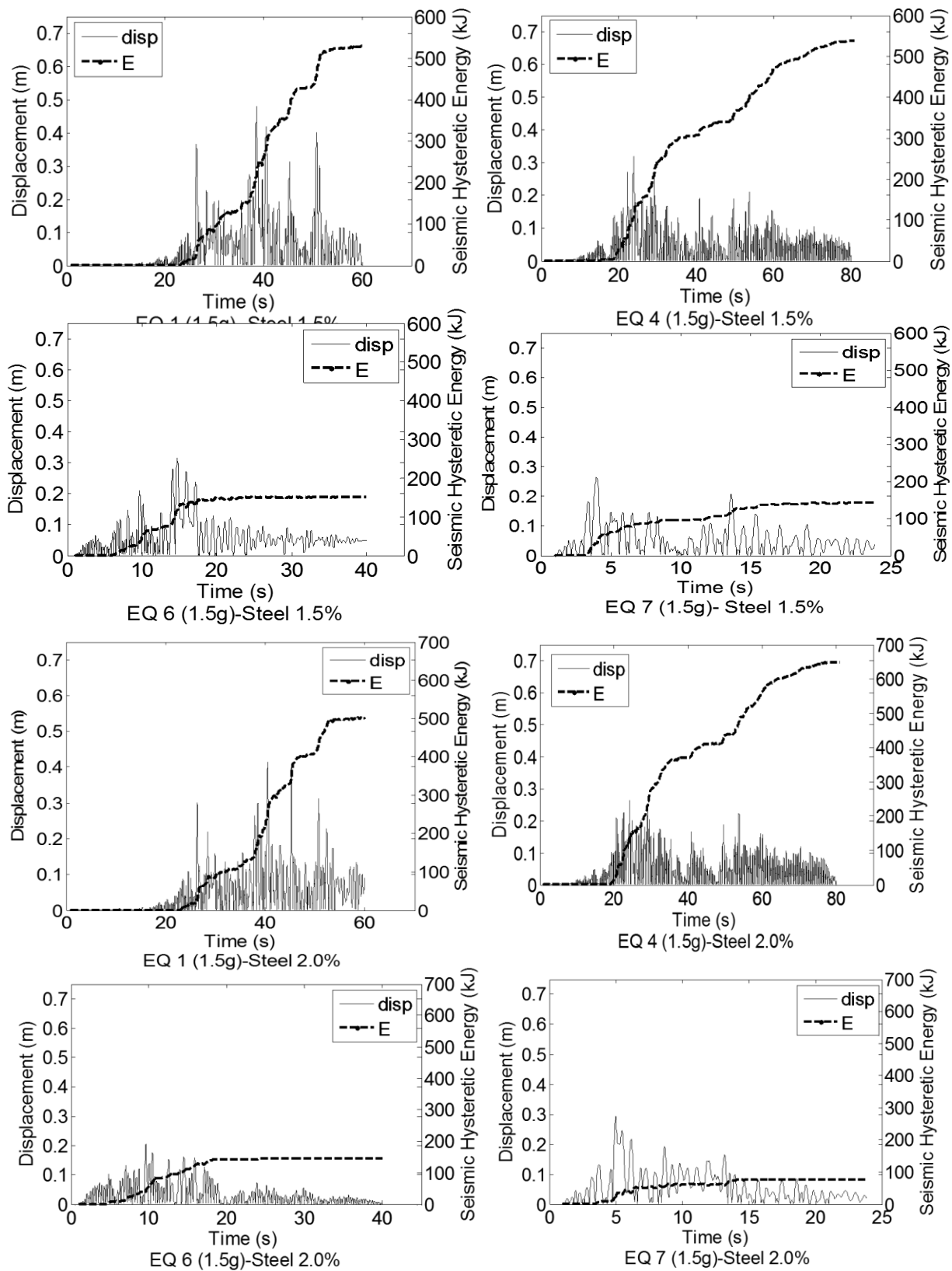


**Figure 91** Hysteretic Energy Plots - Frame 2 (cont.)

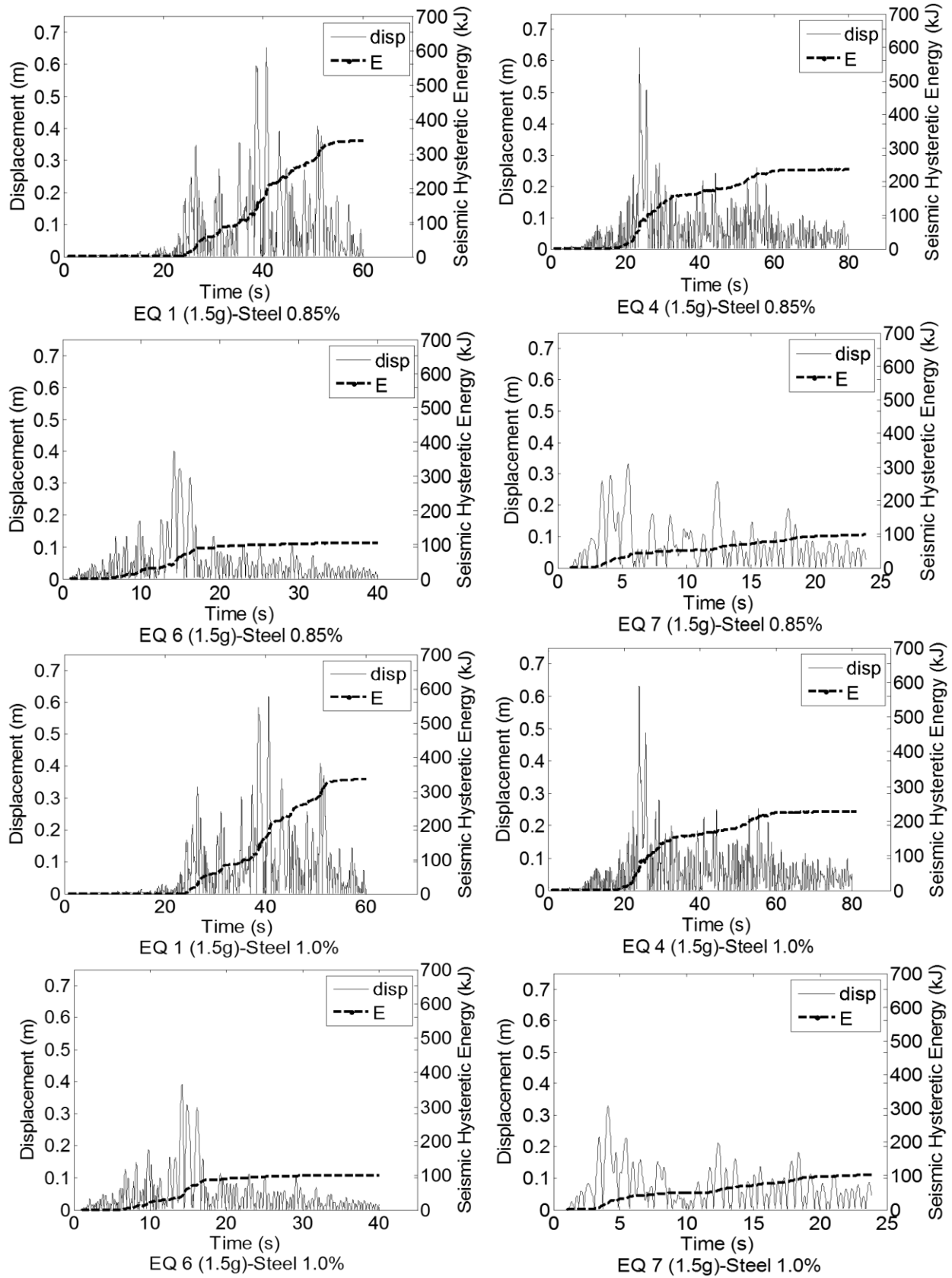
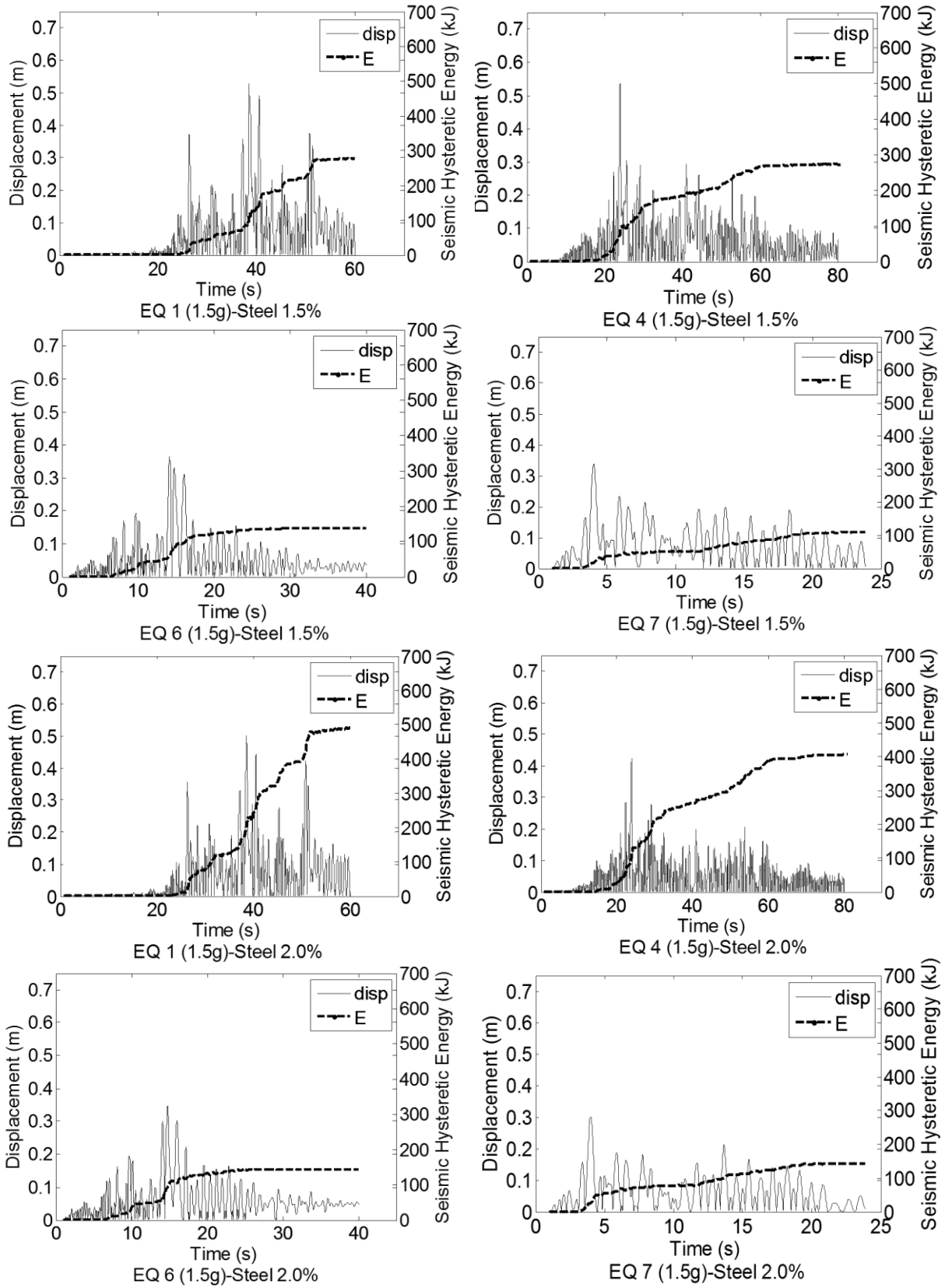
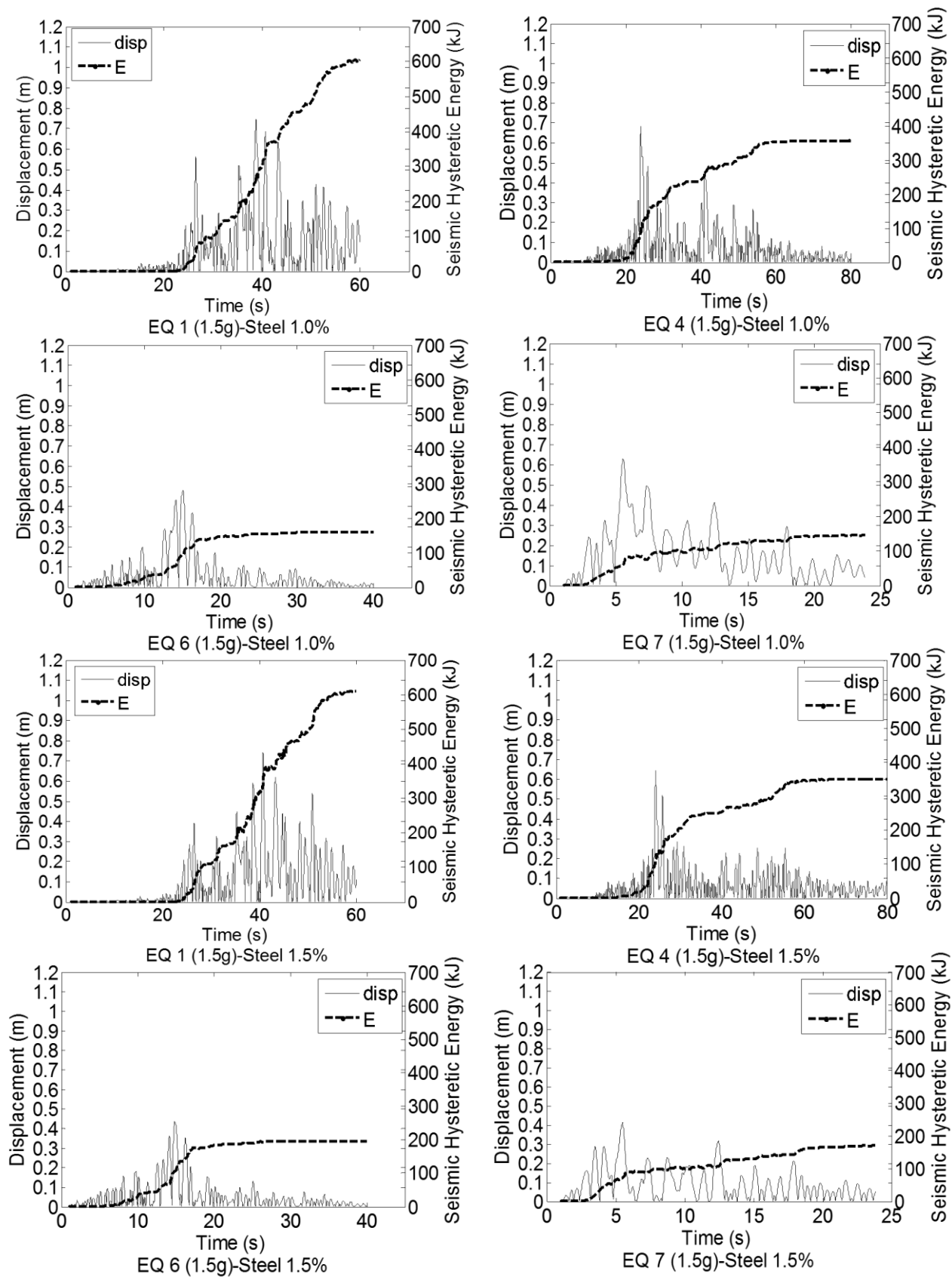


Figure 92 Hysteretic Energy Plots - Frame 3



**Figure 93** Hysteretic Energy Plots - Frame 3 (cont.)



**Figure 94** Hysteretic Energy Plots - Frame 4

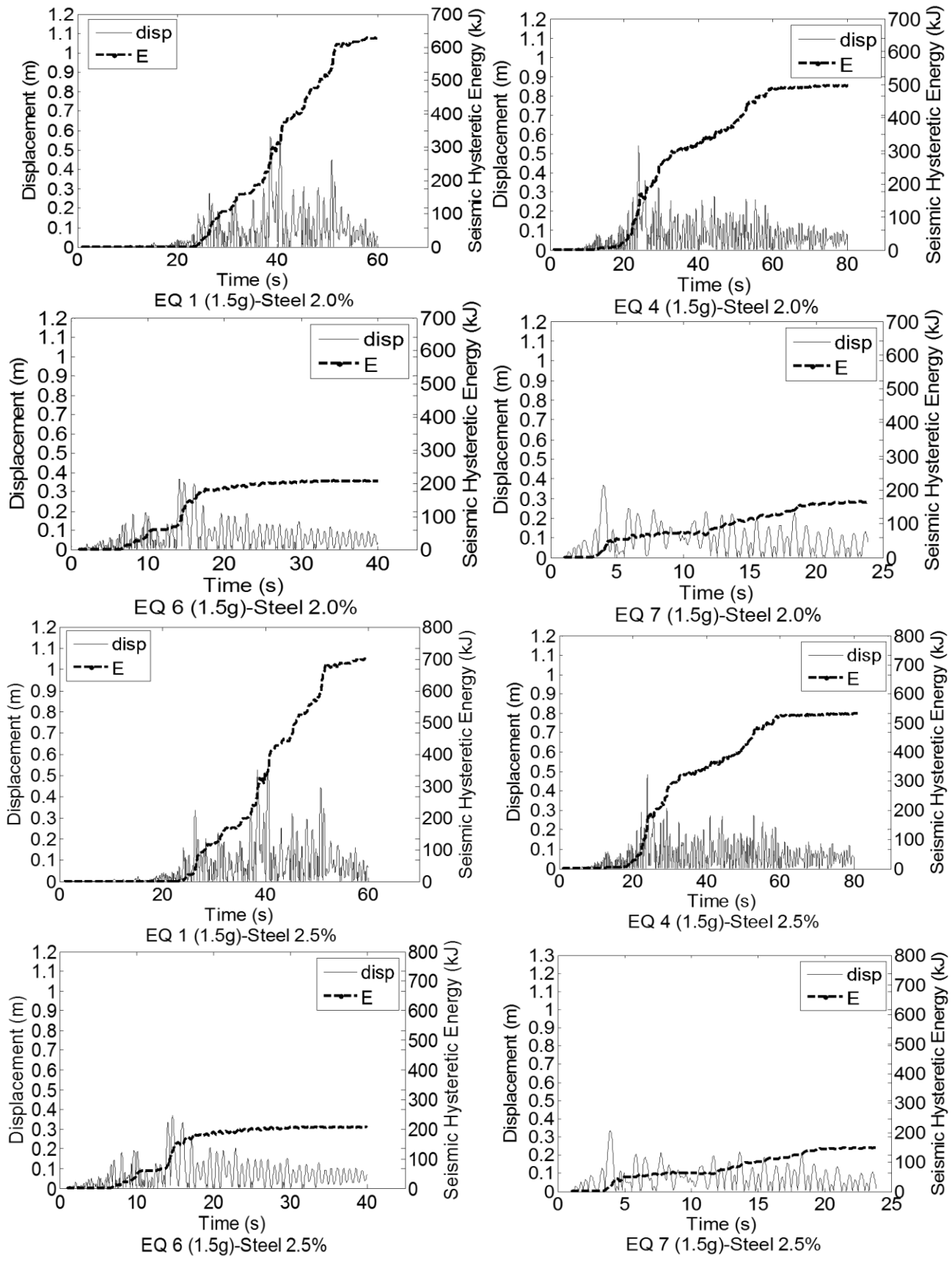


**Figure 95** Hysteretic Energy Plots - Frame 4 (cont.)

## Appendix II: Strain values at Different Limit States

**Table 10** Yield Beam and Yield Frame Strains - Frame 1 0.85%

Yield Beam				Yield Frame				
Earthquake	PGA	Steel Strain	PGA	Min. Concrete Strain	PGA	Steel Strain	PGA	Min. Concrete Strain
Chi-Chi	0.4	0.018639	0.4	-0.00117	0.4	0.021231	0.4	-0.000994382
Imperial Valley	0.4	0.010346	0.4	-0.000583	0.5	0.013675	0.4	-0.000644676
Kobe	0.4	0.00933	0.4	-0.000762	0.6	0.013757	0.4	-0.000407569
Kocaeli	0.4	0.012584	0.4	-0.001019	0.5	0.016225	0.4	-0.000926607
Loma Prieta	0.3	0.008191	0.3	-0.000764	0.3	0.012549	0.3	-0.000853669
Northridge	0.5	0.009317	0.5	-0.000684	0.7	0.01442	0.5	-0.000403146
Tabas	0.5	0.00868	0.5	-0.000379	0.6	0.011378	0.5	-0.000924217
<b>Average</b>		0.0110		-0.0008		0.0147		-0.0007
<b>Max</b>		0.0186		-0.0004		0.0212		-0.0004
<b>Min</b>		0.0082		-0.0012		0.0114		-0.0010
<b>standard deviation</b>		0.0037		0.0003		0.0032		0.0003

**Table 11** Steel Strain at Limit States - Frame 1 0.85%

Steel Strain						
Earthquake	PGA <sub>IO</sub>	IO	PGA <sub>LS</sub>	LS	PGA <sub>CP</sub>	CP
Chi-Chi	0.4	0.016961	0.5	0.023169	1.1	0.04647
Imperial Valley	0.3	0.008257	0.6	0.016502	1	0.037378
Kobe	0.3	0.007391	0.6	0.016083	1.1	0.036441
Kocaeli	0.4	0.011545	0.8	0.021893	1.4	0.043177
Loma Prieta	0.2	0.006784	0.4	0.01538	0.7	0.035324
Northridge	0.4	0.007582	0.9	0.017973	1.3	0.039175
Tabas	0.4	0.00681	0.6	0.013992	1.3	0.031867
<b>Average</b>		0.0093		0.0179		0.0385
<b>Max</b>		0.0170		0.0232		0.0465
<b>Min</b>		0.0068		0.0140		0.0319
<b>standard deviation</b>		0.0037		0.0034		0.0049

**Table 12** Concrete Strain at Limit States - Frame 1 0.85%

Minimum Concrete Strain						
Earthquake	PGA <sub>IO</sub>	IO	PGA <sub>LS</sub>	LS	PGA <sub>CP</sub>	CP
Chi-Chi	0.4	-0.00121	0.5	-0.0009	1.1	-0.00071
Imperial Valley	0.3	-0.00076	0.6	-0.00056	1	-0.00063
Kobe	0.3	-0.00078	0.6	-0.00042	1.1	-0.00071
Kocaeli	0.4	-0.001	0.8	-0.00063	1.4	-0.00055
Loma Prieta	0.2	-0.00072	0.4	-0.00092	0.7	-0.00175
Northridge	0.4	-0.00076	0.9	-0.00039	1.3	-0.00042
Tabas	0.4	-0.00051	0.6	-0.00112	1.3	-0.00082
<b>Average</b>		-0.0008		-0.0007		-0.0008
<b>Max</b>		-0.0005		-0.0004		-0.0004
<b>Min</b>		-0.0012		-0.0011		-0.0017
<b>standard deviation</b>		0.0002		0.0003		0.0004

**Table 13 Seismic Hysteretic Energy at Limit States (kJ) - Frame 1 0.85%**

Seismic Hysteretic Energy						
Earthquake	PGA <sub>IO</sub>	IO	PGA <sub>LS</sub>	LS	PGA <sub>CP</sub>	CP
Chi-Chi	0.4	11.463072	0.5	24.664237	1.1	174.494439
Imperial Valley	0.3	2.953483	0.6	23.757747	1	89.558456
Kobe	0.3	6.409273	0.6	28.133338	1.1	75.870588
Kocaeli	0.4	8.372676	0.8	124.935616	1.4	364.396061
Loma Prieta	0.2	3.584096	0.4	9.619667	0.7	27.890041
Northridge	0.4	4.799678	0.9	52.909542	1.3	121.016303
Tabas	0.4	6.984189	0.6	19.015736	1.3	71.738542
<b>Average</b>		6.3666		40.4337		132.1378
<b>Max</b>		11.4631		124.9356		364.3961
<b>Min</b>		2.9535		9.6197		27.8900
<b>standard deviation</b>		2.9504		39.5443		112.0687

**Table 14 Yield Beam and Yield Frame Strains - Frame 1 1.0%**

Earthquake	Yield Beam			Yield Frame				
	PGA	Steel Strain	PGA	Min. Concrete Strain	PGA	Steel Strain	PGA	Min. Concrete Strain
Chi-Chi	0.3	0.015923	0.3	-0.001144	0.4	0.02091	0.4	-0.00106763
Imperial Valley	0.3	0.007344	0.3	-0.000624	0.4	0.010511	0.4	-0.000997765
Kobe	0.3	0.007784	0.3	-0.000909	0.4	0.011701	0.4	-0.000705651
Kocaeli	0.4	0.012011	0.4	-0.001054	0.5	0.015754	0.5	-0.000861151
Loma Prieta	0.2	0.006247	0.2	-0.000875	0.3	0.010191	0.3	-0.000851235
Northridge	0.3	0.007997	0.3	-0.000737	0.6	0.011753	0.6	-0.000424137
Tabas	0.4	0.006766	0.4	-0.00053	0.6	0.010928	0.6	-0.001250314
<b>Average</b>		0.0092		-0.0008		0.0131		-0.0009
<b>Max</b>		0.0159		-0.0005		0.0209		-0.0004
<b>Min</b>		0.0062		-0.0011		0.0102		-0.0013
<b>standard deviation</b>		0.0035		0.0002		0.0039		0.0003

**Table 15 Steel Strain at Limit States - Frame 1 1.0%**

Steel Strain						
Earthquake	PGA <sub>IO</sub>	IO	PGA <sub>LS</sub>	LS	PGA <sub>CP</sub>	CP
Chi-Chi	0.3	0.0143	0.5	0.024158	1	0.041176
Imperial Valley	0.3	0.006139	0.5	0.013025	1	0.030182
Kobe	0.2	0.006424	0.6	0.014184	0.9	0.031207
Kocaeli	0.3	0.010891	0.6	0.0194	1.2	0.038156
Loma Prieta	0.2	0.005061	0.4	0.012658	0.6	0.030658
Northridge	0.3	0.006145	0.7	0.014959	1.3	0.031591
Tabas	0.3	0.005099	0.6	0.013515	1	0.033355
<b>Average</b>		0.0077		0.0160		0.0338
<b>Max</b>		0.0143		0.0242		0.0412
<b>Min</b>		0.0051		0.0127		0.0302
<b>standard deviation</b>		0.0035		0.0043		0.0042

**Table 16** Concrete Strain at Limit States - Frame 1 1.0%

Minimum Concrete Strain						
Earthquake	PGA <sub>IO</sub>	IO	PGA <sub>LS</sub>	LS	PGA <sub>CP</sub>	CP
Chi-Chi	0.3	-0.00124	0.5	-0.00107	1	-0.00081
Imperial Valley	0.3	-0.00078	0.5	-0.00097	1	-0.00065
Kobe	0.2	-0.00085	0.6	-0.00043	0.9	-0.00085
Kocaeli	0.3	-0.00111	0.6	-0.00092	1.2	-0.00067
Loma Prieta	0.2	-0.00079	0.4	-0.00083	0.6	-0.00208
Northridge	0.3	-0.00078	0.7	-0.00046	1.3	-0.00069
Tabas	0.3	-0.00062	0.6	-0.00142	1	-0.00156
<b>Average</b>		-0.0009		-0.0009		-0.0010
<b>Max</b>		-0.0006		-0.0004		-0.0007
<b>Min</b>		-0.0012		-0.0014		-0.0021
<b>standard deviation</b>		0.0002		0.0003		0.0006

**Table 17** Seismic Hysteretic Energy at Limit States (kJ) - Frame 1 1.0%

Seismic Hysteretic Energy						
Earthquake	PGA <sub>IO</sub>	IO	PGA <sub>LS</sub>	LS	PGA <sub>CP</sub>	CP
Chi-Chi	0.3	9.635293	0.5	53.14558	1	230.7358
Imperial Valley	0.3	2.834515	0.5	21.2011	1	87.04341
Kobe	0.2	3.882614	0.6	24.90995	0.9	83.91635
Kocaeli	0.3	10.72546	0.6	76.65787	1.2	456.162
Loma Prieta	0.2	2.637609	0.4	9.753388	0.6	26.03795
Northridge	0.3	3.710111	0.7	45.75272	1.3	137.2385
Tabas	0.3	3.261295	0.6	26.67779	1	84.16224
<b>Average</b>		5.2410		36.8712		157.8995
<b>Max</b>		10.7255		76.6579		456.1620
<b>Min</b>		2.6376		9.7534		26.0379
<b>standard deviation</b>		3.4173		22.9297		146.0658

**Table 18** Yield Beam and Yield Frame Strains - Frame 1 1.5%

Earthquake	Yield Beam				Yield Frame			
	PGA	Steel Strain	PGA	Min. Concrete Strain	PGA	Steel Strain	PGA	Min. Concrete Strain
Chi-Chi	0.3	0.007907	0.3	-0.001222	0.4	0.011565	0.4	-0.001336
Imperial Valley	0.3	0.003694	0.3	-0.000914	0.5	0.006642	0.5	-0.000946
Kobe	0.3	0.003699	0.3	-0.000921	0.4	0.006317	0.4	-0.001066
Kocaeli	0.3	0.006012	0.3	-0.001094	0.6	0.00844	0.6	-0.001258
Loma Prieta	0.3	0.003801	0.3	-0.000812	0.4	0.006324	0.4	-0.000676
Northridge	0.3	0.0039	0.3	-0.000935	0.4	0.006609	0.4	-0.000906
Tabas	0.4	0.003114	0.4	-0.000867	0.6	0.005281	0.6	-0.000971
<b>Average</b>		0.0046		-0.0010		0.0073		-0.0010
<b>Max</b>		0.0079		-0.0008		0.0116		-0.0007
<b>Min</b>		0.0031		-0.0012		0.0053		-0.0013
<b>standard deviation</b>		0.0017		0.0001		0.0021		0.0002

**Table 19** Steel Strain at Limit States - Frame 1 1.5%

Steel Strain						
Earthquake	PGA <sub>IO</sub>	IO	PGA <sub>LS</sub>	LS	PGA <sub>CP</sub>	CP
Chi-Chi	0.3	0.006486	0.5	0.013345	0.9	0.0237
Imperial Valley	0.3	0.00279	0.5	0.008282	1.1	0.017845
Kobe	0.3	0.002752	0.5	0.007925	1.1	0.021555
Kocaeli	0.3	0.004757	0.6	0.009898	1.3	0.021028
Loma Prieta	0.2	0.002903	0.4	0.007463	0.7	0.018909
Northridge	0.2	0.002946	0.6	0.008467	0	0.017617
Tabas	0.4	0.002377	0.7	0.006568	1.1	0.017712
<b>Average</b>		0.0036		0.0088		0.0198
<b>Max</b>		0.0065		0.0133		0.0237
<b>Min</b>		0.0024		0.0066		0.0176
<b>standard deviation</b>		0.0015		0.0022		0.0024

**Table 20** Concrete Strain at Limit States - Frame 1 1.5%

Minimum Concrete Strain						
Earthquake	PGA <sub>IO</sub>	IO	PGA <sub>LS</sub>	LS	PGA <sub>CP</sub>	CP
Chi-Chi	0.3	-0.00114	0.5	-0.00128	0.9	-0.00096
Imperial Valley	0.3	-0.00082	0.5	-0.00071	1.1	-0.00088
Kobe	0.3	-0.00084	0.5	-0.00103	1.1	-0.00164
Kocaeli	0.3	-0.001	0.6	-0.001	1.3	-0.00049
Loma Prieta	0.2	-0.00083	0.4	-0.00069	0.7	-0.0016
Northridge	0.2	-0.00084	0.6	-0.00068	0	-0.00063
Tabas	0.4	-0.00076	0.7	-0.00113	1.1	-0.0022
<b>Average</b>		-0.0009		-0.0009		-0.0012
<b>Max</b>		-0.0008		-0.0007		-0.0005
<b>Min</b>		-0.0011		-0.0013		-0.0022
<b>standard deviation</b>		0.0001		0.0002		0.0006

**Table 21** Seismic Hysteretic Energy at Limit States (kJ) - Frame 1 1.5%

Seismic Hysteretic Energy						
Earthquake	PGA <sub>IO</sub>	IO	PGA <sub>LS</sub>	LS	PGA <sub>CP</sub>	CP
Chi-Chi	0.3	5.072972	0.5	46.72209	0.9	206.9028
Imperial Valley	0.3	1.025008	0.5	16.7986	1.1	90.55653
Kobe	0.3	0.474299	0.5	23.76231	1.1	107.7082
Kocaeli	0.3	5.341352	0.6	37.53777	1.3	547.0421
Loma Prieta	0.2	0.884135	0.4	14.07259	0.7	40.26928
Northridge	0.2	0.661568	0.6	29.67648	0	203.8761
Tabas	0.4	0.490165	0.7	24.9887	1.1	83.38628
<b>Average</b>		1.9928		27.6512		182.8202
<b>Max</b>		5.3414		46.7221		547.0421
<b>Min</b>		0.4743		14.0726		40.2693
<b>standard deviation</b>		2.2061		11.4740		172.2610

**Table 22** Yield Beam and Yield Frame - Frame 1 2.0%

Yield Beam					Yield Frame			
Earthquake	PGA	Steel Strain	PGA	Min. Concrete Strain	PGA	Steel Strain	PGA	Min. Concrete Strain
Chi-Chi	0.3	0.007179	0.3	-0.001534	0.4	0.012175	0.4	-0.002005
Imperial Valley	0.4	0.002795	0.4	-0.001056	0.5	0.00621	0.5	-0.001349
Kobe	0.3	0.003205	0.3	-0.001066	0.4	0.006133	0.4	-0.001388
Kocaeli	0.4	0.004782	0.4	-0.001303	0.5	0.009373	0.5	-0.001653
Loma Prieta	0.3	0.003674	0.3	-0.001127	0.5	0.007114	0.5	-0.001229
Northridge	0.4	0.002766	0.4	-0.001044	0.5	0.007012	0.5	-0.001159
Tabas	0.5	0.002713	0.5	-0.001015	0.7	0.005289	0.7	-0.001309
<b>Average</b>		0.0039		-0.0012		0.0076		-0.0014
<b>Max</b>		0.0072		-0.0010		0.0122		-0.0012
<b>Min</b>		0.0027		-0.0015		0.0053		-0.0020
<b>standard deviation</b>		0.0016		0.0002		0.0024		0.0003

**Table 23** Steel Strain at Limit States - Frame 1 2.0%

Steel Strain						
Earthquake	PGA <sub>IO</sub>	IO	PGA <sub>LS</sub>	LS	PGA <sub>CP</sub>	CP
Chi-Chi	0.3	0.005395	0.5	0.014915	1	0.030697
Imperial Valley	0.3	0.002211	0.6	0.008587	1.3	0.022171
Kobe	0.3	0.002414	0.5	0.008219	1.3	0.027306
Kocaeli	0.4	0.003295	0.7	0.011557	1.3	0.022296
Loma Prieta	0.3	0.002372	0.6	0.00834	0.8	0.02368
Northridge	0.3	0.002158	0.5	0.008915	0	0.019784
Tabas	0.4	0.001815	0.9	0.007408	1.4	0.020782
<b>Average</b>		0.0028		0.0097		0.0238
<b>Max</b>		0.0054		0.0149		0.0307
<b>Min</b>		0.0018		0.0074		0.0198
<b>standard deviation</b>		0.0012		0.0026		0.0039

**Table 24** Concrete Strain at Limit States - Frame 1 2.0%

Minimum Concrete Strain						
Earthquake	PGA <sub>IO</sub>	IO	PGA <sub>LS</sub>	LS	PGA <sub>CP</sub>	CP
Chi-Chi	0.3	-0.00136	0.5	-0.00188	1	-0.00157
Imperial Valley	0.3	-0.00091	0.6	-0.00115	1.3	-0.00135
Kobe	0.3	-0.00091	0.5	-0.00144	1.3	-0.00289
Kocaeli	0.4	-0.00114	0.7	-0.00189	1.3	-0.00305
Loma Prieta	0.3	-0.00093	0.6	-0.00108	0.8	-0.00216
Northridge	0.3	-0.0009	0.5	-0.00102	0	-0.00079
Tabas	0.4	-0.00082	0.9	-0.00116	1.4	-0.00352
<b>Average</b>		-0.0010		-0.0014		-0.0022
<b>Max</b>		-0.0008		-0.0010		-0.0008
<b>Min</b>		-0.0014		-0.0019		-0.0035
<b>standard deviation</b>		0.0002		0.0004		0.0010

**Table 25** Seismic Hysteretic Energy at Limit States (kJ) - Frame 1 2.0%

Seismic Hysteretic Energy						
Earthquake	PGA <sub>IO</sub>	IO	PGA <sub>LS</sub>	LS	PGA <sub>CP</sub>	CP
Chi-Chi	0.3	2.660987	0.5	42.2331	1	267.5279
Imperial Valley	0.3	0.367086	0.6	18.96455	1.3	140.0073
Kobe	0.3	0.509676	0.5	10.99789	1.3	179.125
Kocaeli	0.4	0.506422	0.7	50.77509	1.3	212.7347
Loma Prieta	0.3	0.767391	0.6	19.33936	0.8	79.10424
Northridge	0.3	0.348859	0.5	17.84187	0	192.3867
Tabas	0.4	0.131808	0.9	15.6406	1.4	118.5779
<b>Average</b>		0.7560		25.1132		169.9234
<b>Max</b>		2.6610		50.7751		267.5279
<b>Min</b>		0.1318		10.9979		79.1042
<b>standard deviation</b>		0.8620		15.0810		62.8864

**Table 26** Yield Beam and Yield Frame - Frame 2 0.85%

Yield Beam					Yield Frame			
Earthquake	PGA	Steel Strain	PGA	Min. Concrete Strain	PGA	Steel Strain	PGA	Min. Concrete Strain
Chi-Chi	0.3	0.01629	0.3	-0.001281	0.4	0.020936	0.4	-0.001119
Imperial Valley	0.3	0.010275	0.3	-0.000705	0.5	0.013705	0.5	-0.000779
Kobe	0.4	0.009687	0.4	-0.000876	0.4	0.014261	0.4	-0.00057
Kocaeli	0.3	0.013522	0.3	-0.001128	0.5	0.017479	0.5	-0.000894
Loma Prieta	0.3	0.008391	0.3	-0.000929	0.4	0.012558	0.4	-0.00113
Northridge	0.4	0.009898	0.4	-0.000721	0.7	0.014026	0.7	-0.000489
Tabas	0.4	0.008861	0.4	-0.000699	0.5	0.012781	0.5	-0.000613
<b>Average</b>		0.0110		-0.0009		0.0151		-0.0008
<b>Max</b>		0.0163		-0.0007		0.0209		-0.0005
<b>Min</b>		0.0084		-0.0013		0.0126		-0.0011
<b>standard deviation</b>		0.0029		0.0002		0.0030		0.0003

**Table 27** Steel Strain at Limit States - Frame 2 0.85%

Steel Strain						
Earthquake	PGA <sub>IO</sub>	IO	PGA <sub>LS</sub>	LS	PGA <sub>CP</sub>	CP
Chi-Chi	0.2	0.013012	0.4	0.020745	0.8	0.038028
Imperial Valley	0.2	0.006871	0.5	0.013565	0.8	0.029974
Kobe	0.2	0.006623	0.4	0.014072	0.9	0.031151
Kocaeli	0.2	0.009764	0.5	0.017167	1.1	0.029699
Loma Prieta	0.3	0.005563	0.4	0.012384	0.6	0.027516
Northridge	0.3	0.006868	0.7	0.013818	1.1	0.031708
Tabas	0.2	0.005862	0.5	0.012628	1.1	0.02768
<b>Average</b>		0.0078		0.0149		0.0308
<b>Max</b>		0.0130		0.0207		0.0380
<b>Min</b>		0.0056		0.0124		0.0275
<b>standard deviation</b>		0.0027		0.0030		0.0035

**Table 28** Concrete Strain at Limit States - Frame 2 0.85%

Minimum Concrete Strain						
Earthquake	PGA <sub>IO</sub>	IO	PGA <sub>LS</sub>	LS	PGA <sub>CP</sub>	CP
Chi-Chi	0.2	-0.001101	0.4	-0.001133	0.8	-0.000519
Imperial Valley	0.2	-0.000729	0.5	-0.00076	0.8	-0.000513
Kobe	0.2	-0.000845	0.4	-0.000583	0.9	-0.000161
Kocaeli	0.2	-0.000964	0.5	-0.000914	1.1	-0.00113
Loma Prieta	0.3	-0.000787	0.4	-0.001122	0.6	-0.00161
Northridge	0.3	-0.00084	0.7	-0.000455	1.1	-0.000496
Tabas	0.2	-0.000818	0.5	-0.000613	1.1	-0.000691
<b>Average</b>		-0.0009		-0.0008		-0.0007
<b>Max</b>		-0.0007		-0.0005		-0.0002
<b>Min</b>		-0.0011		-0.0011		-0.0016
<b>standard deviation</b>		0.0001		0.0003		0.0005

**Table 29** Seismic Hysteretic Energy at Limit States (kJ) - Frame 2 0.85%

Seismic Hysteretic Energy						
Earthquake	PGA <sub>IO</sub>	IO	PGA <sub>LS</sub>	LS	PGA <sub>CP</sub>	CP
Chi-Chi	0.2	3.304262	0.4	16.551506	0.8	116.101056
Imperial Valley	0.2	2.376772	0.5	22.169064	0.8	50.330936
Kobe	0.2	2.126122	0.4	15.453854	0.9	74.558403
Kocaeli	0.2	10.717707	0.5	60.401422	1.1	104.295793
Loma Prieta	0.3	2.048543	0.4	7.658161	0.6	24.627702
Northridge	0.3	2.901216	0.7	22.801283	1.1	66.962472
Tabas	0.2	2.52877	0.5	7.203776	1.1	59.626343
<b>Average</b>		3.7148		21.7484		70.9290
<b>Max</b>		10.7177		60.4014		116.1011
<b>Min</b>		2.0485		7.2038		24.6277
<b>standard deviation</b>		3.1190		18.1294		31.3012

**Table 30** Yield Beam and Yield Frame Strains - Frame 2 1.0%

Earthquake	Yield Beam				Yield Frame			
	PGA	Steel Strain	PGA	Min. Concrete Strain	PGA	Steel Strain	PGA	Min. Concrete Strain
Chi-Chi	0.3	0.017219	0.3	-0.001402	0.4	0.022111	0.4	-0.001276
Imperial Valley	0.3	0.010874	0.3	-0.000691	0.6	0.014658	0.6	-0.000597
Kobe	0.4	0.010145	0.4	-0.00074	0.5	0.014238	0.5	-0.000747
Kocaeli	0.3	0.01427	0.3	0.001286	0.5	0.018533	0.5	-0.000289
Loma Prieta	0.3	0.008897	0.3	-0.00101	0.4	0.012917	0.4	-0.001209
Northridge	0.4	0.01037	0.4	-0.000747	0.7	0.014351	0.7	-0.000432
Tabas	0.4	0.008991	0.4	-0.000841	0.6	0.013146	0.6	-0.000611
<b>Average</b>		0.0115		-0.0006		0.0157		-0.0007
<b>Max</b>		0.0172		0.0013		0.0221		-0.0003
<b>Min</b>		0.0089		-0.0014		0.0129		-0.0013
<b>standard deviation</b>		0.0031		0.0009		0.0034		0.0004

**Table 31 Steel Strain at Limit States - Frame 2 1.0%**

<b>Steel Strain</b>						
<b>Earthquake</b>	<b>PGA<sub>IO</sub></b>	<b>IO</b>	<b>PGA<sub>LS</sub></b>	<b>LS</b>	<b>PGA<sub>CP</sub></b>	<b>CP</b>
Chi-Chi	0.2	0.013631	0.4	0.021914	0.8	0.041994
Imperial Valley	0.2	0.007011	0.4	0.014435	0.8	0.031576
Kobe	0.2	0.006673	0.5	0.013992	0.9	0.032418
Kocaeli	0.2	0.010255	0.5	0.018409	1.1	0.032081
Loma Prieta	0.2	0.006552	0.4	0.012739	0.6	0.029159
Northridge	0.2	0.006916	0.6	0.0142	1.1	0.033644
Tabas	0.2	0.005771	0.6	0.012927	1.1	0.028618
<b>Average</b>		0.0081		0.0155		0.0328
<b>Max</b>		0.0136		0.0219		0.0420
<b>Min</b>		0.0058		0.0127		0.0286
<b>standard deviation</b>		0.0028		0.0034		0.0044

**Table 32 Concrete Strain at Limit States - Frame 2 1.0%**

<b>Minimum Concrete Strain</b>						
<b>Earthquake</b>	<b>PGA<sub>IO</sub></b>	<b>IO</b>	<b>PGA<sub>LS</sub></b>	<b>LS</b>	<b>PGA<sub>CP</sub></b>	<b>CP</b>
Chi-Chi	0.2	-0.001198	0.4	-0.001289	0.8	-0.000743
Imperial Valley	0.2	-0.000756	0.4	-0.000569	0.8	-0.000588
Kobe	0.2	-0.000896	0.5	-0.000752	0.9	-0.000207
Kocaeli	0.2	0.001783	0.5	-0.000199	1.1	-0.001267
Loma Prieta	0.2	-0.000885	0.4	-0.0012	0.6	-0.001784
Northridge	0.2	-0.000904	0.6	-0.000414	1.1	-0.000476
Tabas	0.2	-0.000849	0.6	-0.000619	1.1	-0.00071
<b>Average</b>		-0.0005		-0.0007		-0.0008
<b>Max</b>		0.0018		-0.0002		-0.0002
<b>Min</b>		-0.0012		-0.0013		-0.0018
<b>standard deviation</b>		0.0010		0.0004		0.0005

**Table 33** Seismic Hysteretic Energy at Limit States (kJ) - Frame 2 1.0%

Seismic Hysteretic Energy						
Earthquake	PGA <sub>IO</sub>	IO	PGA <sub>LS</sub>	LS	PGA <sub>CP</sub>	CP
Chi-Chi	0.2	2.53863	0.4	17.149907	0.8	135.03905
Imperial Valley	0.2	2.586197	0.4	15.249404	0.8	58.863029
Kobe	0.2	2.336921	0.5	18.963949	0.9	77.687209
Kocaeli	0.2	9.942591	0.5	62.611604	1.1	125.75734
Loma Prieta	0.2	2.092575	0.4	7.38602	0.6	26.365045
Northridge	0.2	2.58646	0.6	25.097644	1.1	69.750915
Tabas	0.2	2.792545	0.6	10.84272	1.1	59.917299
<b>Average</b>		3.5537		22.4716		79.0543
<b>Max</b>		9.9426		62.6116		135.0390
<b>Min</b>		2.0926		7.3860		26.3650
<b>standard deviation</b>		2.8259		18.5908		38.6306

**Table 34** Yield Beam and Yield Frame Strains - Frame 2 1.5%

Yield Beam					Yield Frame			
Earthquake	PGA	Steel Strain	PGA	Min. Concrete Strain	PGA	Steel Strain	PGA	Min. Concrete Strain
Chi-Chi	0.3	0.014884	0.3	-0.001658	0.4	0.019983	0.4	-0.001994
Imperial Valley	0.3	0.007164	0.3	-0.001059	0.4	0.011134	0.4	-0.000712
Kobe	0.4	0.006859	0.4	-0.001142	0.5	0.012468	0.5	-0.001682
Kocaeli	0.3	0.010217	0.3	0	0.5	0.014949	0.5	0
Loma Prieta	0.3	0.005709	0.3	-0.000635	0.4	0.010703	0.4	-0.001465
Northridge	0.4	0.007112	0.4	-0.00106	0.6	0.010895	0.6	-0.000755
Tabas	0.2	0.005905	0.2	-0.001075	0.7	0.009501	0.7	-0.000879
<b>Average</b>		0.0083		-0.0009		0.0128		-0.0011
<b>Max</b>		0.0149		-0.0006		0.0200		-0.0007
<b>Min</b>		0.0057		-0.0017		0.0095		-0.0020
<b>standard deviation</b>		0.0033		0.0005		0.0036		0.0007

**Table 35** Steel Strain at Limit States - Frame 2 1.5%

Steel Strain						
Earthquake	PGA <sub>IO</sub>	IO	PGA <sub>LS</sub>	LS	PGA <sub>CP</sub>	CP
Chi-Chi	0.3	0.010587	0.4	0.019781	0.9	0.034283
Imperial Valley	0.2	0.004402	0.4	0.010984	0.9	0.025741
Kobe	0.2	0.004129	0.5	0.012214	0.8	0.024526
Kocaeli	0.2	0.006185	0.5	0.014769	1.2	0.03096
Loma Prieta	0.2	0.00402	0.4	0.010465	0.6	0.019738
Northridge	0.2	0.004267	0.6	0.010746	1.2	0.024142
Tabas	0.2	0.00333	0.7	0.009376	1.2	0.018405
<b>Average</b>		0.0053		0.0126		0.0254
<b>Max</b>		0.0106		0.0198		0.0343
<b>Min</b>		0.0033		0.0094		0.0184
<b>standard deviation</b>		0.0025		0.0036		0.0057

**Table 36** Concrete Strain at Limit States - Frame 2 1.5%

Minimum Concrete Strain						
Earthquake	PGA <sub>IO</sub>	IO	PGA <sub>LS</sub>	LS	PGA <sub>CP</sub>	CP
Chi-Chi	0.3	-0.001392	0.4	-0.00198	0.9	-0.00084
Imperial Valley	0.2	-0.000905	0.4	-0.000732	0.9	-0.001118
Kobe	0.2	-0.000886	0.5	-0.001656	0.8	-0.001018
Kocaeli	0.2	0.000183	0.5	0.000455	1.2	0.00238
Loma Prieta	0.2	-0.000436	0.4	-0.001433	0.6	-0.001979
Northridge	0.2	-0.000894	0.6	-0.000758	1.2	-0.001044
Tabas	0.2	-0.000857	0.7	-0.000867	1.2	-0.000803
<b>Average</b>		-0.0007		-0.0010		-0.0006
<b>Max</b>		0.0002		0.0005		0.0024
<b>Min</b>		-0.0014		-0.0020		-0.0020
<b>standard deviation</b>		0.0005		0.0008		0.0014

**Table 37** Seismic Hysteretic Energy at Limit States (kJ) - Frame 2 1.5%

Seismic Hysteretic Energy						
Earthquake	PGA <sub>IO</sub>	IO	PGA <sub>LS</sub>	LS	PGA <sub>CP</sub>	CP
Chi-Chi	0.3	4.746465	0.4	26.308416	0.9	176.35541
Imperial Valley	0.2	1.012191	0.4	9.299918	0.9	74.431443
Kobe	0.2	1.666647	0.5	18.170447	0.8	58.82842
Kocaeli	0.2	2.09458	0.5	66.228163	1.2	381.53054
Loma Prieta	0.2	0.950707	0.4	6.131701	0.6	23.95255
Northridge	0.2	1.776937	0.6	23.385862	1.2	81.52305
Tabas	0.2	0.57421	0.7	8.214199	1.2	39.844971
<b>Average</b>		1.8317		22.5341		119.4952
<b>Max</b>		4.7465		66.2282		381.5305
<b>Min</b>		0.5742		6.1317		23.9526
<b>standard deviation</b>		1.3919		20.7863		125.5131

**Table 38** Yield Beam and Yield Frame Strains - Frame 2 2.0%

Earthquake	Yield Beam				Yield Frame			
	PGA	Steel Strain	PGA	Min. Concrete Strain	PGA	Steel Strain	PGA	Min. Concrete Strain
Chi-Chi	0.4	0.010422	0.4	-0.001976	0.5	0.014062	0.5	-0.002507
Imperial Valley	0.3	0.003499	0.3	-0.001184	0.4	0.008615	0.4	-0.001068
Kobe	0.3	0.004371	0.3	-0.001256	0.4	0.008528	0.4	-0.000977
Kocaeli	0.3	0.006081	0.3	-0.001487	0.4	0.010133	0.4	-0.001962
Loma Prieta	0.3	0.004054	0.3	-0.0009	0.4	0.006703	0.4	-0.000963
Northridge	0.3	0.004297	0.3	-0.001186	0.6	0.008541	0.6	-0.000966
Tabas	0.4	0.003666	0.4	-0.001079	0.6	0.007621	0.6	-0.000895
<b>Average</b>		0.0052		-0.0013		0.0092		-0.0013
<b>Max</b>		0.0104		-0.0009		0.0141		-0.0009
<b>Min</b>		0.0035		-0.0020		0.0067		-0.0025
<b>standard deviation</b>		0.0025		0.0003		0.0024		0.0006

**Table 39** Steel Strain at Limit States - Frame 2 2.0%

<b>Steel Strain</b>						
<b>Earthquake</b>	<b>PGA<sub>IO</sub></b>	<b>IO</b>	<b>PGA<sub>LS</sub></b>	<b>LS</b>	<b>PGA<sub>CP</sub></b>	<b>CP</b>
Chi-Chi	0.2	0.006559	0.5	0.0139	0.9	0.026795
Imperial Valley	0.2	0.00263	0.4	0.008401	1	0.018229
Kobe	0.2	0.002675	0.4	0.008295	1	0.018713
Kocaeli	0.2	0.003585	0.4	0.009966	1.2	0.021923
Loma Prieta	0.2	0.002286	0.4	0.006639	0.7	0.018613
Northridge	0.2	0.00233	0.6	0.008496	1.5	0.018495
Tabas	0.3	0.002022	0.6	0.0075	1.1	0.016196
<b>Average</b>		0.0032		0.0090		0.0199
<b>Max</b>		0.0066		0.0139		0.0268
<b>Min</b>		0.0020		0.0066		0.0162
<b>standard deviation</b>		0.0016		0.0024		0.0035

**Table 40** Concrete Strain at Limit States - Frame 2 2.0%

<b>Minimum Concrete Strain</b>						
<b>Earthquake</b>	<b>PGA<sub>IO</sub></b>	<b>IO</b>	<b>PGA<sub>LS</sub></b>	<b>LS</b>	<b>PGA<sub>CP</sub></b>	<b>CP</b>
Chi-Chi	0.2	-0.001561	0.5	-0.002483	0.9	-0.00183
Imperial Valley	0.2	-0.000951	0.4	-0.001073	1	-0.00129
Kobe	0.2	-0.000964	0.4	-0.001027	1	-0.001164
Kocaeli	0.2	-0.001171	0.4	-0.001942	1.2	-0.001434
Loma Prieta	0.2	-0.000904	0.4	-0.000929	0.7	-0.00356
Northridge	0.2	-0.000937	0.6	-0.000974	1.5	-0.001267
Tabas	0.3	-0.000849	0.6	-0.000899	1.1	-0.002561
<b>Average</b>		-0.0010		-0.0013		-0.0019
<b>Max</b>		-0.0008		-0.0009		-0.0012
<b>Min</b>		-0.0016		-0.0025		-0.0036
<b>standard deviation</b>		0.0002		0.0006		0.0009

**Table 41** Seismic Hysteretic Energy at Limit States (kJ) - Frame 2 2.0%

Seismic Hysteretic Energy						
Earthquake	PGA <sub>IO</sub>	IO	PGA <sub>LS</sub>	LS	PGA <sub>CP</sub>	CP
Chi-Chi	0.2	3.130773	0.5	25.09414	0.9	153.106779
Imperial Valley	0.2	0.415252	0.4	11.14502	1	69.823561
Kobe	0.2	0.611056	0.4	16.0416	1	76.945308
Kocaeli	0.2	0.964242	0.4	21.82951	1.2	421.44149
Loma Prieta	0.2	0.375088	0.4	6.750935	0.7	24.22268
Northridge	0.2	0.274287	0.6	23.30713	1.5	136.826043
Tabas	0.3	0.223645	0.6	16.48896	1.1	40.288828
<b>Average</b>		0.8563		17.2368		131.8078
<b>Max</b>		3.1308		25.0941		421.4415
<b>Min</b>		0.2236		6.7509		24.2227
<b>standard deviation</b>		1.0336		6.6924		136.1180

**Table 42** Yield Beam and Yield Frame Strains - Frame 3 0.85%

Earthquake	Yield Beam				Yield Frame			
	PGA	Steel Strain	PGA	Min. Concrete Strain	PGA	Steel Strain	PGA	Min. Concrete Strain
Chi-Chi	0.3	0.020622	0.3	-0.00126	0.5	0.026525	0.5	-0.001154
Imperial Valley	0.4	0.008599	0.4	-0.000881	0.5	0.017381	0.5	-0.000465
Kobe	0.3	0.010056	0.3	-0.000867	0.4	0.014921	0.4	-0.00095
Kocaeli	0.3	0.014318	0.3	-0.001167	0.5	0.021672	0.5	-0.000596
Loma Prieta	0.3	0.010125	0.3	-0.001005	0.4	0.014682	0.4	-0.001228
Northridge	0.5	0.01032	0.5	-0.000759	0.6	0.017151	0.6	-0.000652
Tabas	0.4	0.008091	0.4	-0.000839	0.7	0.012628	0.7	-0.000769
<b>Average</b>		0.0117		-0.0010		0.0179		-0.0008
<b>Max</b>		0.0206		-0.0008		0.0265		-0.0005
<b>Min</b>		0.0081		-0.0013		0.0126		-0.0012
<b>standard deviation</b>		0.0044		0.0002		0.0048		0.0003

**Table 43** Steel Strain at Limit States - Frame 3 0.85%

Steel Strain						
Earthquake	PGA <sub>IO</sub>	IO	PGA <sub>LS</sub>	LS	PGA <sub>CP</sub>	CP
Chi-Chi	0.2	0.014824	0.4	0.024564	0.7	0.036828
Imperial Valley	0.2	0.007169	0.4	0.014607	0.7	0.029226
Kobe	0.2	0.006147	0.4	0.012904	0.8	0.028345
Kocaeli	0.2	0.010381	0.4	0.01921	0.9	0.031925
Loma Prieta	0.2	0.006038	0.4	0.013005	0.6	0.027386
Northridge	0.3	0.00689	0.6	0.014244	0.9	0.029928
Tabas	0.2	0.005921	0.6	0.012053	1	0.025121
<b>Average</b>		0.0082		0.0158		0.0298
<b>Max</b>		0.0148		0.0246		0.0368
<b>Min</b>		0.0059		0.0121		0.0251
<b>standard deviation</b>		0.0033		0.0045		0.0037

**Table 44** Concrete Strain at Limit States - Frame 3 0.85%

Minimum Concrete Strain						
Earthquake	PGA <sub>IO</sub>	IO	PGA <sub>LS</sub>	LS	PGA <sub>CP</sub>	CP
Chi-Chi	0.2	-0.001196	0.4	-0.001189	0.7	-0.000966
Imperial Valley	0.2	-0.000855	0.4	-0.000567	0.7	-0.000687
Kobe	0.2	-0.000744	0.4	-0.000889	0.8	-0.000815
Kocaeli	0.2	-0.000941	0.4	-0.000772	0.9	-0.001204
Loma Prieta	0.2	-0.00078	0.4	-0.001151	0.6	-0.001618
Northridge	0.3	-0.000838	0.6	-0.000779	0.9	-0.00045
Tabas	0.2	-0.000797	0.6	-0.000679	1	-0.001187
<b>Average</b>		-0.0009		-0.0009		-0.0010
<b>Max</b>		-0.0007		-0.0006		-0.0005
<b>Min</b>		-0.0012		-0.0012		-0.0016
<b>standard deviation</b>		0.0002		0.0002		0.0004

**Table 45** Seismic Hysteretic Energy at Limit States (kJ) - Frame 3 0.85%

Seismic Hysteretic Energy						
Earthquake	PGA <sub>IO</sub>	IO	PGA <sub>LS</sub>	LS	PGA <sub>CP</sub>	CP
Chi-Chi	0.2	2.802367	0.4	19.585275	0.7	80.106542
Imperial Valley	0.2	1.637014	0.4	16.342564	0.7	27.712427
Kobe	0.2	1.568384	0.4	8.380181	0.8	37.026571
Kocaeli	0.2	7.391769	0.4	25.569509	0.9	97.700099
Loma Prieta	0.2	1.054508	0.4	9.622822	0.6	13.027965
Northridge	0.3	2.966103	0.6	12.462804	0.9	37.141672
Tabas	0.2	0.927138	0.6	8.209369	1	32.814155
<b>Average</b>		2.6210		14.3104		46.5042
<b>Max</b>		7.3918		25.5695		97.7001
<b>Min</b>		0.9271		8.2094		13.0280
<b>standard deviation</b>		2.2476		6.5383		30.5200

**Table 46** Yield Beam and Yield Frame Strains - Frame 3 1.0%

Earthquake	Yield Beam				Yield Frame			
	PGA	Steel Strain	PGA	Min. Concrete Strain	PGA	Steel Strain	PGA	Min. Concrete Strain
Chi-Chi	0.3	0.018121	0.3	-0.001285	0.4	0.023582	0.4	-0.001294
Imperial Valley	0.4	0.009328	0.4	-0.00066	0.5	0.014868	0.5	-0.000465
Kobe	0.3	0.009815	0.3	-0.000886	0.4	0.015399	0.4	-0.000766
Kocaeli	0.3	0.012515	0.3	-0.001152	0.5	0.019136	0.5	-0.000647
Loma Prieta	0.3	0.008658	0.3	-0.001003	0.4	0.012783	0.4	-0.00122
Northridge	0.5	0.01032	0.5	-0.000759	0.6	0.017151	0.6	-0.000652
Tabas	0.4	0.008091	0.4	-0.000839	0.7	0.012628	0.7	-0.000769
<b>Average</b>		0.0110		-0.0009		0.0165		-0.0008
<b>Max</b>		0.0181		-0.0007		0.0236		-0.0005
<b>Min</b>		0.0081		-0.0013		0.0126		-0.0013
<b>standard deviation</b>		0.0035		0.0002		0.0039		0.0003

**Table 47** Steel Strain at Limit States- Frame 3 1.0%

Steel Strain						
Earthquake	PGA <sub>IO</sub>	IO	PGA <sub>LS</sub>	LS	PGA <sub>CP</sub>	CP
Chi-Chi	0.2	0.013168	0.4	0.021749	0.7	0.035619
Imperial Valley	0.2	0.00594	0.4	0.012889	0.7	0.02676
Kobe	0.2	0.005394	0.4	0.013353	0.9	0.026521
Kocaeli	0.2	0.008858	0.4	0.01708	0.9	0.030523
Loma Prieta	0.2	0.005074	0.4	0.011268	0.6	0.023588
Northridge	0.3	0.00689	0.6	0.014244	0.9	0.029928
Tabas	0.2	0.005921	0.6	0.012053	1	0.025121
<b>Average</b>		0.0073		0.0147		0.0283
<b>Max</b>		0.0132		0.0217		0.0356
<b>Min</b>		0.0051		0.0113		0.0236
<b>standard deviation</b>		0.0029		0.0036		0.0041

**Table 48** Concrete Strain at Limit States - Frame 3 1.0%

Minimum Concrete Strain						
Earthquake	PGA <sub>IO</sub>	IO	PGA <sub>LS</sub>	LS	PGA <sub>CP</sub>	CP
Chi-Chi	0.2	-0.001193	0.4	-0.001303	0.7	-0.000636
Imperial Valley	0.2	-0.000851	0.4	-0.000524	0.7	-0.000566
Kobe	0.2	-0.000804	0.4	-0.00083	0.9	-0.000456
Kocaeli	0.2	-0.000944	0.4	-0.000774	0.9	-0.000737
Loma Prieta	0.2	-0.000796	0.4	-0.001143	0.6	-0.001732
Northridge	0.3	-0.000838	0.6	-0.000779	0.9	-0.00045
Tabas	0.2	-0.000797	0.6	-0.000679	1	-0.001187
<b>Average</b>		-0.0009		-0.0009		-0.0008
<b>Max</b>		-0.0008		-0.0005		-0.0005
<b>Min</b>		-0.0012		-0.0013		-0.0017
<b>standard deviation</b>		0.0001		0.0003		0.0005

**Table 49** Seismic Hysteretic Energy at Limit States (kJ) - Frame 3 1.0%

Seismic Hysteretic Energy						
Earthquake	PGA <sub>IO</sub>	IO	PGA <sub>LS</sub>	LS	PGA <sub>CP</sub>	CP
Chi-Chi	0.2	2.347806	0.4	17.904137	0.7	94.549863
Imperial Valley	0.2	1.239073	0.4	17.38619	0.7	36.352281
Kobe	0.2	2.867228	0.4	10.940913	0.9	48.169927
Kocaeli	0.2	6.979053	0.4	25.447562	0.9	126.775653
Loma Prieta	0.2	0.921529	0.4	9.626477	0.6	12.239561
Northridge	0.3	2.966103	0.6	12.462804	0.9	37.141672
Tabas	0.2	0.927138	0.6	8.209369	1	32.814155
<b>Average</b>		2.6068		14.5682		55.4347
<b>Max</b>		6.9791		25.4476		126.7757
<b>Min</b>		0.9215		8.2094		12.2396
<b>standard deviation</b>		2.1179		6.0536		40.3084

**Table 50** Yield Beam and Yield Frame Strain - Frame 3 1.5%

Earthquake	Yield Beam				Yield Frame			
	PGA	Steel Strain	PGA	Min. Concrete Strain	PGA	Steel Strain	PGA	Min. Concrete Strain
Chi-Chi	0.3	0.013903	0.3	-0.001519	0.4	0.017747	0.4	-0.001817
Imperial Valley	0.4	0.006859	0.4	-0.000914	0.5	0.010262	0.5	-0.001106
Kobe	0.3	0.006697	0.3	-0.001075	0.4	0.010854	0.4	-0.001119
Kocaeli	0.3	0.011261	0.3	-0.001366	0.5	0.013873	0.5	-0.001383
Loma Prieta	0.3	0.006219	0.3	-0.001049	0.4	0.009644	0.4	-0.001273
Northridge	0.4	0.007352	0.4	-0.001012	0.7	0.01173	0.7	-0.000642
Tabas	0.5	0.006275	0.5	-0.001028	0.5	0.009228	0.5	-0.000995
<b>Average</b>		0.0084		-0.0011		0.0119		-0.0012
<b>Max</b>		0.0139		-0.0009		0.0177		-0.0006
<b>Min</b>		0.0062		-0.0015		0.0092		-0.0018
<b>standard deviation</b>		0.0030		0.0002		0.0030		0.0004

**Table 51** Steel Strain at Limit States - Frame 3 1.5%

Earthquake	Steel Strain					
	PGA <sub>IO</sub>	IO	PGA <sub>LS</sub>	LS	PGA <sub>CP</sub>	CP
Chi-Chi	0.2	0.010665	0.4	0.016286	0.8	0.030795
Imperial Valley	0.2	0.004244	0.5	0.008903	0.8	0.021278
Kobe	0.2	0.00384	0.4	0.009242	0.9	0.023524
Kocaeli	0.2	0.007892	0.4	0.012353	1.1	0.025831
Loma Prieta	0.2	0.00312	0.4	0.008402	0.6	0.019216
Northridge	0.3	0.003795	0.5	0.0096	1	0.023272
Tabas	0.2	0.003239	0.5	0.008132	1.1	0.018518
<b>Average</b>		0.0053		0.0104		0.0232
<b>Max</b>		0.0107		0.0163		0.0308
<b>Min</b>		0.0031		0.0081		0.0185
<b>standard deviation</b>		0.0029		0.0029		0.0042

**Table 52** Concrete Strain at Limit States - Frame 3 1.5%

Earthquake	Minimum Concrete Strain					
	PGA <sub>IO</sub>	IO	PGA <sub>LS</sub>	LS	PGA <sub>CP</sub>	CP
Chi-Chi	0.2	-0.001251	0.4	-0.001706	0.8	-0.000963
Imperial Valley	0.2	-0.000878	0.5	-0.001004	0.8	-0.000622
Kobe	0.2	-0.000861	0.4	-0.001116	0.9	-0.000308
Kocaeli	0.2	-0.00117	0.4	-0.001391	1.1	-0.000647
Loma Prieta	0.2	-0.0008	0.4	-0.001193	0.6	-0.001967
Northridge	0.3	-0.000874	0.5	-0.000792	1	-0.000607
Tabas	0.2	-0.000816	0.5	-0.001007	1.1	-0.000899
<b>Average</b>		-0.0010		-0.0012		-0.0009
<b>Max</b>		-0.0008		-0.0008		-0.0003
<b>Min</b>		-0.0013		-0.0017		-0.0020
<b>standard deviation</b>		0.0002		0.0003		0.0005

**Table 53** Seismic Hysteretic Energy at Limit States (kJ) - Frame 3 1.5%

Seismic Hysteretic Energy						
Earthquake	PGA <sub>IO</sub>	IO	PGA <sub>LS</sub>	LS	PGA <sub>CP</sub>	CP
Chi-Chi	0.2	2.558274	0.4	11.665363	0.8	95.74429
Imperial Valley	0.2	0.843222	0.5	14.092191	0.8	42.789707
Kobe	0.2	0.886051	0.4	9.469667	0.9	62.659855
Kocaeli	0.2	7.244241	0.4	32.93227	1.1	137.70712
Loma Prieta	0.2	0.578491	0.4	6.83378	0.6	21.290005
Northridge	0.3	1.464263	0.5	11.926939	1	53.088479
Tabas	0.2	0.553513	0.5	3.781264	1.1	44.775385
<b>Average</b>		2.0183		12.9574		65.4364
<b>Max</b>		7.2442		32.9323		137.7071
<b>Min</b>		0.5535		3.7813		21.2900
<b>standard deviation</b>		2.4080		9.4594		39.1375

**Table 54** Yield Beam and Yield Frame Strains - Frame 3 2.0%

Earthquake	Yield Beam				Yield Frame			
	PGA	Steel Strain	PGA	Min. Concrete Strain	PGA	Steel Strain	PGA	Min. Concrete Strain
Chi-Chi	0.3	0.011881	0.3	-0.001624	0.5	0.015617	0.5	-0.001952
Imperial Valley	0.4	0.005054	0.4	-0.001113	0.6	0.007795	0.6	-0.001347
Kobe	0.4	0.005428	0.4	-0.001179	0.5	0.007474	0.5	-0.001235
Kocaeli	0.3	0.008734	0.3	-0.001434	0.5	0.011043	0.5	-0.00145
Loma Prieta	0.3	0.003974	0.3	-0.001029	0.4	0.006548	0.4	-0.001231
Northridge	0.4	0.005105	0.4	-0.001153	0.6	0.008033	0.6	-0.001139
Tabas	0.4	0.004218	0.4	-0.001059	0.6	0.006251	0.6	-0.001217
<b>Average</b>		0.0063		-0.0012		0.0090		-0.0014
<b>Max</b>		0.0119		-0.0010		0.0156		-0.0011
<b>Min</b>		0.0040		-0.0016		0.0063		-0.0020
<b>standard deviation</b>		0.0029		0.0002		0.0033		0.0003

**Table 55** Steel Strain at Limit States - Frame 3 2.0%

Steel Strain						
Earthquake	PGA <sub>IO</sub>	IO	PGA <sub>LS</sub>	LS	PGA <sub>CP</sub>	CP
Chi-Chi	0.2	0.006239	0.4	0.0146	0.8	0.026453
Imperial Valley	0.2	0.002944	0.4	0.006532	0.8	0.016206
Kobe	0.2	0.002473	0.4	0.006353	0.8	0.017197
Kocaeli	0.2	0.005054	0.4	0.010117	1	0.022113
Loma Prieta	0.2	0.00226	0.4	0.005576	0.6	0.012757
Northridge	0.2	0.002336	0.5	0.006952	1	0.017775
Tabas	0.2	0.002054	0.6	0.005217	1.1	0.011381
<b>Average</b>		0.0033		0.0079		0.0177
<b>Max</b>		0.0062		0.0146		0.0265
<b>Min</b>		0.0021		0.0052		0.0114
<b>standard deviation</b>		0.0016		0.0034		0.0052

**Table 56** Concrete Strain at Limit States - Frame 3 2.0%

Minimum Concrete Strain						
Earthquake	PGA <sub>IO</sub>	IO	PGA <sub>LS</sub>	LS	PGA <sub>CP</sub>	CP
Chi-Chi	0.2	-0.001169	0.4	-0.00186	0.8	-0.00103
Imperial Valley	0.2	-0.00084	0.4	-0.0012	0.8	-0.000752
Kobe	0.2	-0.000824	0.4	-0.00121	0.8	-0.001055
Kocaeli	0.2	-0.001066	0.4	-0.00151	1	-0.000812
Loma Prieta	0.2	-0.000808	0.4	-0.00116	0.6	-0.001713
Northridge	0.2	-0.000834	0.5	-0.0012	1	-0.000743
Tabas	0.2	-0.000752	0.6	-0.00114	1.1	-0.001117
<b>Average</b>		-0.0009		-0.0013		-0.0010
<b>Max</b>		-0.0008		-0.0011		-0.0007
<b>Min</b>		-0.0012		-0.0019		-0.0017
<b>standard deviation</b>		0.0002		0.0003		0.0003

**Table 57** Seismic Hysteretic Energy at Limit States (kJ) - Frame 3 2.0%

Seismic Hysteretic Energy						
Earthquake	PGA <sub>IO</sub>	IO	PGA <sub>LS</sub>	LS	PGA <sub>CP</sub>	CP
Chi-Chi	0.2	1.358845	0.4	16.53275	0.8	125.483113
Imperial Valley	0.2	0.489348	0.4	5.523577	0.8	48.171745
Kobe	0.2	0.426338	0.4	6.794231	0.8	47.085009
Kocaeli	0.2	5.506911	0.4	50.73686	1	199.801542
Loma Prieta	0.2	0.200136	0.4	2.77107	0.6	21.071546
Northridge	0.2	0.280521	0.5	7.339913	1	50.092365
Tabas	0.2	0.156196	0.6	2.617692	1.1	21.691596
<b>Average</b>		1.2026		13.1880		73.3424
<b>Max</b>		5.5069		50.7369		199.8015
<b>Min</b>		0.1562		2.6177		21.0715
<b>standard deviation</b>		1.9413		17.2006		65.7954

**Table 58** Yield Beam and Yield Frame Strains - Frame 4 1.0%

Earthquake	Yield Beam				Yield Frame			
	PGA	Steel Strain	PGA	Min. Concrete Strain	PGA	Steel Strain	PGA	Min. Concrete Strain
Chi-Chi	0.4	0.03194	0.4	-0.002273	0.4	0.035878	0.4	-0.002265
Imperial Valley	0.4	0.012671	0.4	-0.001201	0.5	0.018495	0.5	-0.001396
Kobe	0.4	0.014887	0.4	-0.001333	0.5	0.019221	0.5	-0.001549
Kocaeli	0.4	0.023463	0.4	-0.00161	0.5	0.027522	0.5	-0.001615
Loma Prieta	0.4	0.013122	0.4	-0.001181	0.5	0.01822	0.5	-0.001478
Northridge	0.4	0.017362	0.4	-0.001325	0.5	0.023057	0.5	-0.00137
Tabas	0.5	0.012166	0.5	-0.001162	0.6	0.014021	0.6	-0.001169
<b>Average</b>		0.0179		-0.0014		0.0223		-0.0015
<b>Max</b>		0.0319		-0.0012		0.0359		-0.0012
<b>Min</b>		0.0122		-0.0023		0.0140		-0.0023
<b>standard deviation</b>		0.0073		0.0004		0.0073		0.0003

**Table 59** Steel Strain at Limit States - Frame 4 1.0%

Steel Strain						
Earthquake	PGA <sub>IO</sub>	IO	PGA <sub>LS</sub>	LS	PGA <sub>CP</sub>	CP
Chi-Chi	0.2	0.027492	0.4	0.032475	0.6	0.04593
Imperial Valley	0.2	0.009538	0.4	0.013248	0.6	0.029603
Kobe	0.2	0.007032	0.4	0.015325	0.8	0.028246
Kocaeli	0.2	0.018843	0.4	0.023591	0.7	0.038213
Loma Prieta	0.2	0.007465	0.4	0.013898	0.6	0.025462
Northridge	0.3	0.008128	0.4	0.018136	0.8	0.031021
Tabas	0.2	0.004919	0.5	0.011738	0.8	0.023376
<b>Average</b>		0.0119		0.0183		0.0317
<b>Max</b>		0.0275		0.0325		0.0459
<b>Min</b>		0.0049		0.0117		0.0234
<b>standard deviation</b>		0.0082		0.0074		0.0079

**Table 60** Concrete Strain at Limit States - Frame 4 1.0%

Minimum Concrete Strain						
Earthquake	PGA <sub>IO</sub>	IO	PGA <sub>LS</sub>	LS	PGA <sub>CP</sub>	CP
Chi-Chi	0.2	-0.0019	0.4	-0.00227	0.6	-0.00145
Imperial Valley	0.2	-0.00102	0.4	-0.00123	0.6	-0.00138
Kobe	0.2	-0.00088	0.4	-0.00136	0.8	-0.00143
Kocaeli	0.2	-0.00145	0.4	-0.00156	0.7	-0.00132
Loma Prieta	0.2	-0.00091	0.4	-0.00123	0.6	-0.00184
Northridge	0.3	-0.00097	0.4	-0.00134	0.8	-0.00083
Tabas	0.2	-0.00077	0.5	-0.00114	0.8	-0.00081
<b>Average</b>		-0.0011		-0.0014		-0.0013
<b>Max</b>		-0.0008		-0.0011		-0.0008
<b>Min</b>		-0.0019		-0.0023		-0.0018
<b>standard deviation</b>		0.0004		0.0004		0.0004

**Table 61** Seismic Hysteretic Energy at Limit States (kJ) - Frame 4 1.0%

Seismic Hysteretic Energy						
Earthquake	PGA <sub>IO</sub>	IO	PGA <sub>LS</sub>	LS	PGA <sub>CP</sub>	CP
Chi-Chi	0.2	9.455912	0.4	29.00956	0.6	93.67952
Imperial Valley	0.2	7.082956	0.4	18.99733	0.6	41.26598
Kobe	0.2	1.842077	0.4	13.33501	0.8	56.5631
Kocaeli	0.2	5.71639	0.4	35.0726	0.7	91.35505
Loma Prieta	0.2	2.438046	0.4	8.8906	0.6	20.40644
Northridge	0.3	3.897393	0.4	18.20968	0.8	42.73277
Tabas	0.2	0.716518	0.5	19.93892	0.8	46.62486
<b>Average</b>		4.4499		20.4934		56.0897
<b>Max</b>		9.4559		35.0726		93.6795
<b>Min</b>		0.7165		8.8906		20.4064
<b>standard deviation</b>		3.1275		8.9322		27.1351

**Table 62** Yield Beam and Yield Frame Strains - Frame 4 1.5%

Yield Beam					Yield Frame			
Earthquake	PGA	Steel Strain	PGA	Min. Concrete Strain	PGA	Steel Strain	PGA	Min. Concrete Strain
Chi-Chi	0.3	0.032238	0.3	-0.002922	0.5	0.031976	0.5	-0.002747
Imperial Valley	0.4	0.008992	0.4	-0.001271	0.5	0.013219	0.5	-0.001516
Kobe	0.4	0.011392	0.4	-0.001439	0.5	0.016497	0.5	-0.001774
Kocaeli	0.4	0.02062	0.4	-0.002017	0.6	0.02779	0.6	-0.001657
Loma Prieta	0.3	0.009949	0.3	-0.001319	0.4	0.013942	0.4	-0.001579
Northridge	0.4	0.011004	0.4	-0.001405	0.5	0.018125	0.5	-0.00133
Tabas	0.5	0.012043	0.5	-0.001279	0.7	0.012657	0.7	-0.001767
<b>Average</b>		0.0152		-0.0017		0.0192		-0.0018
<b>Max</b>		0.0322		-0.0013		0.0320		-0.0013
<b>Min</b>		0.0090		-0.0029		0.0127		-0.0027
<b>standard deviation</b>		0.0084		0.0006		0.0077		0.0005

**Table 63** Steel Strain at Limit States - Frame 4 1.5%

Steel Strain						
Earthquake	PGA <sub>IO</sub>	IO	PGA <sub>LS</sub>	LS	PGA <sub>CP</sub>	CP
Chi-Chi	0.2	0.023561	0.4	0.032227	0.6	0.040782
Imperial Valley	0.2	0.004376	0.4	0.0096	0.7	0.022038
Kobe	0.2	0.00469	0.4	0.012097	0.8	0.031201
Kocaeli	0.2	0.01389	0.5	0.020863	0.8	0.031546
Loma Prieta	0.2	0.004751	0.3	0.010402	0.7	0.021444
Northridge	0.2	0.004694	0.5	0.011972	0.8	0.026635
Tabas	0.2	0.002469	0.6	0.012732	0.8	0.017434
<b>Average</b>		0.0083		0.0157		0.0273
<b>Max</b>		0.0236		0.0322		0.0408
<b>Min</b>		0.0025		0.0096		0.0174
<b>standard deviation</b>		0.0077		0.0082		0.0079

**Table 64** Concrete Strain at Limit States - Frame 4 1.5%

Minimum Concrete Strain						
Earthquake	PGA <sub>IO</sub>	IO	PGA <sub>LS</sub>	LS	PGA <sub>CP</sub>	CP
Chi-Chi	0.2	-0.00222	0.4	-0.00293	0.6	-0.00262
Imperial Valley	0.2	-0.0009	0.4	-0.0013	0.7	-0.00183
Kobe	0.2	-0.00099	0.4	-0.00148	0.8	-0.00106
Kocaeli	0.2	-0.0015	0.5	-0.00199	0.8	-0.00159
Loma Prieta	0.2	-0.00094	0.3	-0.00135	0.7	-0.00213
Northridge	0.2	-0.00098	0.5	-0.0014	0.8	-0.00111
Tabas	0.2	-0.00074	0.6	-0.00136	0.8	-0.00191
<b>Average</b>		-0.0012		-0.0017		-0.0018
<b>Max</b>		-0.0007		-0.0013		-0.0011
<b>Min</b>		-0.0022		-0.0029		-0.0026
<b>standard deviation</b>		0.0005		0.0006		0.0006

**Table 65** Seismic Hysteretic Energy at Limit States (kJ) - Frame 4 1.5%

Seismic Hysteretic Energy						
Earthquake	PGA <sub>IO</sub>	IO	PGA <sub>LS</sub>	LS	PGA <sub>CP</sub>	CP
Chi-Chi	0.2	9.593921	0.4	29.05369	0.6	126.3554
Imperial Valley	0.2	2.447784	0.4	15.23915	0.7	50.26053
Kobe	0.2	1.164645	0.4	18.17456	0.8	118.1602
Kocaeli	0.2	5.14997	0.5	25.07101	0.8	155.0229
Loma Prieta	0.2	2.807459	0.3	9.533577	0.7	32.36683
Northridge	0.2	1.843639	0.5	17.04673	0.8	51.22759
Tabas	0.2	0.191113	0.6	17.02792	0.8	53.58286
<b>Average</b>		3.3141		18.7352		83.8537
<b>Max</b>		9.5939		29.0537		155.0229
<b>Min</b>		0.1911		9.5336		32.3668
<b>standard deviation</b>		3.1715		6.4496		47.9732

**Table 66** Yield Beam and Yield Frame Strains - Frame 4 2.0%

Earthquake	Yield Beam				Yield Frame			
	PGA	Steel Strain	PGA	Min. Concrete Strain	PGA	Steel Strain	PGA	Min. Concrete Strain
Chi-Chi	0.4	0.023655	0.4	-0.003171	0.5	0.029242	0.5	-0.003615
Imperial Valley	0.3	0.006486	0.3	-0.001447	0.5	0.013215	0.5	-0.001208
Kobe	0.3	0.008425	0.3	-0.001671	0.5	0.013216	0.5	-0.002179
Kocaeli	0.4	0.017901	0.4	-0.002674	0.5	0.023211	0.5	-0.002854
Loma Prieta	0.3	0.007773	0.3	-0.001581	0.4	0.011195	0.4	-0.001926
Northridge	0.4	0.010133	0.4	-0.001832	0.7	0.013221	0.7	-0.001468
Tabas	0.4	0.005251	0.4	-0.001328	0.5	0.009829	0.5	-0.001898
<b>Average</b>		0.0114		-0.0020		0.0162		-0.0022
<b>Max</b>		0.0237		-0.0013		0.0292		-0.0012
<b>Min</b>		0.0053		-0.0032		0.0098		-0.0036
<b>standard deviation</b>		0.0068		0.0007		0.0072		0.0008

**Table 67** Steel Strain at Limit States - Frame 4 2.0%

Steel Strain						
Earthquake	PGA <sub>IO</sub>	IO	PGA <sub>LS</sub>	LS	PGA <sub>CP</sub>	CP
Chi-Chi	0.2	0.016976	0.4	0.02424	0.8	0.033658
Imperial Valley	0.2	0.002306	0.4	0.007474	0.8	0.019332
Kobe	0.2	0.003165	0.3	0.009114	0.8	0.021171
Kocaeli	0.2	0.00618	0.4	0.018518	0.9	0.026953
Loma Prieta	0.2	0.002282	0.3	0.008669	0.6	0.017127
Northridge	0.2	0.002438	0.5	0.010479	0.9	0.022679
Tabas	0.2	0.001661	0.4	0.005881	1.1	0.012262
<b>Average</b>		0.0050		0.0121		0.0219
<b>Max</b>		0.0170		0.0242		0.0337
<b>Min</b>		0.0017		0.0059		0.0123
<b>standard deviation</b>		0.0055		0.0067		0.0069

**Table 68** Concrete Strain at Limit States - Frame 4 2.0%

Minimum Concrete Strain						
Earthquake	PGA <sub>IO</sub>	IO	PGA <sub>LS</sub>	LS	PGA <sub>CP</sub>	CP
Chi-Chi	0.2	-0.00239	0.4	-0.00325	0.8	-0.00336
Imperial Valley	0.2	-0.0009	0.4	-0.00145	0.8	-0.00159
Kobe	0.2	-0.00106	0.3	-0.00174	0.8	-0.00207
Kocaeli	0.2	-0.00132	0.4	-0.00273	0.9	-0.00282
Loma Prieta	0.2	-0.00087	0.3	-0.00168	0.6	-0.0026
Northridge	0.2	-0.00095	0.5	-0.00185	0.9	-0.00135
Tabas	0.2	-0.00074	0.4	-0.00139	1.1	-0.00203
<b>Average</b>		-0.0012		-0.0020		-0.0023
<b>Max</b>		-0.0007		-0.0014		-0.0014
<b>Min</b>		-0.0024		-0.0032		-0.0034
<b>standard deviation</b>		0.0006		0.0007		0.0007

**Table 69** Seismic Hysteretic Energy at Limit States (kJ) - Frame 4 2.0%

Seismic Hysteretic Energy						
Earthquake	PGA <sub>IO</sub>	IO	PGA <sub>LS</sub>	LS	PGA <sub>CP</sub>	CP
Chi-Chi	0.2	5.160594	0.4	19.34016	0.8	179.7441
Imperial Valley	0.2	0.475006	0.4	10.54555	0.8	64.2863
Kobe	0.2	1.011851	0.3	8.514524	0.8	76.45042
Kocaeli	0.2	4.651804	0.4	30.4996	0.9	216.7197
Loma Prieta	0.2	0.505536	0.3	12.5174	0.6	31.57685
Northridge	0.2	0.560475	0.5	13.96461	0.9	75.81842
Tabas	0.2	0.150429	0.4	2.154969	1.1	77.24824
<b>Average</b>		1.7880		13.9338		103.1206
<b>Max</b>		5.1606		30.4996		216.7197
<b>Min</b>		0.1504		2.1550		31.5769
<b>standard deviation</b>		2.1500		8.9931		67.7355

**Table 70** Yield Beam and Yield Frame Strains - Frame 4 2.5%

Earthquake	Yield Beam				Yield Frame			
	PGA	Steel Strain	PGA	Min. Concrete Strain	PGA	Steel Strain	PGA	Min. Concrete Strain
Chi-Chi	0.4	0.019595	0.4	-0.003173	0.5	0.025407	0.5	-0.003927
Imperial Valley	0.3	0.004593	0.3	-0.001407	0.5	0.009991	0.5	-0.001405
Kobe	0.3	0.005788	0.3	-0.001586	0.4	0.010564	0.4	-0.002153
Kocaeli	0.4	0.010783	0.4	-0.002197	0.5	0.019171	0.5	-0.003185
Loma Prieta	0.3	0.005738	0.3	-0.001538	0.5	0.008739	0.5	-0.001896
Northridge	0.4	0.006846	0.4	-0.001705	0.7	0.00996	0.7	-0.001837
Tabas	0.4	0.003623	0.4	-0.001269	0.6	0.00723	0.6	-0.00169
<b>Average</b>		0.0081		-0.0018		0.0130		-0.0023
<b>Max</b>		0.0196		-0.0013		0.0254		-0.0014
<b>Min</b>		0.0036		-0.0032		0.0072		-0.0039
<b>standard deviation</b>		0.0055		0.0007		0.0067		0.0009

**Table 71 Steel Strain at Limit States - Frame 4 2.5%**

<b>Steel Strain</b>						
<b>Earthquake</b>	<b>PGA<sub>IO</sub></b>	<b>IO</b>	<b>PGA<sub>LS</sub></b>	<b>LS</b>	<b>PGA<sub>CP</sub></b>	<b>CP</b>
Chi-Chi	0.2	0.012553	0.4	0.020264	0.8	0.035767
Imperial Valley	0.2	0.002079	0.4	0.005054	0.8	0.016775
Kobe	0.2	0.002266	0.3	0.006357	0.7	0.016614
Kocaeli	0.2	0.0043	0.4	0.01269	0.9	0.025082
Loma Prieta	0.2	0.001669	0.3	0.006449	0.6	0.013933
Northridge	0.2	0.001856	0.4	0.008226	0.9	0.018562
Tabas	0.3	0.001413	0.4	0.004069	1.1	0.014199
<b>Average</b>		0.0037		0.0090		0.0201
<b>Max</b>		0.0126		0.0203		0.0358
<b>Min</b>		0.0014		0.0041		0.0139
<b>standard deviation</b>		0.0040		0.0057		0.0078

**Table 72 Concrete Strain at Limit States - Frame 4 2.5%**

<b>Minimum Concrete Strain</b>						
<b>Earthquake</b>	<b>PGA<sub>IO</sub></b>	<b>IO</b>	<b>PGA<sub>LS</sub></b>	<b>LS</b>	<b>PGA<sub>CP</sub></b>	<b>CP</b>
Chi-Chi	0.2	-0.002264	0.4	-0.003275	0.8	-0.004195
Imperial Valley	0.2	-0.000883	0.4	-0.001464	0.8	-0.002169
Kobe	0.2	-0.000892	0.3	-0.001653	0.7	-0.002672
Kocaeli	0.2	-0.001341	0.4	-0.002431	0.9	-0.00278
Loma Prieta	0.2	-0.000817	0.3	-0.001639	0.6	-0.002566
Northridge	0.2	-0.000914	0.4	-0.00187	0.9	-0.001525
Tabas	0.3	-0.000705	0.4	-0.001344	1.1	-0.003068
<b>Average</b>		-0.0011		-0.0020		-0.0027
<b>Max</b>		-0.0007		-0.0013		-0.0015
<b>Min</b>		-0.0023		-0.0033		-0.0042
<b>standard deviation</b>		0.0005		0.0007		0.0008

**Table 73 Seismic Hysteretic Energy at Limit States (kJ) - Frame 4 2.5%**

<b>Seismic Hysteretic Energy</b>						
<b>Earthquake</b>	<b>PGA<sub>IO</sub></b>	<b>IO</b>	<b>PGA<sub>LS</sub></b>	<b>LS</b>	<b>PGA<sub>CP</sub></b>	<b>CP</b>
Chi-Chi	0.2	4.905324	0.4	14.971395	0.8	188.162028
Imperial Valley	0.2	0.495556	0.4	5.449603	0.8	59.762792
Kobe	0.2	0.805287	0.3	6.14268	0.7	67.303525
Kocaeli	0.2	3.718363	0.4	29.826072	0.9	176.578546
Loma Prieta	0.2	0.154927	0.3	6.841938	0.6	29.884099
Northridge	0.2	0.134162	0.4	8.974465	0.9	67.352746
Tabas	0.3	0.038565	0.4	1.429327	1.1	64.596895
<b>Average</b>		1.4646		10.5194		93.3772
<b>Max</b>		4.9053		29.8261		188.1620
<b>Min</b>		0.0386		1.4293		29.8841
<b>standard deviation</b>		1.9921		9.4513		62.2540